Photon Counting in Astronomy:
Evaluation of avalanche photodiode detectors

Johan Ingjald

Lund Observatory
Lund University

2010-EXA37

Degree project of 30 higher education credits (for a degree of Master)
May 2010

Lund Observatory
Box 43
SE-221 00 Lund
Sweden

Abstract

With the rise of modern physics in the 20th century, in particular quantum physics, a mix of confusion and interest came along. This meant new challenges and rethinking what actually measuring something means (with Heisenberg's uncertainty principle in mind). This created a need - a need for high speed and great accuracy in the instruments, in order to examine the newly discovered phenomena. One can say that, some of the resulting instruments is what we evaluate in this thesis. In particular we look at single-photon-counting avalanche photo-diode (APD) detectors.

We start by introducing a few different photon detectors; photomultiplier tubes (PMTs), charge-coupled devices (CCDs) and avalanche photo-diodes. Then we go through some basic properties of the APDs and also present various projects in the field of high-speed instrumentation and High Time Resolution Astrophysics (HTRA). The project section also features several introductions of alternative detectors, such as superconducting tunnel junctions (STJs) and transition edge sensors (TESs), as well as applications, e.g., lucky imaging.

In the following experiment section we take a look at our equipment, which mainly consists of photon detectors, a hardware-correlator and an oscilloscope. The detectors that are up for evaluation are the following: id Quantique's id100-50, MPD's PDM series (PD1C0B), PerkinElmer's SPCM-AQR-14, RCA Electro Optics' (now PerkinElmer's) SPCM-100-PQ, SensL's PCDMini0100 and SensL's SPMPC. We give a short presentation of each detector and their properties (as stated in the manufacturers' data sheets). We test the detectors by looking at the auto- and crosscorrelation functions obtained from the hardware-correlator in real time. We use a standard 100 Hz tube lamp as a white light source in order to obtain the signature for each detector. We also look at the pulse waveforms in an oscilloscope in order to check for possible issues resulting from long coaxial cables, cable joints or high photon count rates. Properties such as operating voltage vs. maximum count rate, dark count rate and dead time are also evaluated. Over 3000 runs of testing were made, using many different setups.

Sammanfattning

Under 1900-talet växte den moderna fysiken fram, speciellt kvantfysiken, vilket ledde till en blandning av både förvirring och intresse. Detta betydde nya utmaningar och en revidering av vad att mäta något faktiskt betyder (med tanke på Heisenbergs osäkerhetsprincip). Detta skapade ett behov - ett behov av hög hastighet och stor precision i utrustningen, för att undersöka de nyupptäckta fenomenen. Man kan säga att några av de resulterande instrumenten är vad vid testar i denna uppsats. Framför allt tittar vi på fotonräknande lavindiod (APD) detektorer.

Vi börjar med att introducera några olika fotondetektorer; fotomultiplikatorer (PMTs), laddningskopplade mekanismer (CCDs) och lavindioder. Sedan går vi igenom några av de grundläggande egenskaperna för APD detektorer och presenterar också ett antal projekt inom området hög-hastighets utrustning och hög-tidsupplöst astrofysik (HTRA). Projektsektionen innehåller även ett flertal introduktioner av alternativa detektorer, t.ex., supraledande tunnelövergångar (STJs) och övergångssensorer (TESs), liksom ett antal tillämpningar, t.ex., "lucky imaging".

I den följande experimentsektionen så tar vi en titt på vår utrustning, vilken framförallt består av fotondetektorer, en hårdvaru-korrelator och ett oscilloskop. Detektorerna som stod till vårt förfogande var följande: id Quantiques id100-50, MPDs PDM series (PD1C0B), PerkinElmers SPCM-AQR-14, RCA Electro Optics' (nu PerkinElmers) SPCM-100-PQ, SensLs PCDMini0100 och SensLs SPMPC. Vi ger en kort presentation av varje detektor och deras egenskaper (tillhandahållet från tillverkarnas datablad). Vi testar detektorerna genom att titta på auto- och korskorrelations funktionerna som vi får från hårdvaru-korrelatorn i realtid. Vi använder oss av ett standard 100 Hz lysrör som vitljuskälla för att kunna få fram en signatur för varje detektor. Vi tittar även på pulsvågformerna i ett oscilloskop för att undersöka och finna eventuella problem härstammande från användning av långa koaxialkablar, kabelskarvar eller höga fotonräknetal. Egenskaper såsom spänning mot maximalt fotonräknetal, mörker räknetal och dödtid undersöks också. Fler än 3000 mätningar har gjorts, med många olika uppsättningar.

Contents

1 Detecting light in astronomy **1**
1.1 High Time Resolution Astrophysics (HTRA) . . . 1

2 Detectors and materials for photon counting **3**
2.1 Photomultiplier tubes (PMTs) . . . 3
2.1.1 Conventional photomultiplier tubes . . . 3
2.1.2 Modern photomultiplier tubes (e.g., MCP-PMTs) . . . 3
2.2 Charge-coupled devices (CCDs) . . . 5
2.3 Avalanche Photodiodes (APDs) . . . 6
2.4 Semiconductor materials in photodiodes . . . 7

3 Geiger-mode avalanche photo-diodes (GM-APDs) **8**
3.1 Efficiency . . . 8
3.1.1 Quantum efficiency . . . 8
3.1.2 Photon detection efficiency . . . 8
3.2 Linear mode, Geiger-mode and breakdowns of photo diodes . . . 8
3.2.1 Linear mode and Geiger-mode . . . 8
3.2.2 Avalanche Breakdown . . . 9
3.2.3 Zener Breakdown . . . 9
3.3 Quenching . . . 10
3.3.1 Passive quenching . . . 10
3.3.2 Active quenching . . . 10
3.4 Resetting . . . 10
3.4.1 Dead time . . . 10

4 Unwanted photon counter properties **11**
4.1 Dark counts . . . 11
4.2 After-pulsing . . . 11
4.3 Optical crosstalk . . . 11
4.4 Connectivity . . . 12
4.5 Fill-factor . . . 12
4.6 Junction heating . . . 12
4.7 Inconsistent sensitivity . . . 12

5 Projects for high time resolution astrophysics and high speed instrumentation **14**
5.1 The High Speed Photometer on the Hubble Space Telescope . . . 14
5.2 High-speed Imaging Photometer for Occultation on board SOFIA, the airborne Stratospheric Observatory for Infrared Astronomy . . . 15
5.3 ULTRACAM and ULTRASPEC . . . 16
5.3.1 ULTRACAM . . . 16
5.3.2 ULTRASPEC . . . 19
5.4 Superconducting Tunnel Junctions (STJs) and Transition Edge Sensors (TESs) . . . 19
5.4.1 Superconducting Tunnel Junctions (STJs) . . . 20
5.4.2 Transition Edge Sensors (TESs) . . . 22
5.4.2.1 Position-Sensitive Transition Edge Sensors (PoSTs) . . . 23
5.5 Optical Pulsar TIMing Analyzer (OPTIMA) . . . 25
5.6 Multichannel Analysis of Nanosecond Intensity Alternations (MANIA) . . . 27
5.7 Fast Variability Optical Registration (FAVOR) . . . 27
5.8 Optical Searches for Extraterrestrial Intelligence (Optical SETI) . . . 29
5.9 Lunar- and Satellite Laser Ranging . . . 31
5.10 Quantum Optical-Spectrometer (QVANTOS) . . . 35
5.11 Lucky Imaging . . . 38
5.12 TRIFFID, MEKASPEK, MCCP, SUBARU, SALT, ESO-VLT and OPTICON . . . 39

5.12.1 TRansputer Instrument For Fast Image Deconvolution (TRIFFID) . . . 39
5.12.2 MEhr-KAnal-SPEKtralphotometer (MEKASPEK) and Multi-Channel multi-Color Photometer (MCCP) . . . 40
5.12.3 SUBARU . . . 40
5.12.4 Southern African Large Telescope (SALT) . . . 42
5.12.5 ESO VLT . . . 43
5.12.6 Optical Infrared Coordination Network for Astronomy (OPTICON) . . . 44

6 Experiments **47**
6.1 Equipment . . . 47
6.1.1 Detectors . . . 47
6.1.1.1 id Quantique . . . 47
6.1.1.1.1 About id Quantique . . . 47
6.1.1.1.2 id100-50 . . . 47
6.1.1.2 Micro Photon Devices (MPD) . . . 49
6.1.1.2.1 About MPD . . . 49
6.1.1.2.2 PDM series, PD1C0B . . . 49
6.1.1.3 PerkinElmer . . . 51
6.1.1.3.1 About PerkinElmer . . . 51
6.1.1.3.2 SPCM-100-PQ . . . 52
6.1.1.3.3 SPCM-AQR-14 . . . 54
6.1.1.4 SensL . . . 57
6.1.1.4.1 About SensL . . . 57
6.1.1.4.2 Passive Quench Circuit (PQC) . . . 57
6.1.1.4.3 PCDMini0100 . . . 57
6.1.1.4.4 SPMPC, Large Area Photon Counting APD . . . 59
6.1.2 Hardware-Correlators . . . 62
6.1.3 Oscilloscope . . . 64
6.1.4 Power Supply . . . 65
6.1.5 Lamp and LEDs (Light Emitting Diodes) . . . 65
6.2 Test descriptions and Methods . . . 65
6.2.1 SensL's PCEdu-1 Photon Counting Fundamentals Educator Pack . . . 65
6.2.2 Photon count rate and coaxial cable length dependence for Auto- and Cross-correlation functions . . . 66
6.2.3 Color sensitivity . . . 67
6.2.4 SensL operating voltage vs. photon count rate . . . 68
6.2.5 Dark count evaluation . . . 68
6.2.6 Dead time estimation . . . 69
6.3 Results . . . 69
6.3.1 SensL's PCEdu-1 Photon Counting Fundamentals Educator Pack . . . 69
6.3.2 Photon count rate and coaxial cable-length dependence for Auto- and Cross-correlation functions . . . 71
6.3.3 Color sensitivity . . . 76
6.3.4 SensL Operating Voltage vs. Photon Count Rate . . . 77
6.3.5 Dark count evaluation . . . 78
6.3.6 Dead time estimation . . . 81
6.3.7 Encounters of weird and unwanted behavior . . . 81

7 Conclusions **83**
7.1 Acknowledgments . . . 84

Bibliography **85**

A Appendix: Auto- and Cross-correlation functions and waveforms **87**
A.1 id Quantique's id100-50 87
A.2 MPD's PDM series, PD1C0B 99
A.3 PerkinElmer's SPCM-100-PQ 111
A.4 PerkinElmer's SPCM-AQR-14 117
A.5 SensL's PCDMini0100 129
A.6 SensL's SPMPC 135

1 Detecting light in astronomy

For many centuries people have looked up into the skies and been stunned and overwhelmed with questions of what may lie beyond Earth and the solar system. With the development of telescopes started in Galileo Galilei's era to the present space-based telescopes and ground-based very/extremely/overwhelmingly large telescopes (V-/E-/OW-/-LT) together with advancements in technology, studies of stellar objects well beyond our solar system are possible. Actually one can almost say that telescopes today are limited by the Universe's structure, i.e. plasma clouds about 300.000 years after the Big Bang, rather than the telescope size when trying to observe further out in space. This limitation as well as other factors emphasizes development of new methods to observe both possibly further but also in greater detail on objects closer to us. Even if many questions in classical astronomy have been answered due to the advances, many remain and new arise.

Today we scan the space in not only the visible region of the electromagnetic spectrum but also in the gamma, radio, ultraviolet and infrared regions. This makes it possible to look through certain areas where visible light is blocked, but still leaves many questions unanswered.

To fill a part of this gap as well as take a large step into new discoveries and advancement in science as well as understanding the Universe and the laws of nature, we can observe the Universe through High Time Resolution Astrophysics (HTRA). This field in astrophysics is new and very much in development. One of the main goals in HTRA is to take the classical astronomy to the quantum physics era, i.e. approach Heisenberg limits and observe the very fundamental particles in action and other rapid events in space. Unfortunately, the adaptation towards this field is not completely smooth as some classical astronomers might not even see the need for this field, which is understandable considering that there are many questions still possible to answer with more time and the present observation methods. Also the complexity that HTRA and quantum physics introduces is a factor as well.

HTRA is very much technology dependent and even though the largest possible telescopes are preferred and eagerly awaited, the advances in the HTRA field is currently focused towards the receiver end, i.e. the photon detectors. These detectors come as different types and have their own development history (see section 2) but the present detectors that enable and are most promising for HTRA are the semi-conductor-based avalanche photodiodes (APDs) operated in Geiger-mode.

Because High Time Resolution Astrophysics (HTRA) is not a major field, the development of APDs is mostly driven by the communication branch striving for new or improved communication methods mostly in the infrared region. However, the need for high-speed observations is present in other fields such as, e.g., single molecule spectroscopy, DNA sequencing, quantum cryptography and laser testing, which all pushes for advances in other fields of the electromagnetic spectrum. This allows for attempts of applying these new high speed photon detectors in astronomy for a big part of the electromagnetic spectrum. Which region of the optical region the detector is sensitive to is primarily a question of the material used.

In this thesis several photon detectors from different manufacturers have been evaluated and compared at various count rates with focus on second-order correlation functions and the waveforms of the pulses, as well as cable-length and cable-joint dependences. Also possible applications in astronomy are discussed and suggested. What are we possibly missing by not observing stellar objects at single-photon resolution?

1.1 High Time Resolution Astrophysics (HTRA)

It has long been stated from various sources that we do not need higher time resolution than say milliseconds when we observe stellar objects because of calculations showing various impossible physical conditions. But as the knowledge and understanding of quantum physics grows, we see that we also have quantum phenomena in optics and thus in astronomy. We also encounter more extreme cases of otherwise well-studied objects such as pulsars, neutron stars and black holes; which conventional astrophysics struggle to explain and further examine.

High Time Resolution Astrophysics (HTRA) opens an important new window to the universe and is a vital step towards understanding a range of phenomena from diverse objects and radiative processes. The motivation and importance of HTRA is shown by the growing number of scientific papers with topics including X-ray binaries, cataclysmic variables, quantum optics, pulsars, stellar oscillations, flare stars and extra-galactic transients; with regards to high-speed phenomena.

In order to explore the field of HTRA, significant technology advancements need to be met but with

the upcoming extremely large telescopes (ELTs) and the rise of high speed detectors such as avalanche photodiodes (APDs); we are on our way to understand the stellar world and its objects even further.

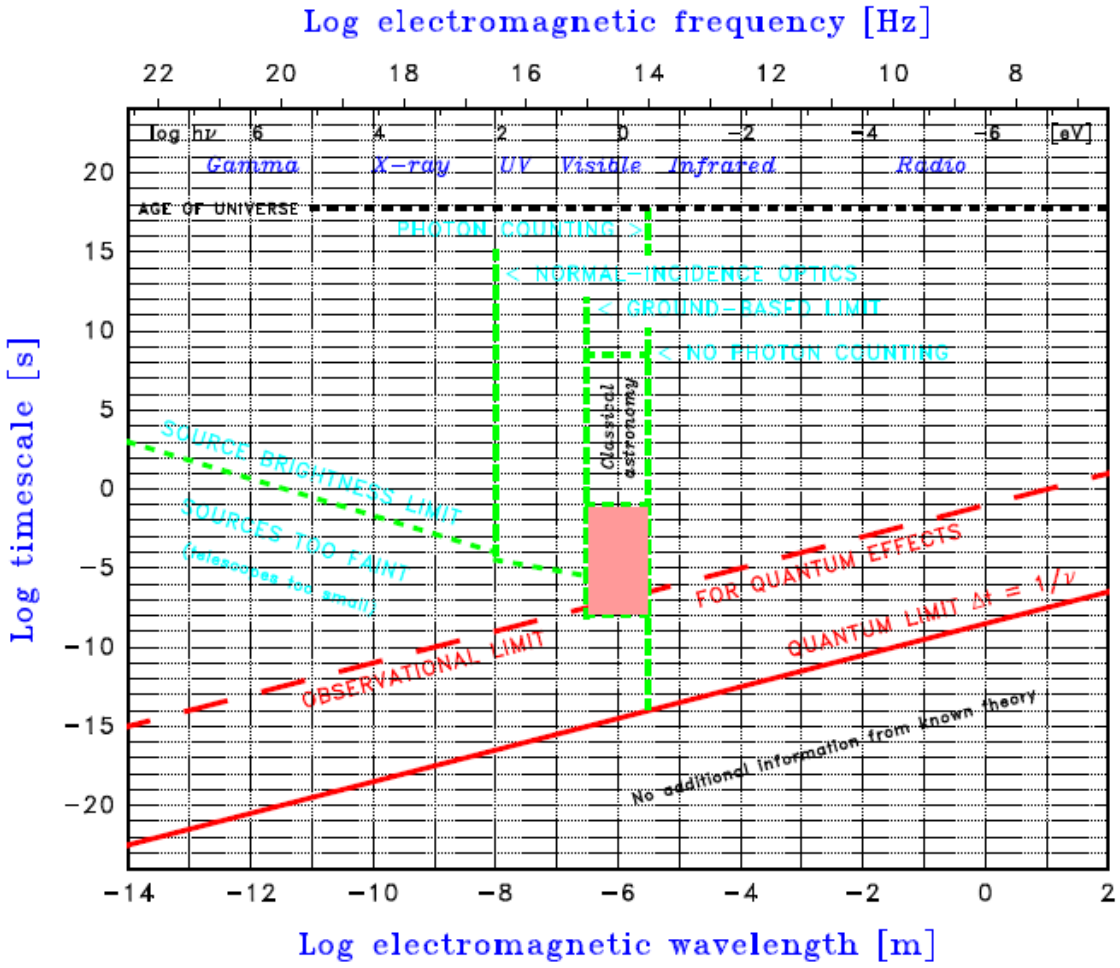

Figure 1.1: Various wavelengths and corresponding phenomena are shown. (Dainis Dravins)

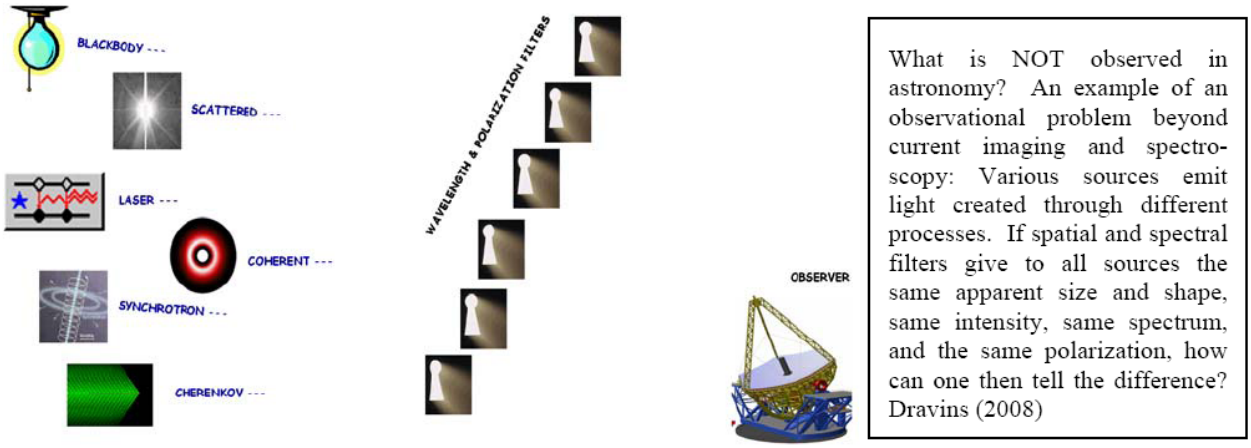

Figure 1.2: Limitations of conventional astrophysics. (Dainis Dravins)

2 Detectors and materials for photon counting

2.1 Photomultiplier tubes (PMTs)

2.1.1 Conventional photomultiplier tubes

Photomultiplier tubes have been around for more than 70 years and have advanced quite a bit in terms of gain, from the first demonstrated PMT of about eight in internal gain to modern ones with several million in internal gain. This makes the modern PMTs capable of counting single photons in theory but they are still in a sense limited by their simplicity. PMTs have rather low quantum efficiency (see section 3.1.1) throughout the optical region, especially lack of sensitivity in the near infrared region.

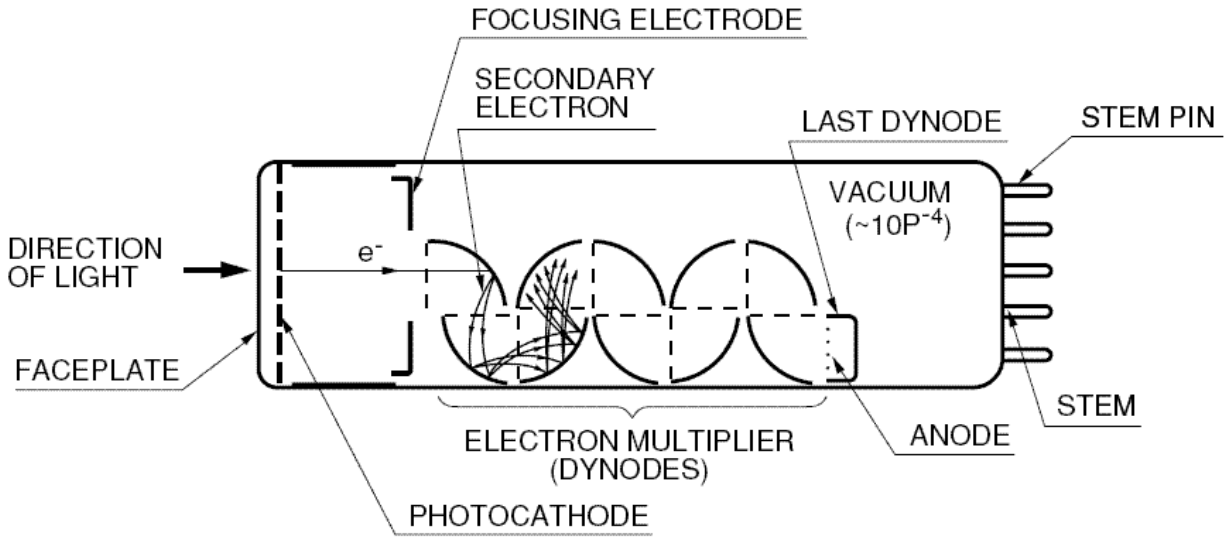

Figure 2.1: Schematic structure of a photomultiplier tube. (Hamamatsu Photonics K.K. 2006, [5])

The basic principle of how PMTs operate is, as Figure 2.1 schematically demonstrates:

1. Incident light enters the PMT through an input window.
2. Photons hit the photocathode and excite electrons which are emitted into vacuum.
3. The photoelectrons are accelerated and focused by the focusing electrode onto the first dynode, where they are multiplied through secondary electron emission.
4. The multiplying process in repeated for every dynode until the electrons are finally collected by the anode.

PMTs of this more conventional type can in some cases be temporarily disabled in the sense that they become less sensitive for a time because of overexposure to light even when not in operating mode because of the material properties in the photocathode. The conventional PMTs often require very high operating voltage as well as sometimes cumbersome interface equipment.

2.1.2 Modern photomultiplier tubes (e.g., MCP-PMTs)

Because of the conventional photomultiplier tubes limitations, shortly and swiftly mentioned in the above section, the need for new improved and more versatile PMTs has grown over the years. This need has evolved into the development of PMTs such as the microchannel plate photomultiplier tubes (MCP-PMTs).

The MCP-PMTs incorporate a microchannel plate (MCP) in place of the conventional electron multipliers (dynodes) and can offer measurements down to picoseconds level as well as low intensity light detection at photon counting level. The MCP consists of a two dimensional array of glass capillaries (channels), each

only a few micrometers in diameter and with a voltage between each end, bundled in parallel and formed into a thin disk. The inner walls of the channels are processed to have the proper electrical resistance and secondary emissive properties. Each channel operates independently as an electron multiplier, thus making the MCP-PMTs more sensitive, with higher internal gain, than the conventional PMTs.

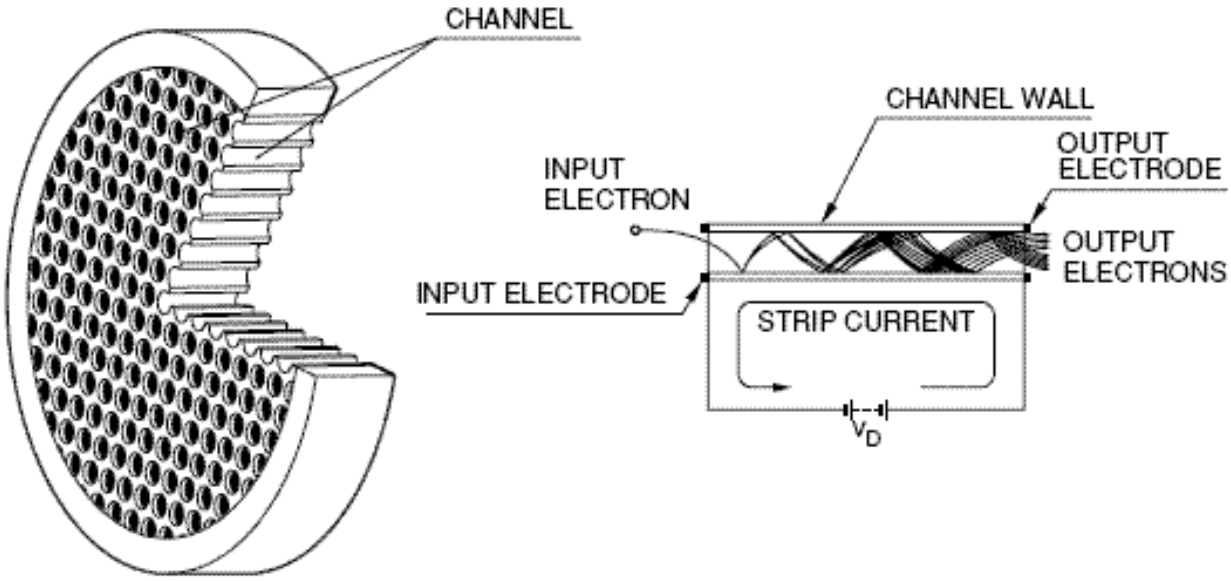

Figure 2.2: Schematic structure the MCP (left) and its multiplying principle (right). (Hamamatsu Photonics K.K. 2006, [5])

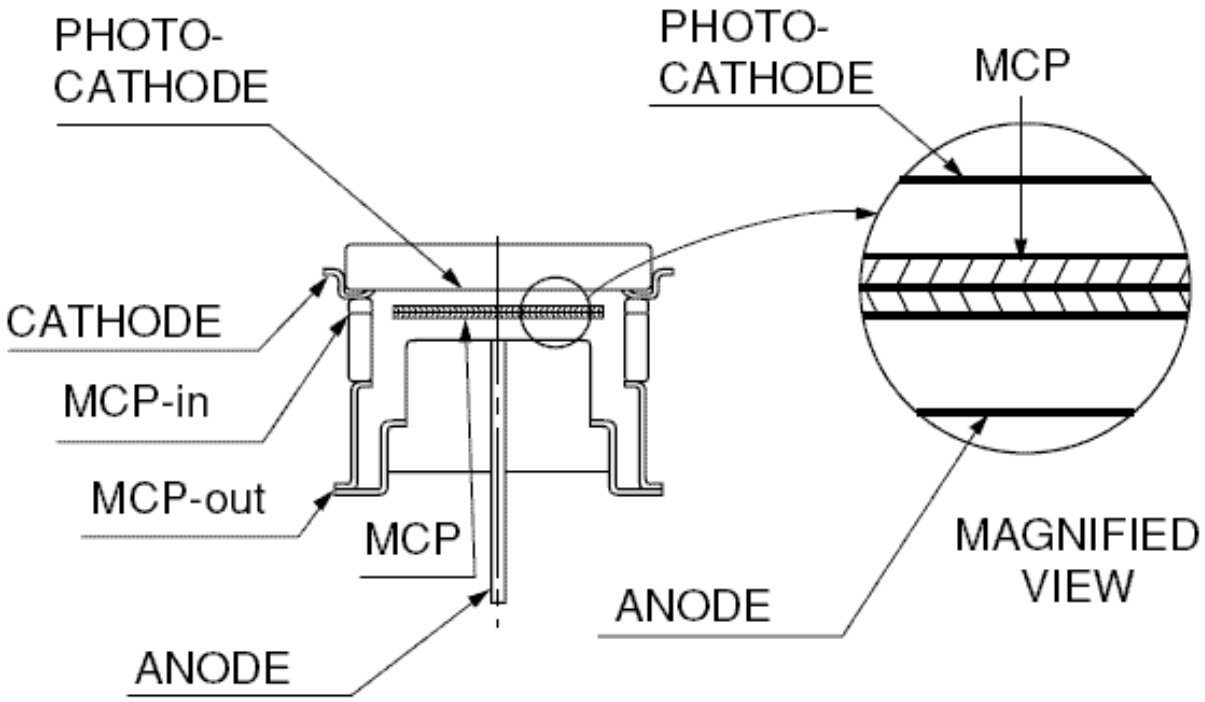

Figure 2.3: Schematic cross section of a typical MCP-PMT. (Hamamatsu Photonics K.K. 2006, [5])

The basic principle of how the MCP-PMTs operate is, as Figure 2.2 (right) and Figure 2.3 schematically demonstrate:

1. Incident light enters the MCP-PMT through a input window.
2. Photons hit the photocathode and excite electrons which are emitted into the channels of the MCP.
3. The photoelectrons hit any of the channels' inner wall and multiply through secondary electron emission.
4. The secondary electrons hits the inner wall again and the multiplying process repeats until the end of the channel.
5. The anode collects the electrons from the MCP.

The advantages of a MCP-PMT over a conventional PMT are many. MCP-PMTs offers high gain despite compact size, fast time response, two-dimensional detection with high spatial resolution, stable operations in strong magnetic fields, sensitivity to charged particles, ultraviolet, X-rays, gamma rays and neutrons, and operates with lower power consumption.

The MCP-PMT has its flaws though; as gain increases to around 10000, severe noise can start to appear, especially if not cooled. MCP-PMTs are also known to be more fragile and more difficult to handle, compared to the conventional PMTs.

2.2 Charge-coupled devices (CCDs)

For almost 50 years the charge-coupled devices (CCDs) have been developed. The first commercial CCD was produced by the company Fairchild (today Fairchild Imaging, http://www.fairchildimaging.com) in 1973 following its invention 1969 at Bell Labs. The CCDs quickly became popular because of their versatility and features such as image capture. Today there are many variations of the CCD design and new are still being developed. Different designs are usually optimized with different applications in focus but in general the CCDs are known to be very reliable, quite simple and can be used in large arrays.

CCDs usually consist of an epitaxial layer of silicon, doped with p+ (e.g., Boron) and put on top of a substrate material, often with p++ doping. This layer of silicon is the photoactive region of the CCD. Capacitor dielectrics are put at the layer.

When incident photons hit this photoactive region each capacitor accumulates a charge proportional to the photon flux (i.e. light intensity). When the array has been exposed for a set amount of time the capacitors operate as a shift register by transferring their accumulated charge to its neighbor. The end capacitor dumps the charge into a charge amplifier, which converts the charge to a voltage. When repeating this process, depleting the CCD arrays in this manner, it creates a sequence of voltages, which are sampled and stored digitally in some type of memory.

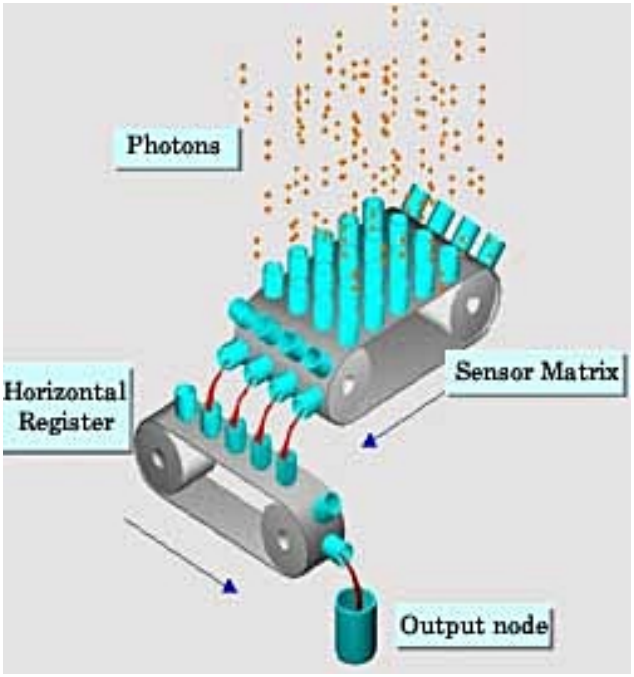

Figure 2.4: A simple sketch of the CCDs readout process. (OpticStar Ltd)

A quite big issue with conventional CCDs is their readout speed, since it can sometimes be measured even in seconds or minutes for large arrays. Newer CCDs may differ and can through other readout processes (e.g., by reading a limited part of the whole CCD array) reach milliseconds.

Another issue with CCDs during the readout process is charges not being transferred, thus are left behind and not registered. To put numbers on this the term *Charge Transfer Efficiency* (CTE) is used. CTE is basically the measurement of how efficient the process of moving charges between the capacitors is. In the past it was not uncommon with CTE at about 98 % or lower but today it can exceed even 99.9999 % in scientific devices. This might tell us that the problem is over but in fact it still makes a difference. Consider a 10000 electron charge packet and 10000 transfers as well as assuming only one pixel/capacitor shift (it can be more, e.g., 3-stage is common). After these 10000 transfers we end up with $(10000e^-) * (0,999999)^{10000} \approx 9900e^-$. 100 charges might have been lost just due to this process. And today it is not uncommon with even larger packets and transfers in CCDs.

To achieve a high CTE it might also be necessary to slow down the readout process by decreasing the clocking rate (i.e. extraction of the photo-generated electrons from the detection site) and/or the digitization rate, thus making CCDs even worse candidates for high speed astrophysics and advancements into quantum astronomy.

The CCDs have, however, made it possible to observe stellar objects in great detail and also made the current digital camera era possible. CCDs are also linear, stable, robust and low-power devices which makes them almost perfect detectors. However, the conventional CCDs do not quite make it to the Heisenberg limits and into quantum physics, which High Time Resolution Astrophysics (HTRA) strives towards. Even though some newer designs including CCDs (e.g., ULTRACAM) do make good attempts and succeed in taking further steps in high speed astrophysics, the problem with CCDs is basically that they are limited to a certain read-out speed while at the same time suffering from read-out noise.

Trying to solve one of the limitations of the CCDs usually ventures another. This creates a need for development and use of other types of detectors for higher temporal resolution observations.

2.3 Avalanche Photodiodes (APDs)

Avalanche Photodiodes (APDs) are high-speed, high sensitivity photodiodes utilizing an internal gain mechanism that functions by applying a reverse voltage. If we compare to a simple PIN photodiode, APDs are

able to measure even lower levels of light and can be used in a wide variety of applications requiring high sensitivity and fast response times such as long-distance optical communications, optical distance measurement, particle detection, astronomical observations, ceilometers (cloud height measurement), optical fiber test and fault location, photometry, ultra sensitive fluorescence, etc.

Ideally we would like an APD to possess zero dark noise, no excess noise, broad spectral and frequency response, a gain range from 1 to 10^6 (at least), and low cost. Basically this would equal a very good PIN photodiode with gain. However, in reality we can currently barely achieve any of these properties because of conflicting design requirements. In other words, one affects the other. More unwanted properties and how they relate on each other are presented in Section 4.

The APD should be seen as a possible replacement for the photomultiplier tubes (PMTs) than the charge-coupled devices (CCDs), but for the extreme photon count rates and time resolution, which high time resolution astrophysics requires, conventional CCDs basically cannot compete.

The actual architecture of an APD will not be described in any greater physical detail in this thesis, because of the variations in design depending on material and application, but the basic properties of APDs are described in Section 3.

2.4 Semiconductor materials in photodiodes

Silicon (Si):
Low dark current, high speed, good sensitivity roughly between 400 and 1000 nm (best around 800 – 900 nm).

Germanium (Ge):
High dark current, slow speed due to large parasitic capacity, good sensitivity roughly between 900 and 1600 nm (best around 1400 – 1500 nm).

Indium Gallium Arsenide Phosphide (InGaAsP):
Expensive, low dark current, high speed, good sensitivity roughly between 1000 and 1350 nm (best around 1100 – 1300 nm).

Indium Gallium Arsenide (InGaAs):
Expensive, low dark current, high speed, good sensitivity roughly between 900 and 1700 nm (best around 1300 – 1600 nm).

[Info above from RP Photonics, `http://www.rp-photonics.com/photodiodes.html`]

The ranges mentioned above are determined by measuring the quantum efficiency (see section 3.1.1) for various wavelengths to examine where it is reasonably high.

One can quite easily understand why many photodiode manufactures choose Silicon; simply because it is cheap, quite easily processed and offers good sensitivity over a pretty broad wavelength range, including the quite often observed visual wavelengths. However, in the high-speed communication branch infrared sensitivity is more valued and the other materials are widely used.

The amount of these material used for a common photon detector is still only about a mere 100×100 μm^2 (e.g., the detectors evaluated in this thesis) or very recently up to one or a few mm^2 in attempts of creating a working array of photodiodes by putting many μm diodes together with some space in between. This gives us a hint of some of the difficult parts concerning the photodiode-material, such as to maintain few defects within the chosen material (as defects, e.g., cause after-pulsing, which can in a way be seen as a quality control) and to attach the electronic wiring needed for the actual device to give an output, rather than attaining the amount of photodiode-material needed. Even if the photodiodes can at first "glimpse" (can actually barely be seen) seem tiny; it is the choice of material used for the photodiode which is critically determining what applications it can be used for.

3 Geiger-mode avalanche photo-diodes (GM-APDs)

3.1 Efficiency

3.1.1 Quantum efficiency

To simplify the understanding of such an intimidating term as *Quantum efficiency*, with the complex field of quantum physics in mind, one can say that Quantum Efficiency (QE) is basically a measurement of input vs. output (i.e. how many incident photons [%] are actually registered by the detector). A high QE is therefore wanted, especially for the actual wavelengths under observation.

For a detector (e.g., an APD) it's sometimes spoken of QE as the ratio between induced current and incident flux. This is often presented as electrons per photon (dimensionless) or ampere/watt.

However, for further understanding one can break down QE into two subterms; *absorption efficiency* and *triggering (or breakdown) probability*.

Absorption efficiency (AE) is essentially the probability for a photon to be absorbed in the active area of the detector device (i.e. the intrinsic region). Absorption efficiency is mainly material dependent, which implies AE being a function of wavelength. This is because different materials have different energy gaps. Therefore one needs to select material after which wavelength that is going to be observed. Photons with long wavelengths (low energy) do not carry enough energy to excite an electron from the valance band to the conduction band in the material. Photons with short wavelengths (high energy) will basically produce electron-hole pairs that will avoid collection in the device and therefore not pass through the multiplication junction.

Triggering (or breakdown) probability (TP) is the probability for a photon-produced electron to trigger a self-sustained avalanche in the device. TP is reliant on excess reverse bias (i.e. voltage above breakdown voltage) and thus also indirectly is temperature dependent because of the breakdown voltage variations with temperature changes. So, in other words, to keep QE constant it is important to keep the temperature of the whole diode constant.

3.1.2 Photon detection efficiency

An alternative and perhaps a more modern and complete way to look at the efficiency of an APD biased in Geiger-mode is to look at Photon detection efficiency (PDE). PDE is a product of quantum efficiency (QE), a geometric factor (ϵ, ratio of sensitive area to total area) and the probability that an incoming photon triggers a breakdown ($P_{trigger}$). $PDE = QE \cdot \epsilon \cdot P_{trigger}$.

QE in this case is defined slightly different from above since the triggering probability has been taken out as its own factor. The geometric factor ϵ needs to be optimized depending on the specific application. This is done by adjusting the area of the cell used for detection. The triggering probability ($P_{trigger}$) depends on where the electron-hole pair was created and on excess bias voltage ($V_{excess} = V_{operating} - V_{breakdown}$).

Also one should consider reflections of the diode surface and use anti-reflection coatings depending on application.

3.2 Linear mode, Geiger-mode and breakdowns of photo diodes

3.2.1 Linear mode and Geiger-mode

There are two main mechanisms in which avalanche photo diodes (APDs) operate, in *linear mode* and in *Geiger-mode*.

In *linear mode* the APD is biased below breakdown voltage and the current registered in the APD is proportional to the incident photon flux. In this mode the APD is easier to calibrate and rather similar to the photomultiplier tubes but has rather limited internal gain.

In *Geiger-mode* the APD is set to a semi-stable state by being biased above the breakdown voltage. An incident photon can then cause the APD to break down in a self-sustained avalanche, which can only be quenched by external electronics (see section 3.3).

3.2.2 Avalanche Breakdown

On the arrival of a photon in the Geiger-mode avalanche photo diode (GM-APD), assuming it is absorbed; it creates an electron-hole pair. Both the electron and the hole can trigger a breakdown. Which is more likely to trigger a breakdown is material dependent. Usually, however, there is some or perhaps only one electron in the valance band of the semi-conductor (e.g., silicon) crystal lattice that is excited into the conduction band where the electrons are accelerated by the strong electric field present within the device. Electrons therefore receive high energy and subsequently collide with, and ionize other atoms (e.g., silicon) in the crystal lattice, thus releasing bound carriers (i.e. high-energy electrons) which themselves can repeat the process. The process is known as impact ionization. In a short amount of time even one triggered electron will indirectly, through these "chain reactions", have produced a big *avalanche* of electrons which easily is detected as an increase in reverse current within the device. This is termed an *avalanche breakdown*.

This massive breakdown phenomenon does not have to become excessively large or be long lasting to be detected, though. Allowing the avalanche breakdown to go to completion in the device is merely a waste of time and because of the high current generated within the device it could also permanently damage the diode. Therefore one usually introduces *quenching* mechanisms (see section 3.3) in the circuits of the APDs. Quenching assists to halt the avalanche and thus makes it possible to more quickly reset the APD operating voltage back to, or above, the breakdown voltage. The quenching mechanisms are essential for the operation of the detector because while breaking down the detector is not very capable (i.e. low probability) of detecting any new incoming photons and needs to be reset before new events can be registered properly. This is of course an issue and the time while the detector is not able to detect new photon-arrivals is termed *dead time* (see section 3.4.1).

Unlike Zener breakdown (see section 3.2.3), avalanche breakdown is highly temperature dependant. The temperature coefficient of the avalanche mechanism varies with breakdown voltage but is positive. That is, as the temperature increases, the breakdown voltage increases. However, the avalanche itself which essentially can be seen as a current flowing through the APD, increases the temperature in a phenomenon termed *junction heating* or s*elf-heating* (see section 4.6). This unwanted property of the APD is being especially noticeable when operating at high counting rates or long durations of time and can cause, e.g., longer dead times, increase of dark counts and alternations to the waveform of the actual pulses seen in, e.g., in an oscilloscope due to breakdown voltage variations. For the latter it, e.g., applies that, since a rise in temperature leads to increased breakdown voltage, the excess bias voltage ($V_{excess} = V_{operating} - V_{breakdown}$) is decreased and thus the amplitude of the pulse, which in many cases is close to the excess bias voltage, is decreased as well. If the excess bias voltage (i.e. the amplitude of the pulse) is too low it cannot trigger an output pulse and thus no pulse is recorded in, e.g., a hardware-correlator, which is used for the experiments in this thesis. The operating voltage, $V_{operating}$, is typically set to 3 – 5 V above the breakdown voltage, $V_{breakdown}$, for APDs, but it can vary.

3.2.3 Zener Breakdown

For highly doped p-n junctions the dominant breakdown mechanism is *Zener breakdown*. The heavy doping makes the depletion layer extremely thin. It is so thin that charge carriers (electrons) cannot be accelerated enough for impact ionization to take place, as in the case for avalanche breakdown. The thin layer, however, allows for very high electric fields.

Zener breakdowns are basically made possible through the quantum mechanical phenomenon called *tunneling*. This can occur because of the depletion region of the junction being sufficiently thin and the electric field sufficiently high. These two factors increase the probability of tunneling enough for it to take place across the junction, i.e. charge carriers (electrons) tunneling through the bandgap of the semi-conductor. Eventually this process leads to complete breakdown of the junction. Tunneling electrons through such a thin depletion layer build up a current which flows through the junction. The current is detected and thus a photon arrival can be registered.

The temperature coefficient of the Zener mechanism is negative. That is, as the temperature increases, the breakdown voltage decreases. The temperature coefficient, unlike for the avalanche mechanism, is usually not dependent on the breakdown voltage.

The photodiodes having the dominant breakdown as Zener breakdown are usually referred to as *Zener diodes*. Sometimes Zener diodes do have dominant avalanche breakdowns though, which can be a bit con-

fusing. At low doping levels and higher voltages the avalanche mechanism dominates while at heavy doping levels and lower voltages the Zener mechanism dominates. And at a certain doping level and, e.g., around 6 V for Silicon, both of the breakdown mechanisms are present with temperature coefficients that just cancel.

Zener diodes with dominant Zener breakdowns are, however, not examined or evaluated in this thesis.

3.3 Quenching

During an avalanche breakdown a large current is present in the APD and the operating voltage has been lowered, thus needs to be reset to or above the breakdown voltage before new photon arrivals can be received and recorded. Quenching is also crucial to avoid damages due to the heat-up accompanying the generated current. To quench the avalanche process and allow the device to reset, quenching mechanisms are needed.

There are two kinds of quenching mechanisms being employed when operating APDs in photon counting mode; passive quenching and active quenching. The former method, passive quenching, is relatively simple but comes with a few drawbacks. For an active quenching circuit the design is rather complex but is still the preferred method.

3.3.1 Passive quenching

A passive quenching circuit basically includes a huge ballast resistor, in the order of kΩ or MΩ, which is put in series with the APD. This limits the current flowing through the device and allows the APD to slowly recharge to the original operating voltage, usually above breakdown voltage (Geiger-mode). The time it takes to recharge is termed dead time (see section 3.4.1) and can be in the order of a few microseconds, thus limiting the maximum count rate to an order of 10^5 Hz (counts per second). In a passive quenching circuit the dead time is often not even possible to keep constant which also limits its use for more precise operation.

Another drawback is that the dark count (see section 4.1) is increased due to the rise of the temperature, which follows the large current present before the quenching has taken place. Also, because of this large current, a huge amount of electrons and holes is present and thus many of them can be trapped in defects within the device. These electrons and holes are after some time released to possibly cause their own avalanches, thus causing after-pulsing (see section 4.2).

Because of the drawbacks, which are all unwanted properties of the APDs but not effectively taken care of by the passive quenching circuits, other methods are needed for high time resolution astrophysics.

3.3.2 Active quenching

The drawbacks from the passive quenching circuits can be rather effectively overcome by using the more complex active quenching circuits (AQC). The AQCs have many different designs and these will not be described in detail here. The main features throughout the designs are that the AQCs effectively and quickly, after breakdown of the APD, can sense and reduce the bias voltage across the APD, thus reducing temperature increase, dark counts and after-pulsing.

The effectiveness of the AQCs together with a cooling system (e.g., a Peltier cooling system) for the APD, allows short dead times on the order of nanoseconds and thus operation of APDs at very high frequencies (count rates), on order of 10^6 Hz and above, for long periods and with high time resolution.

3.4 Resetting

3.4.1 Dead time

Dead time or recovery time is the time it takes for the APD to be quenched and reset to operating at Geiger-mode (biased above breakdown voltage) again, thus being ready for a new photon arrivals. Dead time can essentially be separated into *quench time*, *hold-off time* and *reset time*.

Quench time is the time it takes for the quenching of the avalanche current to finish. *Hold-off time* is the time you can set to keep the device below breakdown voltage for a time (e.g., to reduce after-pulsing by waiting for the trapped electrons to be released). *Reset time* is the time it takes to reset the device to above breakdown voltage.

Because of the dead time, the measured count rate is not a true representation of the statistically true count rate. Under ideal conditions, however, it is possible to account for the dead time and arrive at the true signal rate, using simple formulas.

4 Unwanted photon counter properties

4.1 Dark counts

One might not expect that a detector of light would get triggered even in complete darkness. However, this occurs and is an unwanted property present for all photon detectors operated in normal conditions (i.e. room/outside temperature, no excess cooling). The reason for this occurrence is electrons being thermally excited from the valance band into the conduction band of the semi-conductor detector.

The current detectors have no way to distinguish photon-produced electrons from thermally excited electrons. Therefore an avalanche is released and a photon event is recorded. This false count is termed a dark count.

There are, however, ways to reduce dark count; the easiest being cooling of the device. Lower operating temperature reduces the thermal energy present in the APD and thus efficiently lowers the probability for an electron to get excited and trigger a false photon count. A temperature decrease of 8 ℃ can lead to a reduction of dark counts by a factor of 2 [1].

The method of cooling the device does come with a cost, that is more than the time and effort spent on cooling. Temperature changes affect a lot of the properties of an APD, which is described in more detail in the coming sections of this report. However, as a crucially affected property one can mention Quantum Efficiency (QE), which is indirectly affected by temperature through changes in reverse bias which subsequently affects the triggering probability of the APD. It is therefore not only important to keep the APD cooled enough for dark counts to occur at a reasonably low rate but also to keep a constant temperature to ensure somewhat constant QE (see section 3.1.1, "Triggering probability").

4.2 After-pulsing

Perfect materials just don't exist; all manufactured or processed materials include impurities and defects. These defects can act as traps for the electrons triggered in the avalanche. After some time, *trap time*, these electrons are released and can continue their journey of ionization. This can happen even after a pulse already has been registered by the device, originating from the other electrons in the same avalanche, thus causing an extra photon count in the detector without any new photons being present.

If cooling is present, trap time is increased. Typically a decrease of 25 ℃ prolongs the trap time by a factor of 3 [1]. Therefore it is important to optimize the temperature, depending on application.

To reduce after-pulsing to quite an extent, one can increase the *dead time* to account for the *trap time*. Even though the trap time is not constant but probability based, it is quite effective to try and optimize the dead time depending on application. This does however come with the cost of no new real photon detections being possible. Long dead times are usually not wanted.

Low after-pulsing in GM-APDs is often considered a sign of quality.

4.3 Optical crosstalk

When we start heading towards developing arrays of avalanche photodiodes, we encounter a fundamental limitation – the creation of photons by an APD after an avalanche breakdown. *Optical crosstalk* is when these created photons manage to reach neighboring pixels in the array, leading to the generation of false photon counts in these pixels. A single pixel detector can also trigger itself if the photons are reflected on, e.g., a protective glass window and the circumstances are unfortunate, i.e. such that the emitted photons' travel time exceeds the dead time (e.g., 50 ns deadtime $\sim$ 15 m travel distance) before it hits the pixel again.

There are techniques which may be taken to overcome this fundamental difficulty. It can be reduced by carefully designing the quenching circuit to rapidly sense increased current due to the avalanche breakdown and quickly quench it before significant light generation takes place. Another approach is to optically insulate the neighboring pixels from each other by incorporating features in the architecture such as filled trench

insulation or by employing mesa structures[1] to limit light coupling between devices. Trench insulation provides the added benefit of electrically insulating the pixels from each other. However, while adding trenches between pixels reduces optical crosstalk it also decreases the array fill-factor for the detector.

4.4 Connectivity

For an APD array each pixel requires its own electrical connection to a control circuit, which is not the case in, e.g., CCD devices. This rather unfortunate requirement makes it extremely difficult to manufacture large two-dimensional arrays. The biggest issue is the connectivity for pixels near the center of the array.

The connectivity issue may be circumvented by using carefully designed routing schemes for the connecting wires and making use of multilayer metal interconnection, thus allowing metal tracks to cross without causing short circuits.

4.5 Fill-factor

The *fill-factor* is basically the ratio between the actual area sensitive to light and the total array area. Because of the required electrical connections to each pixel and features such as trenches in the architecture, the fill-factor may be even less than 50 %.

The fill-factor may be increased by using a monolithic lenslet module with the APD array. With a lenslet array in front of it (at the focal plane of the telescope) you may get a pupil image on each of the pixels. However, adding a lenslet array may decrease the throughput of light, e.g., because of reflection.

4.6 Junction heating

A rather unfortunate feature of devices such as an APD, which essentially strives for photon counting at a single photon level, is the phenomenon called *junction heating* or *self heating*. This unwanted property arises from the avalanche breakdown process, and causes the diode to heat up. The heat up scales with increasing photon count rate, and can cause significant temperature variations.

Since so many of the APD essential properties are temperature dependent, we are required to implement a stable and accurate temperature control. The often included cooling system with Peltier cooling of the diode is in many cases not enough for accurate high count rate runs with an APD.

4.7 Inconsistent sensitivity

We strive for as high quantum efficiency (QE) as possible for an APD, but at various wavelengths we see rather big variations in detected photons. As mentioned in section 2.4, the wavelength range which is most sensitive to incident photons depends on the material. This means we have to build APDs using different diode materials depending on what we expect or want to find. Using different materials also changes other properties such as after-pulsing, dark counts and QE. We usually only achieve a high sensitivity for a narrow wavelength region while the sensitivity gradually decreases to the sides of the peak wavelength. We may also have inconsistent sensitivity for the actual diode's active area, as seen below.

[1]The structure of a semiconductor device in which the size of the p-n junction is limited by physical removal of unwanted material leaving a small table (mesa) on the chip surface. (Webster's Online Dictionary)

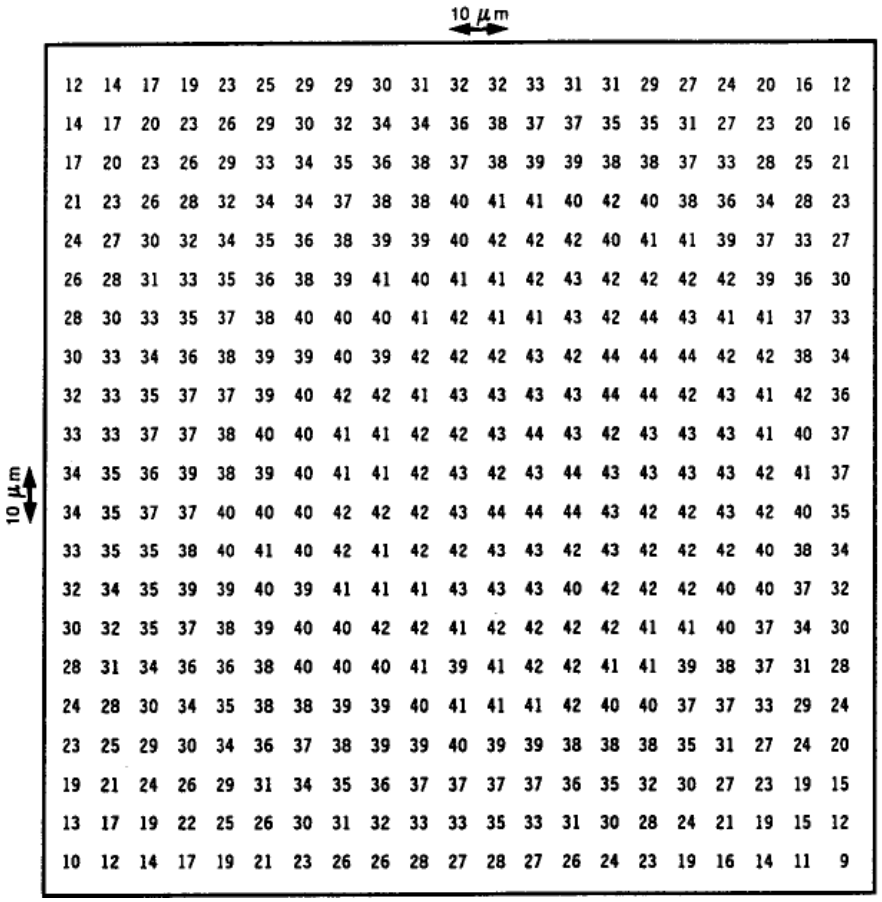

Figure 4.1: Typical Photon Detection Efficiency (%) vs. Position, for PerkinElmer's SPCM-100-PQ. (General Electric Canada Inc., Electro Optics)

5 Projects for high time resolution astrophysics and high speed instrumentation

In this section we present some projects and instrumentation, which in some way or another relate or compete with the high speed instrumentation evaluated in this thesis. The purpose with this chapter is to highlight some pioneering projects for high time resolution astrophysics, some of the current ongoing projects and some competing technology, as well as partly emphasize the fact that the majority of the current projects in the world are CCD-based. This occasionally results in most of the funding going into developments of bigger and bigger CCDs rather than faster, and at the same time other very promising technologies potentially fall short.

Please note that many other projects exist as well but all of them cannot possibly fit in this thesis. We used [14] as a form of template for which projects to include, but we try to include updates on the projects and also present some new or excluded projects.

5.1 The High Speed Photometer on the Hubble Space Telescope

The High Speed Photometer (HSP) on the Hubble Space Telescope (HST) was one of the four original axial instruments on the HST. It was designed to make photometric measurements of astrophysical sources in a variety of filters and passbands from the near ultraviolet to the visible wavelengths at rates up to 10^5 Hz [2]. The HSP was also supposed to measure very low amplitude variability (especially for hotter stars in the UV) as well as linear polarization in the near UV.

The HSPs design was rather unusual for the time since it had no moving parts. The HSP consisted of five detectors, four being image dissector tubes (IDTs) and one a photomultiplier tube. The IDTs were of different types, two of the IDTs had CsTe photocathodes on MgF2 faceplates (sensitive from 120 nm to 300 nm) and the other two had bi-alkali cathodes on suprasil faceplates (sensitive from 160 nm to 700 nm) [2].

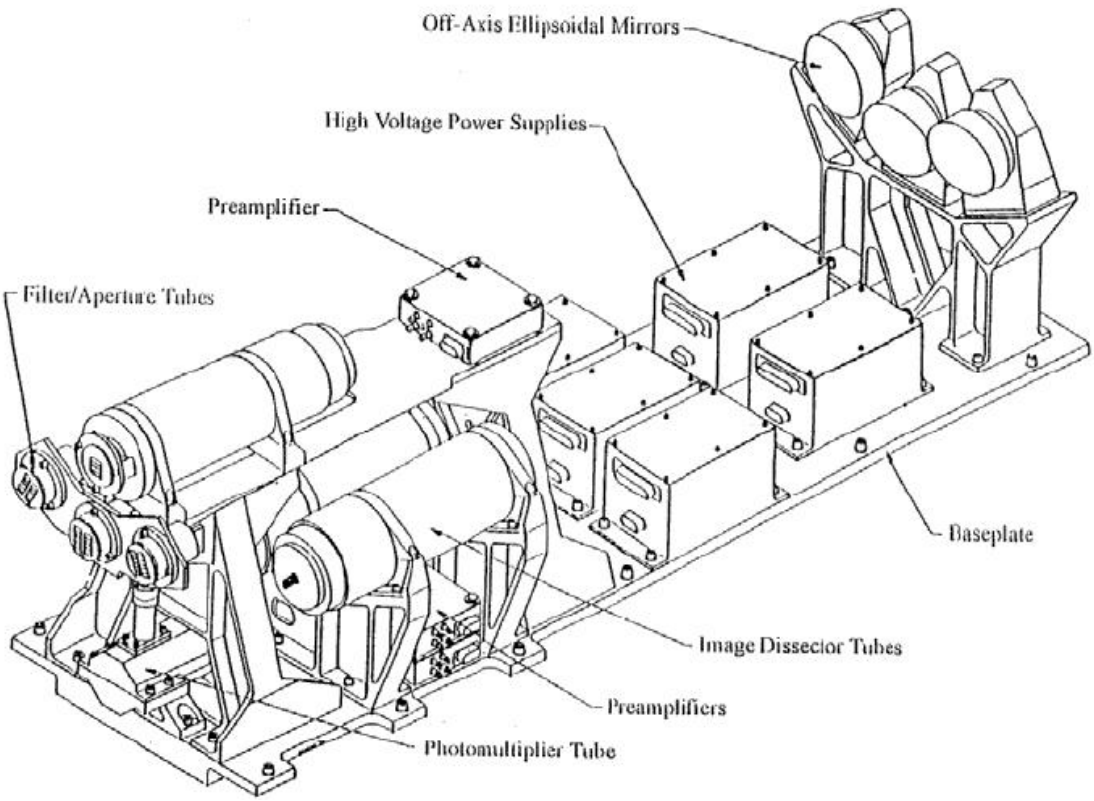

Figure 5.1: The High Speed Photometer's detectors and optics (Bless 1999, [3])

Since the HSP was attached on the HST, a space-based telescope, it had several advantages over similar ground-based instruments [2]:

1. It could properly observe UV wavelength.
2. The apertures could be designed in smaller size, permitting higher spatial resolution and reducing the sky background.
3. Atmospheric absorption or scintillation is not present, leading to higher photometric accuracy and the ability to use very short sample times.

Even though the HSP on the HST looked promising for high speed observations before the launch in 1990, the HST's faultily designed primary mirror (which was discovered after launch), prevented it to do proper observations.

On the first HST service mission in 1993, the HSP was replaced by the Corrective Optics Space Telescope Axial Replacement (COSTAR). The HSP had to be removed to leave room for the COSTAR, which was to correct the primary mirror. A later inspection of the HSP on the ground revealed that the HSP was still in top condition. As a consequence of the removal of the HSP, the possibility to step into a new era of astronomical photometry was lost.

[More information: `http://setas-www.larc.nasa.gov/HUBBLE/HARDWARE/hubble_HSP.html`]

5.2 High-speed Imaging Photometer for Occultation on board SOFIA, the airborne Stratospheric Observatory for Infrared Astronomy

The High-speed Imaging Photometer for Occultation (HIPO) on the Stratospheric Observatory for Infrared Astronomy's (SOFIA's) airborne telescope is a special-purpose science instrument designed to provide simultaneous high-speed time resolved imaging photometry at two optical wavelengths. By co-mounting the HIPO with a side-camera called the First Light Infrared Test Experiment CAMera (FLITECAM), the setup (shown in Figure 5.2) allows for observation of a near infrared wavelength as well as the two optical wavelengths. The HIPO is then used for a variety of time-resolved precise photometry observations, including stellar occultations by solar system objects, transits by extrasolar planets and asteroseismological observations. Since occulation photometry involves time-resolved and precisely time-tagged photometry the HIPO is also capable of high speed CCD imaging, allowing for applications such as the latter two mentioned above.

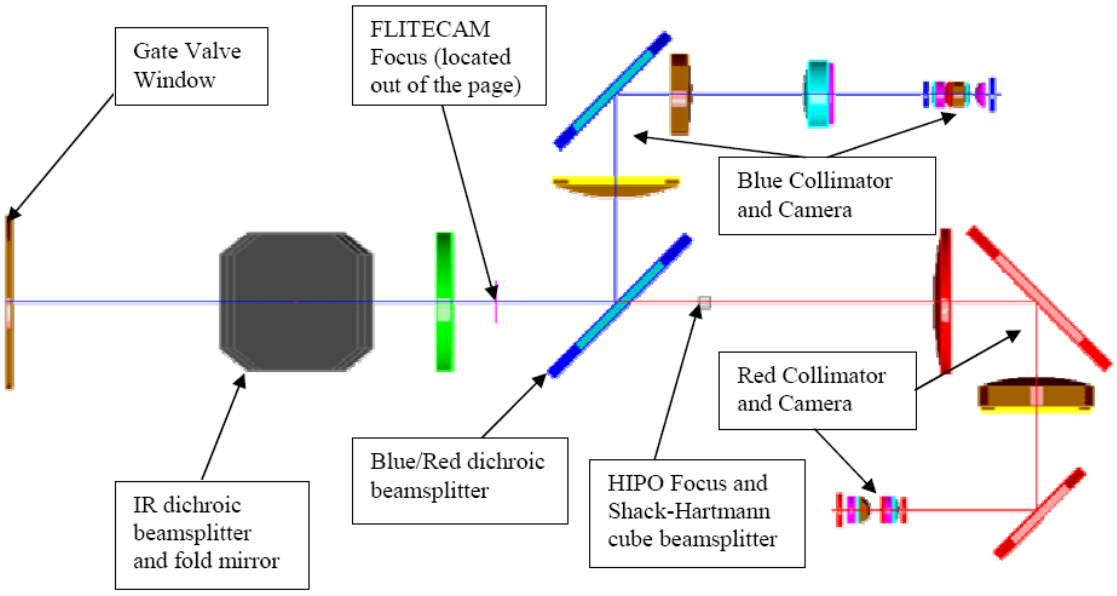

Figure 5.2: A schematic view of the optical layout for HIPO together with the co-mounted side-camera FLITECAM. (Dunham 2003, [4])

Airborne observations are not new. The HIPO is a successor to an earlier attempt of airborne photometry called SNAPSHOT on KAO, the Kuiper Airborne Observatory.

Because of being airborne the HIPO has some advantages over ground-based telescopes aiming for similar observations, e.g.:

1. Low atmospheric scintillation, allowing for the potential to detect P-mode stellar oscillations in stars similar to our sun as well as excellent photometry of stellar transits by extrasolar planets.
2. The telescope is mobile, allowing for flight and observation at good atmospheric conditions.
3. Since the telescope can move between northern and southern hemispheres, observations of sources anywhere in the sky are possible.

5.3 ULTRACAM and ULTRASPEC

Two very active projects at the present time are ULTRACAM and ULTRASPEC, both with pretty much the same research teams behind them and very ambitious goals. Both projects' instrumentation aims for pushing the CCDs detectors to new levels of speed and low read-out noise. These goals render these projects especially interesting for this thesis.

5.3.1 ULTRACAM

CCDs are the dominant detectors on all of the largest ground-based telescopes and thus also the resources of the observatories have understandably been targeted towards increasing the area and sensitivity of their detectors rather than high read-out speeds. As a result, astronomers have encountered difficulties in achieving higher frame rates than $\sim$1 frame per second. This was one of the biggest scientific motivations for the development of a new high speed instrument. Therefore this new instrument was developed after establishing a list of six crucial requirements for the capabilities on a new high-speed photometer. These were [6]:

1. Short exposure times (from milliseconds to seconds).
2. Negligible dead time between exposures.
3. Multi-channels (3 or more) covering a wide wavelength range.
4. Simultaneous measurement of the different wavelength bands.
5. Imaging capability.
6. High efficiency and portability.

The result was ULTRACAM (for ULTRA-fast CAMera) and it achieved them all and that was, and perhaps still is, something unique for similar and comparable instruments.

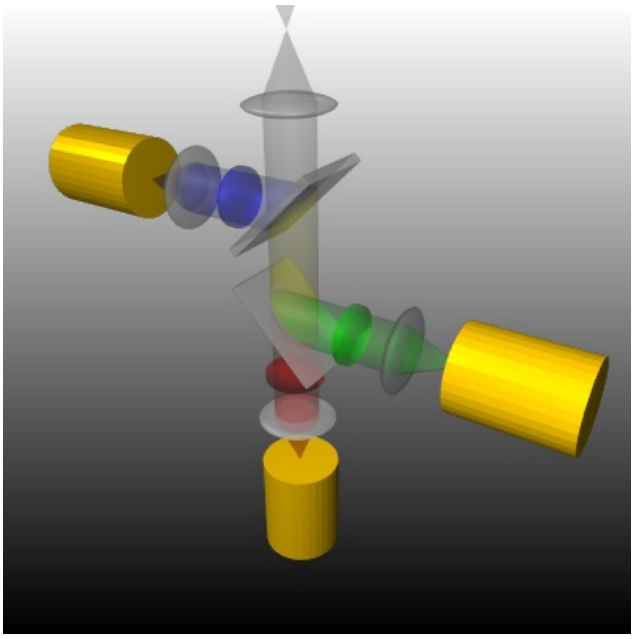

Figure 5.3: Schematic representation of ULTRACAM.

ULTRACAM is a portable, high-speed imaging photometer with a triple-beam CCD camera, which has been designed for studies of faint astronomical objects at high temporal resolution. Since ULTRACAM employs frame-transfer CCD chips (Marconi 47-20) as the detectors, the dead time between exposures is negligible as long as the exposure time is longer than the time it takes to read the data. The triple-beam CCD (i.e. the three frame-transfer CCDs with 1024x1024 pixels) also allows for three-color optical imaging at frame rates up to 500 Hz (2 ms time resolution). This is considered ultra-fast for CCDs and has opened up for some high temporal resolution studies.

However, to achieve the highest frame rates ULTRACAM has to be operated in a certain mode of the ULTRACAM's three readout modes, the *Drift scan mode*. The three readout modes are as follows [7]:

(a) Full frame mode:
This mode provides a slower readout but gives a wider field of view (e.g., 5 arcminutes at 0.3 arcseconds per pixel on the William Herschel Telescope (WHT)). At maximum readout speed a full frame can be read out in about 2 seconds. A faster readout time (of about 1.3 seconds) with reduced dead time can be achieved using a full frame mode in which the CCD is not reset between exposures.

(b) Windowed mode:
ULTRACAM achieves high speeds in windowed readout mode. Frame rates of up to 100 Hz can be achieved. Only the pixels from up to three variable-sized pairs of windows are read out.

(c) Drift scan mode:
In this mode ULTRACAM achieves its fastest speed by repeatedly making an exposure and rapidly shifting the charge into the frame storage area. The resultant stack of windows is continuously shifted down the frame storage area and read out at the bottom, while at the same time new frames are exposed and added at the top. This mode significantly reduces any dead time between exposures, allowing frame rates up to 500 Hz to be realized.

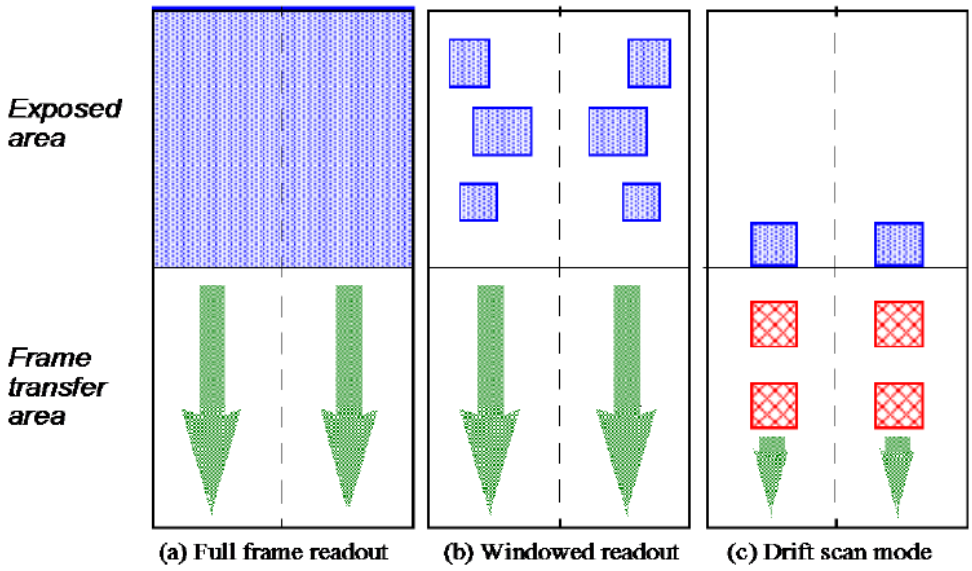

Figure 5.4: ULTRACAM's readout modes.

The ULTRACAM has been employed on ground-based telescopes such as the 4.2 m William Herschel Telescope (WHT) on La Palma in 2002 and the 8.2 m Very Large Telescope (VLT) visitor focus on "Melipal" in Chile in 2006. During the operation of the ULTRACAM mounted on these telescopes the following were observed: white dwarfs, brown dwarfs, pulsars, black-hole/neutron-star X-ray binaries, gamma ray bursts, cataclysmic variables, eclipsing binary stars, extrasolar planets, flare stars, ultra-compact binaries, active galactic nuclei, asteroseismology and occultations by Solar System objects (Titan, Pluto and Kuiper Belt objects).

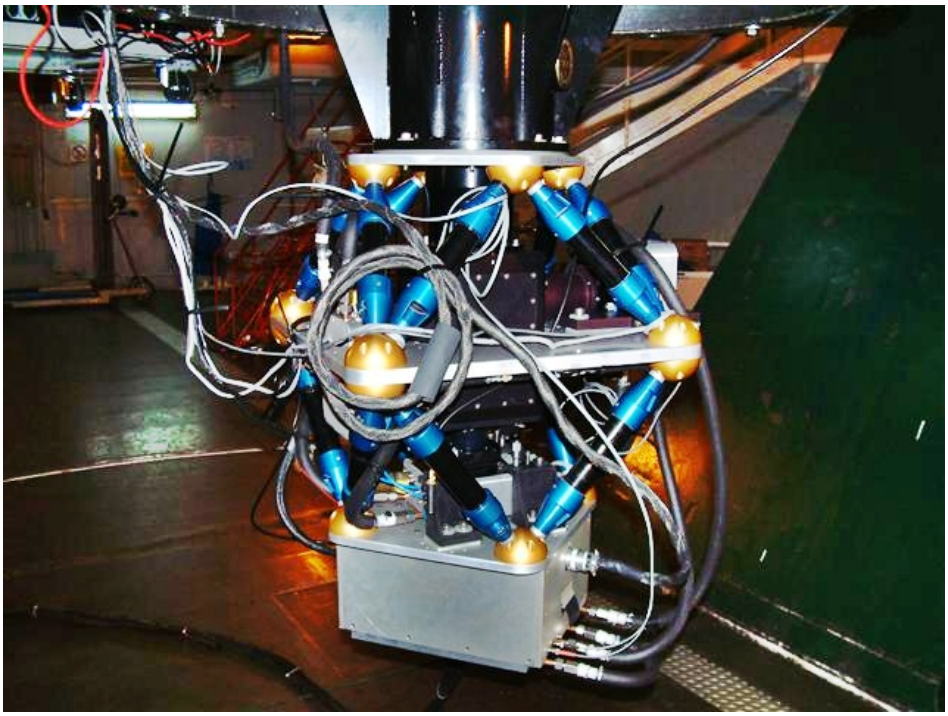

Figure 5.5: ULTRACAM mounted on the 4.2 m William Herschel Telescope (WHT) on La Palma. (Courtesy of Vik Dhillon (Sheffield) and Tom Marsh (Warwick), taken May 2002)

The ULTRACAM project is ambitious and therefore includes a vigorous enhancement program, focused on three important areas for high time resolution astrophysics: increasing the maximum frame rate, reducing the readout noise and minimizing downtime/inefficiency. The ULTRACAM's instrumentation has in 4 years since the first commissions, increased its performance by at least a factor of two in these three areas. In longer term the ULTRACAM team is also exploring the possibility of building ULTRACAM-II, which would be dedicated for use in Chile and which would have four channels, a larger field of view and, if available, use multi-channel, split frame-transfer electron-multiplying CCDs. [6]

[More information: `http://www.vikdhillon.staff.shef.ac.uk/ultracam/`]

5.3.2 ULTRASPEC

"ULTRASPEC is a high-speed, spectroscopic camera based on low-light-level CCDs (L3CCDs) and the data acquisition system of ULTRACAM. The project is a collaboration between the Universities of Sheffield, Warwick and the UK Astronomy Technology Centre, with funding provided by the European Commission under the auspices of OPTICON Joint Research Activity 3: Fast readout, high-performance optical detectors. ULTRASPEC was tested for the first time on-sky in December 2006 on the EFOSC2 spectrograph mounted at the Cassegrain focus of the ESO 3.6-m telescope at La Silla. The first 17-night science run with ULTRASPEC took place in January 2008 on the ESO 3.6-m, and a second 21-night run on the NTT was successfully completed in June 2009."

[Quoted from and more information at: `http://www.vikdhillon.staff.shef.ac.uk/ultraspec/ultraspec.html`]

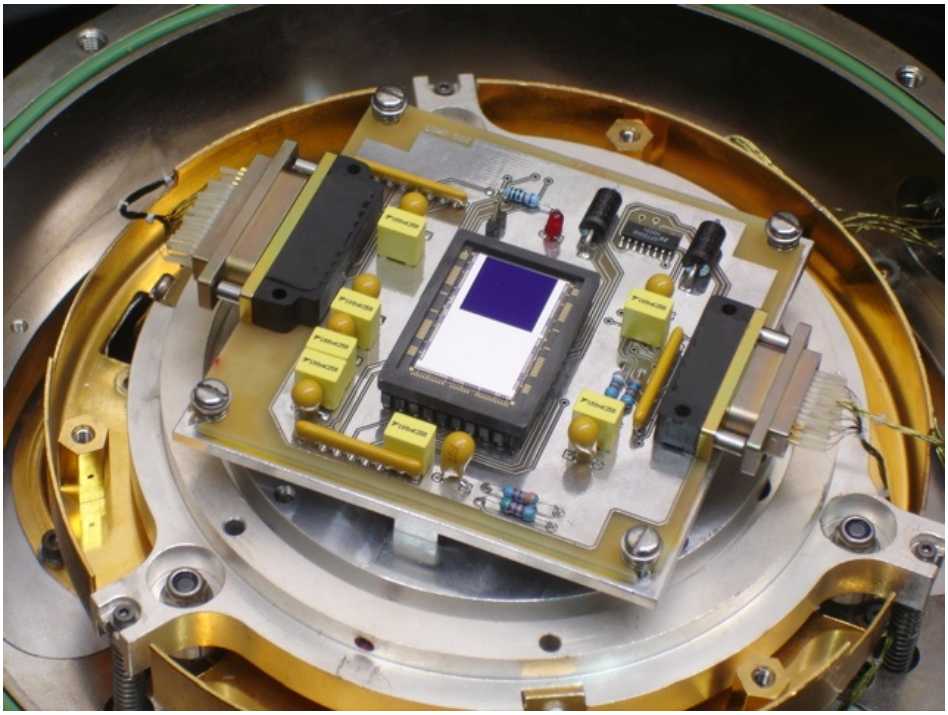

Figure 5.6: Photo of ULTRASPEC from the commissioning run in December 2006. (ULTRASPEC team)

5.4 Superconducting Tunnel Junctions (STJs) and Transition Edge Sensors (TESs)

Some very promising detectors are the Superconducting Tunnel Junctions (STJs) and the Transition Edge Sensors (TESs). These can measure most of an individual photon's attributes with exceptional precision. They can do so throughout the infrared, optical, ultraviolet, X-ray and gamma parts of the electromagnetic

spectrum. For optical astronomy, the cameras using STJ detectors have been developed by ESA/ESTEC, and the TES cameras by Stanford University. Both were developed in the 1990's. New cameras are, however, still being developed as the detectors are far from reaching their full potential because of the need of modern cryogenic technologies, perhaps beyond even present technology.

[Part reference: `https://www.llnl.gov/str/Labov.html`]

5.4.1 Superconducting Tunnel Junctions (STJs)

Superconducting Tunnel Junctions (STJs) utilize the *Josephson effect*. This effect is a phenomenon of current (*Josephson current*) flow across two thin films of a superconducting metal such as niobium, tantalum or hafnium, separated by a very thin insulating barrier. This occurs because of the superconductors acting to preserve their long-range order across the insulating barrier. And with thin enough barrier, the phase of the electron wave-function in a superconductor remains in a fixed relationship with the phase of the wave-function in the other superconductor. This linkage of phase is called *phase coherence* and is the essence of the Josephson effect. This is why the STJs are also known as Josephson junctions. The terms of "Josephson" are named after a British physicist, Brian David Josephson, who predicted the existence of the effect in 1962.

[Part reference: `http://nonlocal.com/hbar/josephsoneffect.html`]

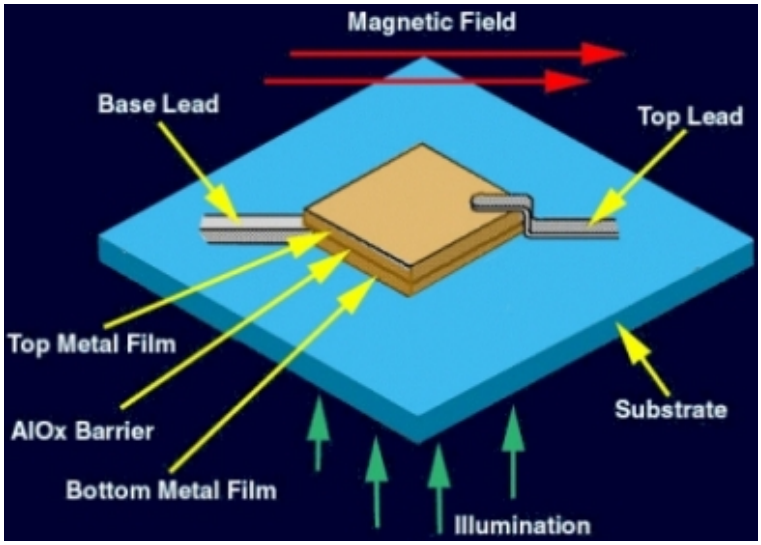

Figure 5.7: "Schematic design of a STJ detector. Illumination of the device can occur either directly from the top or from below through a transparent optical substrate such as sapphire or magnesium fluoride. The latter method is preferred for optical/UV applications since the properties of the lowermost film can be more carefully controlled during manufacture. Back illumination also leaves the top surface free for the wiring required for the manufacture of two dimensional arrays of STJ devices." (ESA)

The STJs operate well below the superconductor's critical temperature (typically below 1 K) and an equilibrium state of the junction is reached. The equilibrium state is easily perturbed by any incoming photons. By applying a small bias voltage cross the junction and a suitable parallel magnetic field to suppress the Josephson current, an electrical charge proportional to the energy of the perturbing photon can be extracted from the device.

Extracting charges reminds one of the CCD detectors and in many ways, STJs seems like a natural next step for astronomical detectors. In semi-conductor CCD detectors, the band gap between the ground state and the excited state reached by absorption of an optical photon is comparable to the photon energy. As a consequence it means that the incoming photon will lose all of its energy, just to release a single electron. Thus only one electron can be extracted from the detector per absorbed photon.

STJs, however, with their superconducting metals such as, e.g., niobium with the equivalent energy gap of some three orders of magnitude lower, allow for thousands of electrons to be released per absorbed optical photon. Even when taking the differing physics of the superconducting detectors compared to the semi-conductor detectors into account and including the release of charge through the breaking of *Cooper pairs*, the amount of charge carriers generated by an absorbed photon is proportional to the energy of the absorbed photon. This allows for determining the wavelength of the incoming photon with certain wavelength resolution.

The STJs abilities do not end with this, they can do more. If a number of STJ devices are arranged into a two dimensional array, a "three dimensional" astronomical detector can be constructed. This allows not just for registering the number of photons in each pixel of the photon but also reveals their distribution in energy throughout the UV, visible and near-IR.

The downside of the STJs is the requirement of very sophisticated cryogenic technologies, as the whole device has to operate stably at below 1 K. Even with current modern technology it is hard to distinguish the relatively feeble charges generated by the STJ detector from the thermal background noise.

[Part reference: `http://sci.esa.int/science-e/www/object/index.cfm?fobjectid=33525`]

The STJs developed by ESA/ESTEC are designated "S-Cam" and has started with S-Cam 1 and officially reached S-Cam 4, but with remote plans for a 5 and a 6 striving for an easier system. For S-Cam 4, the "Distributed Read Out Imaging Detector" (DROID) was introduced, which offered a solution to the serious degradation in performance from the larger dimensioned pixels introduced. DROID's design is based on the original concept by Kraus et al. The main difference is that the photons are not absorbed directly in the STJ but in a superconducting absorber strip.

The S-Cams have been tested on the William Herschel Telescope. There have been discussions of deploying a STJ detector on the Hubble Space Telescope but it has not been realized.

Detector	12x10 Ta/Al STJs
Pixel size	33 x 33 μm^2
Fill factor	76 %
Plate scale	0.8"/pixel
FOV	11" $\times$ 9"
Pass band	330 – 745 nm
Maximum detection efficiency (@ 500 nm)	30 %
$\lambda/\Delta\lambda$ **@** λ **= 500 nm**	8 – 11
Event time resolution	~ 5 μs
Max. event rate/pixel	$>$ 8000 cts/s
Max. overall event rate	$\sim 10^6$ cts/s
Max. observation time	24 h
Operating temperature	285 mK

Table 5.1: Summary of S-Cam 3 specifications as used on the William Herschel Telescope. (ESA)

As seen in Table 5.1, STJ detectors do not typically have anything close to extreme in terms of count rates ($>$ MHz) or time resolutions ($<$ ns) yet. Also as seen, the maximum quantum efficiency is rather low in comparison with, e.g., the APDs evaluated in this thesis (up to 80 %). Although STJs currently have some limitations and challenges to conquer, they are still plausible and good candidates in the future when they have been developed even further, but for now cannot be seen as strong contenders for use in high time resolution astrophysics.

[More on S-Cam and DROIDs can be found on: `http://sci.esa.int/`]

5.4.2 Transition Edge Sensors (TESs)

The Transition Edge Sensors (TESs), or Transition Edge Microcalorimeters as they also are known as, were invented with U.S. Department of Energy's support as part of a physics experiment called the Cryogenic Dark Matter Search, and patented by Stanford in 1997. The TES was designed as a new detector for elementary particles called WIMPs (Weakly Interacting Massive Particles). The motivation for the development of TESs was the proposed ideas of possible explaining the missing mass in the universe with WIMPs. Studies of the rotation of visible galaxies had convinced scientists that 50 % or more of the galaxies' matter must be invisible to telescopes. Transition Edge Sensors can be used to detect the virtually invisible WIMPs, through detecting the heat produced by occasional interactions of the WIMPs with nuclei in crystalline material.

[Part reference: `http://www.xs4all.nl/~carlkop/tes.html`]

Transition Edge Sensors (TESs) are in a way thermometers made from a superconducting film operated near its transition temperature, T_c. There are many different types of superconducting metal films which can be used as a TES. The most essential requirement for a TES is that while in its transition from superconducting to normal metal, a very small change in temperature must correspond to a large change in resistance. The transition widths are typically on the order of milliKelvin (Figure 5.8). To maintain operation in this superconducting-to-normal transition region, the TES is biased at a constant voltage in order to set up a negative electrothermal feedback mechanism. The extremely low temperatures are not only needed for the superconductivity but it also follows that the energy resolution of TESs scales with temperature.

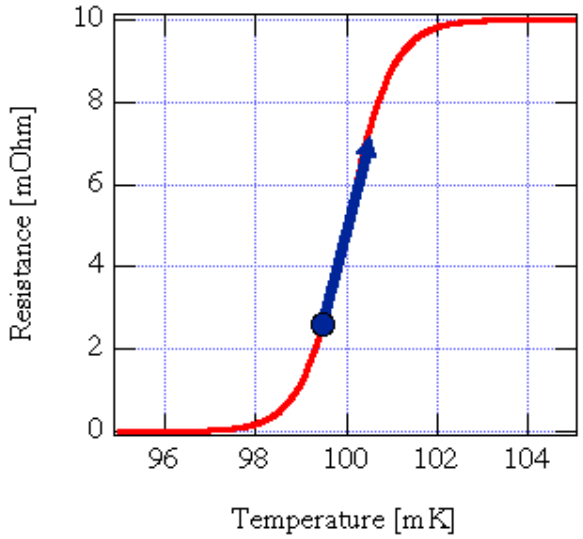

Figure 5.8: Resistance vs. Temperature - example of a transition. (Figueroa Group, MIT)

As a TES absorbs an incoming photon's energy, it is heated, causing it to move up in the transition region. The subsequent increase in resistance at the constant voltage lowers the current passing through the TES. The TES returns very quickly to its equilibrium state but through clever circuit design, including a low noise SQUID amplifier, one can measure the current pulse and reconstruct the energy of the incident photon.

[Part reference and figure: `http://web.mit.edu/figueroagroup/ucal/ucal_tes/`, Figueroa Group, MIT]

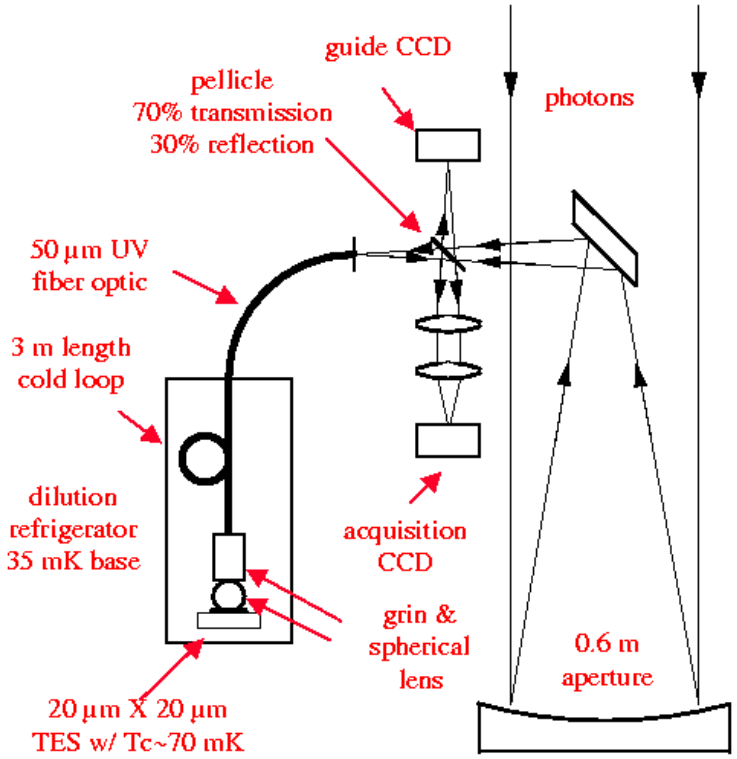

Figure 5.9: Schematic of a TES fiber coupled system at the Stanford Observatory. (Romani et al. [8])

An apparent limitation for the Transition Edge Sensors as a contender for studies in high speed astrophysics is the rather low single-pixel maximum count rate (kHz). Despite the limitation, imaging TES arrays seem promising and are being developed. TES areal spectrophotometry could potentially open up for a whole new class of studies, providing morphology, red-shift, spectral classification and chemical evolution studies at present limits of visibility in the universe [8].

5.4.2.1 Position-Sensitive Transition Edge Sensors (PoSTs) A step further in the development of the Transition Edge Sensors (TESs) is the very interesting Position-Sensitive Transition Edge Sensors (PoSTs). These sensors take over where the approach of using a TES array as a single pixel microcalorimeter runs into some challenges. The primary challenges among them are the area on the chip required to bring out the wiring from the central pixels, the increased heat dissipation on chip due to the large number of biased TESs and the increased number of channels required to read out the TESs. The PoST concept addresses these issues by providing both a position and an energy measurement of the absorbed photon (primarily X-rays). [9]

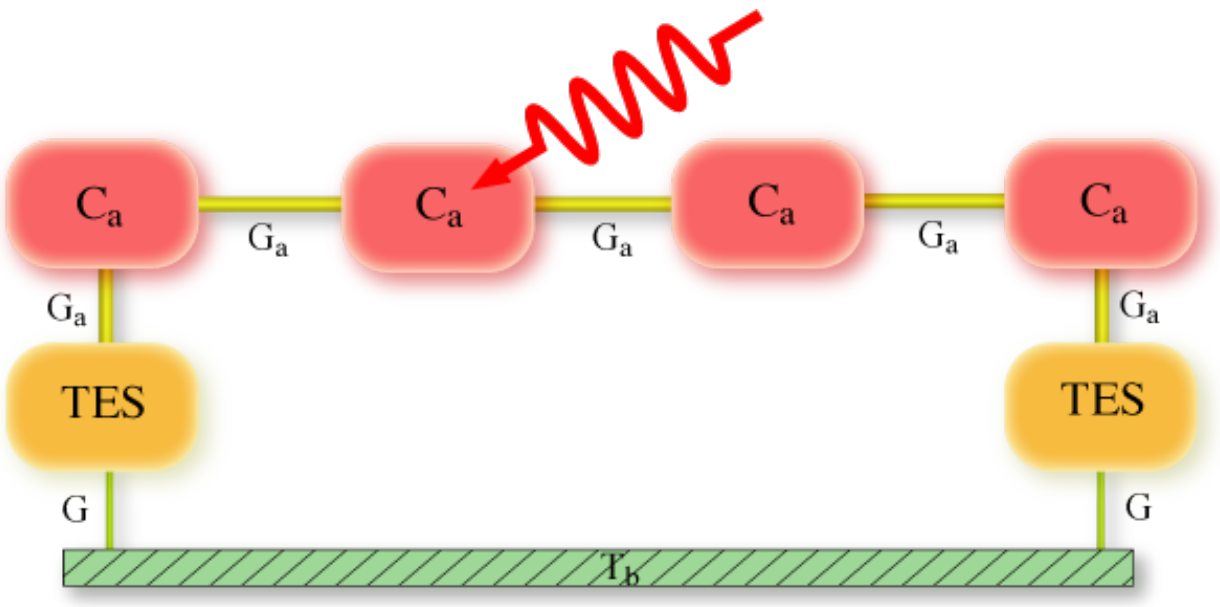

Figure 5.10: Schematic of a PoST thermal model. (Figueroa Group, MIT)

"A Position-Sensitive Transition-Edge Sensor (PoST) is a novel microcalorimeter we are developing for large format imaging spectrometers. The idea is very simple: several absorbers are strung together thermally with a thermal conductance Ga between each. TES thermometers are placed at either end of the absorber chain and connected to a cold bath at temperature Tb through a thermal conductance G. When a photon hits the PoST, heat flows to either end and is readout by the TESs. The position of the photon is inferred from difference in pulse heights between the two TESs. The energy of the X-ray is determined from the sum of the two pulses. A PoST with 10 absorbers and two TESs would provide 5 times more pixels than a single-pixel TES."

[Citation above from `http://web.mit.edu/figueroagroup/ucal/ucal_post/`, Figueroa Group, MIT]

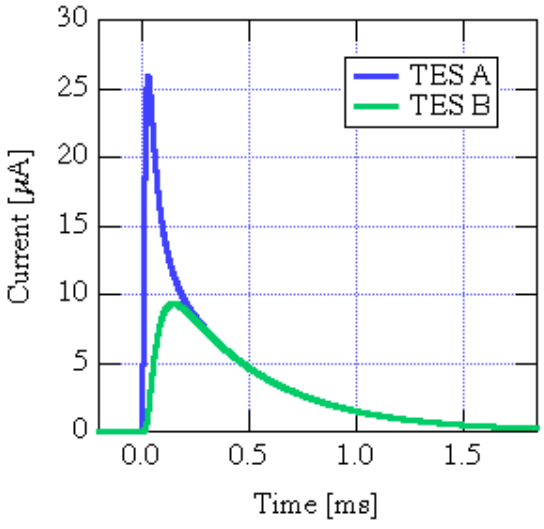

Figure 5.11: Example of two TES pulses. (Figueroa Group, MIT)

5.5 Optical Pulsar TIMing Analyzer (OPTIMA)

OPTIMA (Optical Pulsar TIMing Analyzer) is a high speed optical photo-polarimeter, which has been designed and developed in the group for gamma-ray astronomy of the Max-Planck-Institute for Extraterrestrial Physics in Garching. OPTIMA is a very sensitive, high time resolution (μs) and portable detector designed to observe optical emissions of sources that radiate mainly at X-ray or gamma-ray energies. These sources mainly include pulsars but also other highly variable compact sources.

The detector system of OPTIMA consists of fiber fed Single Photon Avalanche Diodes (SPADs), a GPS timing receiver, a CCD camera for target acquisition and a computerized control unit. Several configurations are available: for photometry a hexagonal bundle with seven channels and one fiber offset for sky background monitoring; for polarimetry a rotating polarization filter in front of the photometer or a newly developed 4-channel double Wollaston system; and for coarse spectroscopy a 4-color prism spectrograph. [10]

Most previous detector systems with the possibility of rather similar applications as OPTIMA, e.g., multi-anode micro-channel arrays (MAMAs) on the TRIFFID camera, arrays of solid-state detectors (e.g., Josephson junctions such as S-Cam 3 described in section 5.4.1) or photomultiplier tubes, have been characterized by either low quantum efficiency, technically challenging operations or narrow wavelength range of sensitivity. They can however offer imaging of a larger field with fine resolution: event selection can be adapted to the viewing and sky background conditions and reference stars are often present in the same exposure. If fine tuned and further developed, these detectors can become advanced fast 2-D photon counting/timing cameras with high sensitivity which may dominate in the future. While waiting for this, the team at the Max-Planck-Institute for Extraterrestrial Physics in Garching decided to first develop a simple photon counting system (OPTIMA) that relies on fixed apertures and is equipped with detectors (SPADs) of high quantum efficiency.

OPTIMA uses fiber fed APDs of type SPCM-AQR-15-FC produced by PerkinElmer. OPTIMA's use of avalanche photodiodes (APDs) allows for not only high quantum efficiency (up to 80 %) but also a wide band of sensitivity ranging from 250 to 1100 nm (in practical use, 320 to 1100 nm due to the Earth's atmosphere) and photon counting rates of several MHz. OPTIMA's data acquisition system was in the earlier stages not able to cope with such rates but has been updated in order to do so. The use of APDs also makes it extra interesting, with this thesis in mind, as the same type of detectors are evaluated in the experiment section.

Since the first development of OPTIMA in 1998, OPTIMA's design has changed and got an additional but optional feature, called OPTIMA-Burst. A schematic layout can be seen before and after 2006 in Figure 5.12 and 5.13, without and with the "-Burst". The alternative OPTIMA-Burst construction allows for polarization measurements of the optical counterparts of Gamma Ray Bursts (GRBs). During the years OPTIMA has also been commissioned at several telescopes, e.g., a 1.3 m telescope (Mt. Skinakas, Crete), a 3.5 m telescope (Calar Alto, Spain), the 2.1 m Guillermo Haro telescope (Cananea, Mexico), the 2.5 m NOT (Nordic Optical Telescope on La Palma), a 74 inch telescope (Mt. Stromlo) and the 2.2 m telescope at the ESO/La Silla observatory.

Rather recently, OPTIMA was operated at the Skinakas observatory (`http://skinakas.physics.uoc.gr/`), where my tutor (Dainis Dravins) also attended in the June/July campaign (2009). On this campaign the object was to observe high time resolution photometry and polarimetry of GRBs immediately after detection with the Swift satellite. Information about the campaigns as well as news and highlights can be found at `http://www.mpe.mpg.de/OPTIMA/results.html`. The latest campaign involving OPTIMA, as of today, was at the end of 2009 at the Nordic Optical Telescope (NOT) on La Palma.

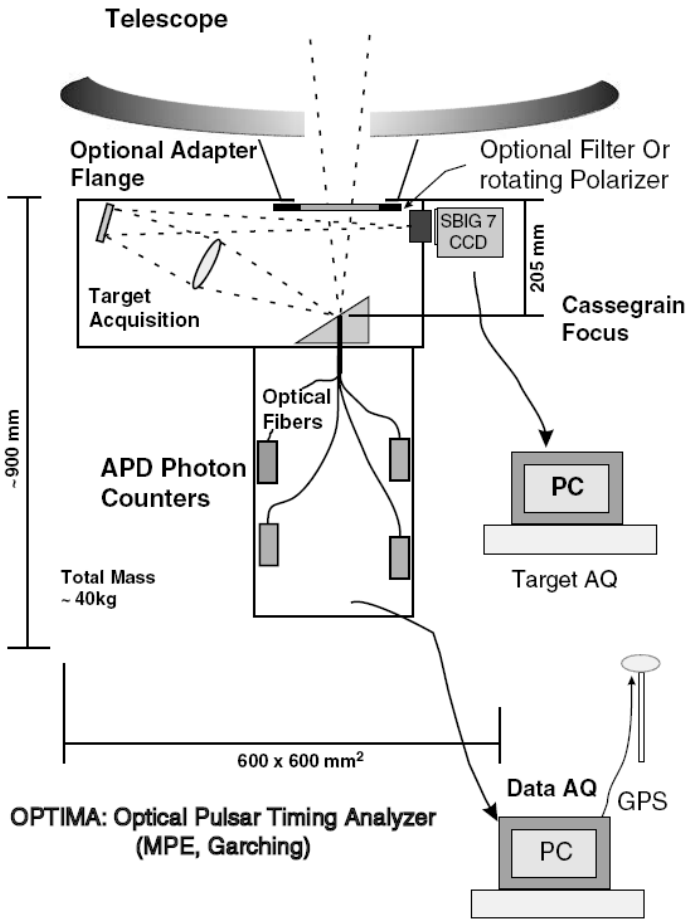

Figure 5.12: Schematic layout of OPTIMA (pre-2006). (G. Kanbach et al. [10])

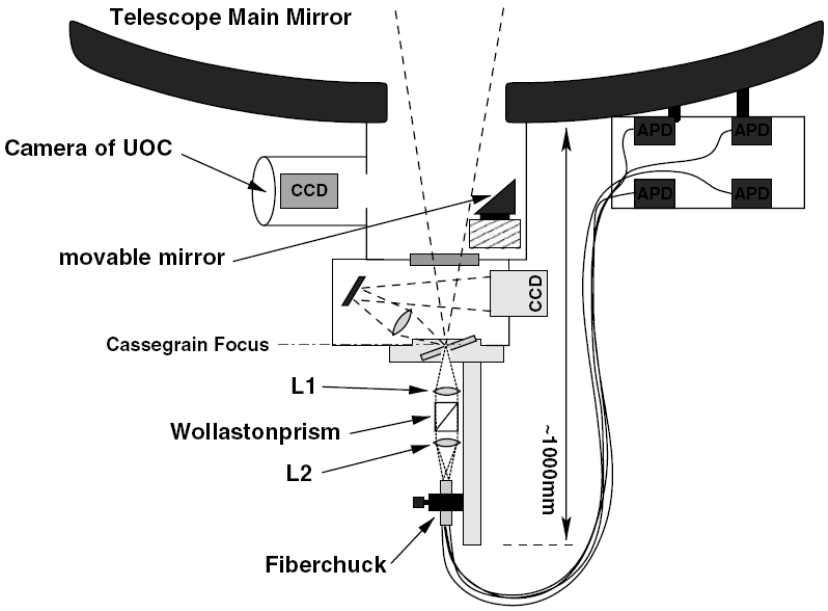

Figure 5.13: Schematic layout of OPTIMA-Burst (post-2006). (G. Kanbach et al. [10])

5.6 Multichannel Analysis of Nanosecond Intensity Alternations (MANIA)

The Multichannel Analysis of Nanosecond Intensity Alternations (MANIA) project was started at the Special Astrophysical Observatory (SAO) in the Northern Caucasus in 1972, initially led by the late Viktorij Shvartsman but more recently led by Gregory Beskin.

MANIA is hardware-and-software-system designed to search for and study optical emission variations of astrophysical objects on time scales from 0.1 μs to 100 s, i.e. superfast photometry (as of 1996). MANIA was more specifically designed to investigate nonstationary processes on flare stars, pulsars, X-ray binaries, etc. The MANIA system utilizes a special time-to-code converter "Quantochron", which allows the system to encode the arrival times of photons registered by a photon detector with a time resolution up to 20 ns in 216 channels (space, colors, polarization, etc.) simultaneously. The dead time is specified as 100 ns and the limiting intensity of flux (i.e. maximum count rate) is 370 kHz or 750 kHz in monochannel mode. [11]

The MANIA project is to be considered a pioneer in the field of High Time Resolution Astrophysics (HTRA). In the early 1990's the team at SAO had pointed out some potentials of quantum optics in polarization measurements. MANIA has been used with both success and "failure". The latter mostly because of technical limitations such as; low maximum photon count rates ($\sim$ 8 kHz using V-filter) and slow data handling rates, at the time.

The official MANIA web page (`http://w0.sao.ru/hq/ra/manija.html`) does not seem to have been updated since 2003 and it is not easy to find any information of the current status of the project. The project has however already in 1996 [11] set future goals such as:

1. A new two-head (6-channel) photometer for simultaneous observations of an object and comparison star will be built.

2. The testing and fitting of the 2D-photometer based on the microchannel detector will be finished. Some test observations have already been carried out.

3. The new "Quantochron 3-24" with a 24-bit storage register for holding coordinate information is being developed.

Today these future plans may be considered close to obsolete due to the development of photon detectors, and computer hardware and software already made.

5.7 Fast Variability Optical Registration (FAVOR)

At the Special Astrophysical Observatory (SAO) in the Northern Caucasus, we also find the Fast Variability Optical Registration (FAVOR) complex which is intended to detect flashes and, more general, variability of any objects in the field. If there, e.g., is a particularly interesting object in the near-Earth space the FAVOR complex can be adjusted to refine orbital elements of satellites and obtain useful information concerning, e.g., meteors. The most important goal, however, is to study Optical Transients (OTs) accompanying Gamma Ray Bursts (GRBs) in a wide field and follow them up with high time resolution investigations.

Even though the full duration of a GRBs covers a 0.01 – 100 s range, the light curves of long ones show substructure in 80 % of the cases, and for 66 % the timescales of rapid variability are shorter than 0.1 of their duration. Millisecond features are also seen in light curves of some long duration GRBs. There are also simulated models which predict the generation of considerable optical flux simultaneously with the GRB, reaching 8 – 12 magnitude. The ratio between optical and gamma-ray photons exceeds a factor of 100 – 1000. This has been confirmed by a unique quasi-synchronous detection of a GRB optical transient. The study of GRBs in high time resolution is therefore important in order to bring decisive information on the nature of this phenomenon. [12]

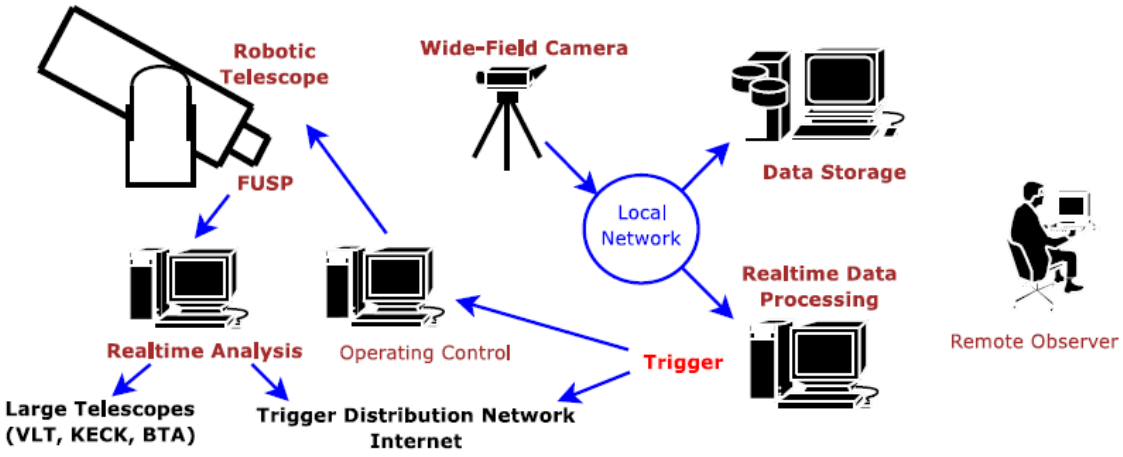

Figure 5.14: Schematics of the FAVOR complex. ([12])

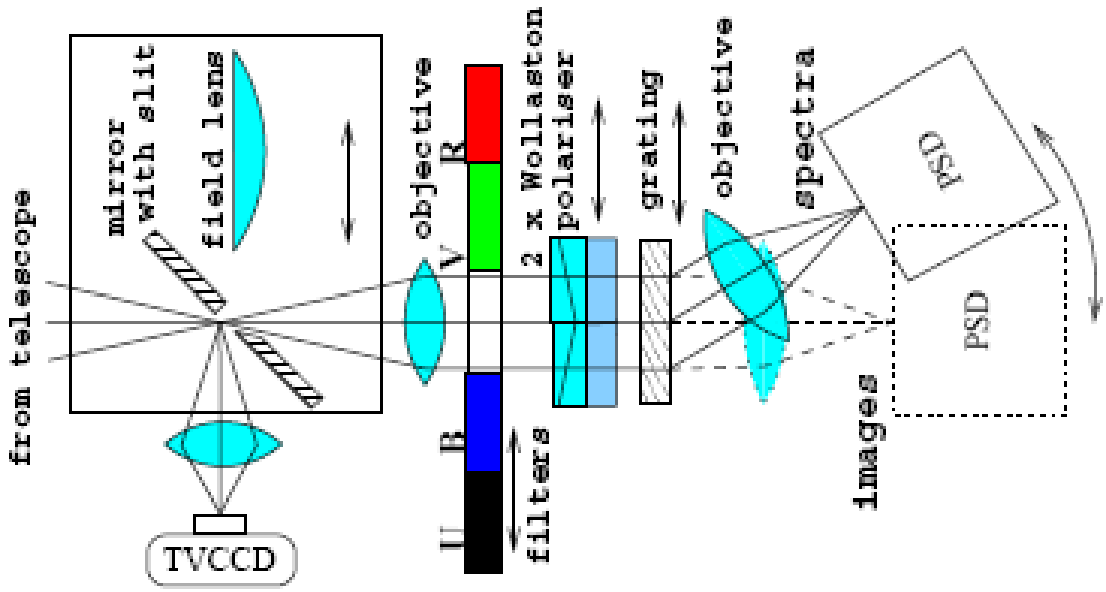

Figure 5.15: Schematics of the Fast Universal Spectro-Polarimeter (FUSP). ([12])

The FAVOR complex consists of a Wide-Field Camera, a real-time data processing computer complex and a robotic telescope equipped with a Fast Universal Spectro-Polarimeter (FUSP). The FUSP consists of an input unit, which allows the choice of three observing modes (photopolarimetry, slitless and slit spectropolarimetry), collimating optics, a polarization unit (a double Wollaston prism), a set of filters, a dispersion element (prism), a position-sensitive detector with time resolution of 1 microsecond, and an acquisition system of type "QUANTOCHRON 4-96". The FUSP is also equipped with a TV-CCD as a guide to control the observations.

Utilizing a new generation of position-sensitive detectors, the FAVOR complex with its FUSP system will be able to achieve a quantum efficiency of 20 – 35 % in the 360 – 850 nm spectrum range while providing a large number of pixels (10^6) and event rates up to 10^5 counts per second (100 kHz). This will allow the FAVOR complex to detect and study Optical Transients (OTs) accompanying Gamma Ray Bursts (GRBs) as faint as 14 magnitudes in high time resolution in just 1 – 60 s after their detection. [12]

5.8 Optical Searches for Extraterrestrial Intelligence (Optical SETI)

Throughout history, humans have speculated about possibilities of other worlds and life elsewhere in the universe. The understanding of how, or the tools to search for such things did however not exist. In 1959, $\sim$ 40 years ago, a famous paper by Cocconi and Morrison in Nature (184, 844, 1959) suggested the possibility of interstellar communication via microwaves (i.e. high frequency radio waves) in the region of GHz. At the time there were no lasers manufactured. Lasers were constructed in 1960 and shortly after, in 1961, suggestions of a laser SETI: "Interstellar Interplanetary Communication by Optical Masers" (Nature, 190, 205, 1961) were presented. A few years later, in 1964, the Nobel Prize was awarded to the laser inventors Schalow and Townes.

The understanding of lasers at the time was very limited and radio searches therefore still dominated as it had been developing for decades and was relatively mature. As laser technology matured, the SETI community started to listen to the pioneers who suggested Optical Searches for Extraterrestrial Intelligence (Optical SETI), and numerous developments and searches have been made since.

[Reference: `http://seti.harvard.edu/OSETI/origins.htm`]

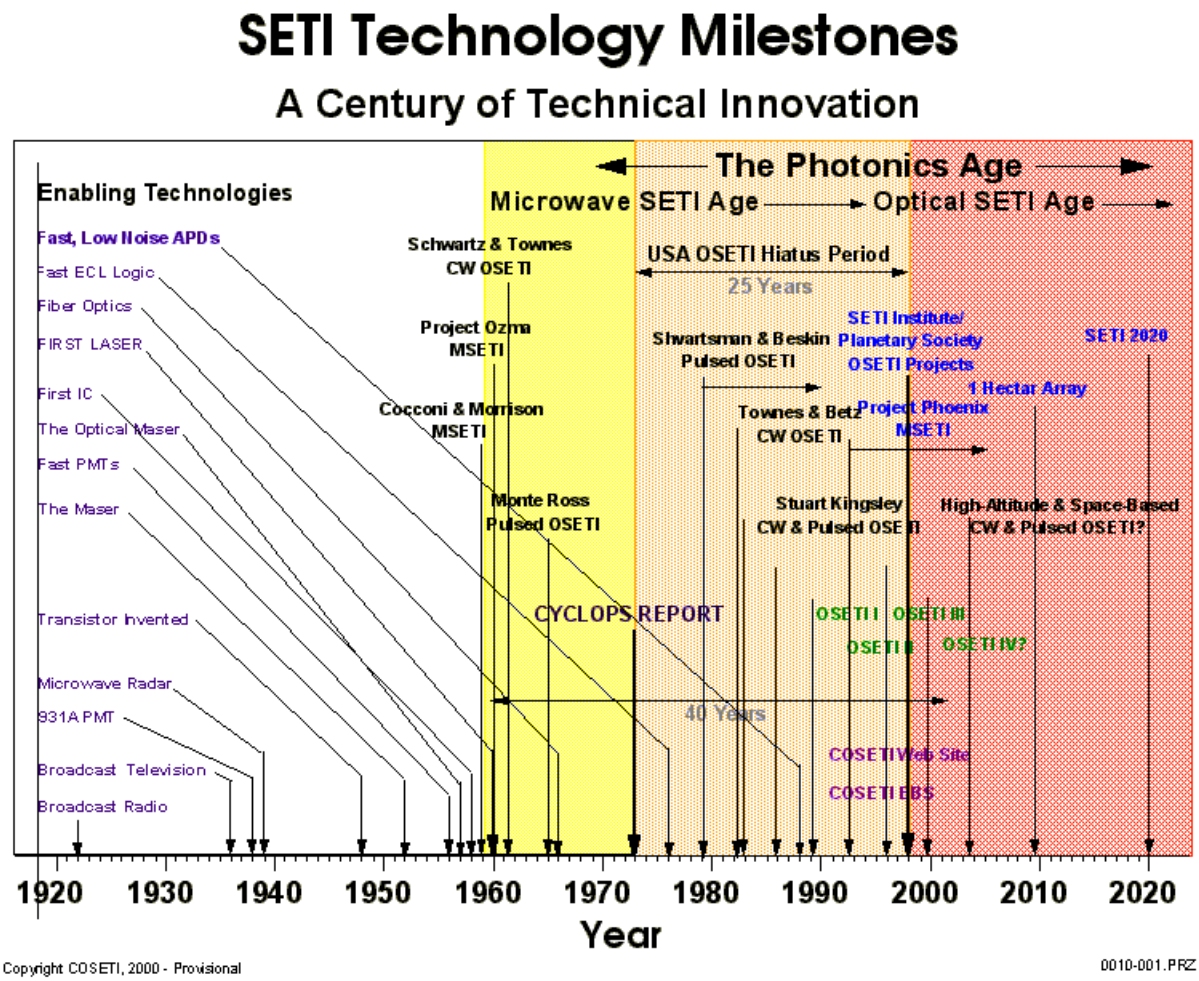

Figure 5.16: Milestones in SETI technology. We see the pioneering OSETI work of Shvartsman & Beskin, using the MANIA-project (section 5.6). (`http://www.coseti.org/mileston.htm`)

Today, there are several Optical SETI programs, e.g., at Harvard (`http://seti.harvard.edu/OSETI/`), Princeton (`http://www.princeton.edu/~willman/observatory/oseti/`), Lick Observatory (`http://seti.ucolick.org/`

optical/oseti_home.htm), Berkeley (http://seti.ssl.berkeley.edu/opticalseti/) and Columbus (http://www.coseti.org/).

With recent technology it has been illustrated that the new picosecond pulse lasers with power exceeding petawatts (10^{15} W) permits to generate a directed laser pulse that outshines the visible light of the Sun by some four orders of magnitude during its short pulse, and within its narrow spectral line; optical interstellar communication is thus technically plausible. Unlike Radio SETI, which permits tuning in to stray signals, Optical SETI requires deliberate high precision targeting of the signals both when sent and received. It also requires sensitive and high resolution instruments, such as high speed photometers or photomultipliers. This makes the Optical SETI projects rather challenging and successful true findings very uncommon (perhaps arguably, but zero confirmed extraterrestrial communications at this time). It is, understandably, very difficult to confirm the source of a detected event.

The Optical SETI project at Berkeley uses a system of beam splitters to feed light to three ultra high speed photomultiplier tubes (PMTs), each followed by a high speed amplifier, a fast discriminator and coincidence detectors. Three detectors are used to reduce or eliminate the risk of "false alarms", which can be caused by, e.g., radioactive decay and scintillation in the PMT glass, cosmic rays and ion feedback. The same or a very similar setup as Berkeley utilizes with their 30 inch automated telescope at Leuschner Observatory seems to be used at the Lick Observatory (see Figure 5.17).

Harvard and Princeton are cooperating with their projects and seem to use two hybrid avalanche photodiodes (Hamamatsu R7110U-07), followed by a pair of multilevel discriminators with levels corresponding to roughly 3, 6, 12 and 24 photoelectrons. By time stamping level crossings, it is possible to approximate the waveforms of incoming pulses with a resolution of 0.6 ns. The time stamping is done by using a GPS clock ($\sim 0.1\ \mu s$ precision and accuracy) together with a computer's internal clock ($\sim$ 1 ms precision, $\sim$ 50 ms accuracy). The two detectors have to detect coincident events for it to count as a plausible Optical SETI event.

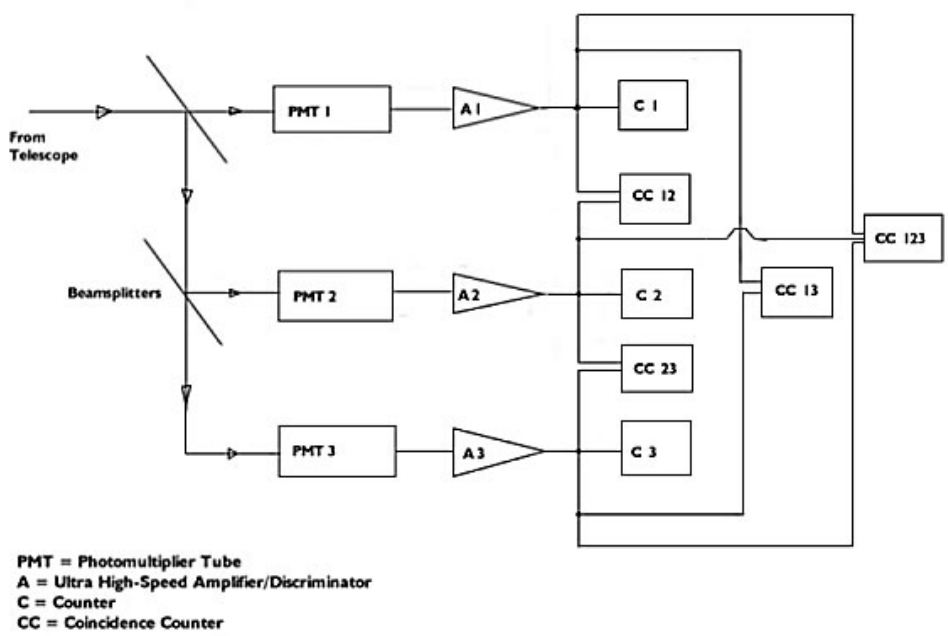

Figure 5.17: Logic diagram of the three detectors. (Berkeley and Lick Observatory)

Figure 5.18: Harvard's Optical SETI system. (Harvard)

The experience gained from developing and using the high speed photon detectors needed to detect the optical photons, as well as the high speed and power lasers, is very valuable towards the pioneering field of High Time Resolution Astrophysics (HTRA).

5.9 Lunar- and Satellite Laser Ranging

After Einstein's revolutionizing new geometric approach on how gravity works with his theory, known as "General relativity" or "General theory of relativity" and published in 1916, some tests followed to confirm the theory. One main goal of the tests was, of course, to test if Einstein's model is a better description of gravity than Newton's thoroughly tested and very successful model. To test if this is true, ultra-precise measurements of distance to, e.g., near-Earth-objects such as the Moon and satellites were and still are carried out by using a technique called laser ranging.

Today, there are several projects in the field of laser ranging, one of the most ambitious being the Apache Point Observatory Lunar Laser-ranging Operation (APOLLO). Laser ranging was, however, perhaps first and foremost truly enabled after the Lunar missions in 1969, when retroreflectors were left on the Moon by the Apollo astronauts, but also by the unmanned Soviet rover (Lunokhod) carrying a French-built reflector, and also Earth-orbiting satellites serve an important role for experiments. Retroreflectors, also called corner-cube prisms, are optical devices that return any incident light back in the exact direction from which it came.

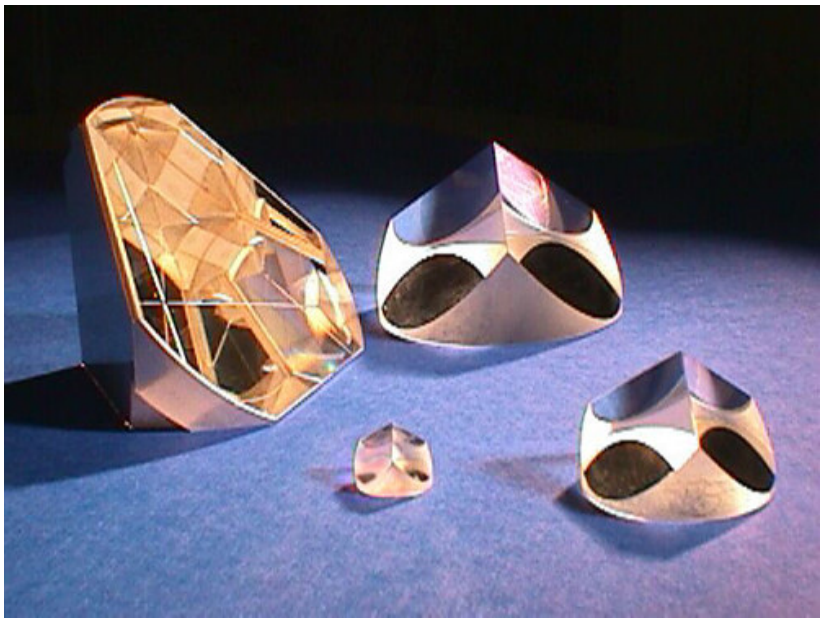

Figure 5.19: Retroreflectors (corner-cube prisms). (APOLLO)

Laser ranging works by sending ultra-short pulses of light towards a target, preferably with a well-defined reflector surface. To do this, lasers with the ability to generate intense bursts of light only ~ 100 picoseconds long are used. Assuming the laser is targeted towards an area of the Moon containing a retroreflector array; an extremely small fraction of the original ~ 300 quadrillion photons are actually returned and collected in the sender's or an adjacent telescope (approximately 1 in 30 million at reflection and another 1 in 30 million at collection, often resulting in mere 1-5 photons per pulse). The total travel-time ranges from anywhere between 2.34 and 2.71 seconds depending on how far away the Moon is (ranges from ~ 351000 to 406000 km).

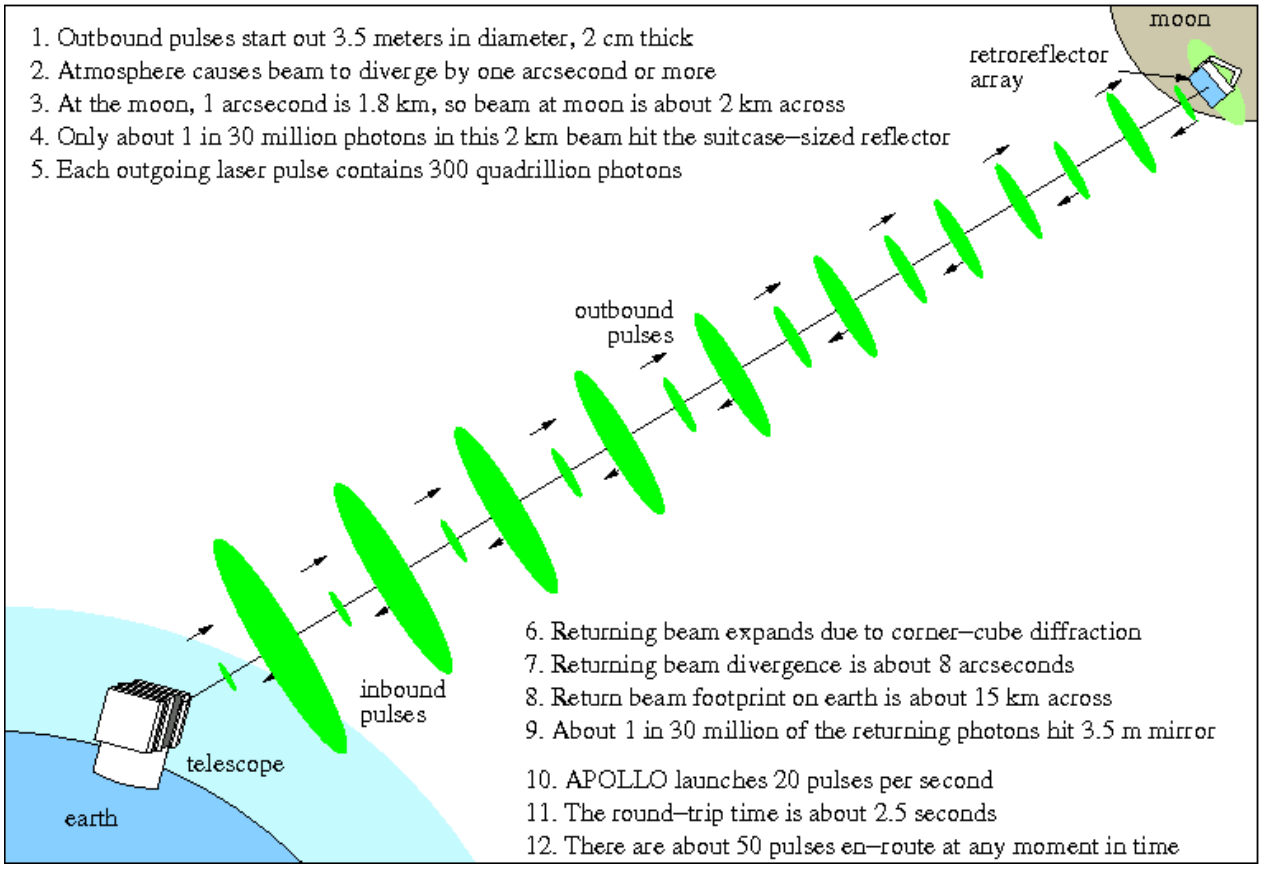

Figure 5.20: Schematics of the procedure for lunar laser ranging. (APOLLO)

The actual receiving part of the procedure, i.e. detection of the returning photons, is done by utilizing various front-line detectors, such as avalanche photodiodes (APDs). These detectors do not, however, quite have to be of similar requirements and sensitivity as the detectors evaluated in this thesis. For example, the usually highly unwanted properties such as dark counts may be overlooked and can be accepted since the returning pulses are measured only during very short time intervals, i.e. when the return is expected, i.e. operating in a gated-mode. Do not misinterpret this as the projects having low standards though.

In the APOLLO project, an 4×4 APD array fabricated by Lincoln Labs is used. Each of the 16 elements has a 30 μm active area diameter on 100 μm centers, which are arranged in a square array (see Figure 5.22). The reason why the APOLLO project uses multiple APD detectors is because an APD array enables simultaneous measurements of multiple photons returning from the Moon. By arranging the elements with space between, optical crosstalk (i.e. an avalanche in one element causing an avalanche in an adjacent element) can be eliminated. The arrangement also allows for preservation of spatial information in the imaging array permitting real-time guiding on the signal. If, e.g., the telescope begins to drift, it is possible to immediately see the returning photon flux drift off to one side, which can then be corrected without directional ambiguity (which would be the case without the spatial information preserved).

The APOLLO detector spends most of its time biased below breakdown voltage, because of the gated-mode operation. Typically the detector is only biased above breakdown voltage for a mere 180 ns window around the time when returning photons are expected.

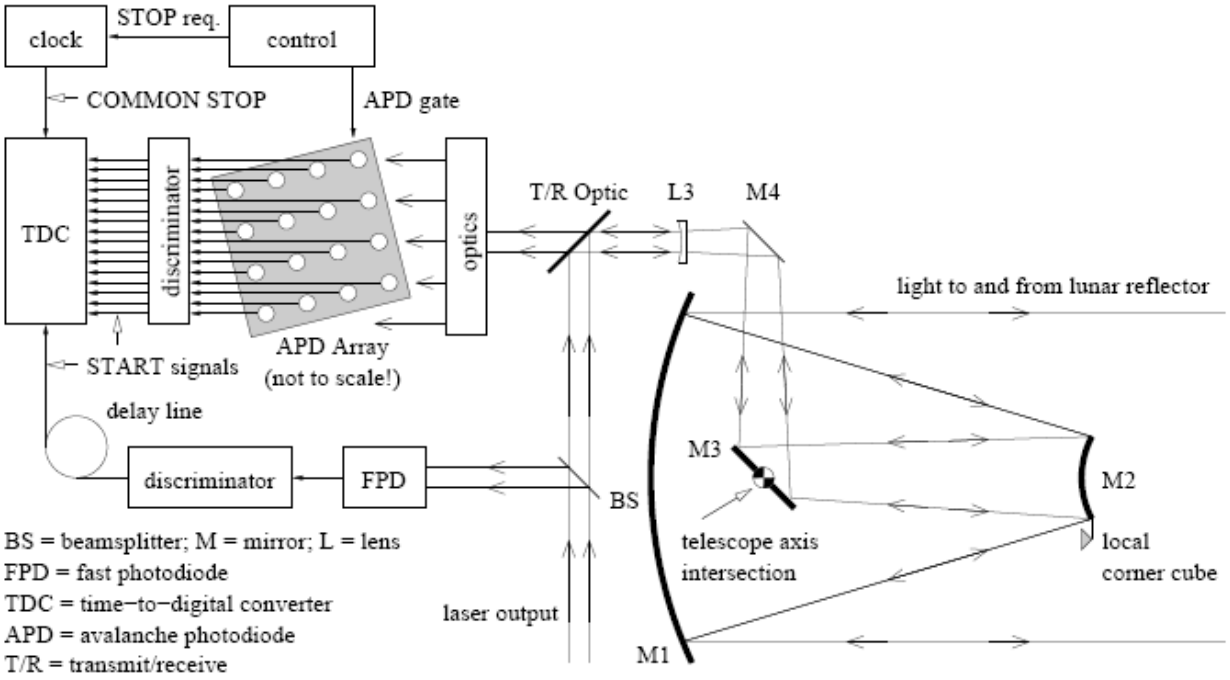

Figure 5.21: Overview of APOLLOs chief components of the system. (APOLLO [13])

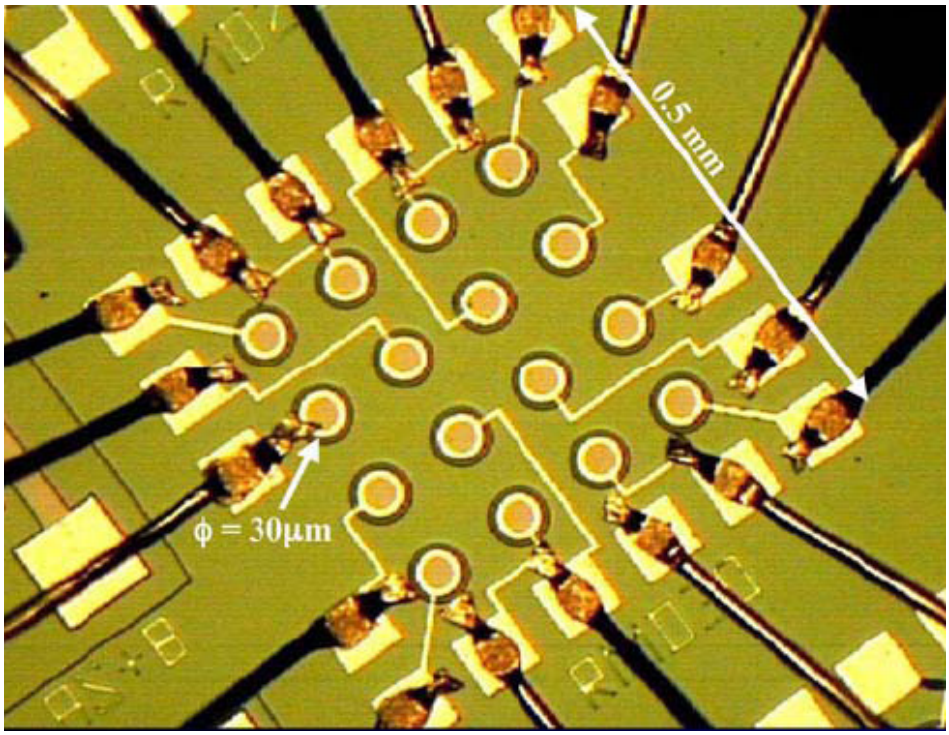

Figure 5.22: APOLLOs 4×4 APD detector array. ([14])

[Part reference and figures: `http://www.physics.ucsd.edu/~tmurphy/apollo/apollo.html`]

While the APOLLO project is ground-base-operated, which can track satellites' height and position; there are also measurements, which require very high precision, involving the tracked satellites. Therefore Satellite Laser Ranging (SLR) is said to contribute to and support several fields of Earth science, e.g., atmosphere-hydrosphere-cryosphere-solid Earth system; direct sensing of surface elevations; sea and ice level monitoring; long-term dynamics of the solid Earth, oceans and atmosphere; tectonic motion; and fundamental physics.

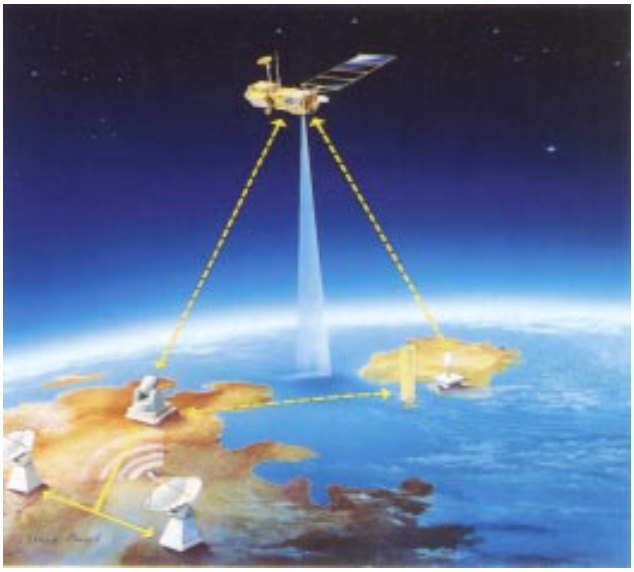

Figure 5.23: A sketch of how a satellite uses satellite laser ranging to calibrate height and position, and then perform its measurements used for topography. (IRLS brochure)

NASA's International Laser Ranging Service (ILRS) writes the following about the next generation of satellite laser ranging in their brochure:
"NASA's next generation SLR station, currently under development, is fully automated, unmanned, inherently eyesafe, and will operate 24 hours a day to the full suite of artificial satellites. The SLR2000 design is expected to greatly reduce station construction, operating and engineering maintenance costs. The low energy, high repetition rate, photon counting approach represents a quantum technological leap over prior low repetition rate, high signal-to-noise ratio designs."

[Reference: `http://ilrs.gsfc.nasa.gov/`]

5.10 Quantum Optical-Spectrometer (QVANTOS)

A project that very recently and still is establishing a stable foundation for the future in the field of High Time Resolution Astrophysics (HTRA) including quantum astronomy is the Lund Observatory's international project "QuantEYE" involving the instrument Quantum Optical-Spectrometer (QVANTOS) and other instrument concepts for Extremely/Overwhelmingly Large Telescopes.

QVANTOS is an instrument developed for the study of extremely rapid astrophysical phenomena (nanosecond time resolution or below). The nanosecond time resolution and other specifications were chosen to ultimately enable also the detection of quantum-optical effects. What really sets QVANTOS apart from other similar instruments is the use of very fast real-time hardware-correlators capable of handling large volumes of data in real time. This means that the data are placed in time bins depending on fluctuations in the signal rather than every single photon's data being saved into a rapidly growing data file. Single photon counting with array detectors can otherwise lead to data rates that exceed terabytes per second, and of course it is unlikely for anyone to be able analyze wholly. Examples of two projects, which generate petabytes of data, are the Large Synoptic Survey Telescope (LSST, `http://www.lsst.org/lsst`) and the Low Frequency ARray (LOFAR, `http://www.lofar.org/`).

What do you do with a night's observation data if its digital file size is reaching terabytes or even petabytes? It is actually not an easy question to answer but one option is to basically save all the data and analyze it for a long time period afterwards. Another option is to analyze the incoming data in real-time, using real-time hardware-correlators and only save the histogram and correlation data. This would however assume that you are, at the time, not interested in time-stamping every single photon.

The QVANTOS instrument is developed in stages, currently Mark I and Mark II. QVANTOS Mark I has been finalized and tested with a telescope on La Palma, with the goal of studying stellar scintillation. The Mark I version utilized photomultiplier tubes (see Figure 5.24), while the newer version (under development) utilizes Single Photon Avalanche Diodes (SPADs). The use of several detectors enable noise reduction because of the use of cross-correlation. While the Mark II version is not completely finalized yet, the electronics have been used for observations at the Skinakas Observatory on Crete together with SPAD detectors in the OPTIMA instrument from MPE Garching (see section 5.5). Laboratory studies have also been carried out in order to better understand how Avalanche Photodiodes (APDs) can be used for accurate photometry. This thesis is in many ways intended just for that.

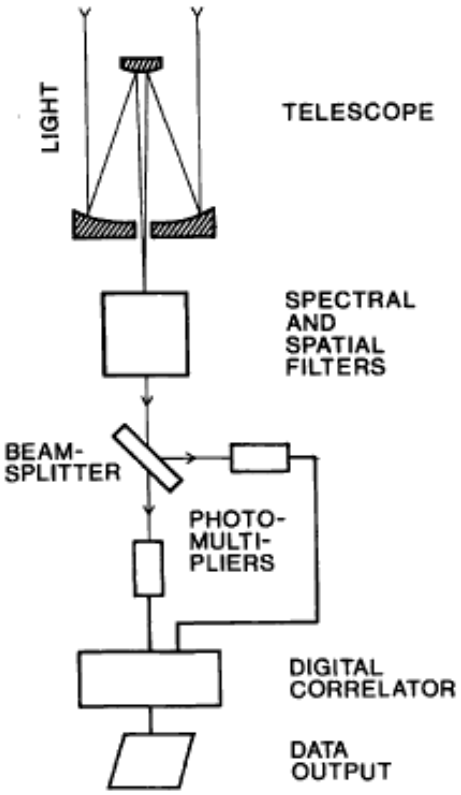

Figure 5.24: Schematic layout of the QVANTOS Mark I instrument. (Dainis Dravins et al., Lund Observatory, [14])

Laboratory experiments are also performed in order to identify optimal strategies for detecting optical variability on microsecond and shorter timescales. In Figure 5.25 it is possible to see results of extremely rapid optical fluctuations in some laboratory sources, captured by the QVANTOS Mark I instrument. Optical fluctuations as rapid as these have, however, not yet been observed in any astronomical object. But without developing and understanding the methods and instruments, which allow such measurement with great accuracy, we cannot exclude the possibility of these fluctuations' existence.

[For more information: `http://www.astro.lu.se/~dainis/HTML/HISPEED.html`]

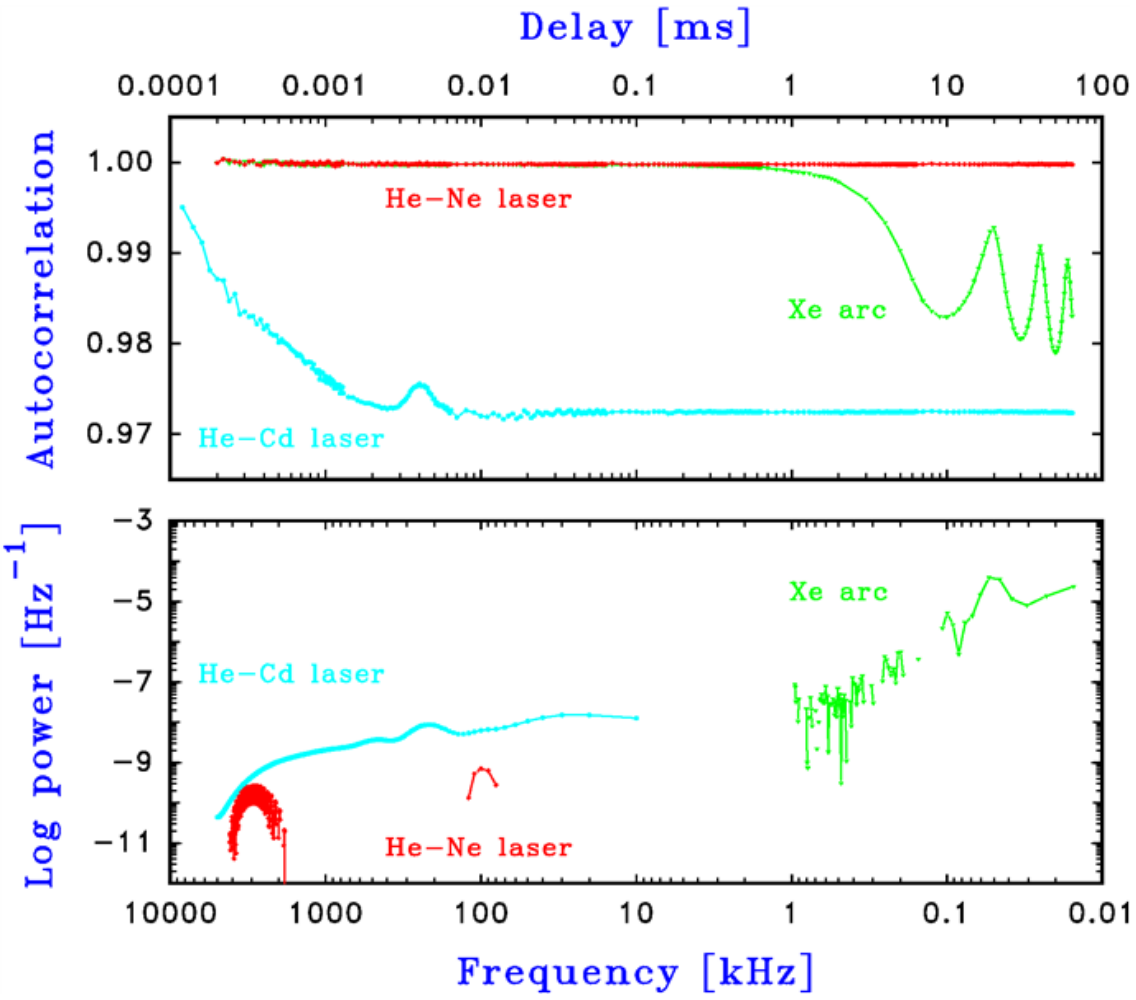

Figure 5.25: Rapid optical variability in different laboratory sources, measured with the QVANTOS Mark I instrument. (Dainis Dravins et al., Lund Observatory, [14])

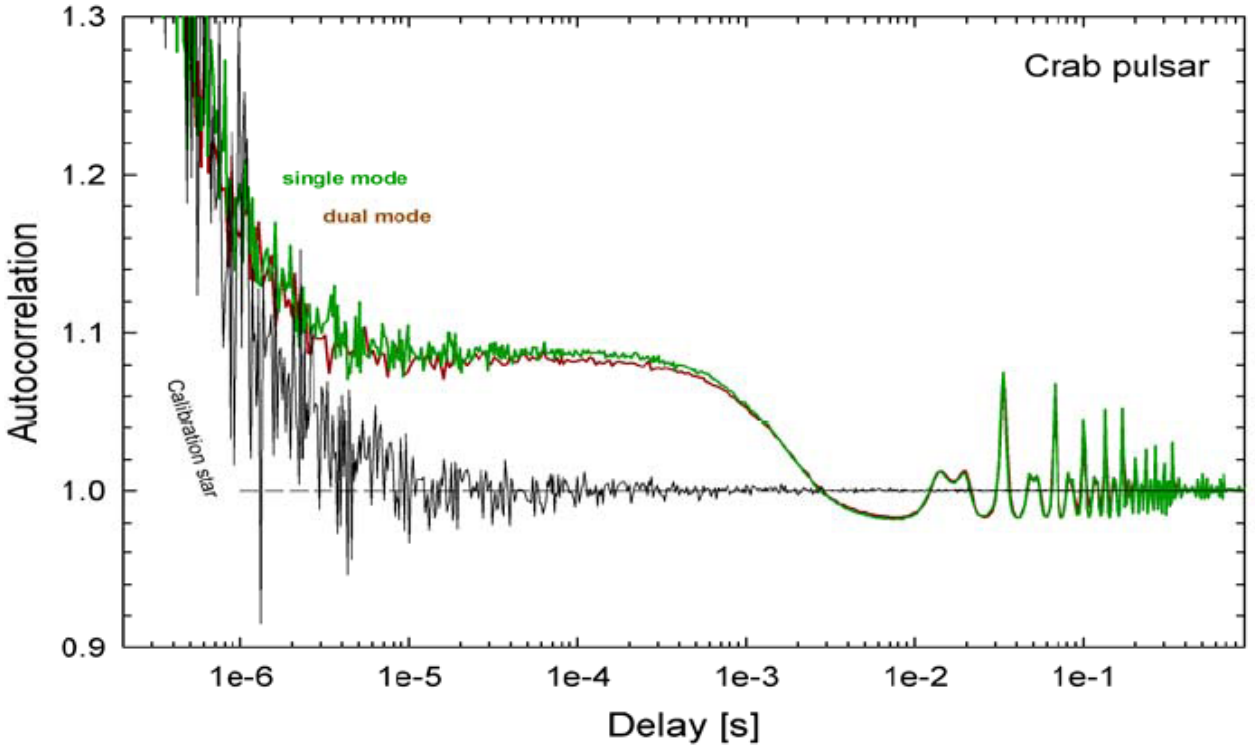

Figure 5.26: Autocorrelation functions recorded for the Crab pulsar (period = 33 ms) using the 1.3 m telescope at the Skinakas Observatory on Crete together with OPTIMA and QVANTOS Mark II (electronics) in October 2004. (Dainis Dravins et al., Lund Observatory, [14])

5.11 Lucky Imaging

It might seem somewhat non-scientific to rely on luck, but that is certainly what Lucky Imaging is all about. Instead of waiting for all the high tech and expensive solutions for solving adaptive optics and image sharpening, extremely large telescopes etc., it is possible to use high speed cameras and take enough images in a short time for some of them to turn out good. By choosing the images that are least affected by the atmosphere and combine them, it is possible to achieve high resolution images.

Lucky Imaging was originally suggested by Fried in 1978 and the principles of Lucky Imaging allow amateur astronomers to produce very high quality images of bright objects such as Mars and the other planets.

Because of the atmosphere's distortion effect on incoming light we have a limitation for ground-based telescopes, which means that even with a larger telescope there is a limit when we do not increase the detail anymore (without adaptive optics). However, using Lucky Imaging it is possible to increase the maximum resolution achievable from the ground by a factor of as much as 5 – 7. This means that using a 2.5 m ground-based telescope it is possible to match the resolution obtained by the 2.5 m space-based telescope, Hubble Space Telescope (HST), at a tiny fraction of the cost. There are no restrictions for using adaptive optics and Lucky Imaging together, as demonstrated with the LuckyCam (`http://www.astro.caltech.edu/palomar/AO/luckycam.html`).

Lucky Imaging requires, as mentioned above, high speed cameras. Most of the the currently active projects are planning to, or are already utilizing CCD cameras, using the newly developed Electron-Multiplying Charge Coupled Devices (EMCCDs) and Low Light Level Charge Coupled Devices (LLLCCDs or L3CCDs). Please have a look at `http://www.ast.cam.ac.uk/~optics/Lucky_Web_Site/guide_to_l3ccds.htm` for a well explained guide of these new CCDs.

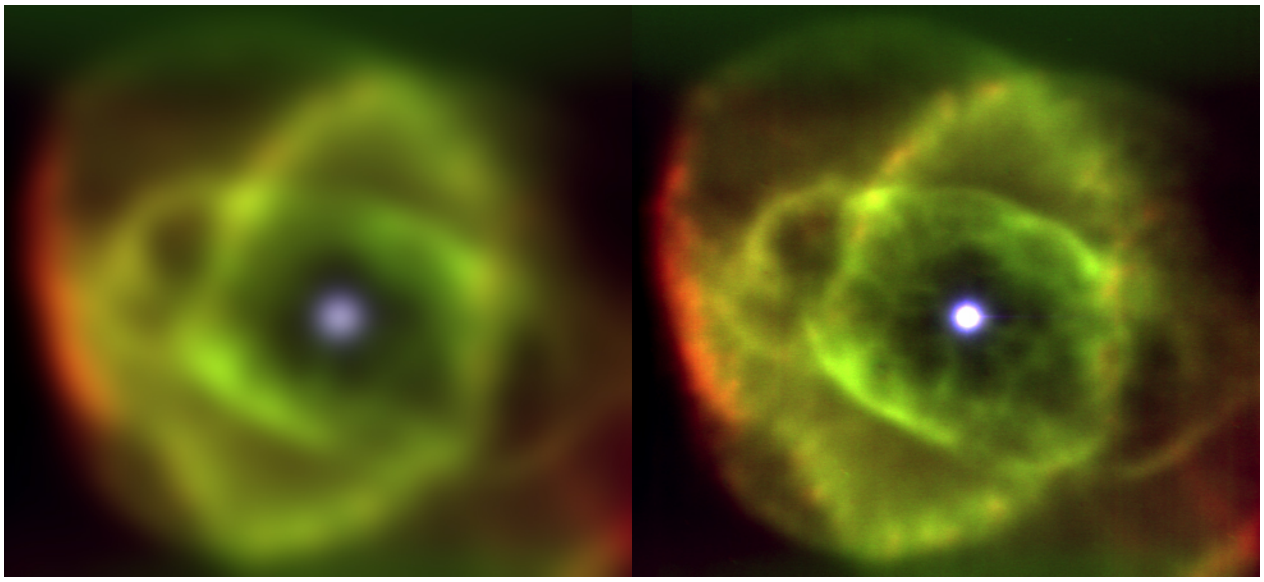

Figure 5.27: The images show the Cat's Eye Nebula (NGC 6543) seen in visible light using the 200-inch Hale Telescope at Palomar Observatory. To the left, "standard mode" for the telescope has been used and to the right adaptive optics enhanced by LuckyCam is being used. (`http://www.astro.caltech.edu/palomar/AO/luckycam.html`)

5.12 TRIFFID, MEKASPEK, MCCP, SUBARU, SALT, ESO-VLT and OPTICON

There are countless other projects, both in small scale and large scale, related to high speed instrumentation and the exploration of new detection procedures in order to push today limits of what is possible even further. Some of these projects are briefly presented below.

5.12.1 TRansputer Instrument For Fast Image Deconvolution (TRIFFID)

The TRansputer Instrument For Fast Image Deconvolution (TRIFFID) is a fast image sharpening camera, built by the University College Galway (today referred to as National University of Ireland (NUI), Galway) in collaboration with the Dunsink Observatory of the Dublin Institute for Advanced Studies (DIAS). TRIFFID utilizes a two-dimensional MultiAnode Multichannel Array (MAMA) detector with fast readout. By recording images in a rapid rate it is possible to overcome some effects of atmospheric seeing and also to achieve a post-exposure image enhancement by a suitable shift-and-add of time-resolved sub-images to compensate for atmospheric tip-tilt distortions.

One of the first real uses of the TRIFFID camera was in January 1993, when it assisted in confirming some observations of two star-like objects seen in a small nebula in the Large Magellanic Cloud (a satellite galaxy to our Milky Way) using the ESO New Technology Telescope (NTT) on La Silla. TRIFFID has been used frequently ever since, including at the WHT and Kapteyn telescopes on La Palma.

A peculiar fact: TRIFFID as an acronym is listed by a Harvard University astrophysics professor, Glen Petitpas, on his "Dumb Or Overly Forced Astronomical Acronyms Site" (DOOFAAS) with the entry:

TRIFFID	TRansputer Instrument For Fast Image Deconvolution (actually, it had no Transputer chips, and didn't even do deconvolution)

Table 5.2: Entry for TRIFFID in DOOFAAS.

[DOOFAAS: `http://www.cfa.harvard.edu/~gpetitpas/Links/Astroacro.html`]

5.12.2 MEhr-KAnal-SPEKtralphotometer (MEKASPEK) and Multi-Channel multi-Color Photometer (MCCP)

The major aim of the MEhr-KAnal-SPEKtralphotometer (or Multi Channel Spectral Photometer) (MEKASPEK) project was to develop a new 4-channel spectral photometer which would be able to achieve the utmost accuracy reachable with then current technology (late 1980's).

The instrumental design for the new photometer was characterized by the following features [15]:

1. High quantum efficiency throughout the whole optical wavelength range in order to keep the photon noise as small as possible.
2. Simultaneous measurements of the object, two comparison stars and sky background for successful elimination of neutral atmospheric extinction effects.
3. Spectral resolution in combination with oversampling allows to eliminate color-dependent atmospheric effects and guarantees an accurate transformation to other broad-band photometric systems.
4. Optimized adaptation of the entrance diaphragm's diameter to the actual seeing conditions.
5. High time resolution up to 10 ms in order to study rapidly variable objects.

The MEKASPEK was able to implement these features by using four optical fibers which could be centered on the stars in the focal plane of the telescope. The fiber bundles fed the slit of a two beam prism spectrograph which had been optimized to reach high transmission throughout the whole optical range of the spectrum. The four spectra were then focused onto the surface of a two-dimensional photon-counting micro-channel plate detector (Mepsicron).

MEKASPEK has been used on several telescopes, including at its "home" on Wendelstein in Bavaria, at Calar Alto and on La Silla. MEKASPEK has been used in observations of flare stars, dwarf nova eruptions, eclipsing binaries, cataclysmic variables and other rapidly variable stars. During an impact of the comet "Shoemaker-Levy 9", MEKASPEK was also used to obtain high-time resolved spectrophotometry of the Galilean moon Europa.

The Multi-Channel multi-Color Photometer (MCCP), which can be seen as a previous instrument version of the MEKASPEK, was developed for precise multicolor aperture photometry of fast variable phenomena. MCCP uses three optical fibers which are positioned by computer control onto three light sources (e.g., a variable star, a calibration star and the sky background) in the focal plane of the telescope. The fibers then feed three prism-spectrographs and the spectra are projected on fiber bundles which allow selecting five overlapping broad band regions corresponding to the Kron-Cousins UBVRI colors. The color channels of each light source feed five photomultiplier tubes operated at -20 ℃, which ultimately meant that the system can use a total of 15 detectors which enable photon counting of three simultaneous light sources with a maximum time resolution of 1 ms.

[MEKASPEK: `http://www.wendelstein-observatorium.de:8002/history/meka/`]
[MCCP: `http://www.wendelstein-observatorium.de:8002/history/mccp/mccp_en.html`]

5.12.3 SUBARU

SUBARU is an 8.2 m optical-infrared telescope at the summit of Mauna Kea on Hawaii, operated by the National Astronomical Observatory of Japan (NAOJ). Several interesting (including some high speed) instruments are used here; COMICS, FMOS, FOCAS, HDS, IRCS, MOIRCS and Suprime-Cam.

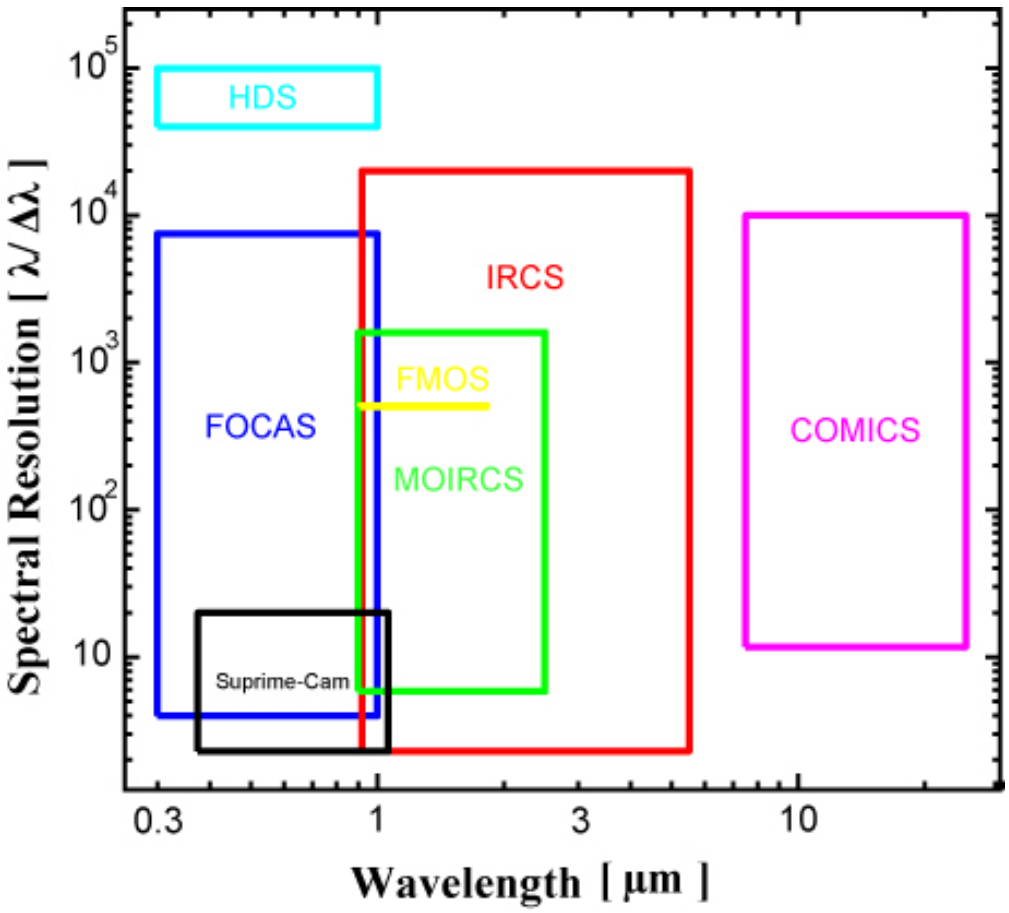

Figure 5.28: The wavelength regions for each of the instruments at SUBARU. (NAOJ)

Instrument	Resolution	Slit length	Pixel scale
COMICS	10000 (0.33")	40"	0.165"
FMOS	500 (1.2"; fiber diameter)	30', multi	-
FOCAS	250 – 7500 (0.4")	6', multi	0.1"
HDS	100000 (0.38")	10", 60"	0.13"
IRCS (grism)	50 – 1400 (0.15 – 0.90")	21", 54"	0.020", 0.052"
IRCS (echelle)	5000 – 20000 (0.14 – 0.55")	4.8 – 9.6"	0.060"
MOIRCS	640 – 1600 (0.5")	multi	0.117"

Table 5.3: The spectrographic capabilities of the SUBARU instruments. (NAOJ)

Instrument	Field of view	Pixel scale	Filters
COMICS	42" × 32"	0.133"	15
FOCAS	6' diameter	0.1"	14
IRCS	21", 54"	0.020", 0.052"	18
MOIRCS	4' × 7'	0.117"	3
Suprime-Cam	34' × 27'	0.20"	10

Table 5.4: The imaging capabilities of the instruments. (NAOJ)

Perhaps the two instruments of most interest for this thesis are the Faint Object Camera And Spectro-

graph (FOCAS) and the High Dispersion Spectrograph (HDS), which both operate in the optical region and aim to reach very high time resolutions. Both are, however, using CCD detectors, which because of long readout times etc. fall short when it comes to the extremely fast operations, that, e.g., detectors of the type evaluated in this thesis (APDs and alike) could perform.

[For more information: `http://www.naoj.org/Observing/Instruments/`]

5.12.4 Southern African Large Telescope (SALT)

The Southern African Large Telescope (SALT) at the South African Astronomical Observatory (SAAO) is the largest single optical telescope in the southern hemisphere. With a hexagonal mirror array 11 meters across, it enables studies of distant stars, galaxies and quasars a billion times too faint to be seen with the unaided eye – as faint as a candle flame at the distance of the Moon. First light was seen in September 2005, using the instrument SALT Imaging CAMera (SALTICAM). The basic properties of the SALTICAM can be seen in the table below.

Image Quality	See SALTICAM Optical Design page. 0.3 arcsec (EE50), combined with SALT 0.6 arcsec (EE50), to give 0.67 arcsec image quality, independent of seeing. EE80 shall be no more than 0.5 arcsec. Distortion shall be less than 1 per cent. The mean plate scale shall be 107 micron/arcsec or 9.35 arcsec/mm within 1 per cent.
Science Field of View	8 arcmin in diameter
Guide Star Field of View	10 arcmin in diameter
Wavelength range	320 – 950 nm
Filters	8 position filter unit: UBVRI + ND + clear filters + short wavelength interference filters at 340 nm (FWHM 35 nm) and 380 nm (FWHM 40 nm) supplied
CCD chips	E2V Technologies 44-82
Format	$2048 \times 4102 \times 15$ micron square pixels per chip
Imaging area per chip	$30.7 \times 61.5\ mm^2$ imaging area per chip
Readout capabilities	2 readout amplifiers per chip
Mosaicing	2×1 mini-mosaic
CTE	better than 99.99 %
Full well	164 and 172 k e^-/pix (for CCDs SALT-01 and SALT-02 respectively)
Dark current	less than 1 e^-/pix/hr at 160 K
Readout noise	less than 3.0 e^-/pix at 100 kHz (10.0 μsec/pix) (slow readout)
CCD Controller	SDSU II (Leach) from Astronomical Research Camera Inc.
Sensitivity	Thinned, back-illuminated. Deep depletion silicon. Astro Broad Band anti-reflection coating.

Table 5.5: The basic properties of SALTICAM. (SALT)

The SALTICAM uses Frame Transfer CCDs, which through several mode options can enable pretty high time resolution but with the cost of having to compensate the exposure area. Continuous photometry of ~ 20 ms integrations might be feasible with windowing, charge shuffling and a suitably fast bus but the typical readout times are, however, in the range over several seconds as seen in Table 5.6.

Mode	Prebin	Observer Specifies	Readout Speed (μsec/pix)	Readout Noise (e^-/pix)	Readout Time (sec)
Full Frame	2×2	Slow	10.0	3.3	11.2
Full Frame	2×2	Fast	4.0	5	4.6
Frame Transfer	2×2	Slow	10.0	3.3	5.7
Frame Transfer	2×2	Fast	4.0	5	2.4

Table 5.6: Readout times. (SALT)

At SALT there are also two other instruments; the Robert Stobie Spectrograph (RSS) (previously known as the Prime Focus Imaging Camera) and the High Resolution Spectrograph (HRS) (currently in development).

[For more information: `http://www.salt.ac.za/`]

5.12.5 ESO VLT

The European Southern Observatory's Very Large Telescope array (ESO VLT) is the flagship facility for European ground-based astronomy at the beginning of the third Millennium. It is the world's most advanced optical instrument, consisting of four unit telescopes with main mirrors of 8.2 m diameter and four mobile 1.8 m Auxiliary Telescopes. The telescopes are arranged in an array in order to be able to work together, in groups of two or three, to form a giant interferometer, the ESO VLT Interferometer (ESO VLTI). The ESO VLTI can with its impressive precision, reconstruct images with an angular resolution of milliarcseconds, equivalent to distinguishing the two headlights of a car at the distance of the Moon.

With the ESO VLT's impressive ability to collect light, it enables studies of extremely faint objects and could serve as a very good testing ground for the instrumentation in the emerging field of High Time Resolution Astrophysics (HTRA), partly covered in this thesis. In the planning of instrumentation for the VLT, various concepts for a high time resolution instrument were considered but not realized. One example of instruments proposed was a Fast Recording Imager and Spectro-Photometric Instrument (FRISPI). It was building upon the experience of MEKASPEK and the time range would have been from 4 seconds for the full image, 1 ms in a binning mode and 0.1 μs in a photon-count time-tagged mode.

The ESO VLT project does, however, include a very ambitious instrumentation plan with the following instruments as of today:

1. **FORS1** (FOcal Reducer and Spectrograph) and its twin, FORS2, are multi-mode instruments that can be used for imaging in the visible and for low-resolution spectroscopy.
2. **ISAAC** (Infrared Spectrometer And Array Camera) is a cryogenic infrared imager and spectrometer, observing in the 1 to 5 μm range.
3. **UVES** (Ultra-violet and Visible Echelle Spectrograph) is the high-dispersion spectrograph of the VLT, observing from 300 nm to 1100 nm, with a maximum spectral resolution of 110,000.
4. **NACO** is an Adaptive Optics facility producing images as sharp as if taken in space.
5. **VIMOS** (VIsible Multi-Object Spectrograph), a four-channel multiobject spectrograph and imager, allows obtaining low-resolution spectra of up to 1000 galaxies at a time.
6. **FLAMES** (Fibre Large Array Multi-Element Spectrograph) offers the unique capability to study simultaneously and at high spectral resolution hundreds of individual stars in nearby galaxies.
7. **VISIR** (VLT Imager and Spectrometer for the mid-InfraRed) provides diffraction-limited imaging at high sensitivity in the two mid infrared (MIR) atmospheric windows (8 to 13 μm and 16.5 to 24.5 μm).
8. **SINFONI** is a near-infrared (1 – 2.5 μm) integral field spectrograph fed by an adaptive optics module.
9. **CRIRES** (CRyogenic high-resolution InfraRed Echelle Spectrograph) provides a resolving power of up to 100,000 in the spectral range from 1 to 5 μm.

10. **HAWK-I** (High Acuity Wide field K-band Imager) is a near-infrared imager with a relatively large field of view.

[For more information: `http://www.eso.org/public/astronomy/teles-instr/paranal.html`]

5.12.6 Optical Infrared Coordination Network for Astronomy (OPTICON)

The Optical Infrared Coordination Network for Astronomy (OPTICON) is a collaboration, until recently funded by the EU Sixth Research and Development Framework Programme (FP6) for a 5-year program 2004-2008. During this period considerable progress was made in technology programmes for adaptive optics, fast detectors, interferometry tools, smart focal plane technologies and VPH gratings for use in astronomical instruments.

Within and after the OPTICON project during the FP6 period some interesting results have come out of it. ESO quite recently released a press release "World's fastest and most sensitive astronomical camera" (ESO 22/09 – Organisation Release, 18 June 2009) which includes the OCam camera with the CCD220 detector. Both of these are results of five years work within the OPTICON project and after development by e2v technologies. However, if the title of the press release really is suitable and completely true is perhaps debatable as this is a CCD camera with maximum frame rate of 1500 frames/second (1.5 kHz or $\sim$ 0.7 ms time resolution). When you compare these numbers with the emerging Avalanche Photodiode (APD) detectors, such as the ones evaluated in this thesis, it can perhaps sound naive and somewhat biased by ESO to call a CCD camera the "World's fastest and most sensitive astronomical camera" when there exist other technology enabling frame rates reaching MHz and higher. One can of course argue that this is for one or a handful of pixels, at the time, but APD arrays are in development.

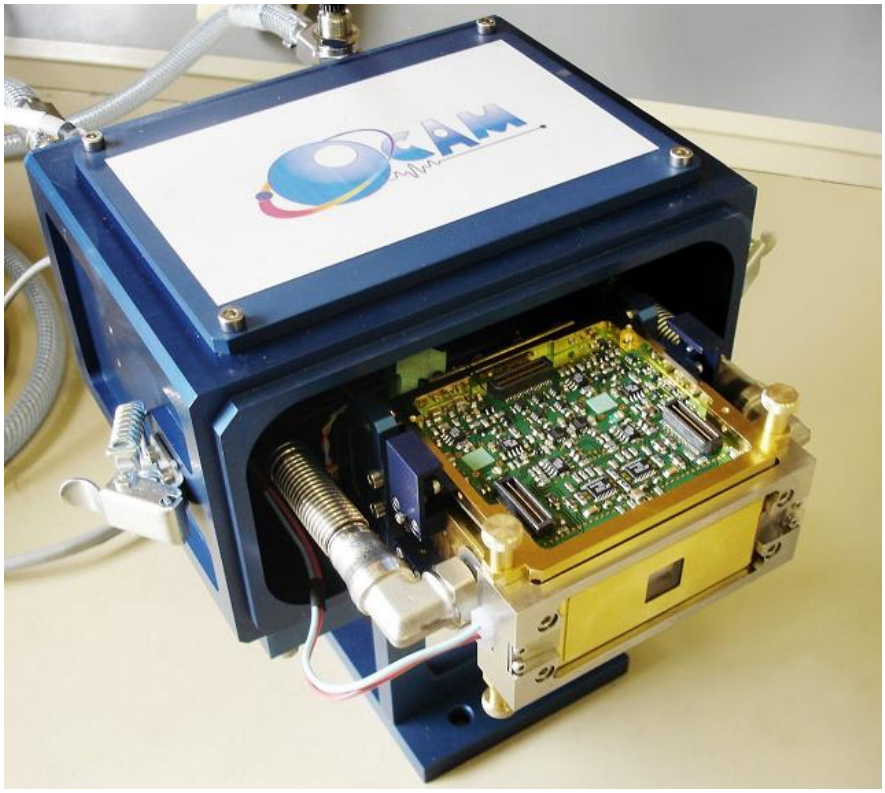

Figure 5.29: "OCam is the world's fastest high precision faint light camera. Developed in Europe, the camera is highly sensitive and able to take 1500 images per second. OCam has been specially designed and built by a team of French engineers from LAM, LAOG and the OHP and uses the CCD220 detector developed by e2v technologies. The technology developed with OCam has been transferred to ESO for use with the second generation instruments of ESO's Very Large Telescope." (ESO)

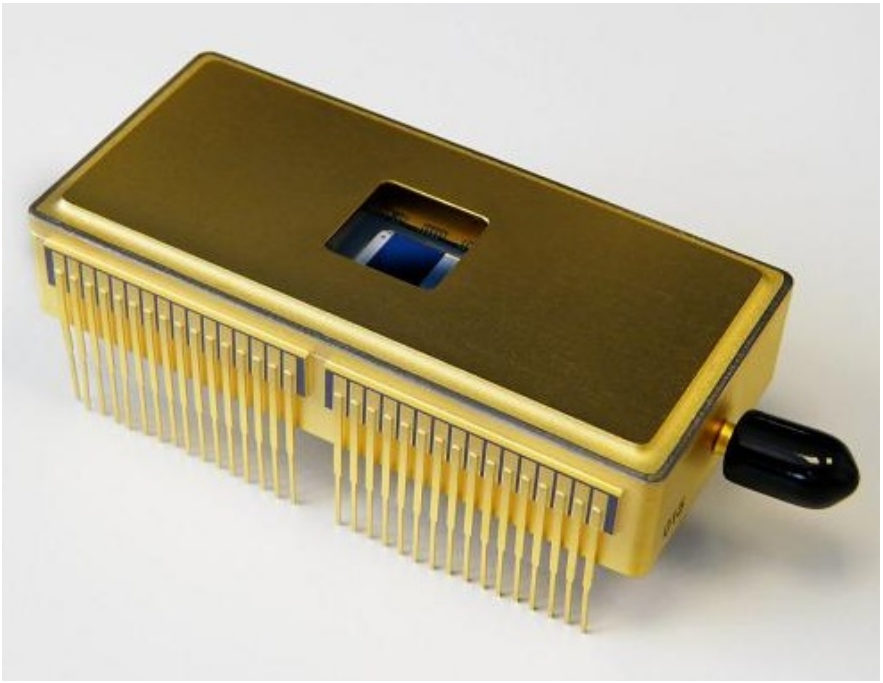

Figure 5.30: "The CCD220 detector at the core of the OCam camera has 240×240 pixels and has a readout noise ten times smaller than detectors in current use, making it ideal for the faint light camera systems to be used on the second generation of Very Large Telescope instruments. It was developed by the British manufacturer e2v technologies." (ESO)

[Information/Press release: `http://www.eso.org/public/outreach/press-rel/pr-2009/pr-22-09.html`]

OPTICON has now entered a new phase, funded by the EU Seventh Research and Development Framework Programme (FP7). OPTICON FP7 incorporates the networking (NA), trans-national access (TNA) and joint research activities (JRA) activities listed in Table 5.7.

Workpackage Number	**Description**
WP1	Adaptive Optics Systems: seeing beyond atmospheric limits
WP2	Laser Guide Star Adaptive Optics detectors
WP3	Astrophotonics
WP4	High Angular Resolution by Interferometry: Enhancing the scientific output and reaching the fundamental limits
WP5	Smart Instrument Technologies
WP6	New Materials and Processes for Astronomical Instrumentation... Work Package description for Transnational Access or Service Activity
WP7	Transnational Access
WP8	Management
WP9	Europe of the Future: Technologies
WP9.1	Key Technologies
WP9.2	Software Standards
WP10	Europe of the Futures: Science
WP10.1	Science Case Development for the European Extremely Large Telescope
WP10.2	European Network for High Time Resolution Astrophysics – HTRA
WP11	Enhancing Community Skills: Strengthening Skills
WP11.1	Community Development
WP11.2	The European Interferometry Initiative
WP12	Enhancing the Community: Optimising Science Access
WP12.1	Telescope Directors' Forum
WP12.2	Planning for a viable future
WP12.3	The European Association for Solar Telescopes (EAST)

Table 5.7: List of OPTICON FP7 activities. (OPTICON)

[OPTICON: `http://www.astro-opticon.org/`]

6 Experiments

6.1 Equipment

6.1.1 Detectors

Figure 6.1: The detector lineup (excluding the SensL PQC and SPMPC). From left to right: PerkinElmer (SPCM-AQR-14), MPD (PDM series, PD1C0B), id Quantique (id100-50), RCA Electro Optics (now PerkinElmer) (SPCM-100-PQ) and SensL (PCDMini0100).

6.1.1.1 id Quantique

6.1.1.1.1 About id Quantique

"id Quantique's focus is to provide innovative and cost-effective solutions by leveraging the tremendous capabilities offered by Quantum Photonics. The company designs and manufactures hardware products serving two main markets: network security and optical instrumentation."

"id Quantique has a growing optical instrumentation business, where the company's core Quantum Photonics technologies provide innovative solutions for industrial, commercial and research applications. Its product offering includes photon-counters for the visible and infrared regions of the optical spectrum, as well as short-pulse laser sources. These products are used in medical/environmental instrumentation, quantum optics, aerospace and defense applications."

[Quoted from id Quantique's "Corporate Profile" (2009-12-17), `http://www.idquantique.com/`]

6.1.1.1.2 id100-50

"The id100 consists of an avalanche photodiode (APD) and an active quenching circuit integrated on the same silicon chip. The chip is mounted on a thermo-electric cooler and packaged in a standard TO5 header with a transparent window cap. A thermistor is used to measure temperature. The APD is operated in Geiger mode, i.e. biased above breakdown voltage. A high voltage supply used to bias the diode is provided by a DC/DC converter. The quenching circuit is supplied with +5V. The module output pulse reflects the arrival of a photon with high timing resolution. The pulse is shaped using a hold-off time circuit and sent to a 50 Ω output driver. All internal settings are preset for optimal operation at room temperature. No user adjustment is necessary. In the fiber-coupled version, the TO5 header and the optical fiber are included in

the housing. The optical input consists of a FC/PC connector on the front side of the module. “

[Quoted from id Quantique's id100-series v. 2.5 specifications as of August 2009 (2009-12-20), `http://www.idquantique.com/products/files/id100-specs.pdf`]

General Specifications at T = 25 ℃				
Parameters	**Minimum**	**Typical**	**Maximum**	**Units**
Spectral range	350		900	nm
Timing resolution [FWHM]		40	60	ps
Photon detection probability				
at 400 nm	15	18		%
at 500 nm	30	35		%
at 600 nm	20	25		%
at 700 nm	15	18		%
at 800 nm	5	7		%
at 900 nm	3	4		%
Afterpulsing probability			3	%
Output pulse width	9	10	15	ns
Output pulse amplitude	1.5	2	2.5	V
Dead time		45	50	ns
Maximum count rate (pulsed light)		20		MHz
Supply voltage	5.6	6	6.5	V
Supply current		100	150	mA
Storage temperature	-40		70	℃
Cooling time			5	s

Table 6.1: General specifications for the id100-50. (id Quantique)

Figure 6.2: id Quantique's id100-50 detector.

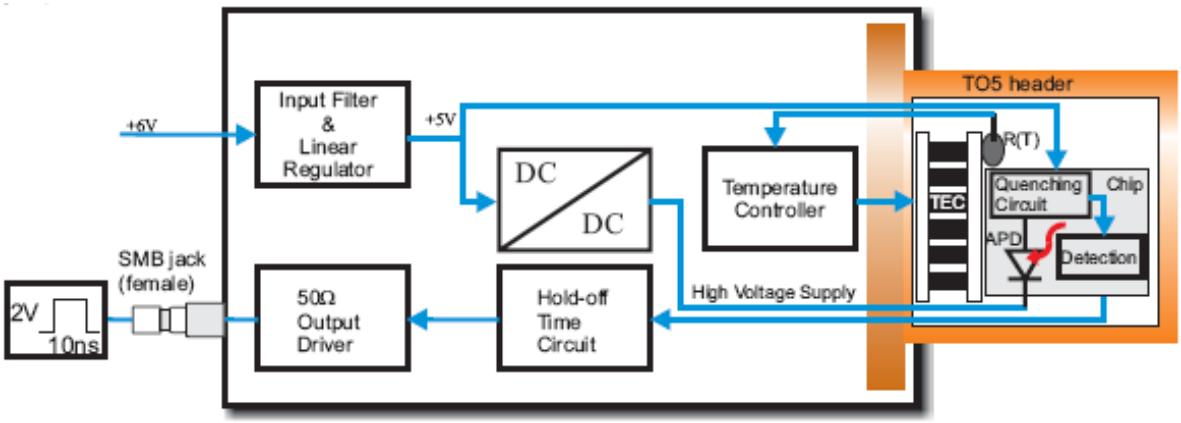

Figure 6.3: Block diagram of the id100 (free-space version, i.e. exposed window (not fiber-coupled)). (id Quantique)

6.1.1.2 Micro Photon Devices (MPD)

6.1.1.2.1 About MPD

"Micro Photon Devices (MPD) is a dynamic production and engineering company based in Bolzano, Italy.The newly founded company benefits of the efforts and the expertise of a research group at Politecnico di Milano, led by Prof. Sergio Cova. Over the past 20 years, Dr. Cova and his team have made many contributions in the field of photon counting – including:

1. Design and production of Single Photon Counting Avalanche Diodes, "SPAD", based on CMOS technology.
2. Active Quenching IC development.

The mission of Micro Photon Devices is the production of photon counting devices based on the technologies developed at Politecnico di Milano. Product engineering and production takes advantage of the experience gained over the years by Microgate (the industrial partner of Micro Photon Devices). Micro Photon Devices is also available to develop custom designs and specific applications related to photon counting detection technology."

[Quoted from MPD (2009-12-17), `http://www.microphotondevices.com/`]

6.1.1.2.2 PDM series, PD1C0B

"The PDM series photon counting detector modules of the PDM series are all solid-state instruments. They have a photon detection efficiency of 49 % at 550 nm and generate a TTL output pulse per detected photon. With fast-timing option (additional circuit board installed) they provide better than 50 ps FWHM photon timing resolution. The excellent photon detection efficiency and superior timing resolution is obtained through the use of epitaxial silicon Single Photon Avalanche Diodes (SPAD) and patented integrated Active Quenching Circuits (iAQC), specifically designed and optimized for photon counting applications. Low-noise SPADs and low-power iAQCs make these modules ideal for portable equipment and all applications requiring low power consumption."

[Quoted from MPD's PDM v. 3.3 datasheet (2009-12-21), `http://www.micro-photon-devices.com/media/pdf/PDM_v3_3.pdf`]

The model name "PD1C0B" is rather cryptic but we can unscramble it by using MPD's ordering guide:
PD(M) – Photon Detection (Module)
1 – 100 μm active area diameter

C– TE (Thermoelectric) Cooled
0 – No timing board
B – Module Grade (See Table 6.3)

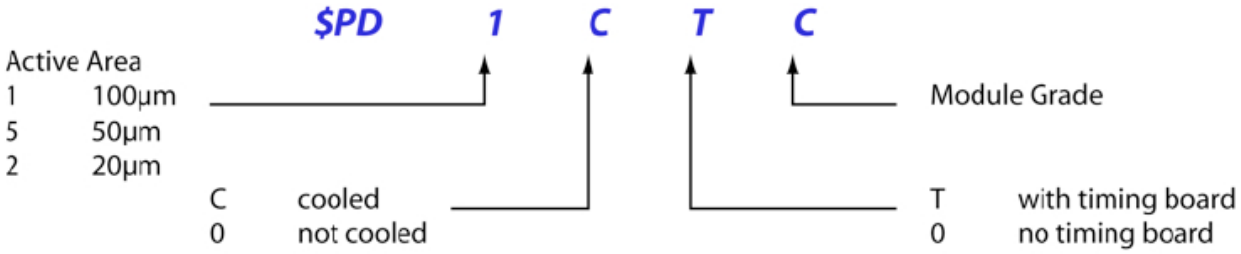

Figure 6.4: MPD's PDM series ordering guide. (MPD)

Specifications @ 25 °C and 5 V overvoltage ($V_{breakdown} + 5$ V)	**Min**	**Typical**	**Max**	**Units**
Photon Detection Efficiency				
at 400nm	21	24		%
at 550nm	45	49		%
at 650nm	34	37		%
Single Photon Timing Resolution				
TTL Counting Output			250	ps (FWHM)
NIM Timing Output (additional internal circuit board required)		35	50	ps (FWHM)
After-pulsing probability	0.1		3	%
Dead Time		77		ns
Supply Voltage	unregulated DC, any value 5 V ∼ 12 V			
TTL Output pulse rise and fall times	< 2 ns on 10 pF load			
Output pulse duration	20 ns typical			
Gating input	TTL control (low level gates detector off)			
Supply input connector	Standard 3.5 mm supply socket			

Table 6.2: General specifications for MPD's PDM series. (MPD datasheet)

	Dark Counts (c/s) TE Cooled			**Dark Counts (c/s) @ 25 °C**
Grade / Active Area Diameter	A	B	C	A
$20\mu m$	< 25			< 250
$50\mu m$	< 250	< 100	< 50	< 5k
$100\mu m$	< 1k	< 500	< 250	< 20k

Table 6.3: Dark Count specifications for MPD's PDM series. (MPD datasheet)

Parameter (Ambient Temperature = 24 ℃)	Measured	Max	Units
Dark Counts	388 / 360		c/s
Maximum count rate (TTL Out)	10.4		Mc/s
Dead time	93 / 93.3		ns
TTL Timing resolution (100 kHz laser, lamb = 675 nm, negligible background noise)	172 / 173	250	ps (FWHM)
TTL Timing resolution (100 kHz laser, lamb = 675 nm, 1 Mc/s background noise)	174 / 183	250	ps (FWHM)
NIM Timing resolution (100 kHz laser, lamb = 675 nm, negligible background noise)		50	ps (FWHM)
NIM Timing resolution (100 kHz laser, lamb = 675 nm, 1 Mc/s background noise)		50	ps (FWHM)
Supply current at 12 V (normal condition)	97 / 96		mA
Supply current at 12 V (startup)	486 / 509		mA
GATE IN check	OK		

Table 6.4: Final test data for the PDM series detectors (SN 00409 / 00410) from MPD as of 8th February 2007. (MPD Test certificate)

Figure 6.5: MPD's PDM Series (PD1C0B) detector.

6.1.1.3 PerkinElmer

6.1.1.3.1 About PerkinElmer

"PerkinElmer is a global technology leader focused on creating a brighter, healthier and safer tomorrow. From energy-efficient illumination to infrared sensing technology for secure homes, we are enhancing your OEM designs with our innovative illumination, detection and digital imaging solutions. As of January, 2009, PerkinElmer is now operating within two businesses - Human Health and Environmental Health. While we are no longer referred to as "PerkinElmer Optoelectronics", you can depend upon the same world-class solutions leveraging our extensive optoelectronics capabilities including:

1. World-class Illumination Solutions for Medical, Safety and Security, Analytical Instrumentation, and Industrial Markets.

2. World-class Detection Solutions for Safety and Security, the Environment, and Human Health.

3. World-class Digital Imaging Solutions for Diagnostic and Therapeutic Applications and Non-destructive Testing (NDT) Applications.

4. Mission-Critical Defense Solutions for Keeping Our Troops Safe.

”

[Quoted from PerkinElmer's “About Us”, `http://www.optoelectronics.perkinelmer.com/`]

PerkinElmer was also contacted in order to obtain some information on the company's name history, which to us seemed a bit confusing at first, when trying to determine the manufacturer of the SPCM-100-PQ detector. We received an answer, which states:
“Originally the companys name was **RCA**. Later it was bought by **General Electric**. In the 1980ies EG&G bought the factory and products from GE, the companys name than changed to **EG&G Canada**. Finally, in 1999, EG&G bought PerkinElmer and changed the name into **PerkinElmer**.”

6.1.1.3.2 SPCM-100-PQ

“The SPCM-100-PQ is a self-contained module which detects single photons of light over the wavelength range from 400 nm to 1060 nm ... a range and sensitivity which often outperforms photomultiplier tubes.

Applications include Lidar, Photon Correlation Spectroscopy, Astronomical Observations, Optical Rangefinding, Optical Fiber Test and Fault Location, Ultrasensitive Spectroscopy etc., where the light being measured can be focused to a small spot.

The module utilizes a unique silicon avalanche photodiode which has a circular active area whose peak photon detection efficiency, within 50 microns of the center, exceeds 40 % at 633 nm. At larger distances from the center, the response decreases, so that at 75 microns from the center the photon detection efficiency is only 20 % (see Figure 4.1).

The module has a so-called “passive quench” circuit, which can count at speeds up to 1,000,000 counts per second. There is a “dead time” of 200 ns between pulses. The avalanche photodiode sensing element is temperature controlled, ensuring stabilized performance despite changes in the ambient temperature.

Single photon arrival times can be measured with an accuracy of 3 ns rms.

The SPCM-100-PQ requires +12, +5, -5 volt power supplies (a mating cable is provided with each module). A digital pulse, 2 volts high and approximately 200 ns wide, is output at the rear BNC connector as each photon is detected. The case temperature should be kept between 5 and 40 ℃ during operation.”

[Quoted from a scanned copy of the SPCM-100-PQ datasheet, which otherwise is hardly available anywhere else, General Electric Canada Inc., Electro Optics]

Note that the SPCM-100-PQ detector may be found under various company names (e.g., RCA, EG&G) but not under PerkinElmer. However, as mentioned in the above About PerkinElmer section, the company has basically just changed names. Therefore we decided to let PerkinElmer be stated as the manufacturer for SPCM-100-PQ throughout this thesis.

Electrical Characteristics	**Minimum**	**Typical**	**Maximum**	**Units**
Supply Voltage Required:				
+ 12 V @ 0.08 A max	11.9	12.0	12.1	V
+ 5 V @ 1.3 A max	4.9	5.0	5.1	V
- 5 V @ 0.02 A max	-4.9	-5.0	-5.1	V
Supply Voltage Ripple (all supplies)	-	-	50	mV rms
Case Operating Temperature	5	-	40	℃
Humidity (Tests in progress)	-	-	70 (estimate)	% R.H.
Photon Detection Efficiency (PDE) within 50 μm of center:				
λ = 1060 nm	-	0.8	-	%
λ = 830 nm	25	32	-	%
λ = 633 nm	40	43	-	%
λ = 400 nm	-	20	-	%
PDE Variation at Constant Case Temperature (12 h)	-	± 1	± 3	% Relative
PDE Variation from 5 ℃ to 40 ℃ compared with 25 ℃ Case Temperature	-	± 5	± 10	% Relative
Dark Count	-	500	1000	Counts/s (Hz)
Dark Count Variation at Constant Case Temperature (12 h with no illumination)	-	± 2	± 10	% Relative
Dark Count Variation from 5 ℃ to 40 ℃ compared with 25 ℃ Case Temperature	-	± 5	± 15	% Relative
Dead time	-	-	200	ms
Output Count Rate Before Saturation	1.3	1.8	-	Mc/s (MHz)
Single Photon Timing Resolution (rms)	-	3	-	ns
Settling Time Following Power Up	-	20	100	s
Threshold Setting Required for Digital Output Pulse (Terminated in 50 ohms)	0.5	1.0	1.5	V

Table 6.5: Specifications for RCA's (PerkinElmer's) SPCM-100-PQ. (General Electric Canada Inc., Electro optics)

Figure 6.6: PerkinElmer's SPCM-100-PQ detector.

6.1.1.3.3 SPCM-AQR-14

"The SPCM-AQR is a self-contained module that detects single photons of light over the 400 nm to 1060 nm wavelength range – a range and sensitivity that often outperforms a photomultiplier tube. The SPCM-AQR uses a unique silicon avalanche photodiode (APD) with a circular active area that achieves a peak photon detection efficiency of more than 65% at 650 nm over a 180 μm diameter. The photodiode is both thermo-electrically cooled and temperature controlled, ensuring stabilized performance despite ambient temperature changes.The SPCM-AQR module can count to speeds exceeding 10 million counts per second (Mc/s) for the SPCM-AQR-1X. There is a "dead time" of 50 ns between pulses.The SPCM-AQR requires a +5 V power supply. A TTL pulse of 2.5 V (minimum) high, in a 50 Ω load and 35 ns wide, is output at the rear BNC connector as each photon is detected. To avoid a degradation of the module linearity and stability, the case temperature should be kept between 5 ℃ and 40 ℃ during operation."

[Partly modified (see note below) but otherwise quoted from PerkinElmer's SPCM-AQRH datasheet (2009-12-22), `http://optoelectronics.perkinelmer.com/content/Datasheets/DTS_SPCMAQRH.pdf`, Old version (2009-12-22): `http://www.htds.fr/doc/optronique/scientifiqueBiomedical/SPCM-AQR.pdf`]

Note: The SPCM-AQR series has been updated in order to be RoHS compliant (EU's Restriction of Hazardous Substances in electrical and electronic equipment) and is now called SPCM-AQRH. This has also meant a few subtle changes in the detectors as well as some completely new detectors in the series. The quoted information has therefore been modified slightly with correct names and also mixed slightly with the old datasheet we had in paper form.

We can unscramble the detector model name "SPCM-AQR-14" by utilizing the ordering guide in the old SPCM-AQR datasheet:
SPCM – Single Photon Counting Module
AQR – Active Quench and Reset
1 – 180 μm active area diameter
4 – Dark Count $<$ 100 c/s
(FC) – Fiber Connection

Specifications SPCM-AQR-WX @ 22 ℃, all models, unless otherwise indicated				
Parameter	**Min**	**Typical**	**Maximum**	**Units**
Supply current		0.5	1.9	A
Supply voltage	4.75	5	5.25	V
PerkinElmer power cable total resistance		0.2		Ω
Case operating temperature	5		40	℃
Active area (diameter) @ minimum PDE	170	175		μm
Photon detection efficiency (PDE)				
at 400 nm	2	5		%
at 650 nm	50	65		%
at 830 nm	35	45		%
at 1060 nm	1	2		%
PDE variation at constant case temperature (2h @ 25 ℃)		± 1	± 3	%
PDE variation 5 ℃ to 40 ℃ case temperature		± 4	± 10	%
Dark Count:				
SPCM-AQR-12			500	c/s
SPCM-AQR-13			250	c/s
SPCM-AQR-14			100	c/s
SPCM-AQR-15			50	c/s
SPCM-AQR-16			25	c/s
Average dark count variation at constant case temperature (6 hrs @ 25 ℃):				
SPCM-AQR-12 & 13			± 10	%
SPCM-AQR-14 & 15 & 16			± 1	σ
Average dark count variation at 5 ℃ to 40 ℃ case temperature:				
SPCM-AQR-12 & 13			± 20	%
SPCM-AQR-14 & 15 & 16			± 2	σ
Single Photon Timing Resolution	Contact factory for availability			
Dead Time (Count rates below 5 Mc/s)		50	60	ns
Output count rate before saturation	10	15		Mc/s
Linearity correction factor:				
at 200 kc/s		1.01		
at 1 Mc/s		1.08	1.15	
at 5 Mc/s		1.40	1.67	
Afterpulsing probability			0.5	%
Settling time following power up (1 % stability) @ 1 Mc/s and 25 ℃		15	30	s
Threshold setting required on counter for digital output pulse (terminate in 50 Ω)	0.75	1.0	2.0	V
Output pulse width		35		ns
Gating turn on/off: (50 Ω output)				
Disable = TTL Low		2	4	ns
Enable = TTL High		45	55	ns
Gating Threshold Voltage: (@ $V_{supply} = 5$ V)				
Low level (sink current > 90 mA)		0	0.4	V
High level (sink current > 30 mA)		3.5	5.25	V

Table 6.6: Specifications for the SPCM-AQR-14 detector. (PerkinElmer's SPCM-AQR datasheet)

Figure 6.7: PerkinElmer's SPCM-AQR-14 detector.

Figure 6.8: PerkinElmer's SPCM-AQR-13-FC detector disassembled. (Vadim Makarov, `http://www.vad1.com/photo/stock/PerkinElmer-SPCM-AQR-13-FC-sn7272-manuf20011005-photos20080603-05.html`, also see arXiv:0809.3408v2 [quant-ph])

6.1.1.4 SensL

6.1.1.4.1 About SensL

"SensL is a private company designing and commercializing revolutionary technology in low light sensing and imaging. Based in Cork, Ireland, SensL has become a global leader with core technology consisting of a range of silicon based low light detectors, modules and systems for applications that use visible low light detection. Based on new silicon fabrication technologies, novel device geometries, and new control circuit design, SensL provides higher specification devices than currently available on the market. Targeted applications include those currently using single photon counting and photomultiplier tube (PMT) technology. The main advantages of SensL's technology are low operating voltage, no excess light damage, high quantum efficiency and low timing jitter. Additionally SensL's detectors are fabricated using CMOS compatible processing steps enabling full electronics integration."

[Quoted from SensL PCEdu-1T Version 1.0 Rev 2 Data Sheet, `http://www.sensl.com/`]

6.1.1.4.2 Passive Quench Circuit (PQC)

The Passive Quench Circuit included in the SensL Photon Counting Fundamentals Educator Pack (PCEdu-1) is essentially a simple passively quenched detector with switches for various resistance modes. It requires a separate power supply and has a SMA connector (SubMiniature version A, i.e. one of the standard coaxial radio-frequency connectors) to enable monitoring of the waveform (shape of the pulse) in an oscilloscope.

Amplitude of the pulse (V)	≈ 3
Dead time (μs)	≈ 40
Dark Count Rate (cps)	≈ 120

Table 6.7: Some properties of the PQC, mentioned in the PCEdu-1 manual.

Figure 6.9: The Passive Quench Circuit (PQC) module included in the SensL's PCEdu-1 Photon Counting Fundamentals Educator Pack.

6.1.1.4.3 PCDMini0100

"SensL's PCDMini Photon Counting Device is the first miniature photon counting system on the market and features SensL's new quenching architecture which stacks with cooling and communication boards for enhanced functionality. The sensor is hermetically sealed and seated on a thermoelectric cooler controlled by the cooler board for applications that require extremely low Dark Count. The USB Interface Board significantly simplifies the task of integrating the PCDMini into any measurement system as its integrated counter functionality eliminates the requirement for a separate data acquisition system. DLL and LabVIEW

drivers supplied with the USB Interface enable the user to easily integrate the module into their system, while the compatibility with SensL's Integrated Environment (SIE) graphical user interface makes system monitoring and configuration extremely user friendly. This ease of integration, combined with the compact and miniature form factor of the product makes the PCDMini the ideal photon counting solution for OEMs."

[Quoted from SensL's PCDMini Datasheet dated May 2009 (2009-12-23), `http://sensl.com/downloads/pcdmini_datasheet.pdf`]

Parameter	Min	Typical	Max	Units	Test Conditions
INPUTS					
Detector Module DC Input Voltage	4.9	5	5.1	V	Typical current: 200 mA at normal operation 700 mA at startup
AC Mains Adapter Supply Voltage	100		240	V	UK, Europe, USA
AC Mains Adapter Supply Frequency	47		63	Hz	UK, Europe, USA
OUTPUTS					
Output Amplitude	2,2	2,4	2,9	V	50 F load
Output Pulse Width		70		ns	
PERFORMANCE					
Breakdown Voltage (V_{br})		27		V	
Dead Time		100		ns	
Maximum Count Rate		10		Mcps	Continuous light
Spectral Range	400		1100	nm	
Cooling Time		10		s	Cooling from room temperature
Setpoint Temperature		-20		℃	Cooling Controller Board
Temperature Setpoint Stability		± 0.1		℃	Cooling Controller Board
Timing Resolution / Time-Bins		200		μs	USB Interface Board (Max)

Table 6.8: General specifications for the PCDMini0100. (SensL's datasheet)

Parameter	Typical values	Units	Test Conditions
INPUTS			
Active Area Diameter	100	μm	
Dark Count	1000	cps	Cooling at -20 ℃
Peak Detection Efficiency	18	%	Typical V_{bias}, λ = 480 nm
Peak After-Pulse Probability	2	%	Typical V_{bias}, Mean Count Rate = 100 kcps
FWHM Jitter	600	ps	Typical V_{bias}, Mean Count Rate = 100 kcps

Table 6.9: Module specifications for the PCDMini0100. (SensL's datasheet)

	Minimum	Typical	Maximum
Breakdown Voltage, V_{br} (V) @ -20 ℃		27.3	
APD Bias Voltage (V) (HV test point)		29.3	31.3
Dark Count (cps) @ 5V over V_{br}		1300	
Dynamic range (cps) @ 5V over V_{br}	1300		$9.6 \cdot 10^6$

Table 6.10: Final test data from SensL for the PCDMini0100 as of 16th April 2009. (SensL's Final Test Sheet)

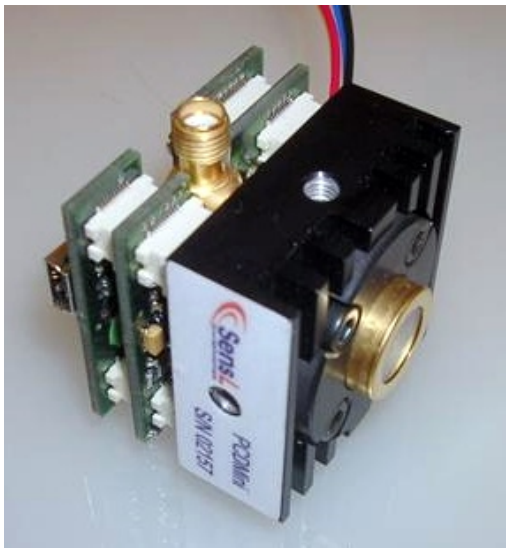

Figure 6.10: The SensL PCDMini0100.

[More information: `http://sensl.com/products/photon-counting-systems/pcdmini/`]

6.1.1.4.4 SPMPC, Large Area Photon Counting APD

"The SPMMini is the first solid state alternative to the long established Photomultiplier Tube (PMT). It combines the high gain (10^6) and high quantum efficiency of the PMT with the well appreciated benefits of silicon including size, low operating voltage, robustness, reliability, magnetic field insensitivity, tolerance of excess/ambient light, and suitability for miniaturization. In addition, the detector has high signal to noise and fast timing properties.

The detector consists of an array of Geiger mode Avalanche Photodiodes (APDs), each individually coupled to integrated quench electronics, and is a type of detector commonly referred to as a Silicon Photomultiplier (SPM). The Geiger mode APD microcells have extremely high internal amplification that allows single photon sensitivity at room temperature. The output of a Geiger mode APD is an identical, fixed charge or current pulse for each single photon detected. By connecting the array of Geiger mode APDs in parallel, the summed output becomes proportional to the number of Geiger mode pulses and hence proportional to the incident photon flux.

The uniform high gain across the array allows the single photoelectron peaks to be clearly resolved permitting both single photon detection and accurate calibration of the photon number. The SPMMini includes transimpedance preamplification, a Peltier cooler driver circuit to enable cooling to -20 ℃ and integrated power supply as standard. A variety of add-on options to enhance functionality are provided, including C-mount (male) adapter and a fiber coupler (adapter and fiber cable included).

The detector die is mounted on a Peltier cooler and housed in a hermetically sealed TO8 can.[2] During normal operation the SPMMini is cooled to -20 ℃. This allows even greater performance over room tem-

[2]The TO8 header ensures smooth transmission of optical signals. TO8 (Transistor Outline 8) is an industry standard, governing the design and size of current-conducting electronic housings.

perature operation as the dark rate is reduced by over an order of magnitude. It is available with an active area of 1 mm circular diameter or 3 mm × 3 mm (square) and with two detector versions: Photon Detection Efficiency optimized or Dynamic Range optimized."

[Quoted from SensL's SPMMini datasheet February 2009 (2010-02-11), `http://sensl.com/downloads/spmmini_datasheet1.pdf`]

Note: We do have the detector with product name SPMMPC, not SPMMini, but because some rather faulty data (e.g., -30 ℃ operating temperature) and since the SPMMini1024X08A1 is the replacement, we decided to quote the SPMMini datasheet. The SPMMPC datasheet can be found here (2010-02-11): `http://www.sensl.com/pdfs/Datasheets/SPMPC_Datasheet.pdf`, dated Aug 2008.

Parameter	**Value**	**Units**	**Notes**
Spectral Range (λ)	400 – 1100	nm	
Peak Spectral Response (λ)	490	nm	See Graphs in datasheet
Breakdown Voltage at -20 ℃ (V_{br})	Typ. 27	V	See test sheet for unit shipped
Operating Voltage (V)	Typ. +2 to 3 V above V_{br}	V	
Microcell Gain	$> 10^6$	-	See Graphs in datasheet
Operating Temperature	-20	℃	
Cooling Time	10	s	From Room Temperature
Temperature Setpoint Stability	-20 ± 0.1	℃	
Max Storage Temperature	40	℃	
Magnetic Sensitivity	2	T	Demonstrated insensitive on signal output up to 2 T. Not tested above 2 T.
Supply Voltage	5 ± 0.1	V	Supplied by integrated Power Board 200 mA at normal operation, 700 mA at startup Wall mounted power supply included
Maximum Output Voltage	2	V	2 V output swing across the dynamic range of the detector with integrated Transimpedance preamplifier

Table 6.11: Key specifications for the SPMMini. (SensL's datasheet)

	Part Number				
Typical Values	SPMMini 1020X08	SPMMini 1035X08	SPMMini 3020X08	SPMMini 3035X08	**Notes**
SPM Pixel Active Area (mm)	Φ1 (diameter)		3 × 3		1 mm detector has circular active area 3 mm detector has square active area
Number of Microcells per SPM Pixel	848	400	8640	3640	
PDE (%)	5 – 20				+1 V to +4 V above V_{br}, see Graphs in datasheet
Dark Rate @ +2 V (kHz)	15	18	400	510	Measured at -20 ℃ and 0.5 p.e. threshold
CrossTalk (%)	4	7	-	-	Measured at 2 p.e. threshold
Dynamic Range	103	103	104	104	
Linear Range	102	102	103	103	
Temp. Dependence of V_{br} (mV/℃)	23				
Single Photon Pulse (ns)	5 – 10	5 – 10	10 – 15	10 – 15	Leading Edge (typ.) using TIA preamp.
Single Photon Pulse (ns)	40 – 60	40 – 60	40 – 60	40 – 60	Falling Edge (typ.) using TIA preamp.

Table 6.12: Typical values for the different SPMMini modules. (SensL's datasheet)

Figure 6.11: SensL's SPMPC. (SensL)

[More information: `http://sensl.com/products/silicon-photomultipliers/spmmini/`]

6.1.2 Hardware-Correlators

There are several hardware-correlators available but we chose to utilize the digital 4-channel-hardware-correlator "Flex03-LQ-01" from Correlator.com (`http://www.correlator.com/`). Flex03-LQ-01 is a multiple function instrument, but when used as a correlator, Flex03-LQ-01 operates as a multiple-tau correlator or a single-tau-arbitrary-delay-correlator. In addition, Flex03-LQ-01 can optionally record and save the intensity series at 100 ns and above sample times on a PC hard drive (using a USB 2.0 interface). In photon history recorder mode, the correlator transfers photon arrival time series to the host PC hard drive. The correlator is also programmable using a specific script language.

The hardware-correlator enables us to observe variations in luminosity in real time by plotting the auto- and cross-correlation functions. We use Correlator.com's correlator-specific-software in order to record data from the correlator and plot normalized correlation functions in real time.

Correlator specifications:
A. Multiple Tau modes (3 modes)
In all multiple tau correlation modes, the intensity history of both channels may be saved to the hard drive.
1. Minimum sample time 100 ns
2. Sample time increment: 12.5 ns
3. Maximum sample time: 65535 * 12.5 ns = 819 μs
4. Real time histogram is calculated.

Mode A. Single auto/cross correlator.
1. Minimum sample time: 1/640 MHz $\sim$ 1.56 ns
2. Auto or cross correlation. (AxA or AxB)
3. Total number of channels: 1120 each
4. Sample times:
5. First 64 channels : 1.56 ns
6. Next 32 channels: 2x1.56 ns
7. Sample times double every 32 channels.
8. Total of 34 segment
9. Delay times: from 1.56 ns to 13.4 minutes.
10. Shift register width: in the order of the segments 1, 1, 1, 2, 3, 4, 5, 6, 7, 8, 9, 10, 11, 12, 13, 14, 15, 32, ... 32.
11. Maximum intensity before overflow: 160 MHz within 6.666 ns, 28.3 MHz continuous.

Mode B: Dual auto/cross correlator.
1. Minimum sample time: 1/640 MHz $\sim$ 1.56 ns
2. Auto or cross correlation. (AxA, BxB, or AxB, BxA)
3. Total number of channels: 624 each
4. Sample times:
5. First 32 channels : 1.56 ns
6. Next 16 channels: 2x1.56 ns
7. Sample times double every 16 channels.
8. Total of 38 segment
9. Delay times: from 1.56 ns to 115 minutes.
10. Shift register width: in the order of the segments 1, 1, 1, 2, 3, 4, 5, 6, 7, 8, 9, 10, 11, 12, 13, 14, 15, 32, ... 32.
11. Maximum intensity before overflow: 160 MHz within 6.666 ns, 28.3 MHz continuous.

Mode C: Quad correlator.
1. Minimum sample time: 1.56 ns
2. Auto and cross correlations. (AxA, BxB, AxB, BxA)
3. Total number of channels: 304
4. Sample times:
5. First 16 channels : 1.56 ns
6. Next 8 channels: 2x1.56 ns
7. Sample times double every 8 channels.
8. Total of 35 segment

9. Delay times: from 1.56 ns to 28.6 minutes.
10. Shift register width: in the order of the segments 1, 1, 1, 2, 3, 4, 5, 6, 7, 8, 9, 10, 11, 12, 13, 32, ... 32.
11. Maximum intensity before overflow: 160 MHz within 6.666 ns, 28.3 MHz continuous.

[Quoted from Correlator.com's "Getting started with your new Flex03LQ-01 USB based Digital correlator".]

Figure 6.12: The digital 4-channel-hardware-correlator "Flex03-LQ-01".

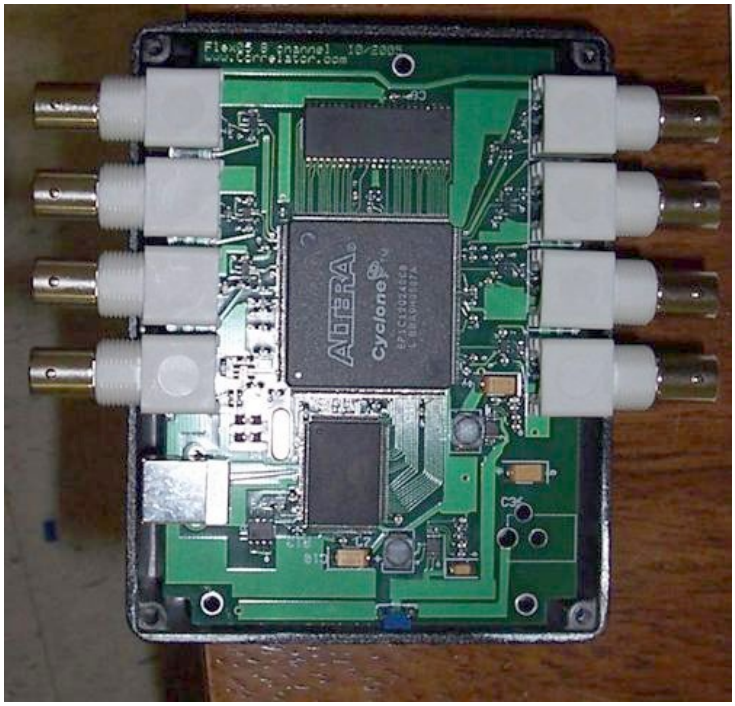

Figure 6.13: The inside of the digital 8-channel-hardware-correlator "Flex05". (Correlator.com)

6.1.3 Oscilloscope

In order to obtain the waveforms (i.e. the shape of the actual output TTL-pulse from the detectors) for the detectors, we used the digital oscilloscope "PicoScope 5203" with the software "PicoScope 6 (ver. 6.2.2.12)", both from Pico Technology (`http://www.picotech.com/`). Detailed specifications can be found on the homepage and partly in the table below.

Oscilloscope specifications	
Number of channels	2
Bandwidth	250 MHz
Maximum sampling rate:	
Real time (one channel in use)	1 GS/s
Real time (both channels in use)	500 MS/s
Equivalent time (for repetitive signals)	20 GS/s
Buffer size	128 M samples (PicoScope 5204) 32 M samples (PicoScope 5203) Shared between channels if two channels enabled
Voltage ranges	± 100 mV to ± 20 V in 8 ranges
Input coupling	1 MΩ AC/DC
Vertical resolution / accuracy	8 bits / 3 %
Timebase accuracy	50 ppm
Overload protection	CHA, CHB, External trigger ± 100 V
Triggers	
Trigger modes	Rising edge, falling edge, dual edge, alternate edges, logic level
Advanced trigger modes	Pulse width, dropout, window, delay

Table 6.13: The digital oscilloscope "PicoScope 5203"'s specifications. (PicoScope 5000 series Data Sheet)

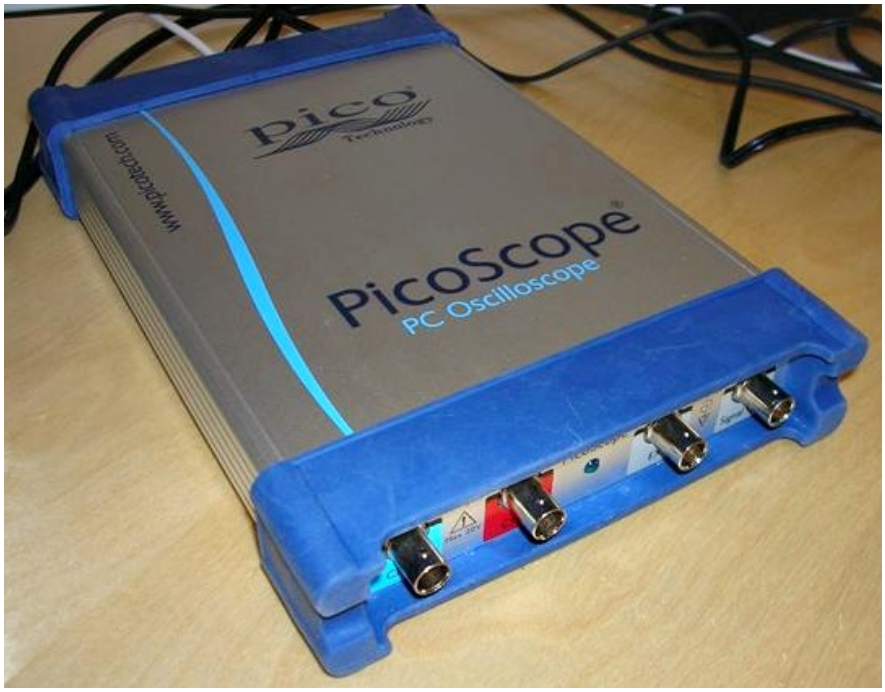

Figure 6.14: The digital oscilloscope "PicoScope 5203".

6.1.4 Power Supply

The power supply used throughout the tests, when needed, was a VOLTCRAFT Laboratory Power Supply "PS 2403 Pro".

6.1.5 Lamp and LEDs (Light Emitting Diodes)

The lamp used throughout the tests as a substitute for a white light source was a 13 W light tube with a standard 100 Hz stability rate (variations in luminosity 100 times per second).

Figure 6.15: The lamp is used as a mobile white light source, and an overview of the working area is seen.

The three LEDs (Light Emitting Diodes) used primarily for the color sensitivity tests were 5.0 mm diameter LEDs with 3 different colors: red, green and blue. These are, however, called "ULTRA RED", "ULTRA PURE GREEN" and "ULTRA BLUE", by the manufacturer and the dominating wavelengths are 625 nm, 525 nm and 460 nm respectively. However, the actual details of these LEDs are not of any significant value for the tests performed.

6.2 Test descriptions and Methods

In this section the tests that were to be carried out are presented and the methods are described.

6.2.1 SensL's PCEdu-1 Photon Counting Fundamentals Educator Pack

The objective was to utilize SensL's PCEdu-1 Photon Counting Fundamentals Educator Pack, including, among some other things, a PIN-photodiode (miniature photon counter) and a passively quenched photon counter with options to choose various modes for the quenching. The educational package was designed to introduce or enhance the user's understanding of how these rather new types of detectors work and what kind of properties they possess.

The package came with an information and guide folder (SensL PCEdu-1, Version 2.0, Rev 1.0) where different concepts, background information and properties of semiconductor photon detectors are presented. There are also a few experiments for the user to carry out after the theoretical parts had been covered. These supposedly educational experiments were what we had on the agenda for this part of the thesis. The details

for these experiments can be found in the SensL PCEdu-1 and will not be presented to any deeper extent here, see the results in section 6.3.1 for further information and explanations of why this is not done.

Figure 6.16: Essentially all the included hardware and software in SensL's PCEdu-1 Photon Counting Fundamentals Educator Pack. A few of these hardware products (the two black boxes next to the PQC and the big black box on top (the calibrated reference detector?)) seen on this picture appear somewhat unfamiliar to us. The PIN-photodiode is not visible either. The wooden box contains various light filters. (SensL, PCEdu-1 Datasheet)

[Some information about an updated version of the educational package:
`http://sensl.com/products/photon-counting-systems/edu-notes/`,
Archived version: `http://www.sensl.com/pdfs/Archived_Products/PCEdu1_Datasheet.pdf`]

6.2.2 Photon count rate and coaxial cable length dependence for Auto- and Cross-correlation functions

This is basically the main experiment for this thesis. What we wanted to examine was whether the autocorrelation and cross-correlation functions could become significantly altered due to various photon count rates and variations in coaxial cable length. In other words we wanted to answer questions like; "How does the photon count rate affect the autocorrelation and cross-correlation functions?" and "Is there a limit for the coaxial cable length where the original pulse is altered and/or blended enough to not be identified at the other end?", i.e. "Can you use a long coaxial cable directly from the detector at the telescope to a remote location with a hardware-correlator or should the electric pulse be converted back to a photon pulse and sent in fiber cables for further analysis?".

We had quite an arsenal of coaxial cables to our disposal. They were all carefully measured and paired based on length in order to enable cross-correlation of 2 (or more) detectors using cables with similar lengths. The cables were of lengths ranging from 1 m and up to about 18 m. For each set of cables and each set of detectors, auto- and cross-correlation functions were obtained using the hardware-correlator "Flex03-LQ-01" and its software from Correlator.com. All correlations were run 10 times for 100 s and each setup (see table below) in Mode A, single auto/cross (see section 6.1.2 for details) in order to maintain maximum detail. Notice that the single cross mode requires 2 detectors but not necessarily the same detector model or manufacturer, although similar characteristics should be preferred. No such tests were recorded for this

thesis however.

	id Quantique id100-50	**MPD PDM series PD1C0B**	**PerkinElmer SPCM-100-PQ**	**PerkinElmer SPCM-AQR-14**	**SensL PCD-Mini0100**	**SensL SPMPC**
Cable length (m)	1(d), d+1, d+2, d+4, d+6, d+10, d+18	1, 2, 4, 6, 10, 18, 4+1+1, 6+4, 2/1	1, 10, 18	1, 10, 18	1(d), d+10, d+18	1(d), d+10, d+18
Single Auto	x	x (not 2/1)	x	x	x	x
Single Cross	x (not d+18)	x (not 18)		x (not 18)		x (not d+18)
Voltage (V)	Default	Default	As specified in datasheet	Default	28.3, 29.3, 30.3, 31.3	Default
Extra	B-detector	B-detector, LED		B-detector		B-detector

Table 6.14: The performed test combinations for each detector. Note: **d** is short for default (cable supplied by manufacturer or cable with "special" connection due to requirements for the detector, it is still $\sim$ 1 m though), **+** indicates a simple cable joint, **2/1** means 2 m cable on A-channel and 1 m cable on B-channel, **B-detector** indicates that a test with the otherwise B-channel detector was tested (alone) in a Single Auto test with default or 1 m cable in A-channel and **LED** indicates that a Single Auto test to distinguish the normal white source from the 3-color LEDs for each color at 5 and 10 MHz with 10 m cable was carried out.

We should state that during the tests it was quite often required to adjust the lamp or detector position in order to remain somewhat close to the targeted count rate. If a correlation run with a detector was suddenly considered too far from target, either by its own (inexplainable behaviour, cable tension, self-heating, etc.) or during adjusting (a minor repositioning (< mm) can equal several kHz), it was discarded and rerun. When using several detectors (single cross mode) the manual adjusting process can be very tedious, which may result in many runs being discarded.

The large amount of test combinations as well as running 10 times for 100 s, for every setup, resulted in almost *3000* supervised runs for this part of the thesis' experiments, many of which are not possible to fit within this thesis.

6.2.3 Color sensitivity

This is a small side-experiment exercised in order to evaluate the color sensitivity for the detectors. This experiment is considered as of lesser scientific significance since it was not possible to properly calibrate the luminosity output from the LEDs, thus the actual intensity was unknown. The experiment does, however, indicate if there exists some sort of significant sensitivity difference between the detector models and manufacturers.

The experiment was, however, performed using our 3-color-LED-setup and using the lowest non-zero intensity possible for our setup, isolating the detector from stray light using an integrating sphere (see Figure 6.17) and noting the difference when turning on the LEDs with different colors; red, green and blue. The integrating sphere's purpose is to spread the light uniformly.

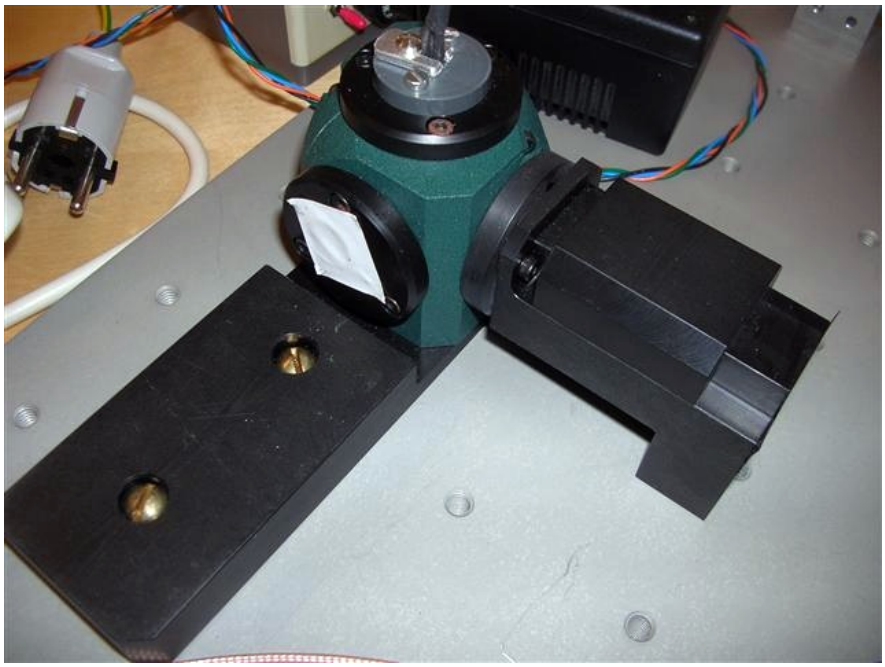

Figure 6.17: The integrating sphere with the three LEDs mounted from the top, here with no detector present. The control-box for the LEDs is partly visible in the top of the image and consists of three switches (on-off for each color) and a variable potentiometer for each color.

6.2.4 SensL operating voltage vs. photon count rate

How does the maximal photon count rate depend on the operating voltage? This is what we wanted to answer by making a quickly performed experiment. This is, however, of quite large importance when you, e.g., take into account that operating voltage has rather big influence on several properties, e.g., heat development. Let us say that you have a celestial source from which you only receive a photon rate of 1 MHz, why would you then want the operating voltage at a level that permits 10 MHz instead of lowering it to a level with an, e.g., 3 MHz maximum count rate when higher operating voltage might result in unwanted effects and putting unnecessary strain on the detector?

This experiment was done using the SensL PCDMini0100, the Power Supply "PS2403 Pro" and the 100 Hz tube light. It was a very straight forward experiment consisting of basically trying to move the light source until some sort of maximum was reached. The maximum count rate was noted at operating voltages varying from 27.3 to 31.3 V with 0.5 V intervals. Because of the breakdown voltage being at 27.3 V, there is no point in setting the operating voltage any lower.The detector's intensity saturation limit has to be taken into account for this kind of experiment; if the detector is saturated by excess light the count rate is lowered in "self-defense" if the actual photon flux is increased further.

6.2.5 Dark count evaluation

The detector-manufacturers usually state some kind of value for typical or maximum dark counts in the data sheets but generally do not include any specific details on the conditions they were tested in. It is also very likely that detectors, despite same model and manufacturer, possess different values in dark counts. We decided to make our own test to make an estimate on the dark count for each detector.

We used long coaxial cables through a specially designed tube into the room next door in order to submerge the test environment in complete darkness. In the test room, two detectors at a time were connected to the hardware-correlator (Flex-LQ-03) in the other room. The room lights were, of course, switched off and the detectors were blocked from any possible stray light and from each other as seen in the figure below, during the evaluation.

The tests were carried out both in a consecutive test form and in a more sporadic test form. Both were done in 10 minute runs in order to keep the intensity history recording resolution. For example this means a consecutive test could consist of 6×10 minute runs after each other and the sporadic tests consist of 10×10 minutes at various unspecified times during the day, without turning the detectors off.

Exceptions in the test methods were made for PerkinElmer's SPCM-100-PQ (only 6×10 minutes consecutive runs) and SensL's PCDMini0100 and SPMPC (tested while isolated from light in the integrated sphere).

Figure 6.18: The dark count test environment.

6.2.6 Dead time estimation

By using the digital oscilloscope and setting it up in infinite persistence mode, i.e. pulses accumulate on the same graph, we were able to estimate the dead times for each detector. The result was obtained by manually checking the time value for when the first pulse after the triggering pulse was able to occur. For example we would use the pulse voltage trigger value of 1 V at time 0 and check the time value for the next pulse at 1 V.

6.3 Results

6.3.1 SensL's PCEdu-1 Photon Counting Fundamentals Educator Pack

Unfortunately this package brought us more trouble than education but let us get into some details.

We followed the experiments' step-by-step guide, starting with Experiment 1 – "Photodiode, Avalanche and Geiger-Mode" in the PCEdu-1 Version 2.0 Rev 1.0 guide. The first part consisted of a Dark Current test, where the SensL PQC (Passive Quench Circuit) was set to 0 Ω and 1 V reverse bias was placed on the diode. Using an ammeter, the current was supposed to be recorded and then noted for different reverse bias. However, nothing sensible was to be recorded on the ammeter. We even tried reversing the circuit and submitting the PQC for low light intensities but again nothing.

We assumed that perhaps something is just unclear with the rather poorly described circuit setup in the PCEdu-1 guide so we proceeded to a latter part in Experiment 1, where the Geiger-mode was to be tested. In this part it was supposed to be possible to use an oscilloscope in order to see the actual pulse output. We used the digital oscilloscope "PicoScope 5203" but got no sensible output, i.e. no signal.

After the above attempts the manufacturer SensL was contacted and some advised tests were performed but with no particular success, resulting in an RMA (Return Merchandise Authorization) request, i.e. the PQC module was sent back for analysis and possible repair. It turned out that the PQC module was not giving any sensible output; the detector and the PQC board both had to be changed, this time free of charge. It was then sent back to us.

The PQC module was now tested again, this time starting with the Geiger-mode test; the oscilloscope gave us a signal and the PQC module was thought to be working. The pulse output was however of the appearance of a positive peak and then exponential decrease towards zero. In the guide there is a picture of a negative peak the exponential "increase" towards zero. No particular intimidating thought was put on this though; it was only considered that it could possibly be that a reverse of the circuit would reverse the pulse form.

Perhaps the module finally was working but when resuming the Experiment 1, where we left off before the RMA, things unfortunately took a turn for the worse again. But this time, to insure that the circuit was at least setup as described in the manual, we had a coworker who is experienced with electronics taking a look at it. It was confirmed to be in order but we did not get any sensible output on the ammeter at first. Therefore we tried to reverse the circuit, with the implication mentioned above in mind, and we were able to get some output on the ammeter, although surprisingly high values (μA was expected). We thought that now we had it setup correctly and that the PQC module finally worked. The coworker left and the experiment was resumed. The result is presented in the table below.

Reverse bias (V)	**Dark Current (mA)**
1	10.74
5	160

Table 6.15: Results of the dark-current test in Experiment 1.

While noting the current at 5 V, 160 mA, it suddenly showed 0 A (or some value in nA). Everything was shut down and we tried the Geiger-mode experiment again but got no signal in the oscilloscope. The PQC module was giving no sensible output, again. After the approximately 15 minutes of "fame" it was done for, a second time.

After this second breakdown we decided to focus on the other experiments in this thesis and let this one be. Even if the first repair was of no charge there were still quite a few expenses in shipping costs as well as in time consumption. Unfortunately not much understanding nor experience was gained with the SensL's PCEdu-1 Photon Counting Fundamentals Educator Pack.

6.3.2 Photon count rate and coaxial cable-length dependence for Auto- and Cross-correlation functions

Because of the huge number of resulting figures, we decided to move most of them to the Appendix A. We do, however, present a few representative figures in this section with a bit of discussions. Since we did not measure any actual distinct events of short time scale fluctuations, we ended up with figures of auto- and cross-correlation functions which represent a form of detector signature.

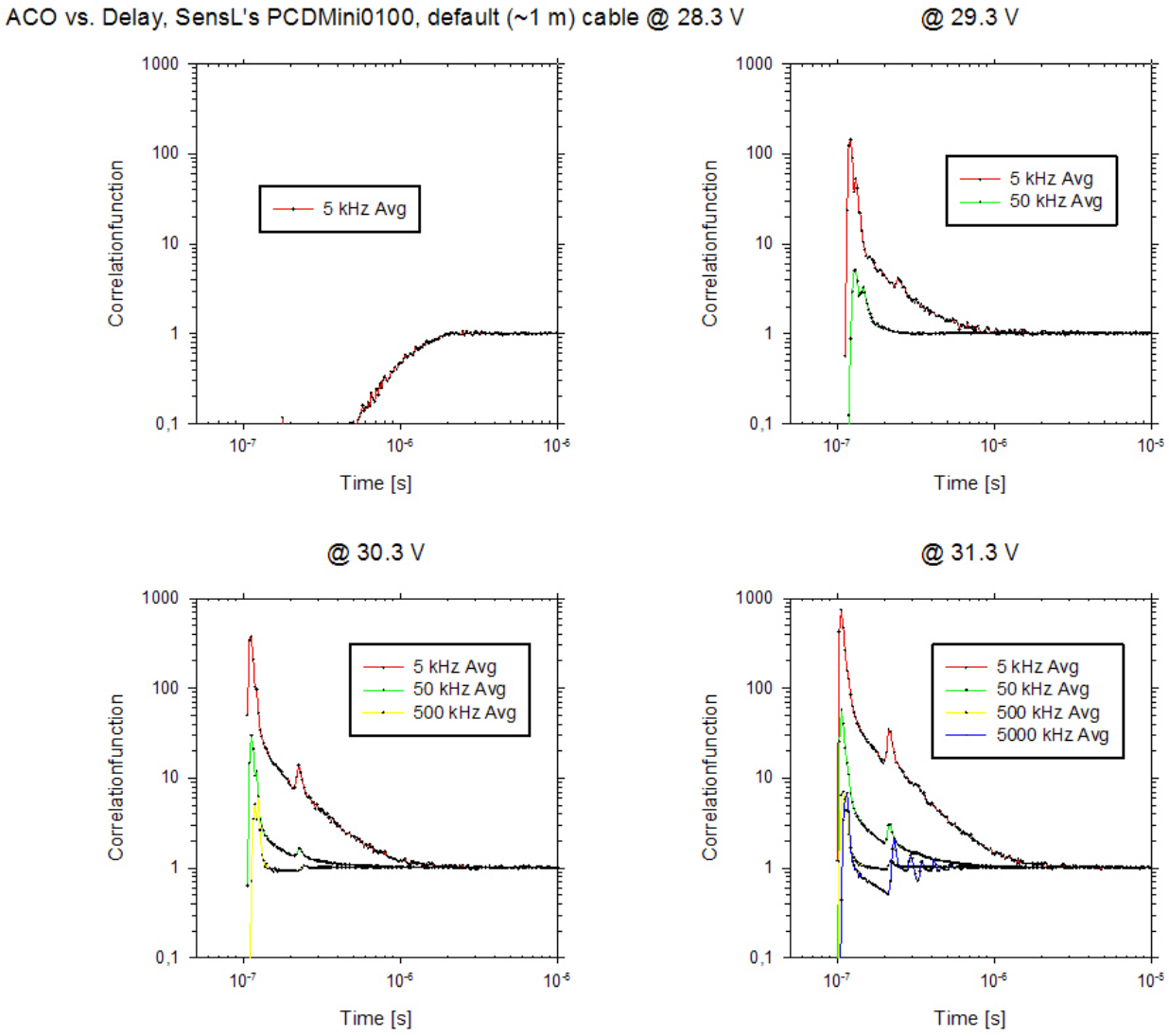

Figure 6.19: Average normalized autocorrelation function vs. time delay for the **SensL's PCDMini0100** at various photon count rates and operating voltages using the default (1 m) cable. Note that both axes use logarithmic scaling.

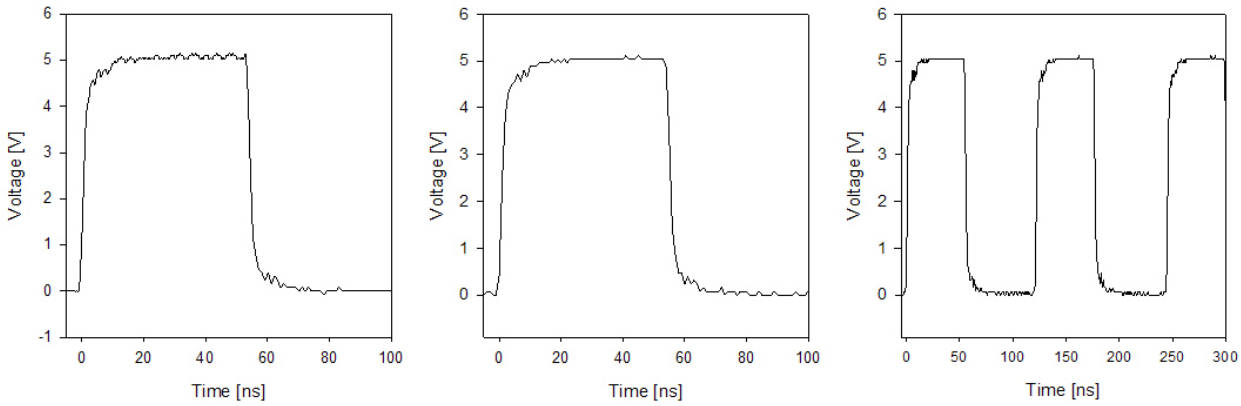

Figure 6.20: Somewhat randomly picked waveforms (pulse shape) in the digital oscilloscope "Picoscope 5203" for some count rates, using **SensL's PCDMini0100** with the default (1 m) cable. From left to right: 5 kHz, 500 kHz, and 5000 kHz.

We picked the two figures above because SensL's PCDMini0100 was the only detector which we adjusted the operating voltage on, thus we can spot some voltage dependencies. And we also see how the waveform for the pulses is extremely well defined, very close to square pulses. We can also compare these pulses with the figure below for PerkinElmer's SPCM-AQR-14, where we encounter a lot of "ringing" (a form of resonance in the cable) for some reason. It should be said that it is possible to get a cleaner waveform if some form of signal damper or adder is used, but the only detector that clearly suffered from "ringing" was PerkinElmer's SPCM-AQR-14. It is not just for SensL's PCDMini0100 that pulses are well-defined, the same applies for SensL's SPMPC. So apparently SensL has managed to get that right.

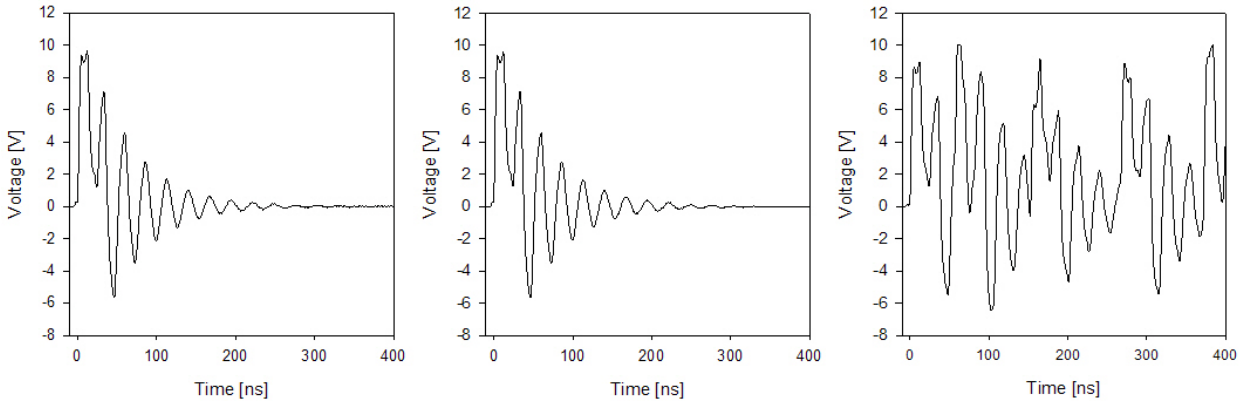

Figure 6.21: Somewhat randomly picked waveforms (pulse shape) in the digital oscilloscope "Picoscope 5203" for some count rates, using **PerkinElmer's SPCM-AQR-14** with a 1 m cable. From left to right: 5 kHz, 500 kHz, and 10000 kHz.

In Figure 6.19 we looked at shorter timescales for auto-correlation functions but we may also look at longer timescales for the auto- and cross-correlation functions. In the two figures below we can identify the tube lamp fluctuations at $\sim$ 100 Hz and we also see that different detectors differ quite a lot. But to determine exactly what is a detector signature and what is merely noise, is very difficult (especially for short runs, like these of 10 averaged 100 s runs).

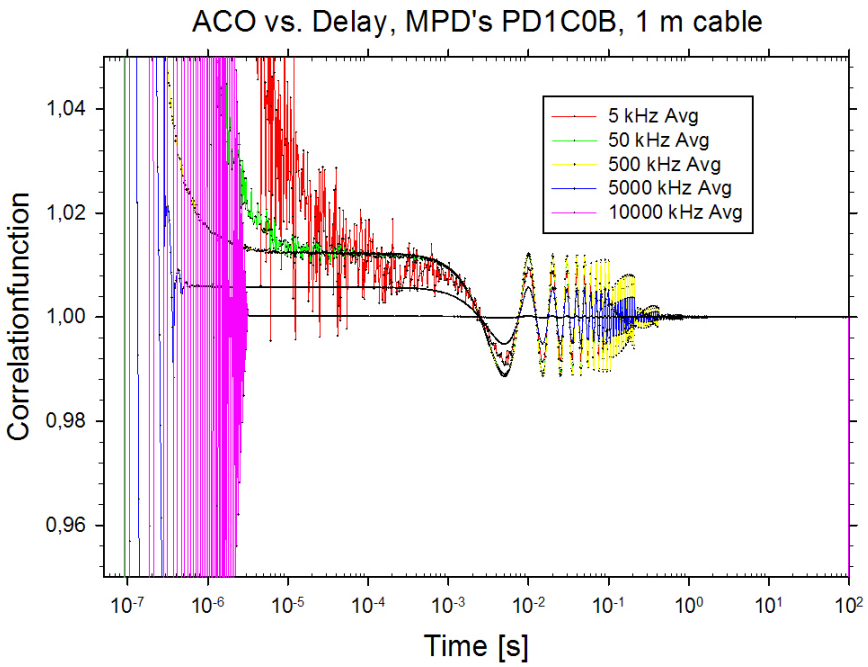

Figure 6.22: Average normalized autocorrelation function vs. time delay for the **MPD's PDM series, PD1C0B** at various photon count rates using 1 m cable. Note that y-axis uses linear scaling and x-axis uses logarithmic scaling.

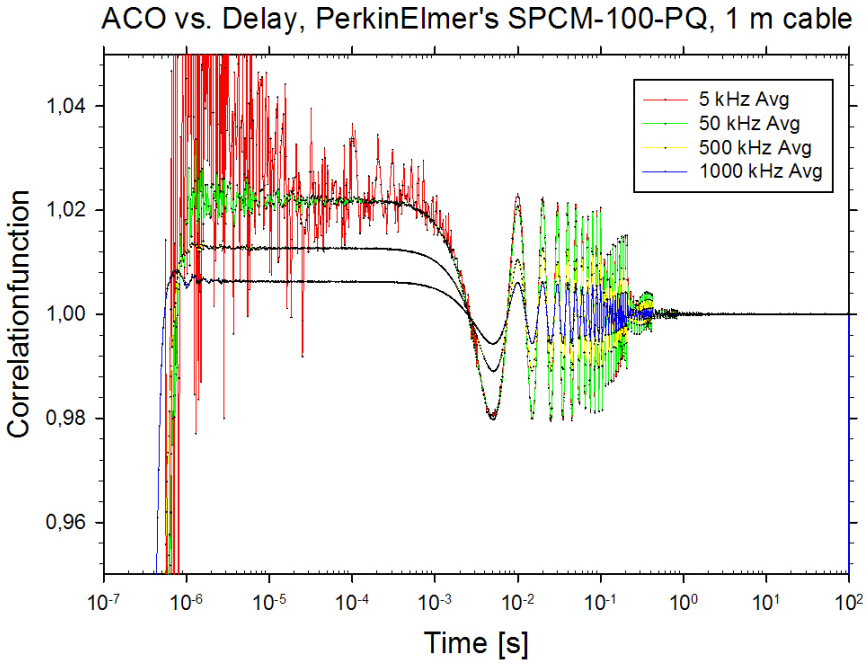

Figure 6.23: Average normalized autocorrelation function vs. time delay for the **PerkinElmer's SPCM-100-PQ** at various photon count rates using 1 m cable. Note that y-axis uses linear scaling and x-axis uses logarithmic scaling.

We can also look at cross-correlation, where 2 (or more) detectors are used and the incoming data compared in real-time – if they correlate with each other, the signal is enhanced. The result for a single

cross-correlation run for id Quantique's id100-50 at both short and long time scales can be seen in the two figures below.

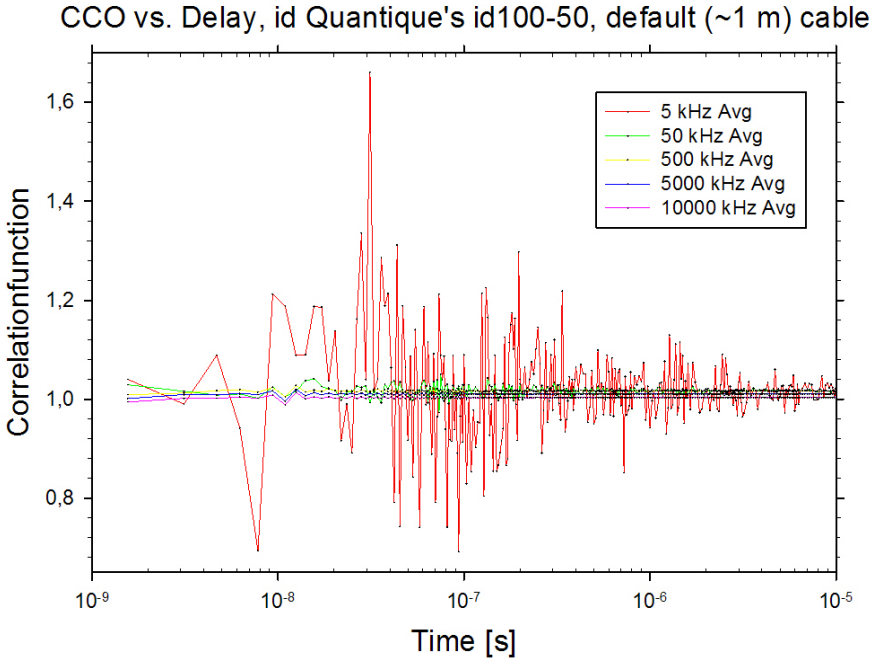

Figure 6.24: Average normalized crosscorrelation function vs. time delay for **id Quantique's id100-50** at various photon count rates using default (1 m) cables. Note that y-axis uses linear scaling and x-axis uses logarithmic scaling.

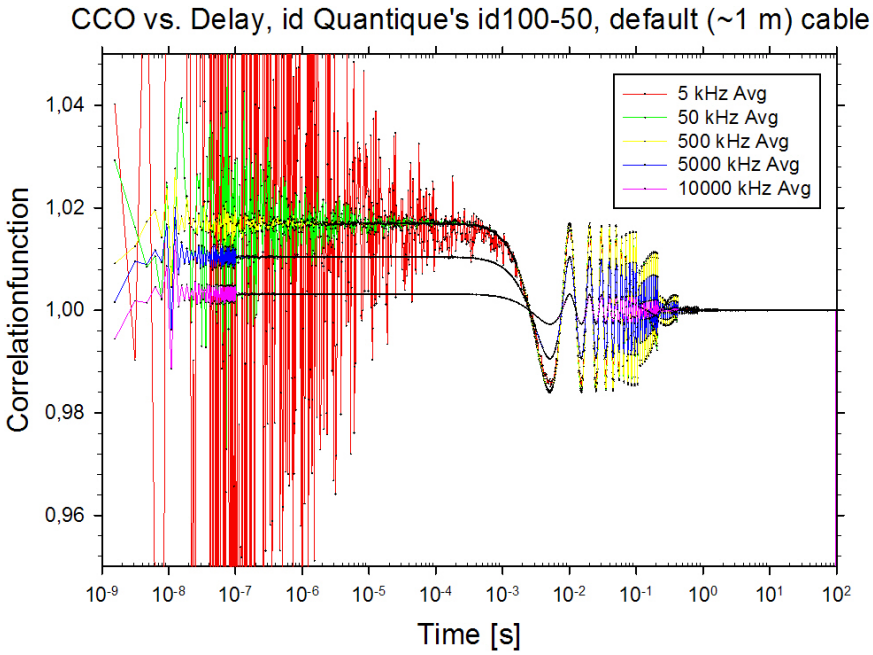

Figure 6.25: Average normalized crosscorrelation function vs. time delay for **id Quantique's id100-50** at various photon count rates using default (1 m) cables. Note that y-axis uses linear scaling and x-axis uses logarithmic scaling.

We did generally choose one detector to be channel A and the other to be channel B (assuming we had 2 detectors of the same model). This meant that all single auto-correlation runs were done using one of the detectors, while the other "B-detector" was used for cross-correlation. But we did however do a quick test in a setup to use the "B-detector" in a single auto-correlation evaluation test and thus we can compare detector signatures from the same manufacturer using the same detector model. The detectors that perhaps differ the most are our two SPMPC detectors from SensL, as shown in the two figures below.

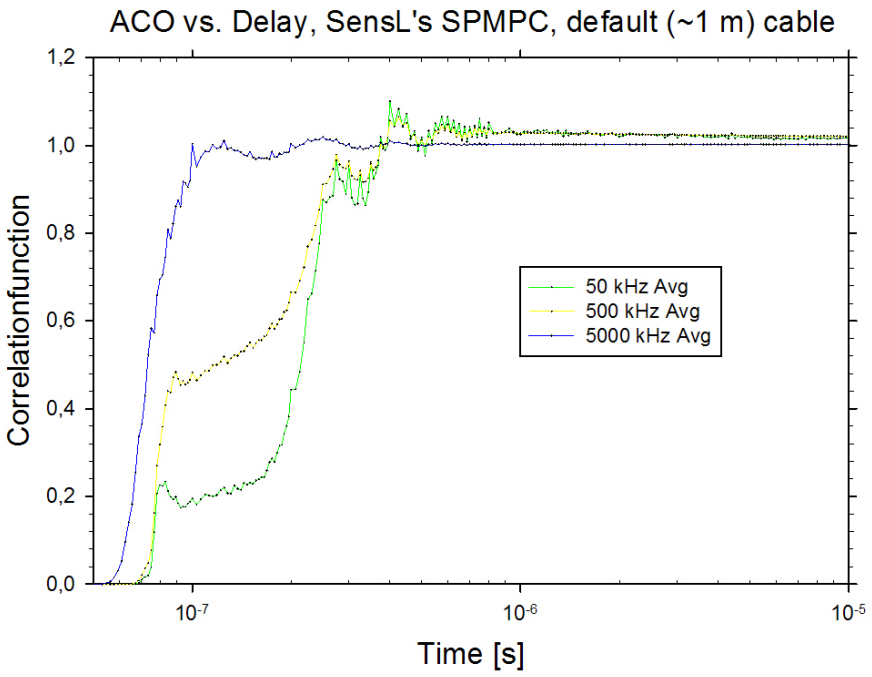

Figure 6.26: Average normalized autocorrelation function vs. time delay for the **SensL's SPMPC** at various photon count rates using default (1 m) cable. Note that y-axis uses linear scaling and x-axis uses logarithmic scaling.

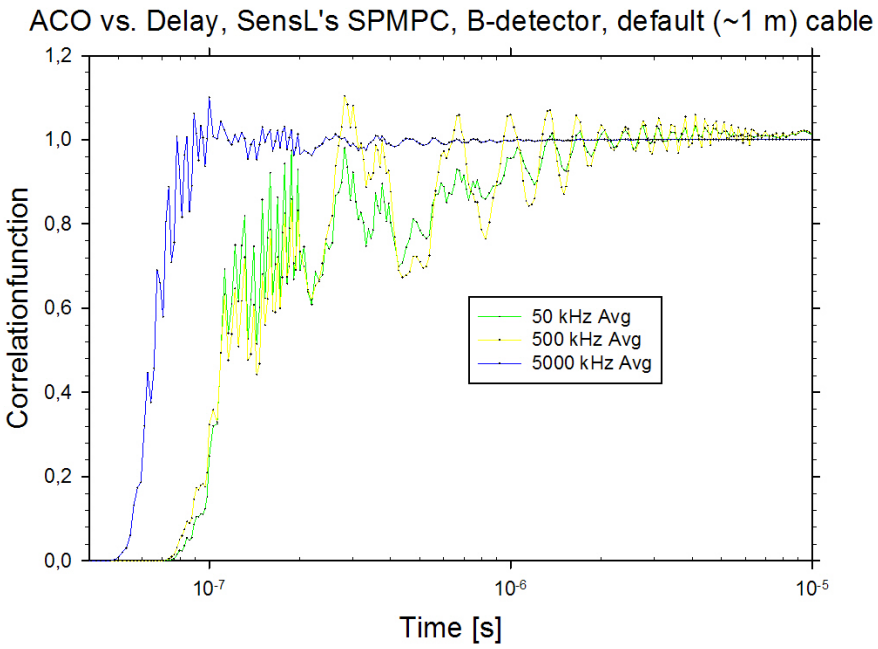

Figure 6.27: Average normalized autocorrelation function vs. time delay for **SensL's SPMPC**, using the 2nd detector (normally used for the B-channel in the hardware-correlator), at various photon count rates using default (1 m) cable. Note that y-axis uses linear scaling and x-axis uses logarithmic scaling.

We did not find any particular or significant differences for auto- or cross-correlation functions when it comes to cable length dependence. But we did see that the waveforms change quite drastically in some cases. They went from showing a distinct identifiable pulse to a chaos of overlapping pulses. Using a infinite persistence mode (let the pulses accumulate and color them depending on how often they appear on same place), it is in most cases possible to identify the original pulse. We also did not see any significant effects of using cable joints. Note that when our setups use cable joints, we indicate it by a + sign at the cable lengths. We therefore refer to the Appendix A to check for cable length and cable joint dependences, as well as a more complete set of figures for the different detectors with the results for this evaluation.

6.3.3 Color sensitivity

LED color	**id Quantique id100-50**	**MPD PDM series PD1C0B**	**PerkinElmer SPCM-100-PQ**	**PerkinElmer SPCM-AQR-14**	**SensL PCD-Mini0100**	**SensL SPMPC**
Dark (kHz)	0.02	0.45	0.225	0.3	0.85	11
Red (kHz)	380	3590	450	14500	5450	4700
Green (kHz)	920	5350	230	14900	7300	5700
Blue (kHz)	2200	7030	380	14800	8050	6000

Table 6.16: The results from the color sensitivity tests.

We see that PerkinElmer's SPCM-AQR-14 was saturated at all colors and not stable at all because of that as well as self-heating (seen as rapid decrease in count rate).

6.3.4 SensL Operating Voltage vs. Photon Count Rate

Voltage (V)	27.3	27.8	28.3	28.8	29.3	29.8	30.3	30.8	31.3
Count rate (Hz)	0	0.9	15	49	307	1437	3754	6355	8703

Table 6.17: The results from the maximum count rate test for SensL's PCDMini0100.

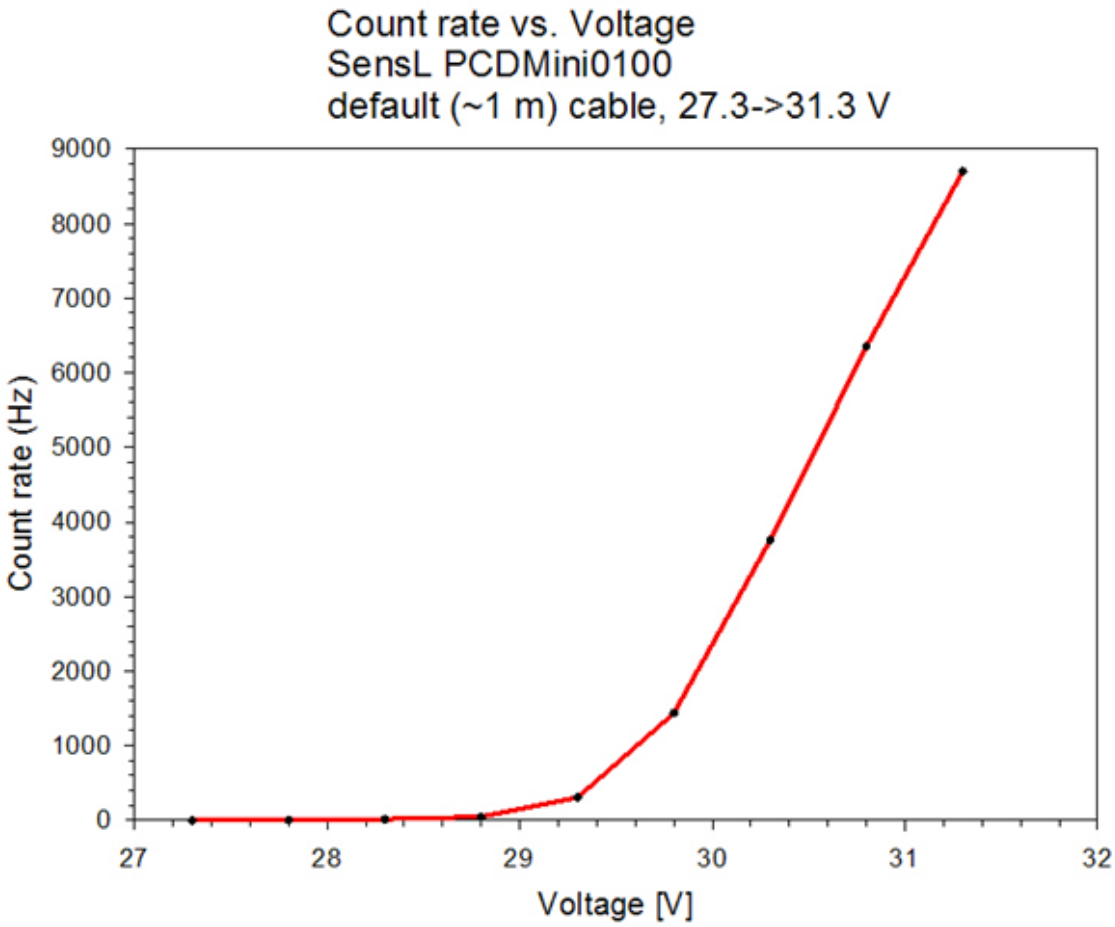

Figure 6.28: The results from the maximum count rate test for SensL's PCDMini0100.

6.3.5 Dark count evaluation

	id Quantique id100-50	MPD PDM series PD1C0B	PerkinElmer SPCM-100-PQ	PerkinElmer SPCM-AQR-14	SensL PCD-Mini0100	SensL SPMPC
Dark Count (C) (Hz)	12	425	187	221	808	10719
Dark Count (NC) (Hz)	12	424	-	221	824	-

Table 6.18: The results from the dark count evaluations. Note: **C** – Consecutive, **NC** – Non-Consecutive. The first value was removed from every data series when producing these average values because of an obviously faulty recording by the software, for some of the runs. All values are rounded to the closest integer value.

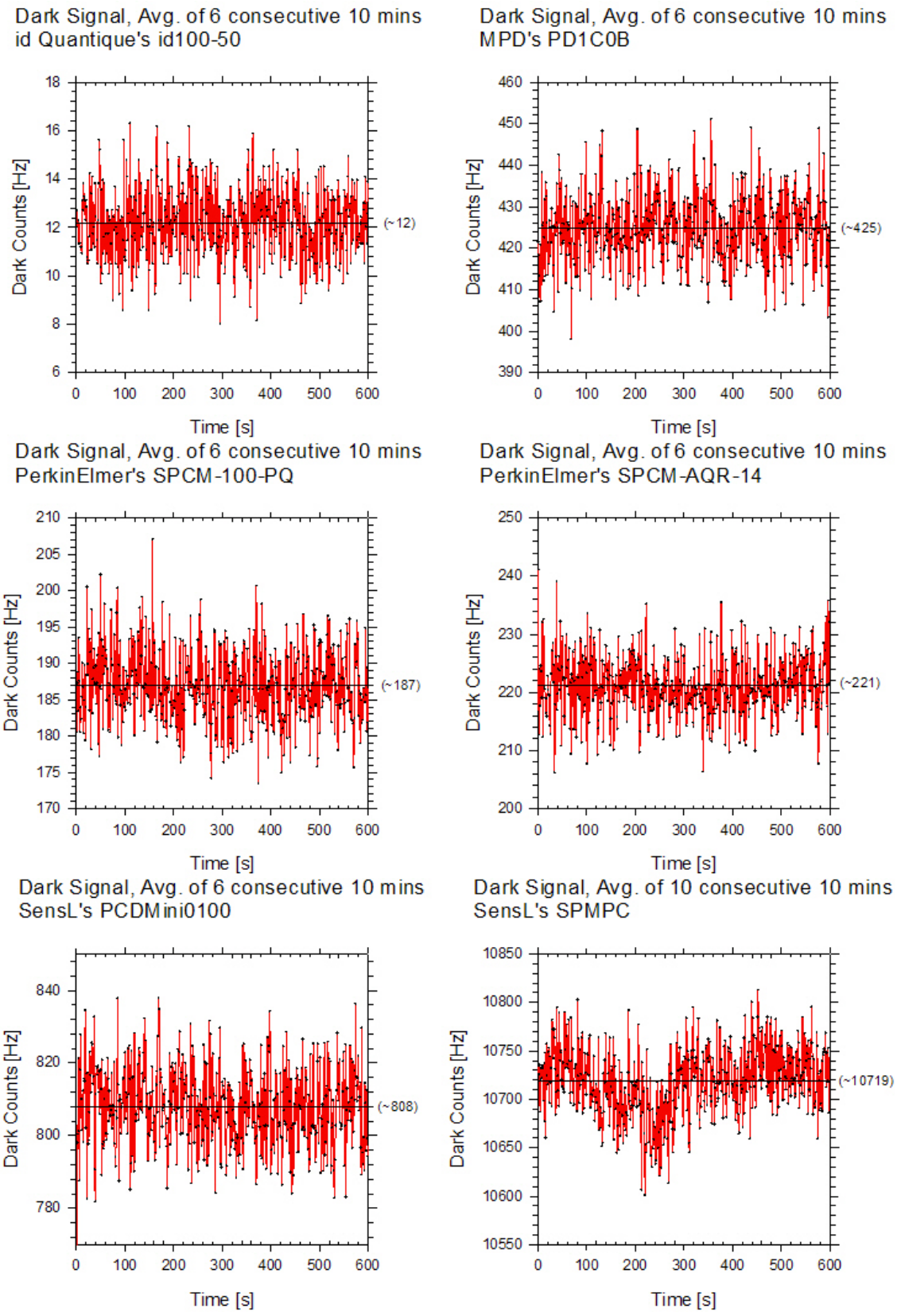

Figure 6.29: The dark count evaluation results for all detectors in consecutive runs. The line representing the mean for each dark signal includes the first value, which in some cases is faulty.

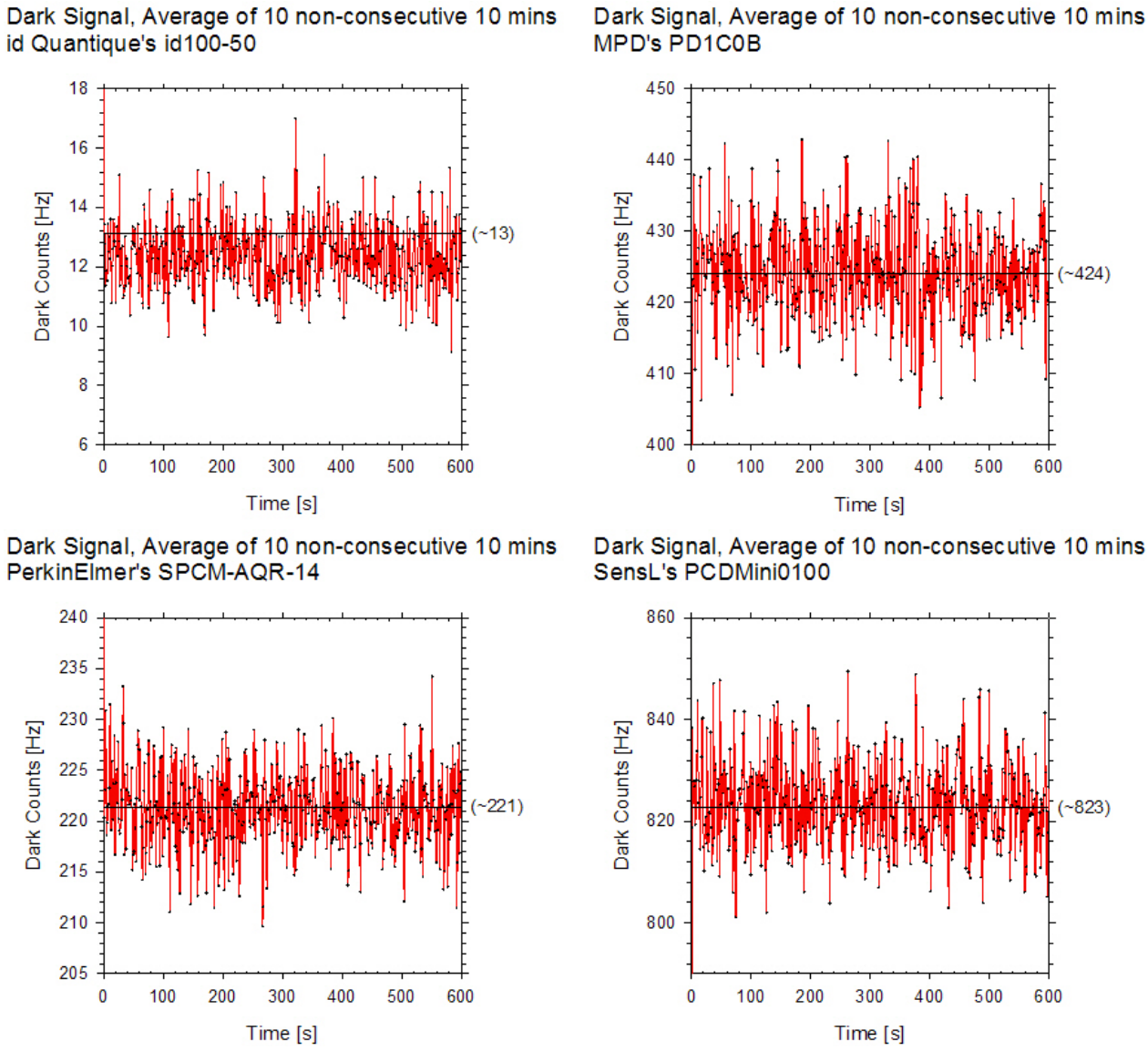

Figure 6.30: The dark count evaluation results for four of the detectors in non-consecutive runs.

We see that the dark count evaluation results were consistent when we compare consecutive and non-consecutive runs, which indicate a rather stable dark signal. The only exception may be SensL's PCDMini0100 where we see a difference of 16 Hz (counts per second). This detector was, however, tested in another environment, involving the integrating sphere, which may possibly have caused some stray light reaching the detector in the longer time frame, which the non-consecutive runs exposed the detector to. A mere variation of only 16 photons per seconds is not enough to draw any conclusions of plausible inconsistencies in the dark signal.

We also noted that PerkinElmer's SPCM-AQR-14 self-heating problem meant having to wait some time in order to let it stabilize, but because it was kept in darkness it did not warm up as much as when a light source is present and therefore it stabilized faster.

6.3.6 Dead time estimation

	id Quantique id100-50	MPD PDM series PD1C0B	PerkinElmer SPCM-100-PQ	PerkinElmer SPCM-AQR-14	SensL PCD-Mini0100	SensL SPMPC
Dead time (ns)	43	94	230	50 – 60	105 – 108	55 – 60

Table 6.19: Estimation of dead times, obtained from the digital oscilloscope "Picoscope 5203", for the detectors.

It is worth to mention that id Quantique's id100-50 was extremely consistent when measuring at various count rates.

6.3.7 Encounters of weird and unwanted behavior

In this section we present some of the strange behavior we encountered throughout the testing.

Pretty much all detectors:
We did encounter some rather weird jumps, both upward and downward in intensity during a run, even though nothing appeared to have changed. This happened with most of the detectors that were able to run at high count rates (> MHz) but was nothing of big concern. We see in the figure below that the jump appears synchronized, both detectors at the same time, which indicates that something in the environment changed and the detectors are not to blame. When such a jump occurred we decided to rerun if our goal was to stay somewhat stable at, e.g., 10 MHz as the situation was for the figure below.

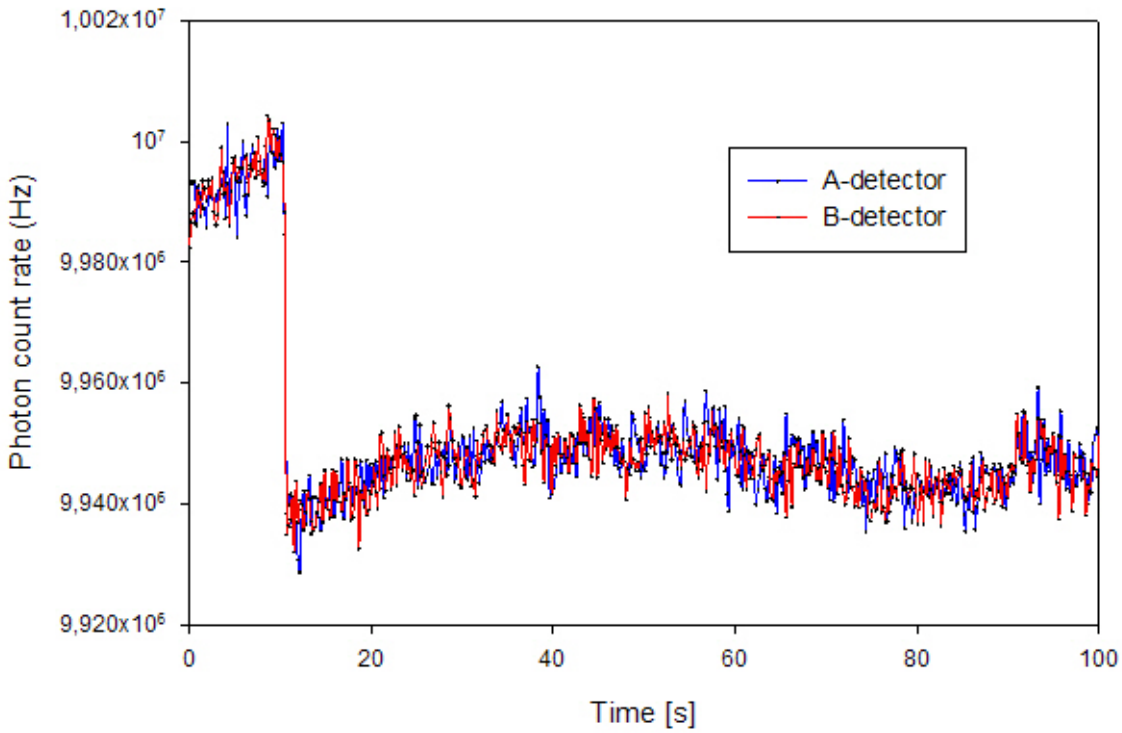

Figure 6.31: A weird jump during a run at 10000 kHz using id Quantique's id100-50 detectors.

PerkinElmer's SPCM-100-PQ casing heat-up:
The longer the SPCM-100-PQ detector was in operation, the more it seemed to heat up, at least when inspecting the casing. We did not notice any particular influences on the measurements though but if memory serves us right, we did after a long run (some hours) somewhat lose contact with the detector or at least were required to let it rest for some time in order to proceed with the measurements.

PerkinElmer's SPCM-AQR-14 self-heating:
When the SPCM-AQR-14 detector is in operation, it heats up, a lot. This can be felt on the casing and seen on the photon count rate, which drops rapidly if it is high (some MHz). This made itself present especially in the color sensitivity evaluation (see section 6.3.3), where for the other detectors we could basically read a somewhat stable value right away, while SPCM-AQR-14's count rate would start at a high value (14 – 15 MHz) and then drop rapidly. We therefore decided to note the value shortly after the exposure had begun (about 5 seconds). At lower count rates the drop was smaller but still noticeable until it had stabilized. The issue of self-heating in this case can most likely be solved with external cooling of the detector, e.g., using a heat-sink. We assume that the actual cooling of the diode is working.

SensL's SPMPC warm-up and B-detector count rate leaps:
Unlike the SPCM-AQR-14 self-heating issue, the SPMPC detector rather possessed a longer than expected warm-up time, i.e. stabilization time (almost 30 min). The difference of the two detectors is that SPMPC needed this time to stabilize pretty much regardless of the initial photon count rate, while SPCM-AQR-14 heats up with increasing photon count rate. Both of our SPMPC detectors possessed this warm-up behavior, i.e. long time to stabilize before use.

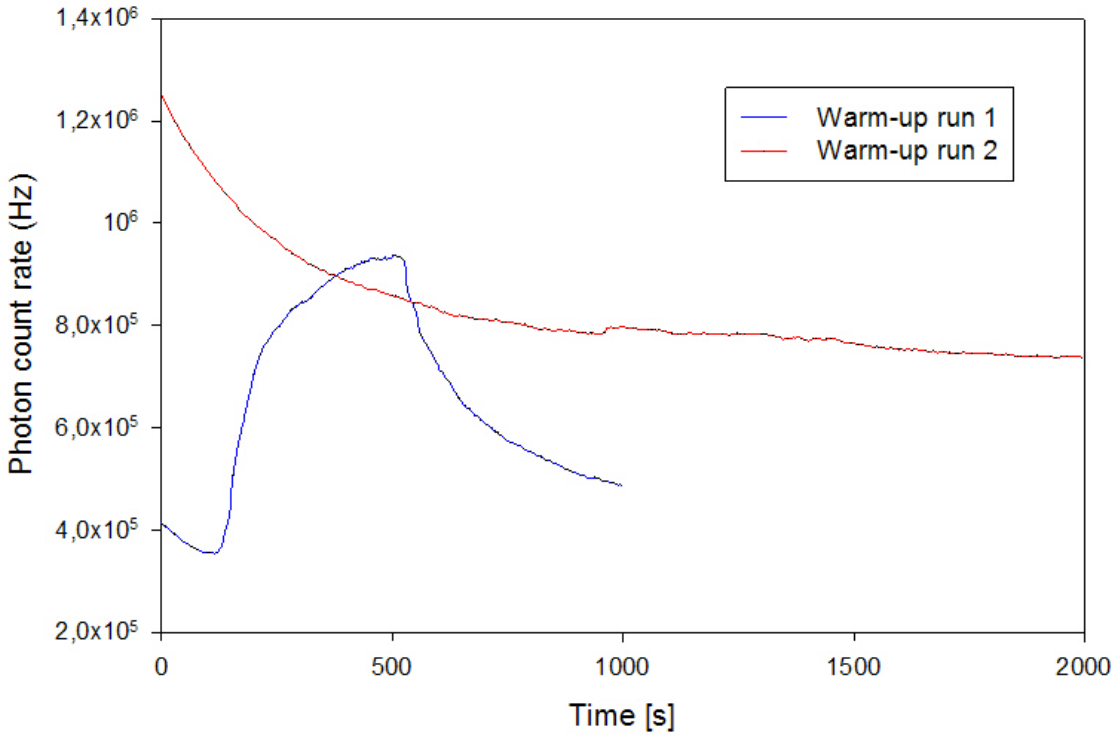

Figure 6.32: Two warm-up curves using SensL's SPMPC.

The blue (bottom) one shows extraordinary weird behavior in the warm-up phase but was not investigated in high detail to ensure it was not something in the environment which caused it to rise, although nothing seemed to have changed. The red (top) curve shows a normal warm-up, which we would expect to see with

the SPMPC. It does render any critical measurements obsolete until the detectors have stabilized though. As we had two detectors of this kind available, both were evaluated even though we focused more on one of the detectors which usually got the A-channel in the hardware-correlator, thus called A-detector. By analogy, we called the other detector, mostly present in cross-correlations, B-detector. This detector was also tested and for the SPMPC B-detector we encountered some very peculiar leaps in photon count rate. Suddenly it could jump to 14 – 15 MHz and "lock" itself there for some time. Since the specified maximum count rate is around 5 – 6 MHz, it is clear that something is not quite all right here. Even covering the detector in darkness, while in this state, has no effect. After some time it restores itself though and acts like nothing has happened. The issue can also be solved by disconnecting the device and turning the power on again, but then you may have to wait almost 30 minutes again for it to stabilize.

Even though we could not nail down the cause for the sudden jump, we do have some form of intuition of that it has something to do with rapid and big changes in intensity. We could not reproduce this at will though, and the other detector which was exposed to the same light source and intensity was not affected. The actual physical reason for the high count rate could be that the pixels, which there are 848 of, may have come into a rare state of triggering each other (optical crosstalk), in a somewhat "infinite loop" fashion.

The hardware-correlator "Flex-LQ-03":
For the very observant reader, you might notice a colored line heading downwards towards zero at almost 100 seconds in the ACO and CCO figures. This is, in this case, nothing of interest with the detector in mind. It is merely a result of the correlator software not registering the last value at exactly 100 s during a 100 s run. Depending on the run time, the software records at different time interval resolution. On a 100 s run it starts with 1.5625 ns and next value at 3.1250 ns but as time goes on the time difference gets larger and end with 97.3078 s, 98.9855 s, 100.6632 s or actually the software adds values up to 429.4963 s with zero values for some reason. The last time coordinate with a proper correlation function value in the graphs above is rather surprisingly 97.3078 s. The intensity history also suffers from these weird time interval bins; it starts at 0 s and has approximately 478 time intervals (varies $\sim \pm 2 - 3$ for unknown reasons) almost equally sized. For a 100 s run this means starting at 0 s and ending at 100.034149 s using intervals of approximately 0.21 s. This scaling of time recording intervals can cause big problems if you want high resolution also on longer runs (which may reduce noise) or long delay times (slow fluctuations) but on the other hand, both the detectors and the hardware-correlator are designed for short time scales. For the longer time scales there are other instruments. Provided you obtain some DLL-files from Correlator.com for the hardware-correlator, the software can of course be custom built as well.

7 Conclusions

The detectors from SensL did unfortunately bring some bad statistics into our detector count. When we first tested SensL's PCDMini0100 it did not give any sensible output and it was then sent back to the manufacturer and we received a repaired one. When we later tried to follow the instructions in the PCEdu-1 Photon Counting Fundamentals Educator Pack, we also encountered a not so pleasant experience of non-functionality. Even after a repair we were not able to get it right and it broke again, leading to us abandoning the PCEdu-1. We also encountered some weird behavior on one of the SPMPC detectors, where it could jump and lock itself into 14 – 15 MHz all of a sudden. So perhaps the statistics speak against SensL but the detectors in general were otherwise very consistent and reliable. The waveforms for SensL's PCDMini0100 (and SPMPC) are the cleanest of all detectors and are almost ideal square waveforms, which is very impressive and almost somewhat unbelievable.

When it comes to the other detectors, PerkinElmer's SPCM-100-PQ and SPCM-AQR-14 both suffered from some warm up issues, and the latter also showed problems of "ringing" in the waveforms. MPD's PDM series, PD1C0B showed good stability and consistency throughout the evaluations. There are almost no special remarks, good or bad, to be made for MPD's detectors, they performed well but did not shine as much as, e.g., SensL's detectors on the waveforms. The same can be said about id Quantique's id100-50, but with a minor additional note that the actual devices feel physically unstable and plastic. This made them more difficult to handle and adjust during the experiments, and it may create a need for modification for some applications where heat disposal for the device is very critical. No noticeable issues with heat during our runs with the id100-50 were detected though.

For all the detectors we noted that no significant cable length or cable joint dependencies were noticeable, except for the waveforms which, in some cases, were greatly distorted because of overlapping pulses when using longer cable lengths. The original pulse shape was still possible to extract in most cases though.

We could see the voltage dependence for maximum count rates for SensL's PCDMini0100, where everything turned out as expected with one exception, for the last value at 31.3 V, which we expected to be a bit higher in order to get a better shaped exponentially increasing curve. It is just a minor difference though, and the numbers would surely change slightly if the experiment was repeated.

For the dark count evaluation we saw that all the detectors were pretty stable, no matter if the measurements were performed consecutively or non-consecutively. We did not see any tendencies for discrete dark count levels, for any of the detectors, which some readers may be aware of, have been encountered by a few other APD users on very rare occasions. The only thing to make a remark about here is rather the hardware-correlator "Flex-LQ-03" and its software, which together mixed up values between the channels at the very start of the run and caused some weird peaks. These were easily identified and removed prior to creating the tables and figures, but is still of grave concern. Have some other values have been incorrectly recorded or swapped between channels?

The final test, "Dead time estimation", did turn out quite consistent with what the manufacturers themselves had stated (that is, if they had stated some value).

All in all, the field of High Time Resolution Astrophysics (HTRA) is really getting a push forward with the development of the Avalanche Photodiodes (APDs) and the various hybrid detectors, as well as by some of the new CCDs (EMCCDs and L3CCDs). The information flow is huge and increases by the minute. Some early versions of APD Arrays have arrived and more are on the way. Everything is set for many years of interesting study as we take another step towards better understanding of the Universe.

A good site to follow the advancements on is `http://www.htra.ie/`.

7.1 Acknowledgments

The experimental work was carried out in the optics laboratories of Lund Observatory, during 2009. I would like to thank my tutor, Dainis Dravins, for helping me to get started with the project as well as assisting whenever help was needed. Torbjörn Wiesel also deserves thanks for the general fixing and for providing assistance with the practical setups, concerning rigging and electricity. And thanks to the staff at Lund Observatory who directly or indirectly made this thesis possible, and to Fredrik Wallinder, at the time at Örebro University, for introducing me to my tutor, Dainis Dravins.

Bibliography

[1] D. Renker, "Geiger-mode avalanche photodiodes, history, properties and problems", Nuclear Instruments and Methods in Physics Research, Section A 567, 48-56 (2006). 11

[2] R. C. Bless, J. W. Percival, L. E. Walter, and R. L. White, "High Speed Photometer Instrument Handbook" ver. 3.0, (1992). 14, 15

[3] R. C. Bless, E. E. Richards, A. Bosh, J. F. Dolan, J. L. Elliot, M. Nelson, J. W. Percival, E. L. Robinson, M. Taylor, G. W. Van Citters, and R. L. White, "The Hubble Space Telescope's High-Speed Photometer", Publications of the Astronomical Society of the Pacific 111, 364-375 (1999). 14

[4] E. W. Dunham, "The Optical Design of HIPO: A High-speed Imaging Photometer for Occultations", in "Airborne Telescope Systems II", Proceedings of the SPIE, vol. 4857, 62-72 (2003). 15

[5] Hamamatsu Photonics K.K., "Photomultiplier tubes - Basics and Applications", Third Edition, Hamamatsu Photonics, Electron Tube Division, (2006). 3, 4

[6] V. S. Dhillon et al., "ULTRACAM: an ultra-fast, triple-beam CCD camera for high-speed astrophysics", Monthly Notices of the Royal Astronomical Society 378, 825-840 (2007). 16, 19

[7] S. Beard, A. Vick, D. Atkinson, V. Dhillon, T. Marsh, S. McLay, M. Stevenson, and C. Tierney, "The ULTRACAM camera control and data acquisition system", in "Advanced Telescope and Instrumentation Control Software II", Proc. SPIE, vol. 4848, 218-229 (2002). 17

[8] R.W. Romani, A.J. Miller, B. Cabrera, and E. Figueroa-Feliciano, "First Astronomical Application of a Cryogenic Transition Edge Sensor Spectrophotometer", The Astrophysical Journal, vol. 521, L153-L156 (1999). 23

[9] T. Saab, S. R. Bandler, K. Boyce, J. A. Chervenak, E. Figueroa-Feliciano, N. Iyomoto, R. L. Kelley, C. A. Kilbourne, F. S. Porter, and J. E. Sadleir, "Optimizing Transition Edge Sensors for High-Resolution X-ray Spectroscopy", in "24th International Conference on Low Temperature Physics - LT24", AIP Conf. Proc. vol. 850, 1605-1608 (2006). 23

[10] G. Kanbach, A. Stefanescu, S. Duscha, M. Mühlegger, F. Schrey, H. Steinle, A. Slowikowska, and H. Spruit, "OPTIMA: A High Time Resolution Optical Photo-Polarimeter", in "High Time Resolution Astrophysics", Astrophysics and Space Science Library, vol. 351, 153-169; Berlin: Springer (2008). 25, 26

[11] V. F. Shvartsman, I. N. Bernstein, G. M. Beskin, V. N. Komarova, V. L. Plokhotnichenko, M. Yu. Popova, and A. V. Zhuravkov, "Superfast Photometry with MANIA Complex", in "Astronomical Data Analysis Software and Systems V", Astronomical Society of the Pacific Conference Series vol. 101, p. 428 (1996). 27

[12] G. Beskin, V. Bad'in, A. Biryukov, S. Bondar, G. Chuntonov, V. Debur, E. Ivanov, S. Karpov, E. Katkova, V. Plokhotnichenko, A. Pozanenko, I. Zolotukhin, K. Hurley, E. Palazzi, N. Masetti, E. Pian, L. Nicastro, C. Bartolini, A. Guarnieri, A. Piccioni, P. Conconi, E. Molinari, F. M. Zerbi, N. Brosch, D. Eichler, A. Shearer, J.-L. Atteia, and M. Boer, "FAVOR (FAst Variability Optical Registration) - A Two-telescope Complex for Detection and Investigation of Short Optical Transients", Il Nuovo Cimento C, vol. 28, p.751 (2005). 27, 28

[13] T.W. Murphy, Jr., E.G. Adelberger, J.B.R. Battat, L.N. Carey, C.D. Hoyle, P. LeBlanc, E. L. Michelsen, K. Nordtvedt, A. E. Orin, J.D. Strasburg, C.W. Stubbs, H.E. Swanson, and E. Williams, "APOLLO: the Apache Point Observatory Lunar Laser-ranging Operation: Instrument Description and First Detections", Publications of the Astronomical Society of the Pacific 120, 20-37 (2008). 34

[14] D. Dravins, C. Barbieri, V. Da Deppo, D. Faria, S. Fornasier, R. A. E. Fosbury, L. Lindegren, G. Naletto, R. Nilsson, T. Occhipinti, F. Tamburini, H. Uthas, and L. Zampieri, "QuantEYE. Quantum Optics Instrumentation for Astronomy", OWL Instrument Concept Study, ESO document OWL-CSR-ESO-00000-0162, 280 pp. (2005). 14, 34, 36, 37, 38

[15] K. H. Mantel, H. Barwig, and S. Kiesewetter, "The MEKASPEK Project - a New Step towards the Utmost Photometric Accuracy", in "Stellar photometry - Current techniques and future developments", proc. IAU Coll. No. 136, p.172; Cambridge: Cambridge University Press (1993). 40

A Appendix: Auto- and Cross-correlation functions and waveforms

A.1 id Quantique's id100-50

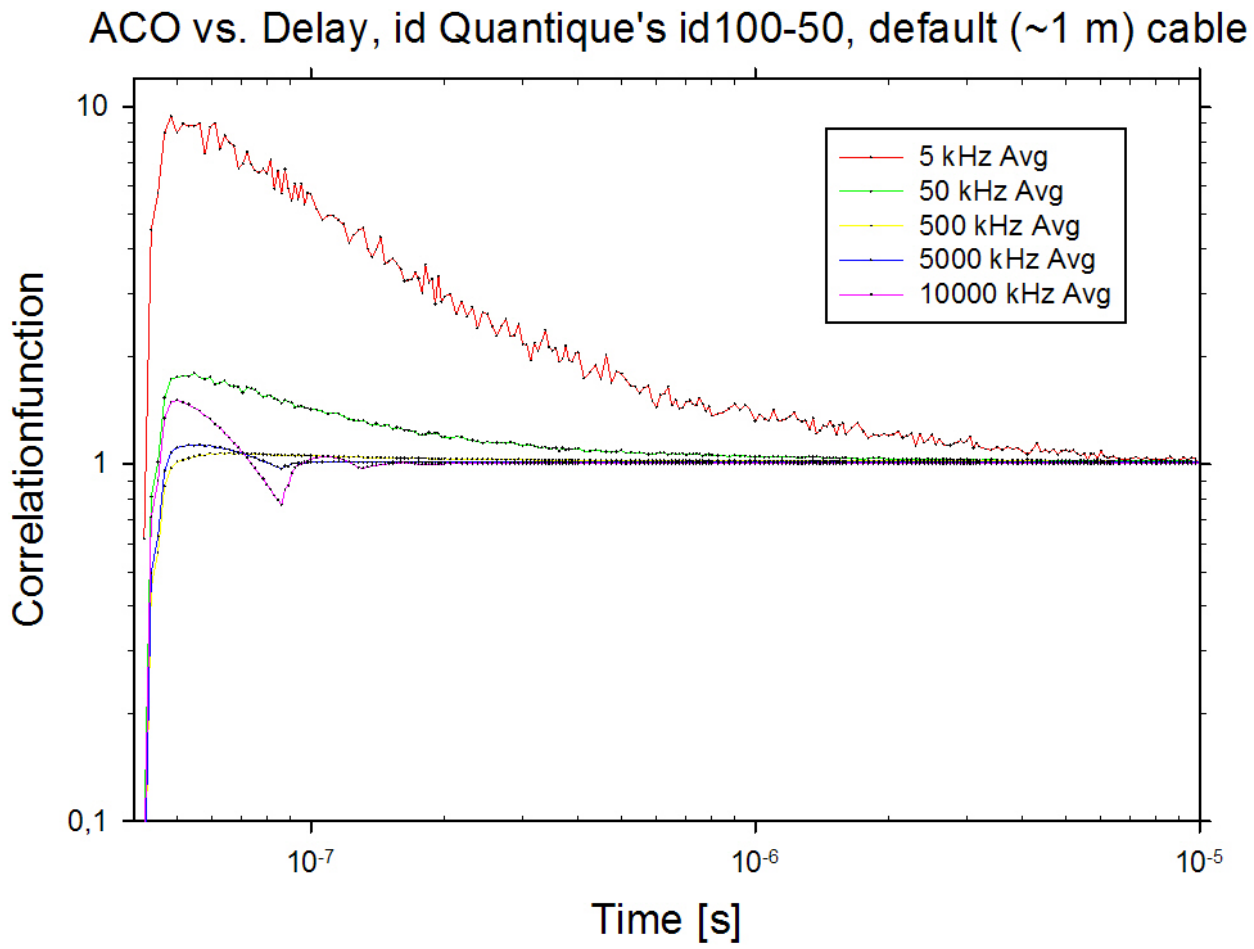

Figure A.1: Average normalized autocorrelation function vs. time delay for **id Quantique's id100-50** at various photon count rates using default (1 m) cable. Note that both axes use logarithmic scaling.

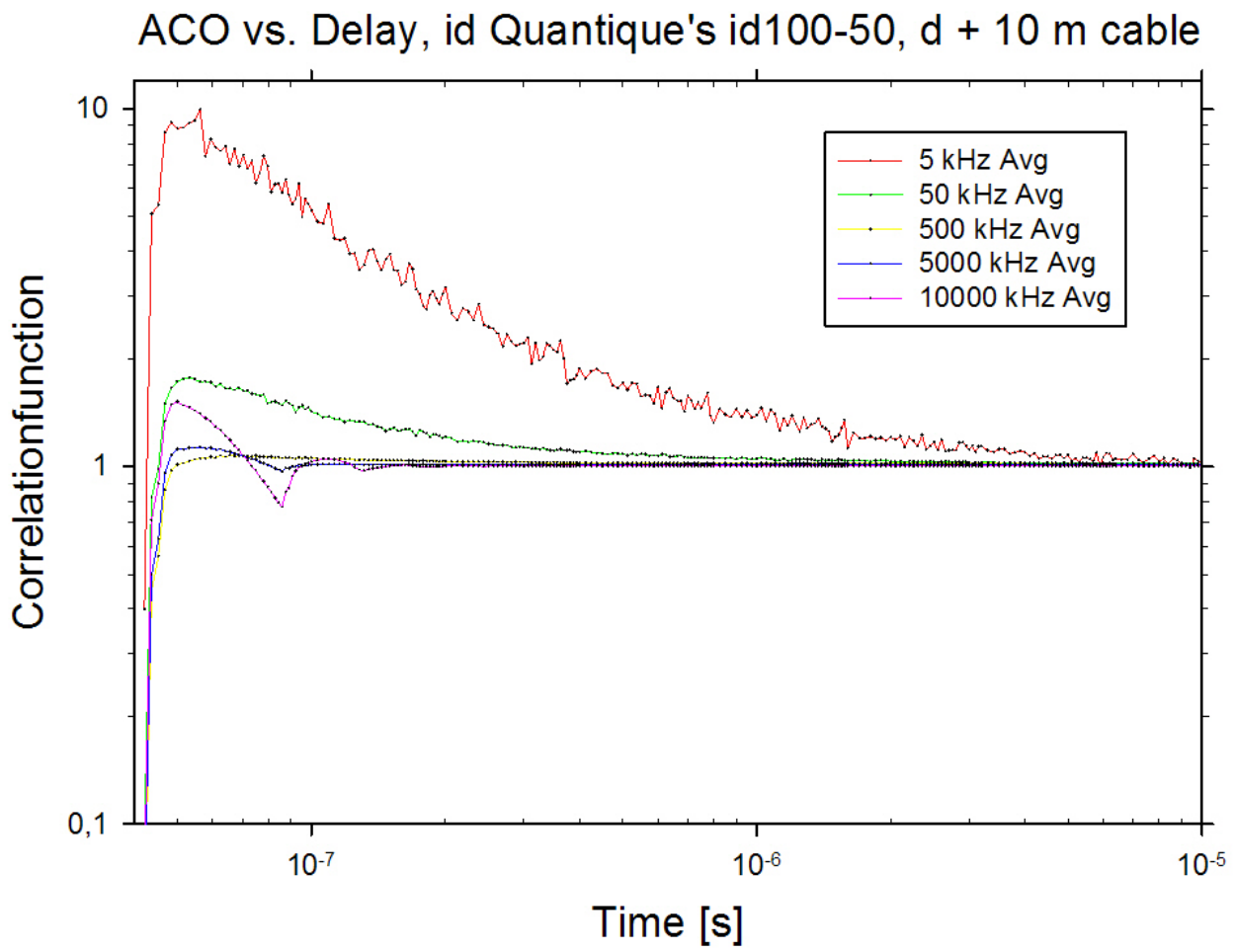

Figure A.2: Average normalized autocorrelation function vs. time delay for **id Quantique's id100-50** at various photon count rates using default (1 m) + 10 m cable. Note that both axes use logarithmic scaling.

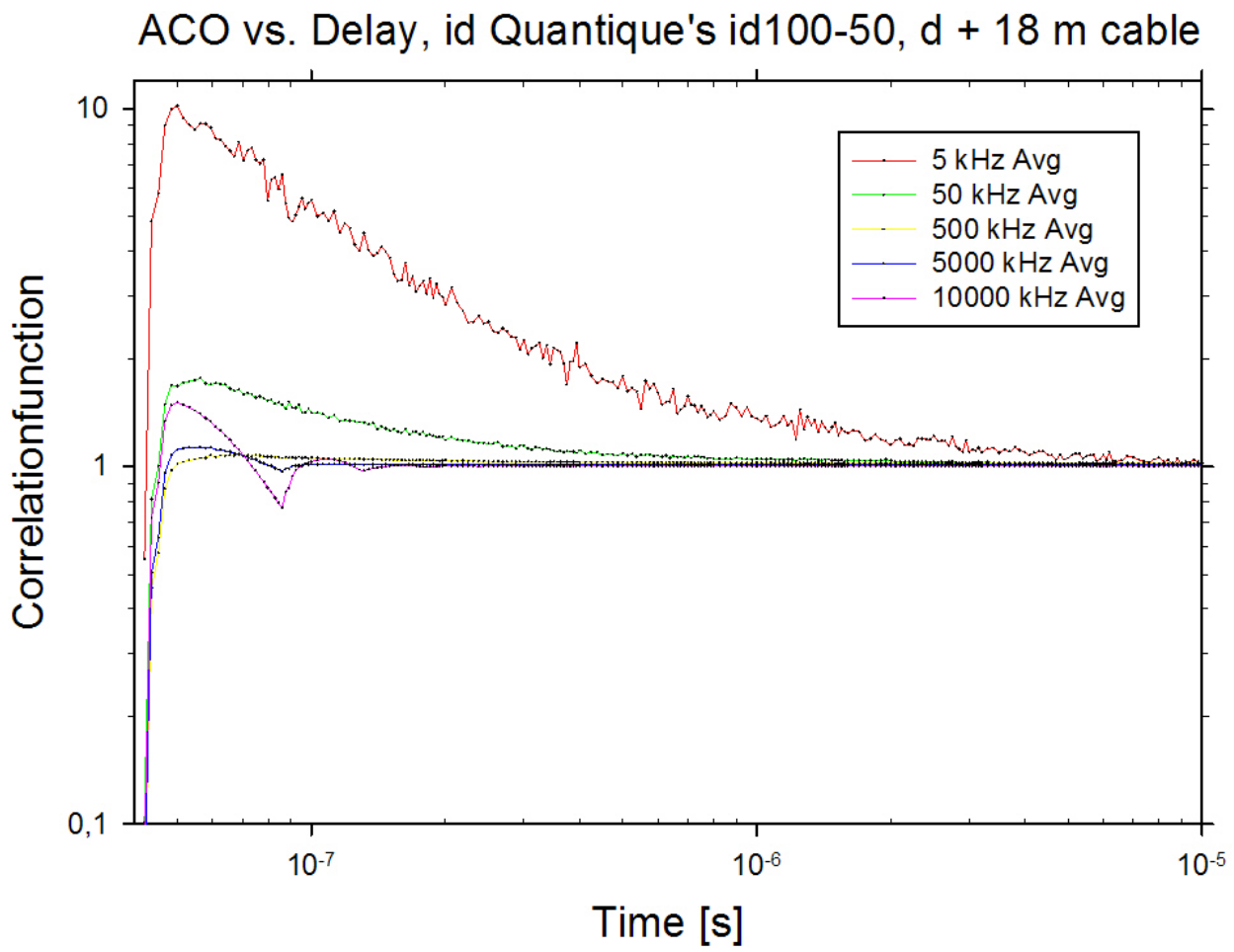

Figure A.3: Average normalized autocorrelation function vs. time delay for **id Quantique's id100-50** at various photon count rates using default (1 m) + 18 m cable. Note that both axes use logarithmic scaling.

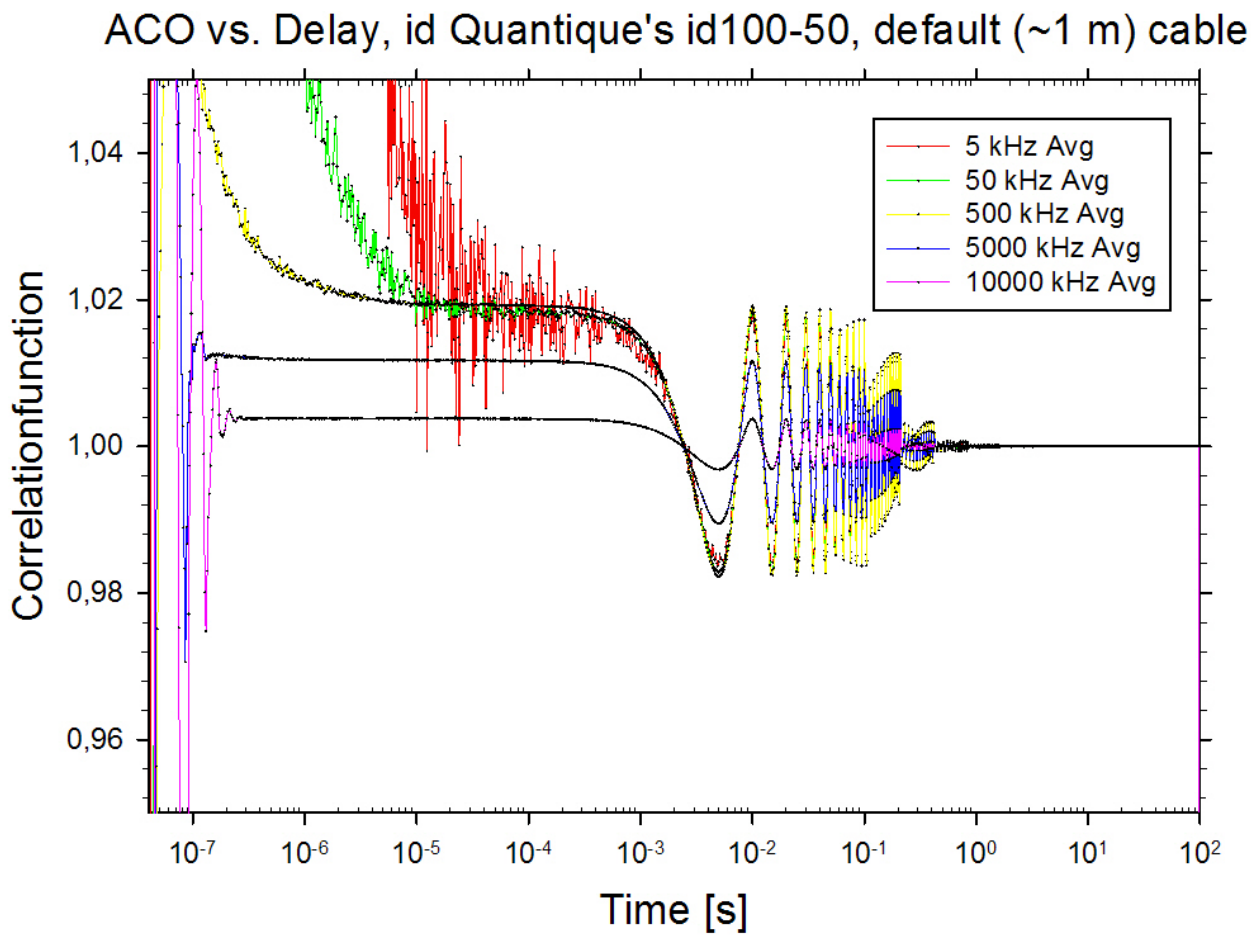

Figure A.4: Average normalized autocorrelation function vs. time delay for **id Quantique's id100-50** at various photon count rates using default (1 m) cable. Note that y-axis uses linear scaling and x-axis uses logarithmic scaling.

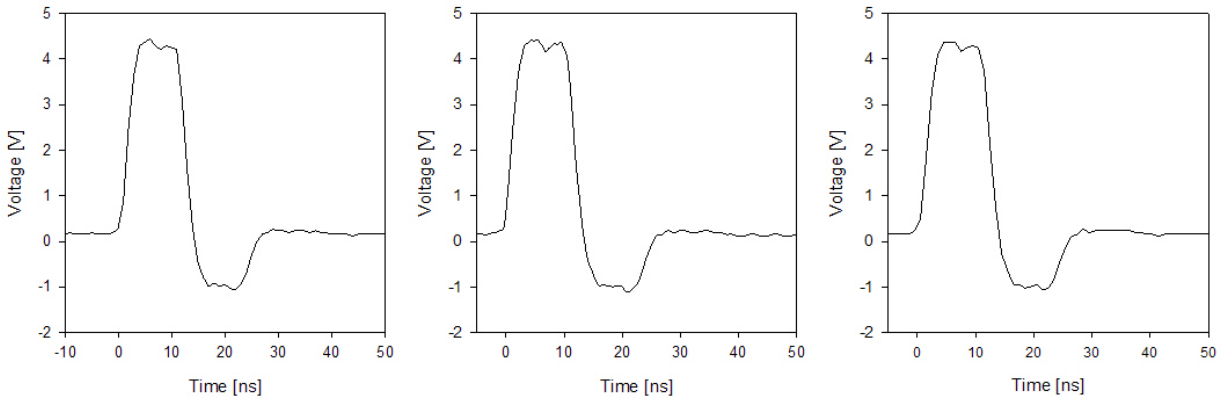

Figure A.5: Somewhat randomly picked waveforms (pulse shape) in the digital oscilloscope "Picoscope 5203" for some count rates, using the same setup as in the previous figure. From left to right: 5 kHz, 500 kHz, and 10000 kHz.

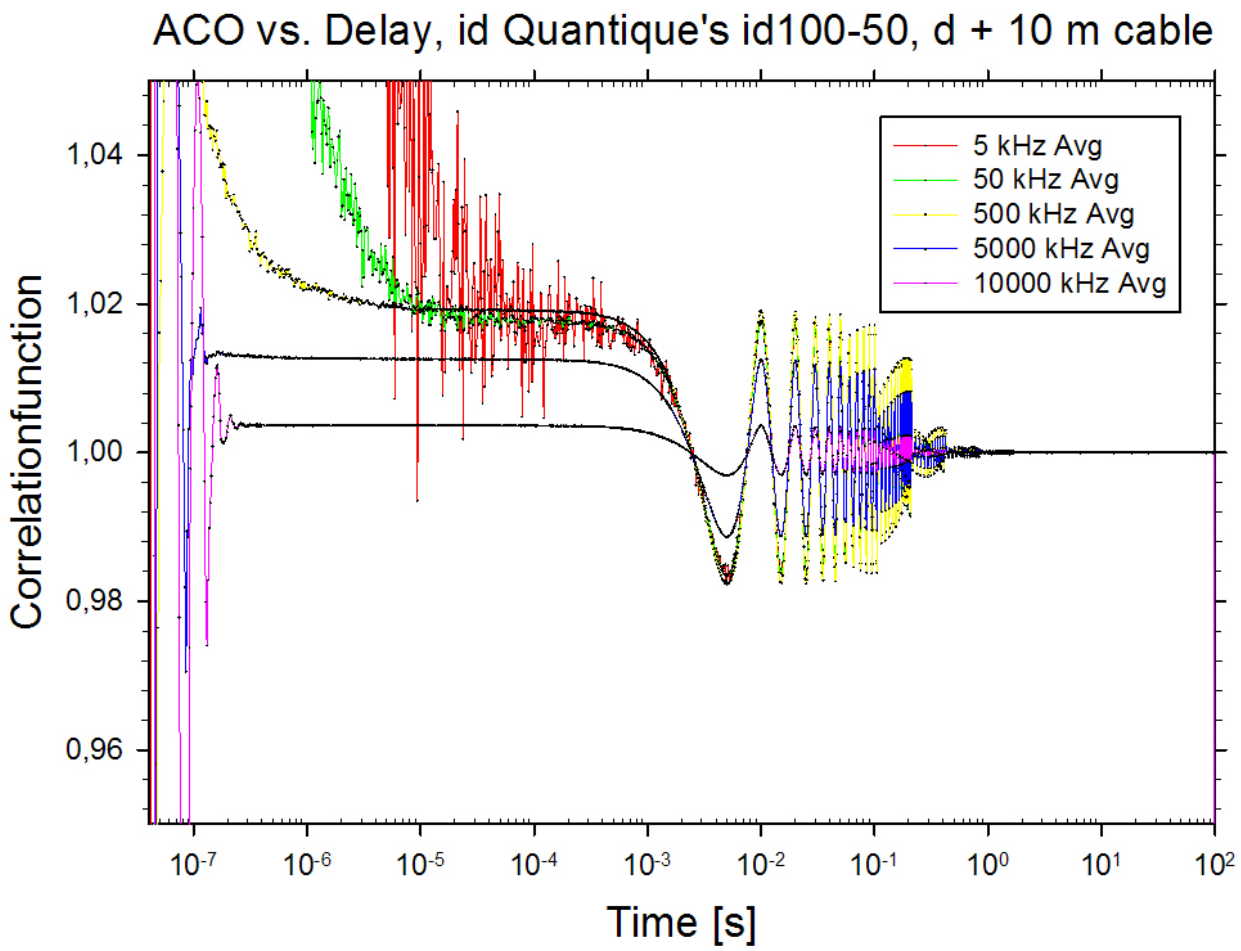

Figure A.6: Average normalized autocorrelation function vs. time delay for **id Quantique's id100-50** at various photon count rates using default (1 m) + 10 m cable. Note that y-axis uses linear scaling and x-axis uses logarithmic scaling.

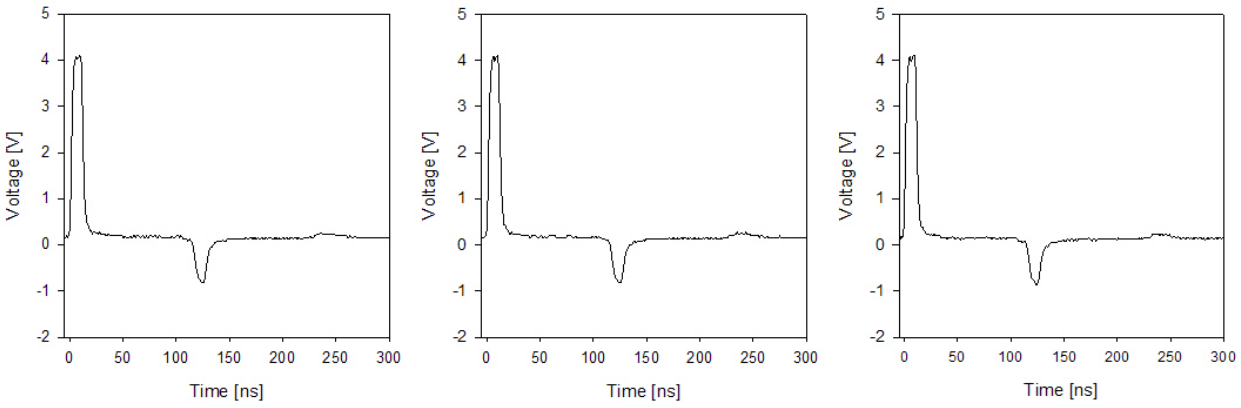

Figure A.7: Somewhat randomly picked waveforms (pulse shape) in the digital oscilloscope "Picoscope 5203" for some count rates, using the same setup as in the previous figure. From left to right: 5 kHz, 500 kHz, and 10000 kHz.

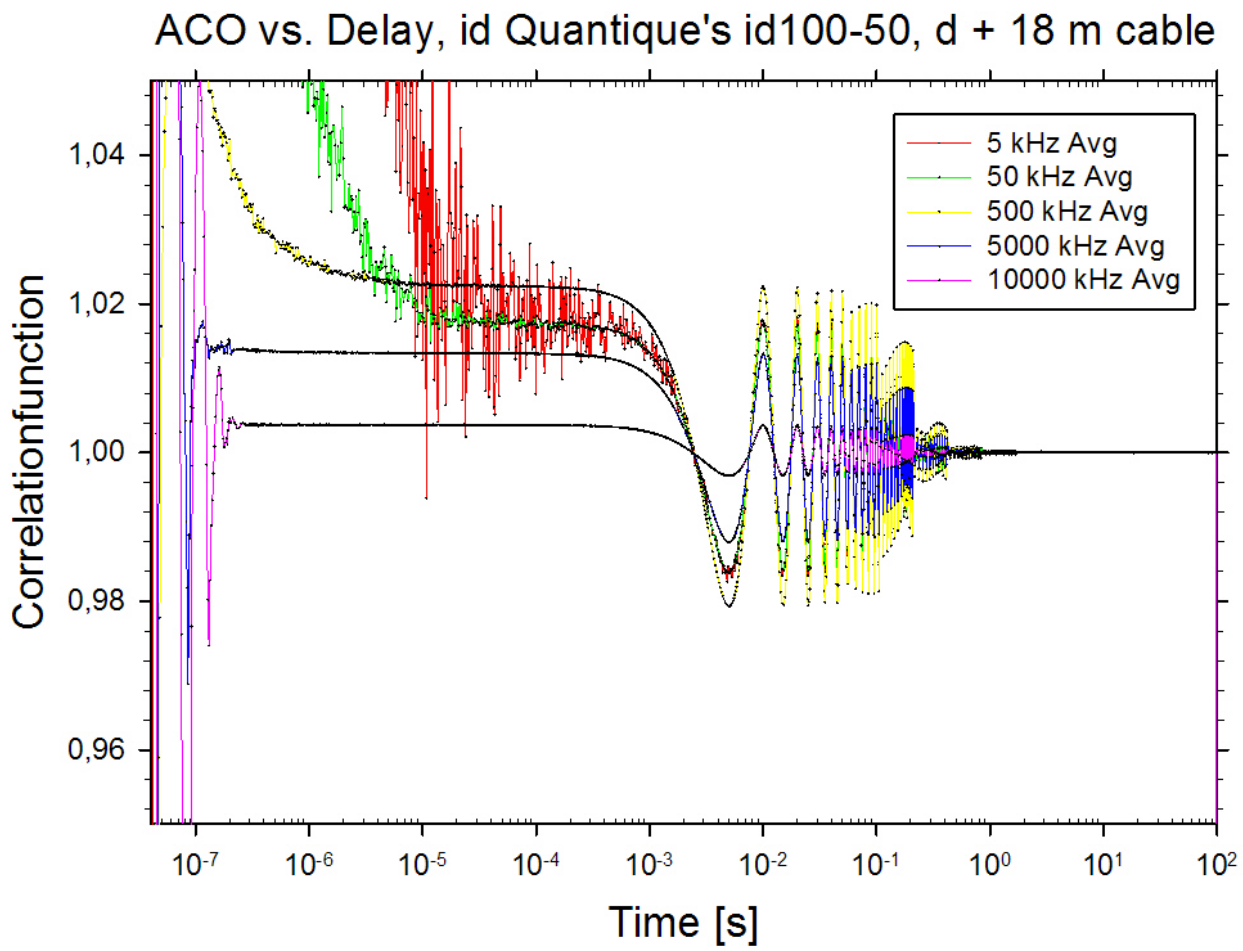

Figure A.8: Average normalized autocorrelation function vs. time delay for **id Quantique's id100-50** at various photon count rates using default (1 m) + 18 m cable. Note that y-axis uses linear scaling and x-axis uses logarithmic scaling.

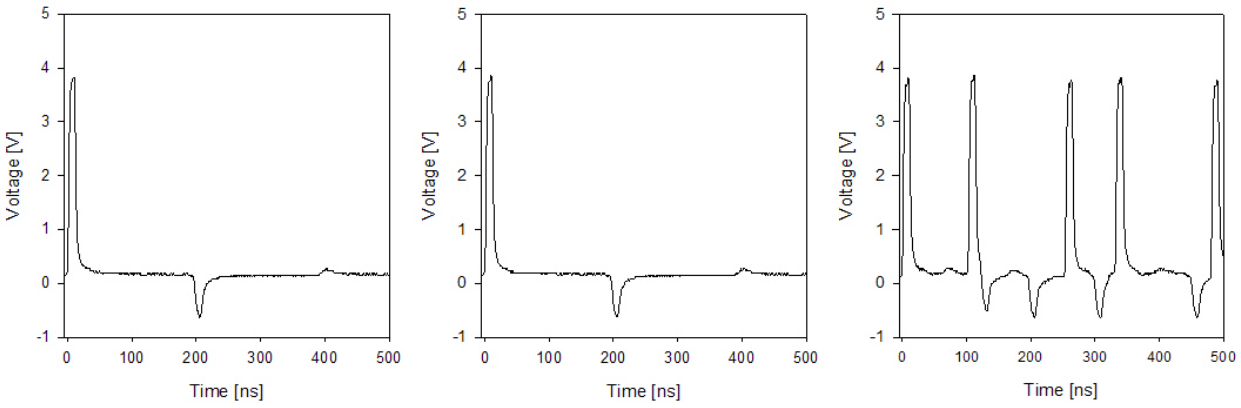

Figure A.9: Somewhat randomly picked waveforms (pulse shape) in the digital oscilloscope "Picoscope 5203" for some count rates, using the same setup as in the previous figure. From left to right: 5 kHz, 500 kHz, and 10000 kHz.

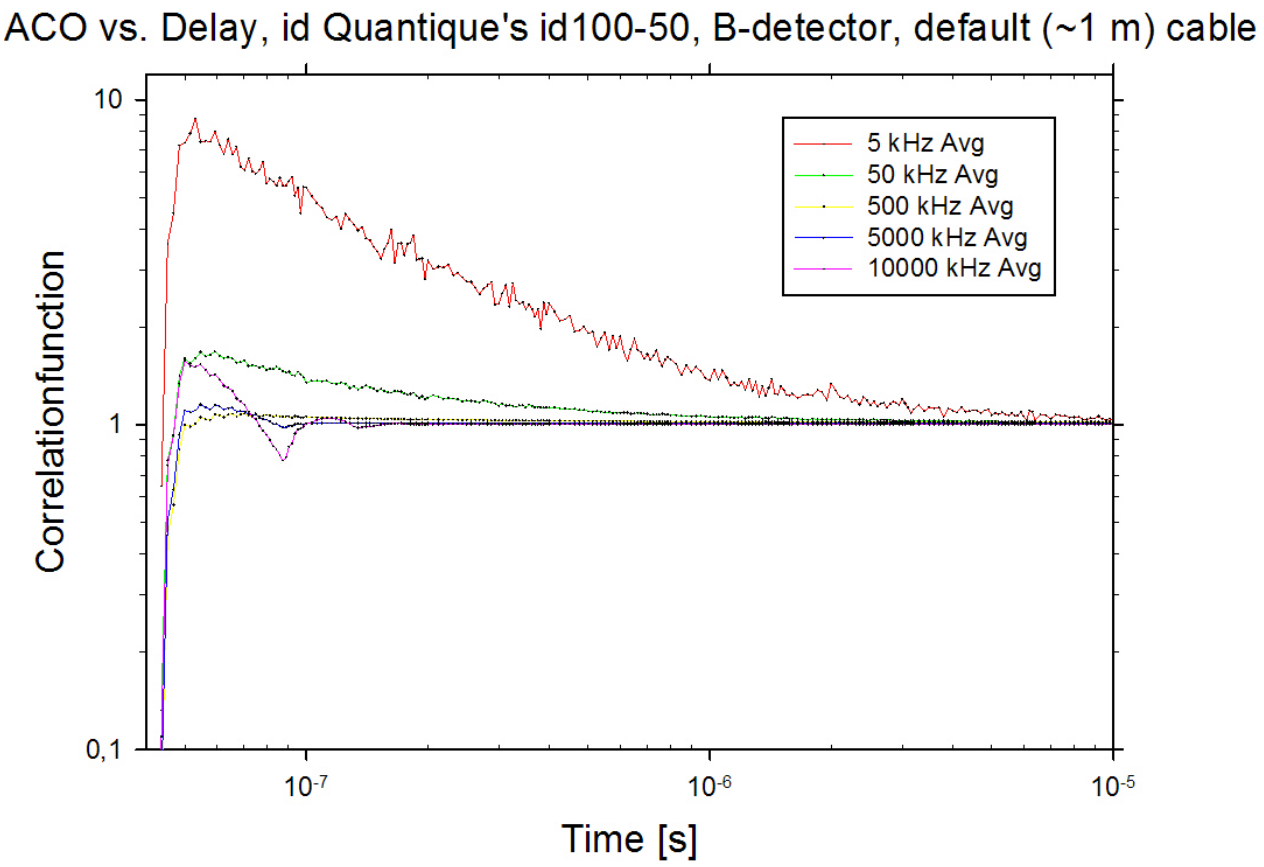

Figure A.10: Average normalized autocorrelation function vs. time delay for **id Quantique's id100-50**, using the 2nd detector (normally used for the B-channel in the hardware-correlator), at various photon count rates using default (1 m) cable. Note that y-axis uses linear scaling and x-axis uses logarithmic scaling.

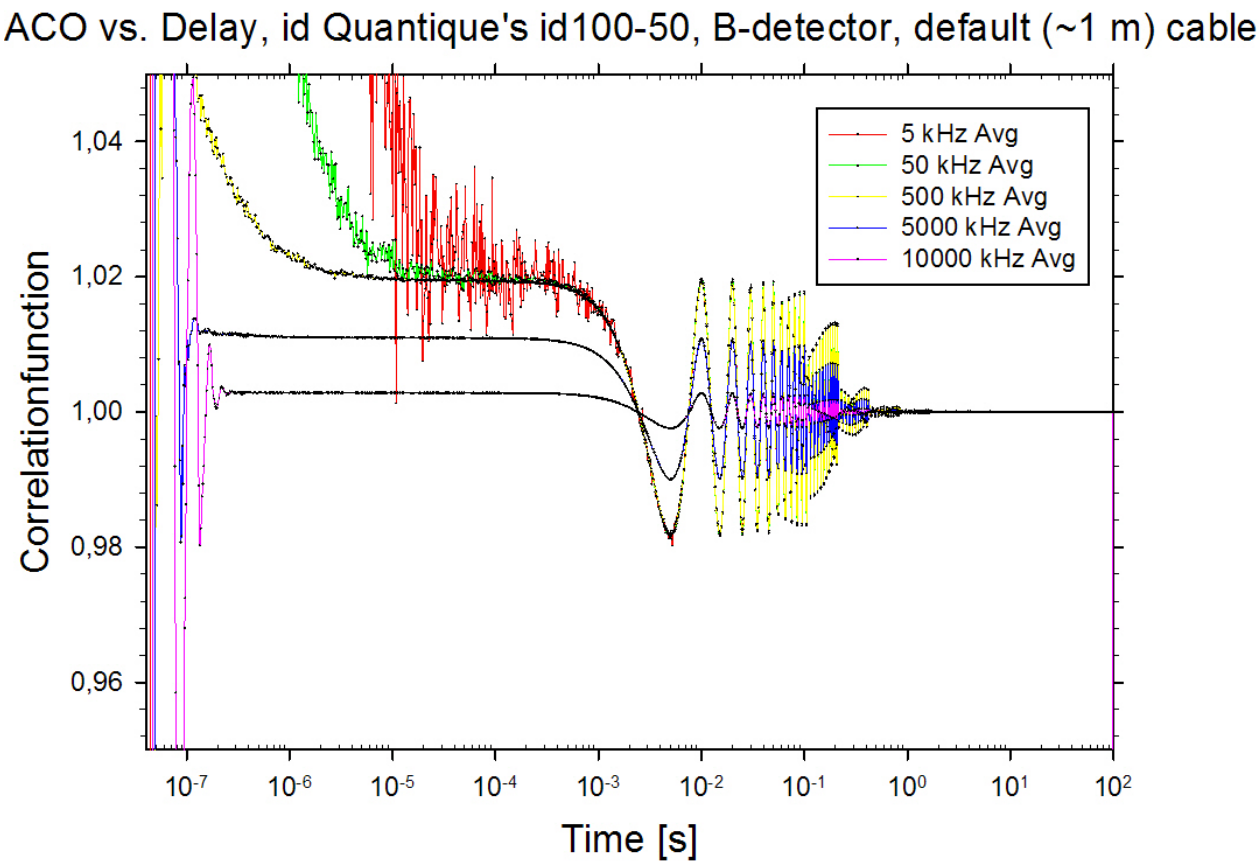

Figure A.11: Average normalized autocorrelation function vs. time delay for **id Quantique's id100-50**, using the 2nd detector (normally used for the B-channel in the hardware-correlator), at various photon count rates using default (1 m) cable. Note that y-axis uses linear scaling and x-axis uses logarithmic scaling.

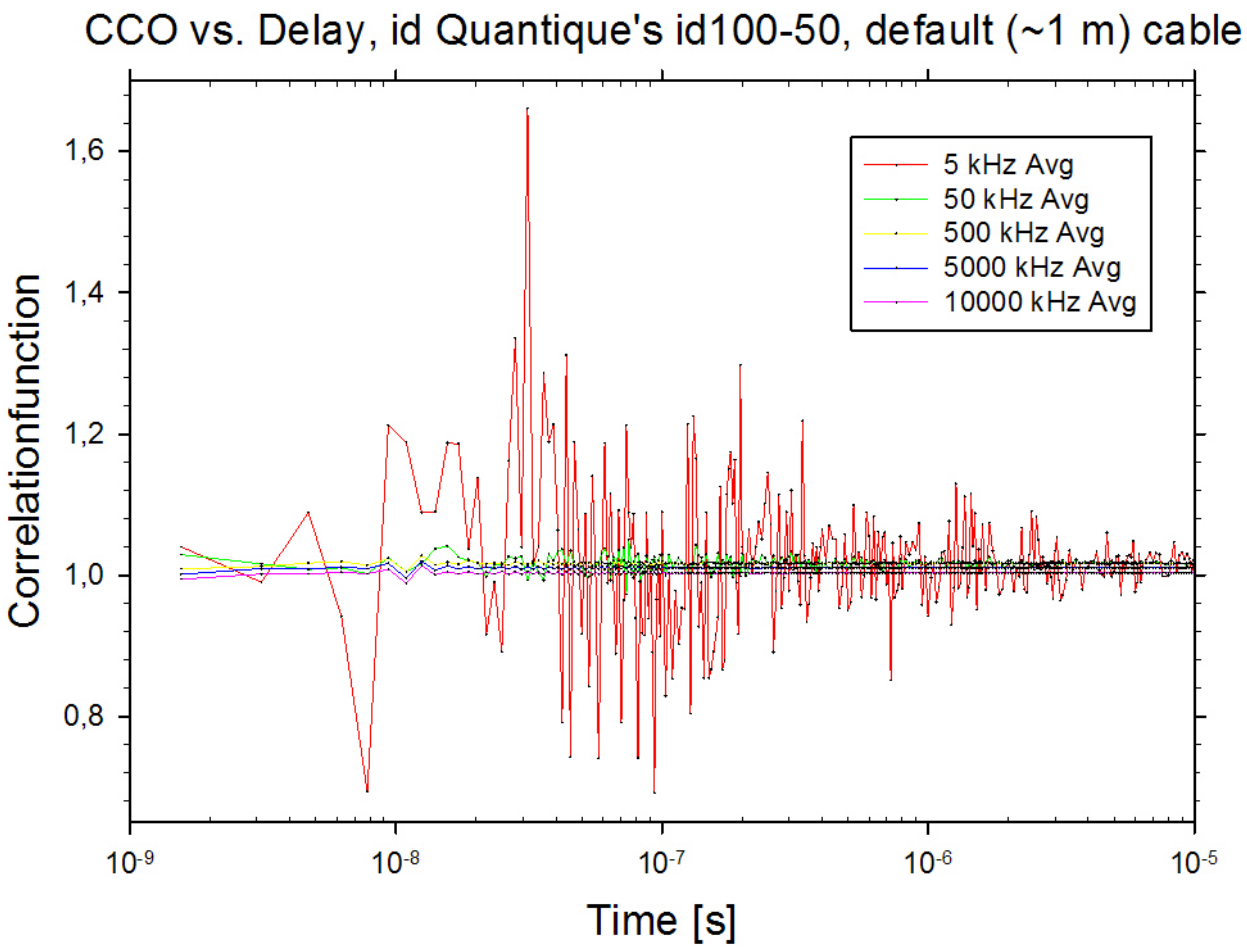

Figure A.12: Average normalized crosscorrelation function vs. time delay for **id Quantique's id100-50** at various photon count rates using default (1 m) cables. Note that y-axis uses linear scaling and x-axis uses logarithmic scaling.

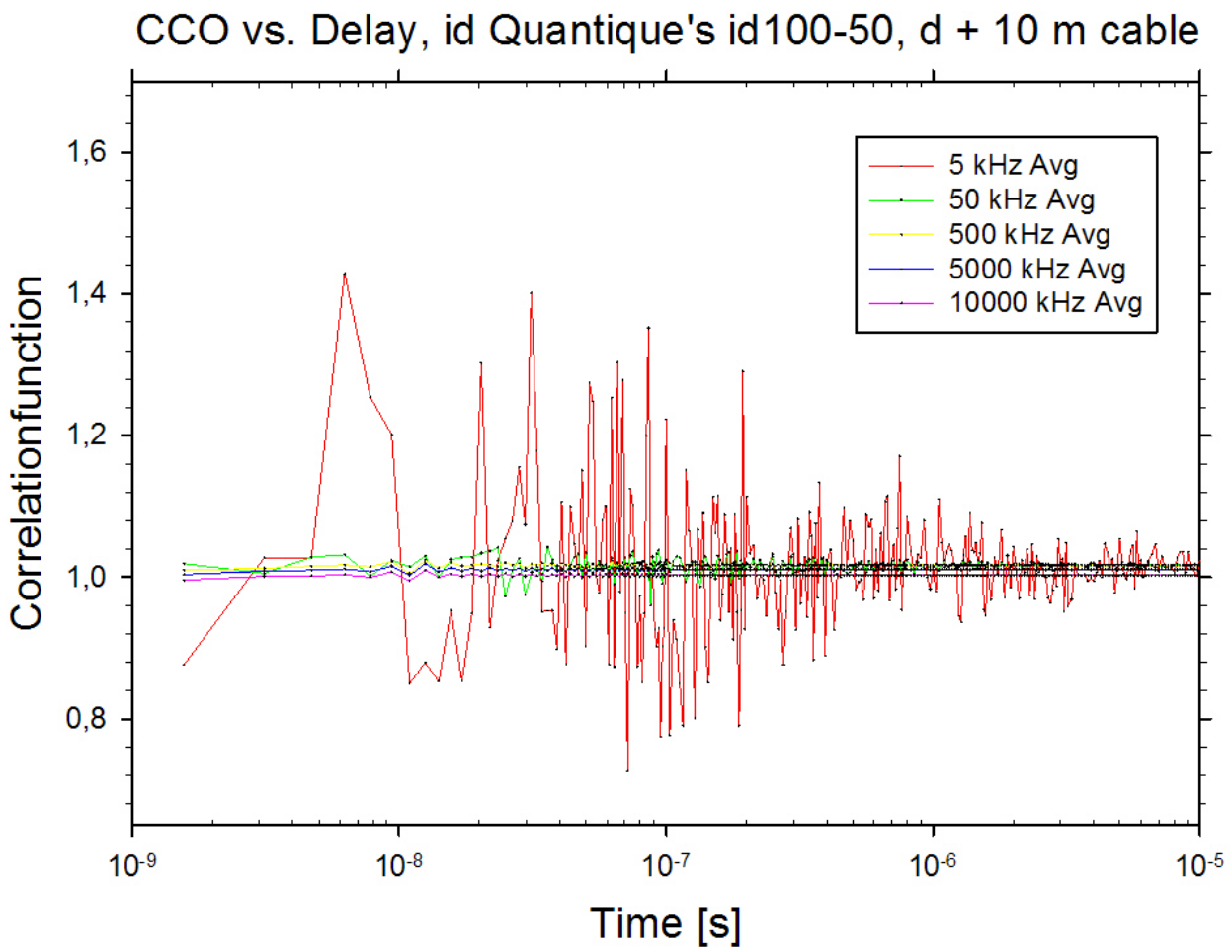

Figure A.13: Average normalized crosscorrelation function vs. time delay for **id Quantique's id100-50** at various photon count rates using default (1 m) + 10 m cables. Note that y-axis uses linear scaling and x-axis uses logarithmic scaling.

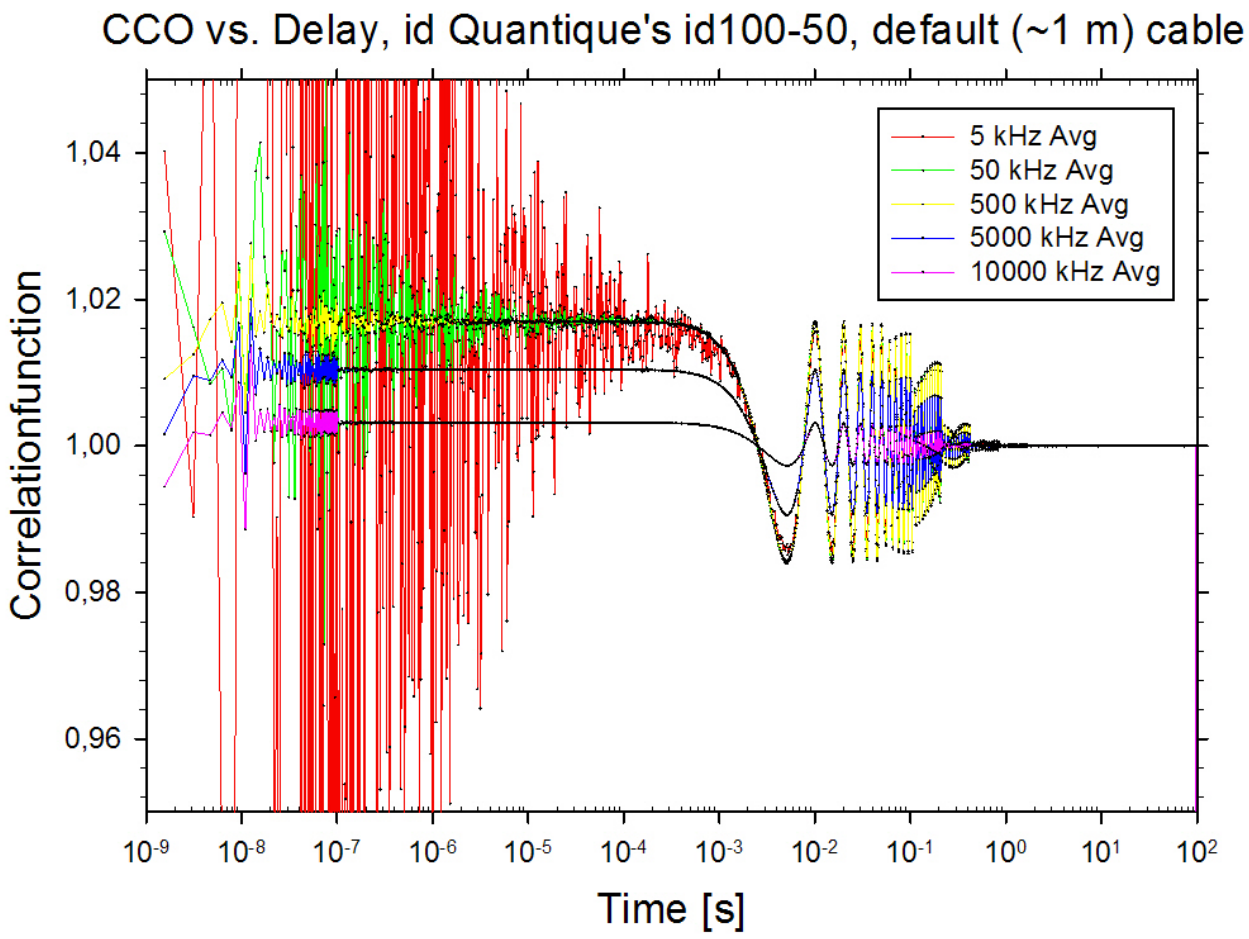

Figure A.14: Average normalized crosscorrelation function vs. time delay for **id Quantique's id100-50** at various photon count rates using default (1 m) cables. Note that y-axis uses linear scaling and x-axis uses logarithmic scaling.

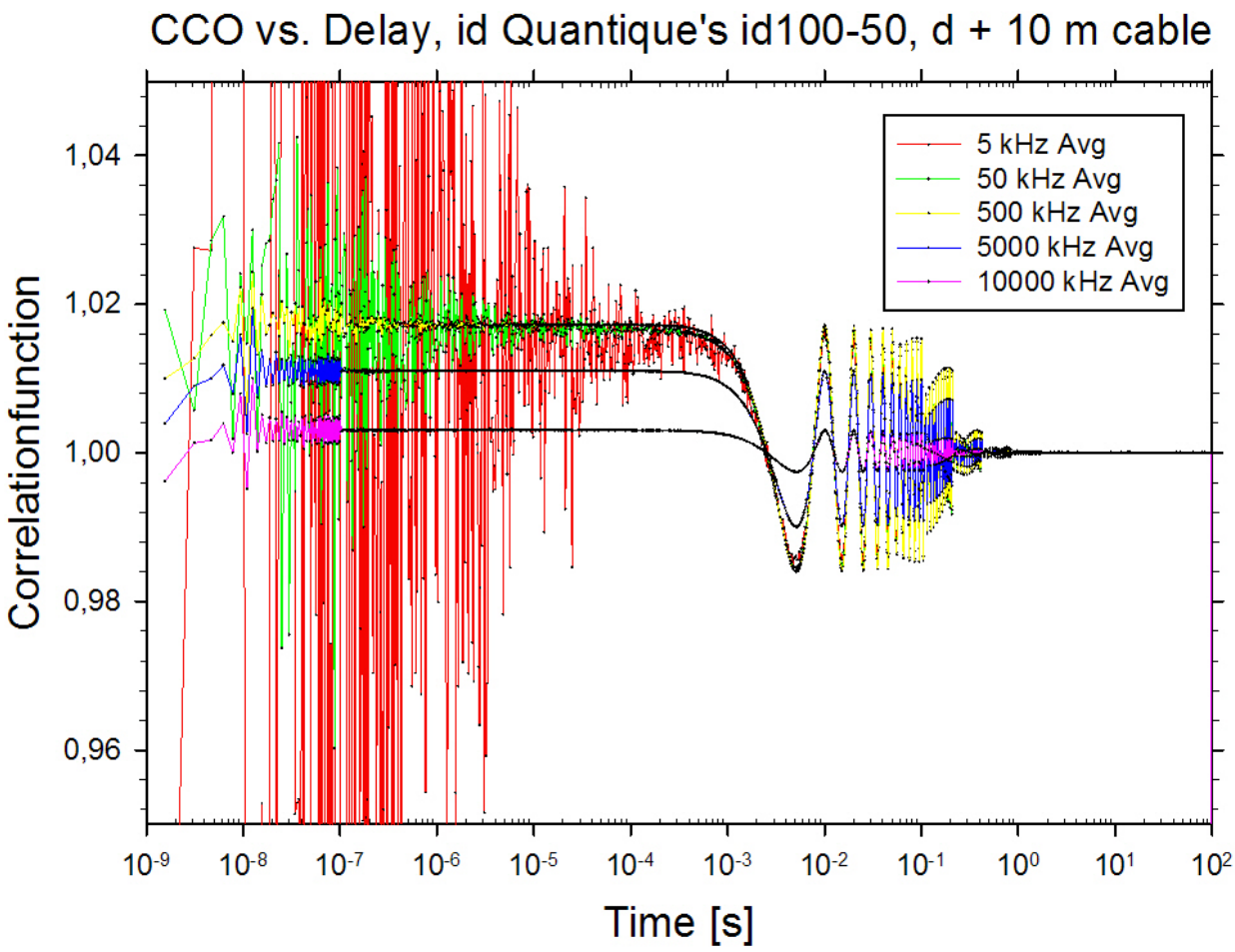

Figure A.15: Average normalized crosscorrelation function vs. time delay for **id Quantique's id100-50** at various photon count rates using default (1 m) + 10 m cables. Note that y-axis uses linear scaling and x-axis uses logarithmic scaling.

A.2 MPD's PDM series, PD1C0B

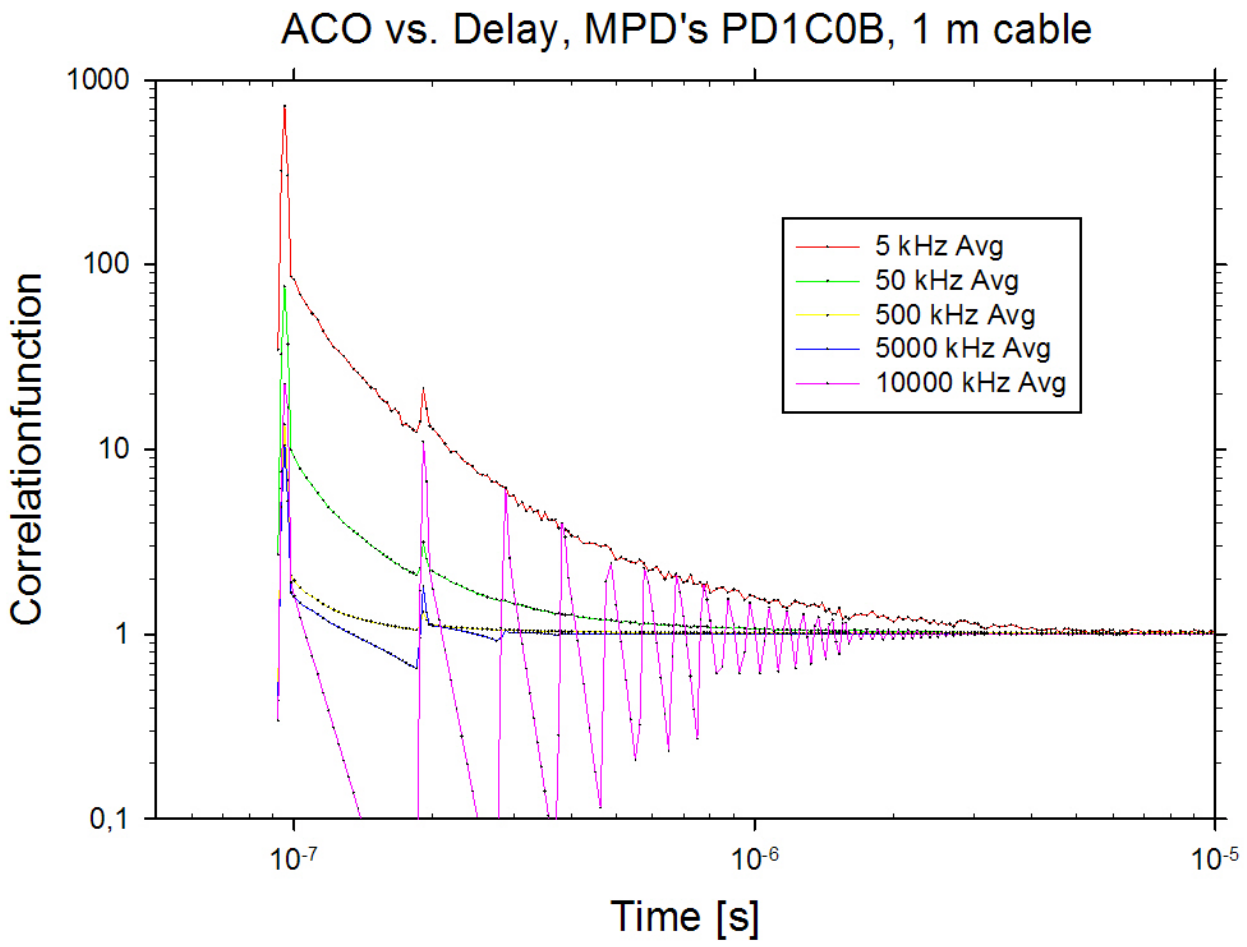

Figure A.16: Average normalized autocorrelation function vs. time delay for **MPD's PDM series, PD1C0B** at various photon count rates using 1 m cable. Note that both axes use logarithmic scaling.

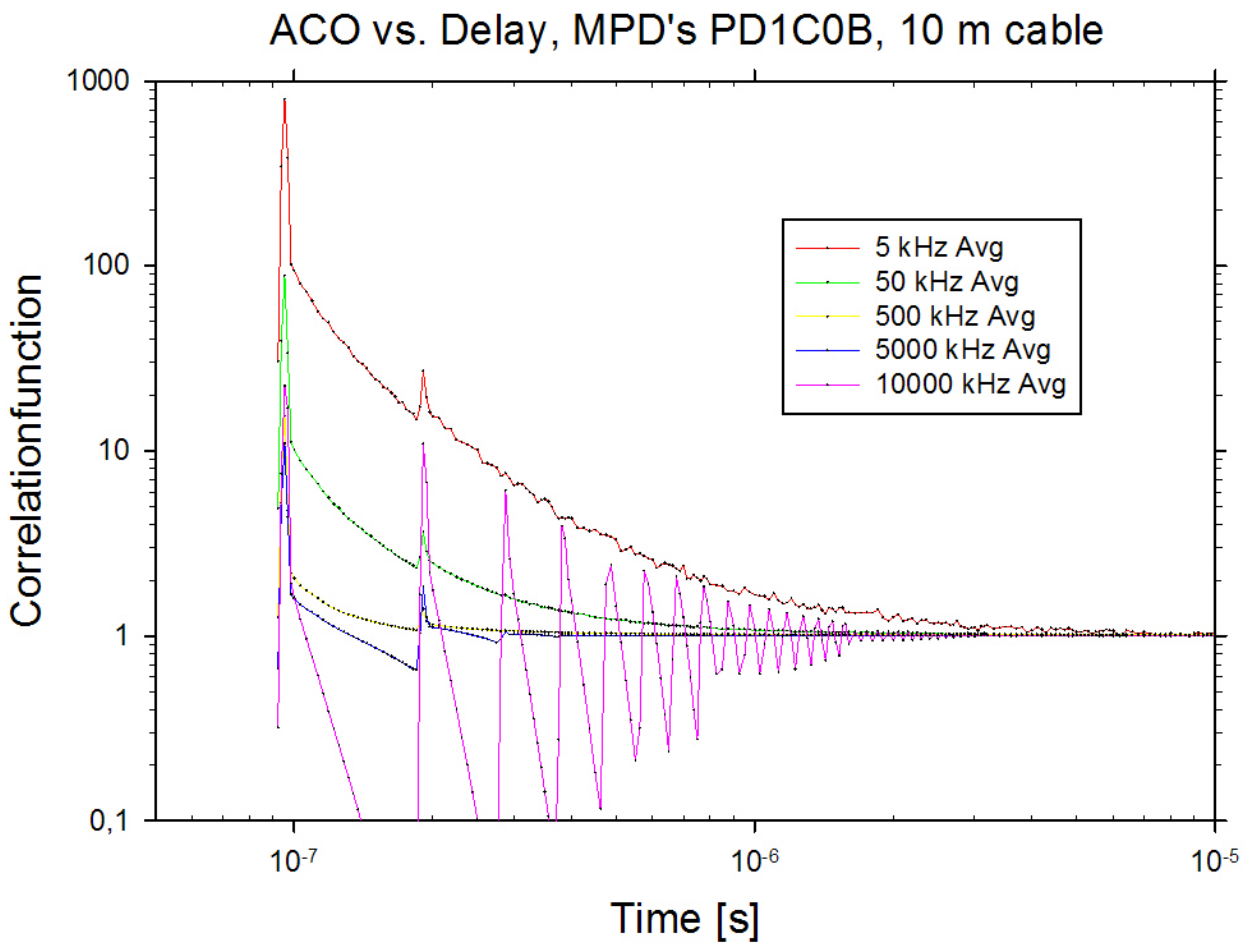

Figure A.17: Average normalized autocorrelation function vs. time delay for **MPD's PDM series, PD1C0B** at various photon count rates using 10 m cable. Note that both axes use logarithmic scaling.

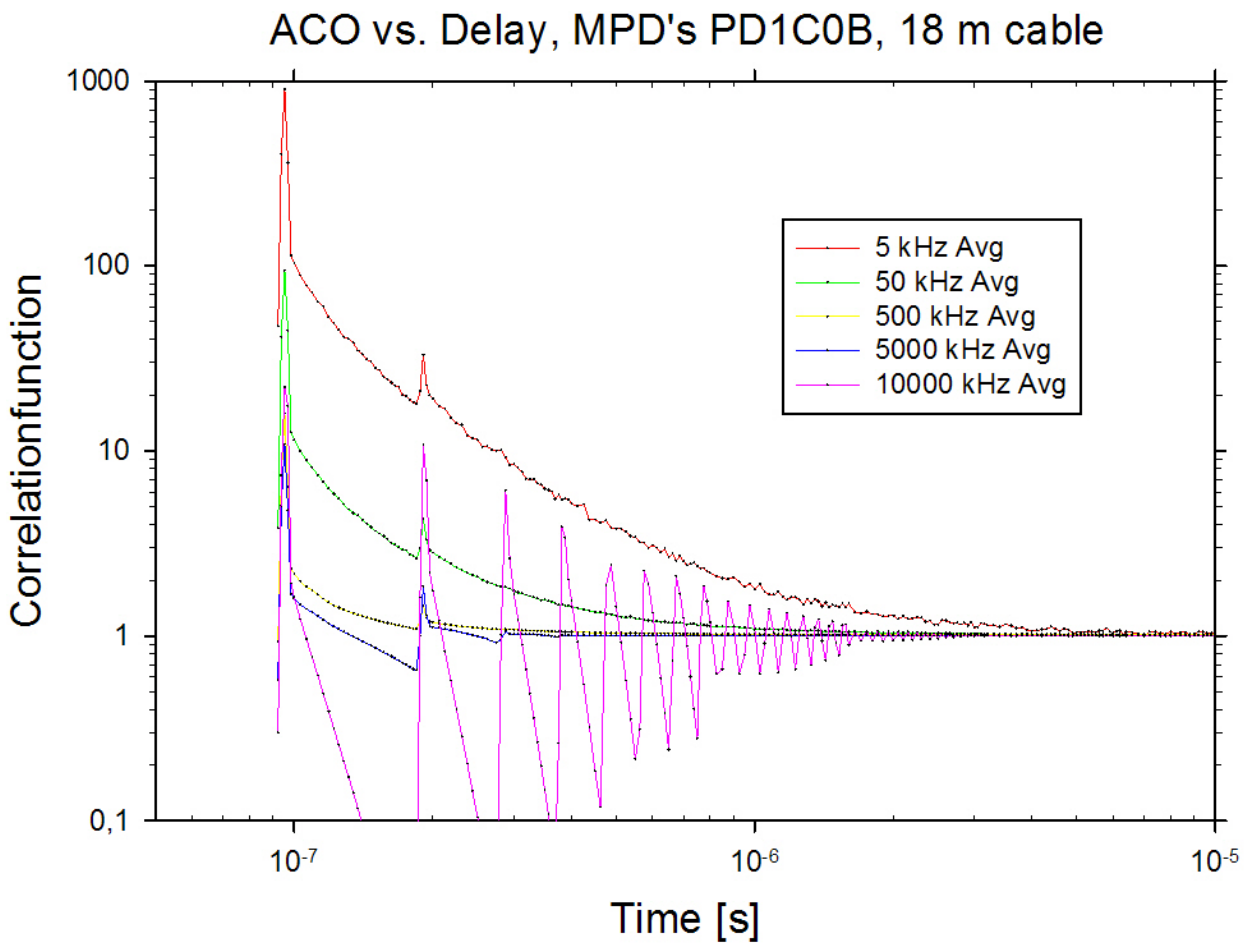

Figure A.18: Average normalized autocorrelation function vs. time delay for **MPD's PDM series, PD1C0B** at various photon count rates using 18 m cable. Note that both axes use logarithmic scaling.

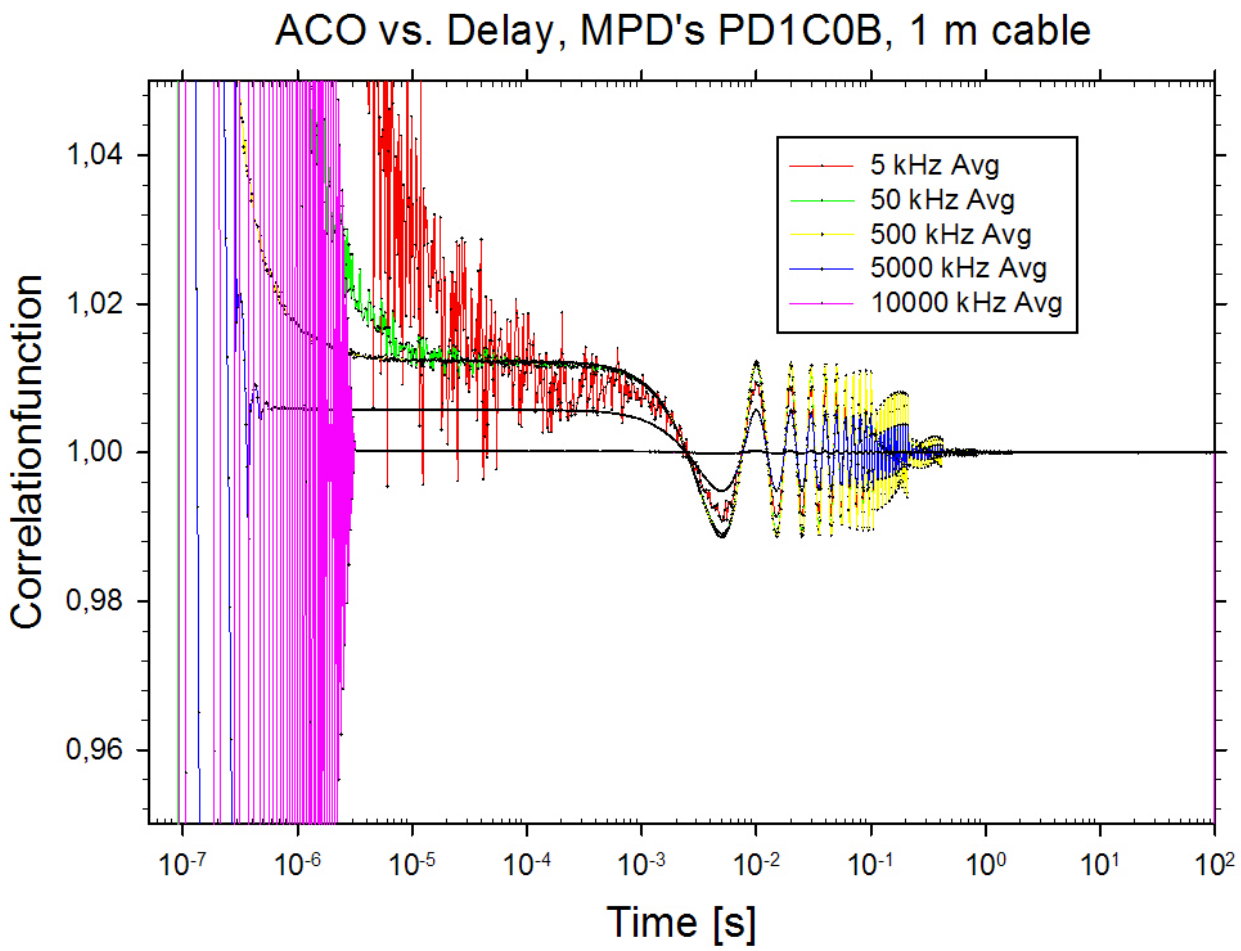

Figure A.19: Average normalized autocorrelation function vs. time delay for the **MPD's PDM series, PD1C0B** at various photon count rates using 1 m cable. Note that y-axis uses linear scaling and x-axis uses logarithmic scaling.

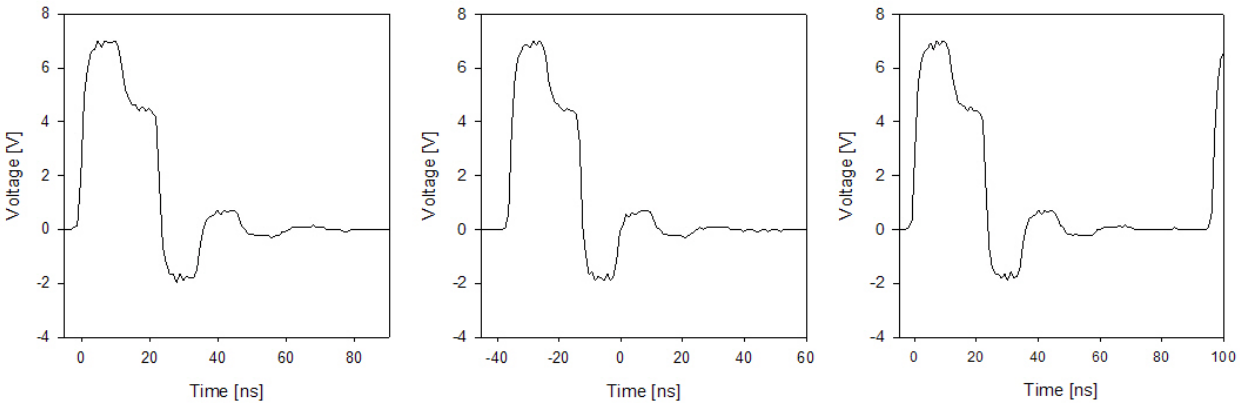

Figure A.20: Somewhat randomly picked waveforms (pulse shape) in the digital oscilloscope "Picoscope 5203" for some count rates, using the same setup as in the previous figure. From left to right: 5 kHz, 500 kHz, and 10000 kHz.

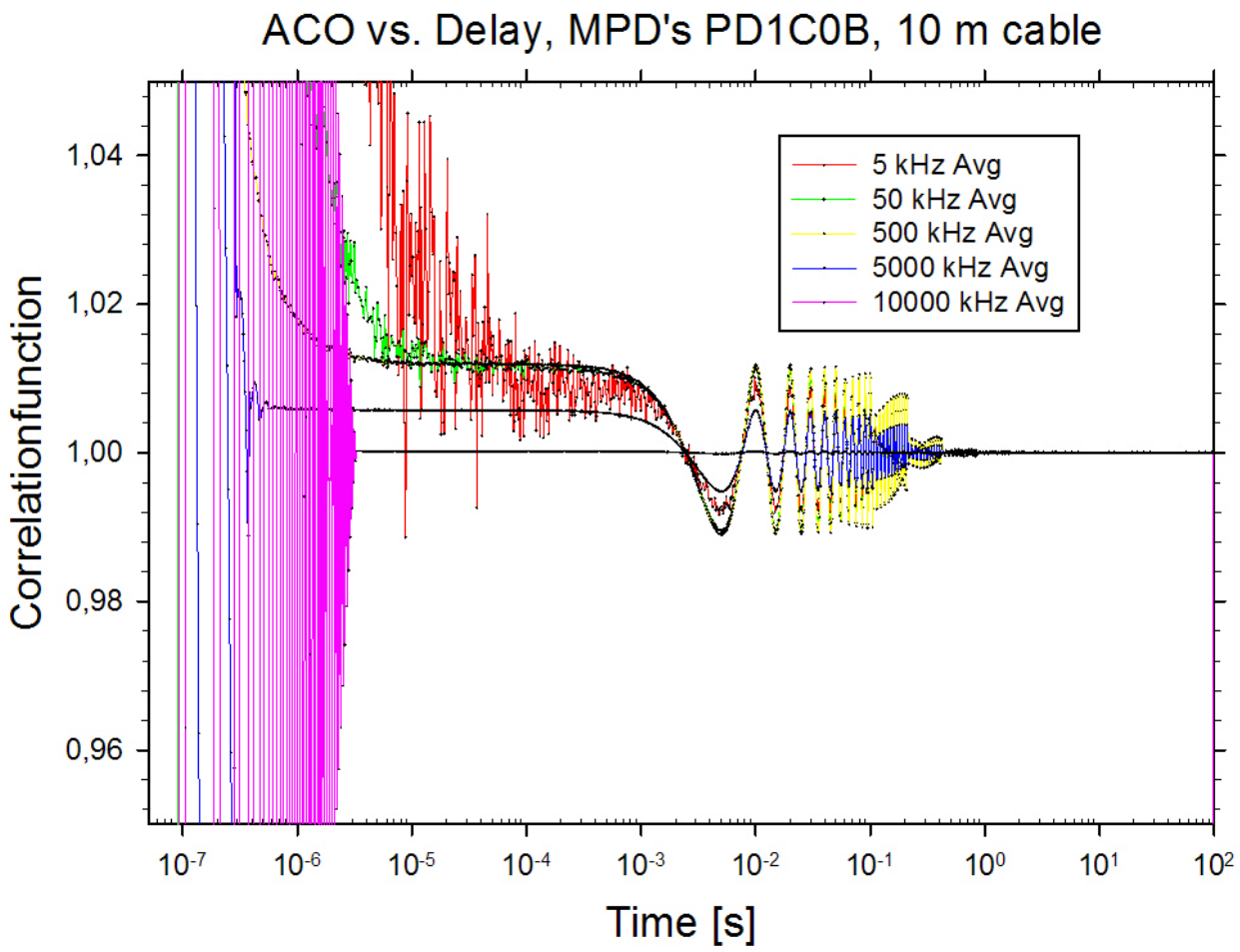

Figure A.21: Average normalized autocorrelation function vs. time delay for the **MPD's PDM series, PD1C0B** at various photon count rates using 10 m cable. Note that y-axis uses linear scaling and x-axis uses logarithmic scaling.

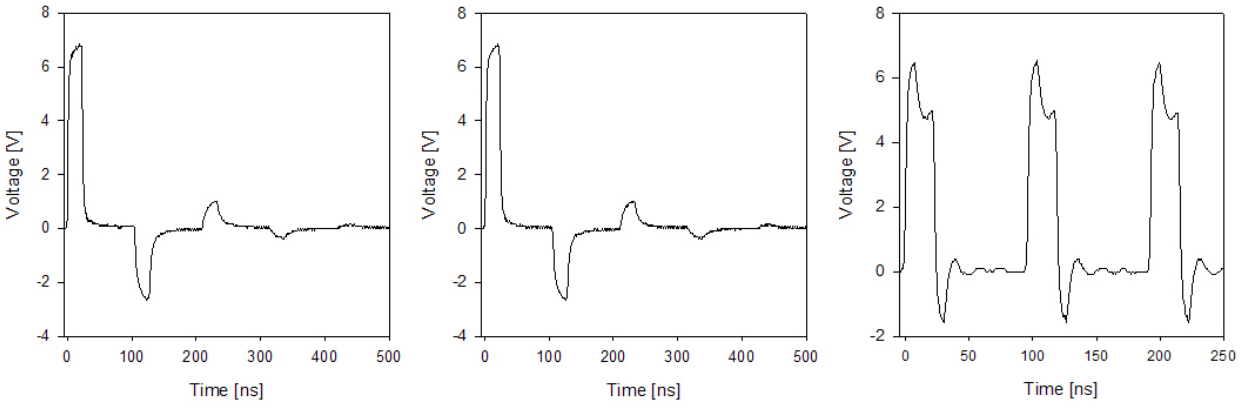

Figure A.22: Somewhat randomly picked waveforms (pulse shape) in the digital oscilloscope "Picoscope 5203" for some count rates, using the same setup as in the previous figure. From left to right: 5 kHz, 500 kHz, and 10000 kHz.

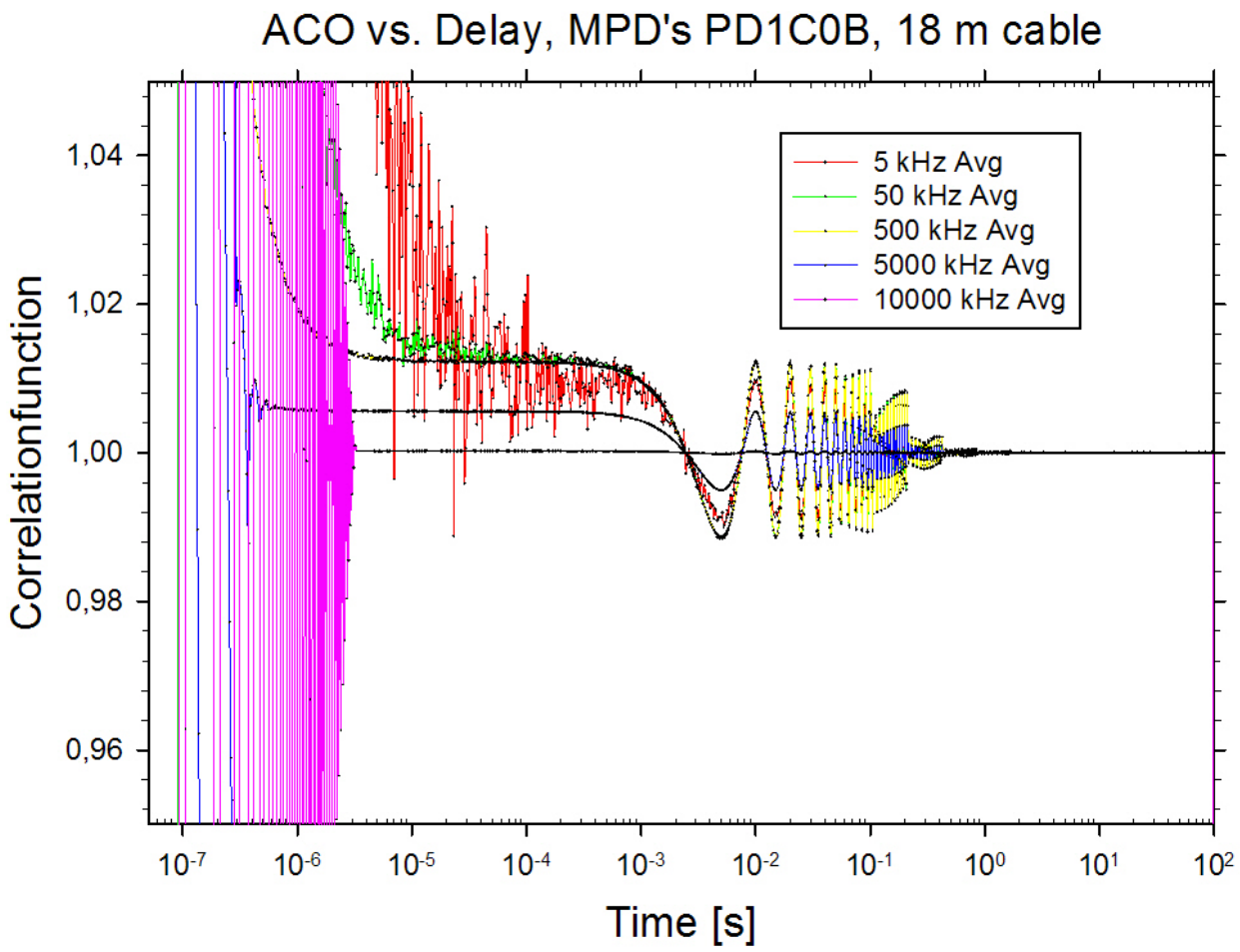

Figure A.23: Average normalized autocorrelation function vs. time delay for **MPD's PDM series, PD1C0B** at various photon count rates using 18 m cable. Note that y-axis uses linear scaling and x-axis uses logarithmic scaling.

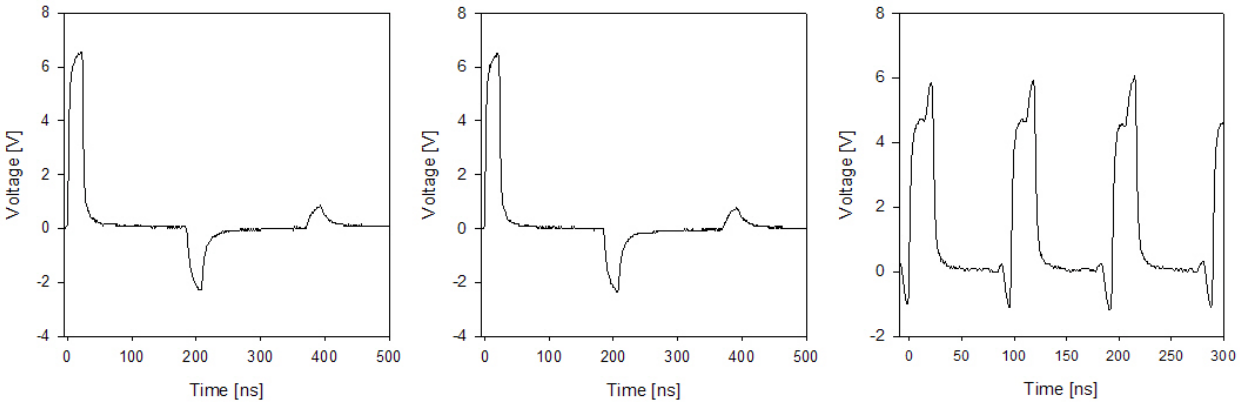

Figure A.24: Somewhat randomly picked waveforms (pulse shape) in the digital oscilloscope "Picoscope 5203" for some count rates, using the same setup as in the previous figure. From left to right: 5 kHz, 500 kHz, and 10000 kHz.

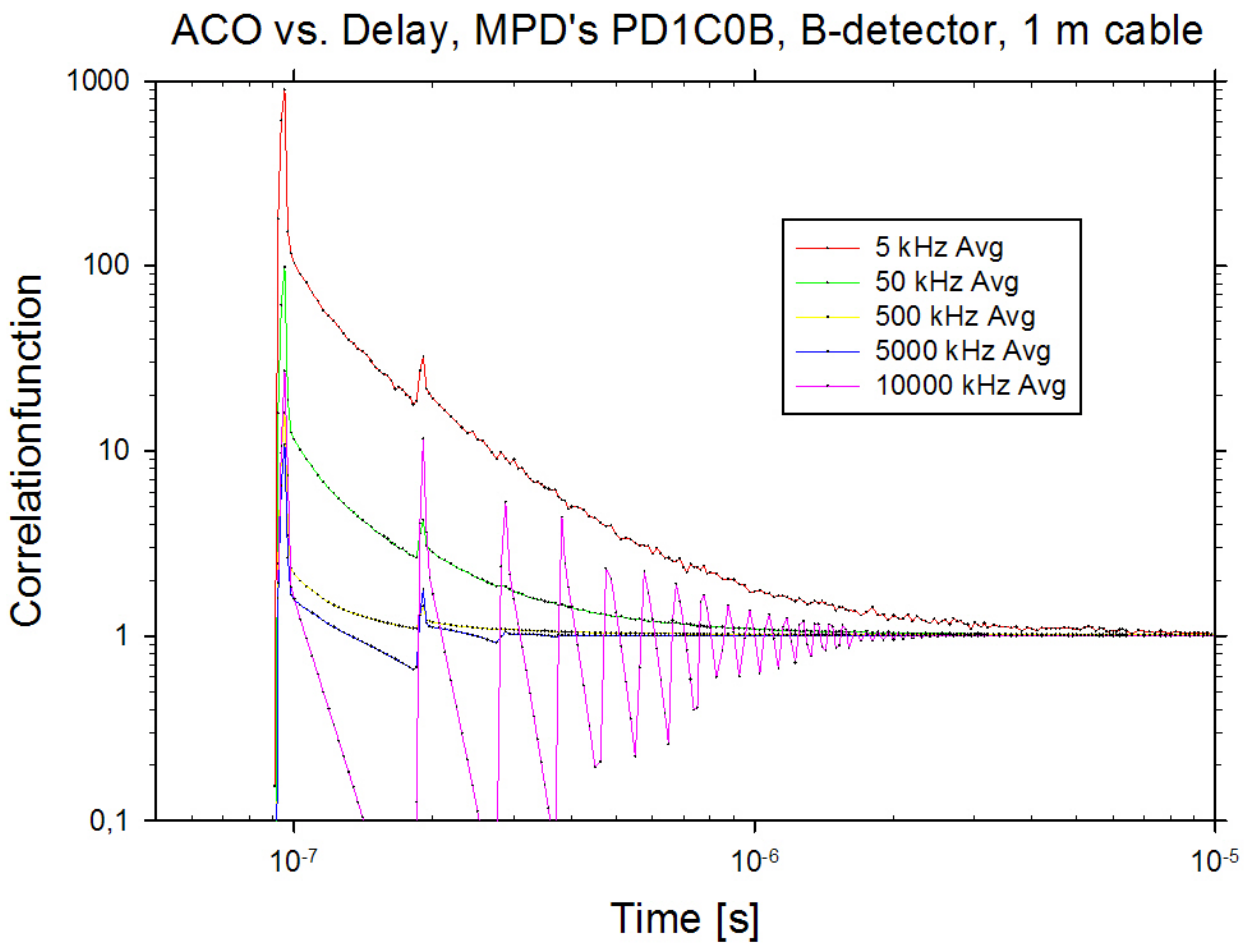

Figure A.25: Average normalized autocorrelation function vs. time delay for **MPD's PDM series, PD1C0B**, using the 2nd detector (normally used for the B-channel in the hardware-correlator), at various photon count rates using 1 m cable. Note that y-axis uses linear scaling and x-axis uses logarithmic scaling.

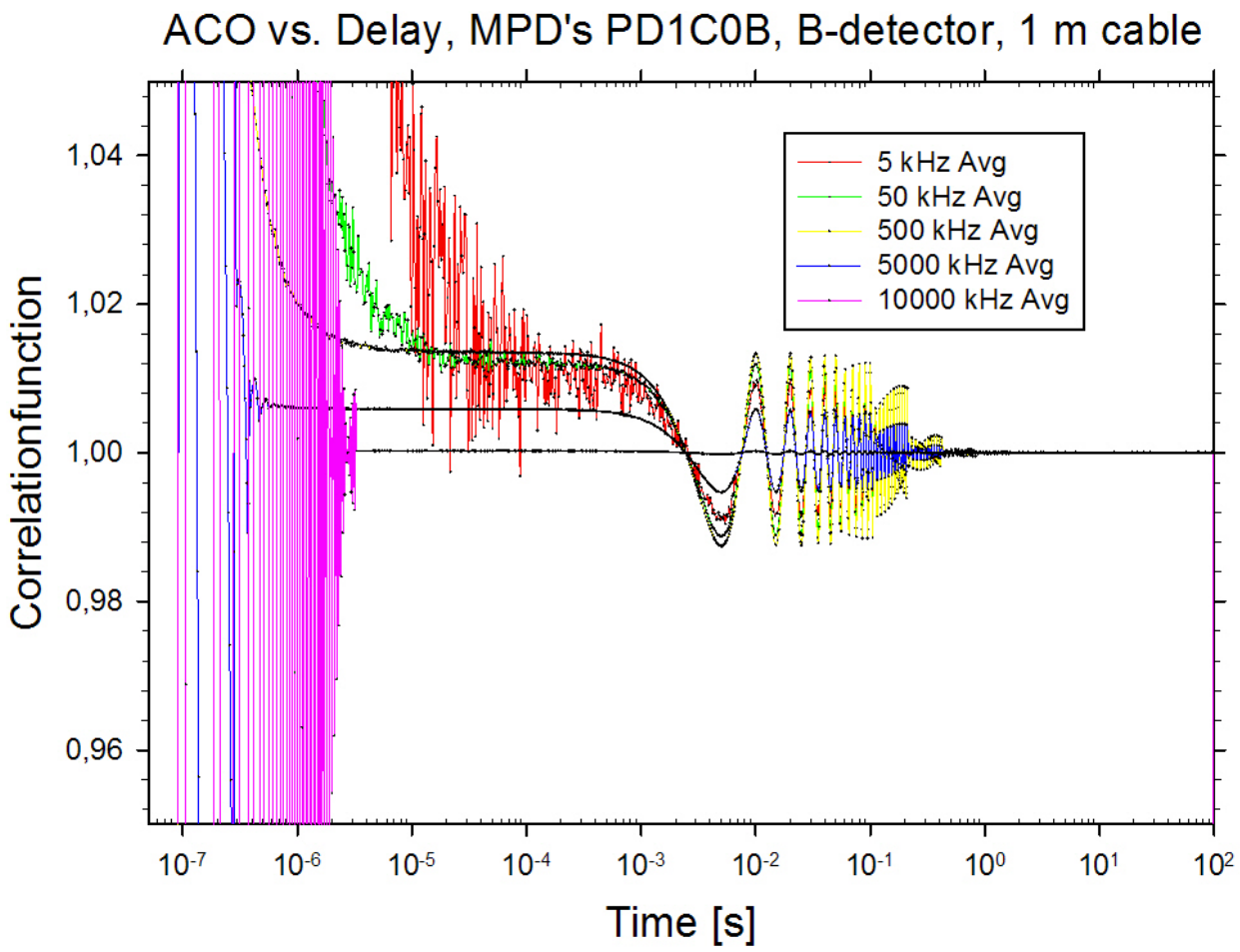

Figure A.26: Average normalized autocorrelation function vs. time delay for **MPD's PDM series, PD1C0B**, using the 2nd detector (normally used for the B-channel in the hardware-correlator), at various photon count rates using 1 m cable. Note that y-axis uses linear scaling and x-axis uses logarithmic scaling.

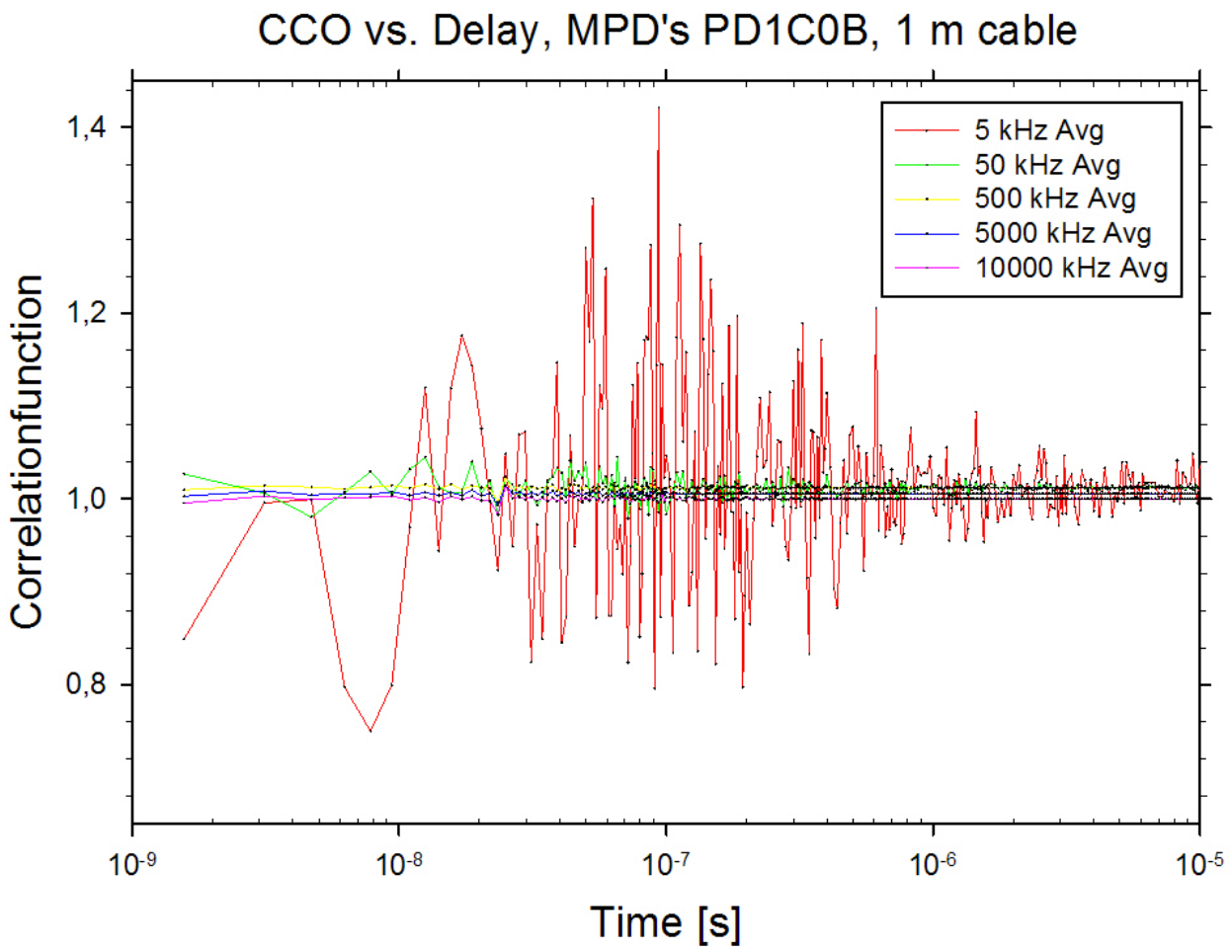

Figure A.27: Average normalized crosscorrelation function vs. time delay for **MPD's PDM series, PD1C0B** at various photon count rates using 1 m cables. Note that y-axis uses linear scaling and x-axis uses logarithmic scaling.

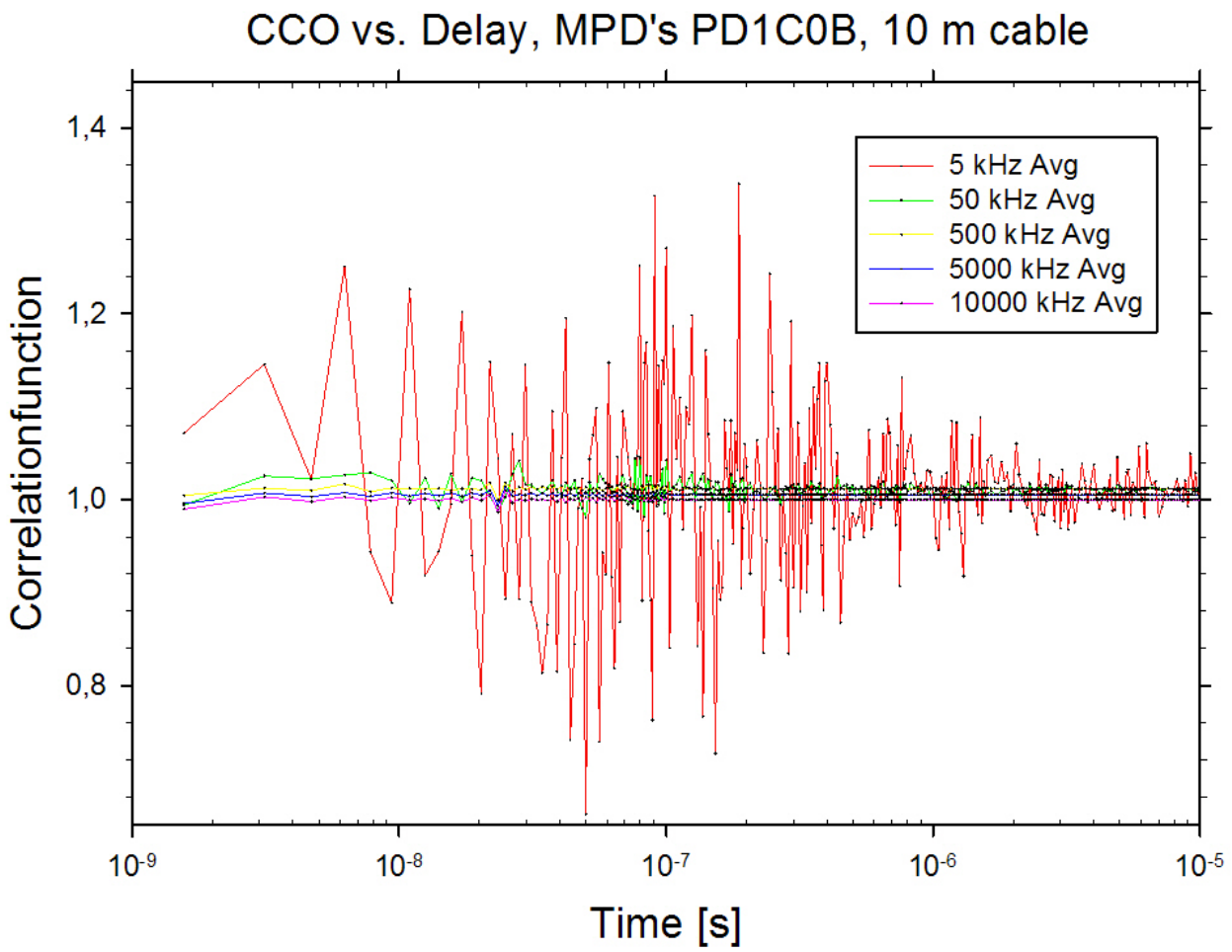

Figure A.28: Average normalized crosscorrelation function vs. time delay for **MPD's PDM series, PD1C0B** at various photon count rates using 10 m cable. Note that y-axis uses linear scaling and x-axis uses logarithmic scaling.

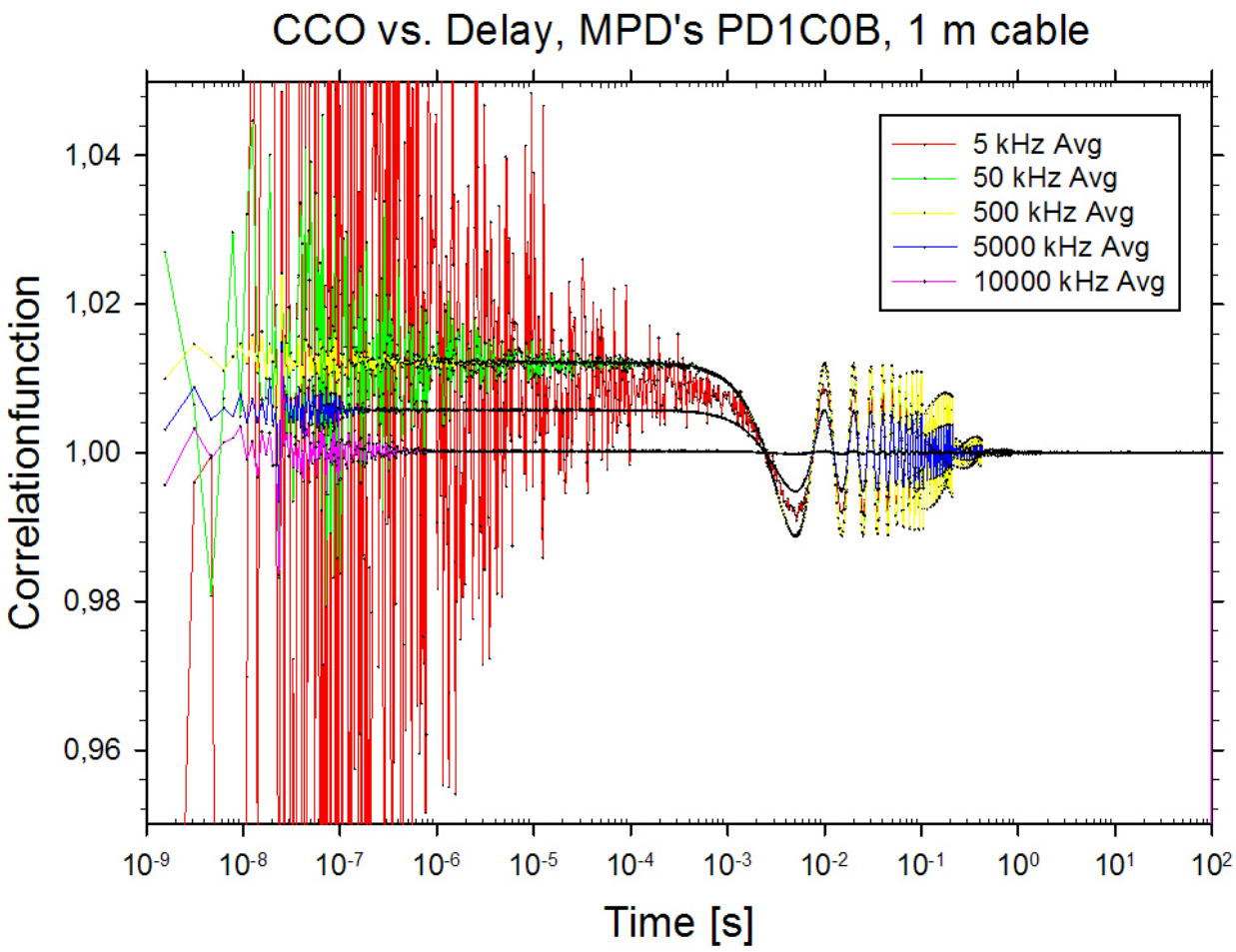

Figure A.29: Average normalized crosscorrelation function vs. time delay for **MPD's PDM series, PD1C0B** at various photon count rates using 1 m cable. Note that y-axis uses linear scaling and x-axis uses logarithmic scaling.

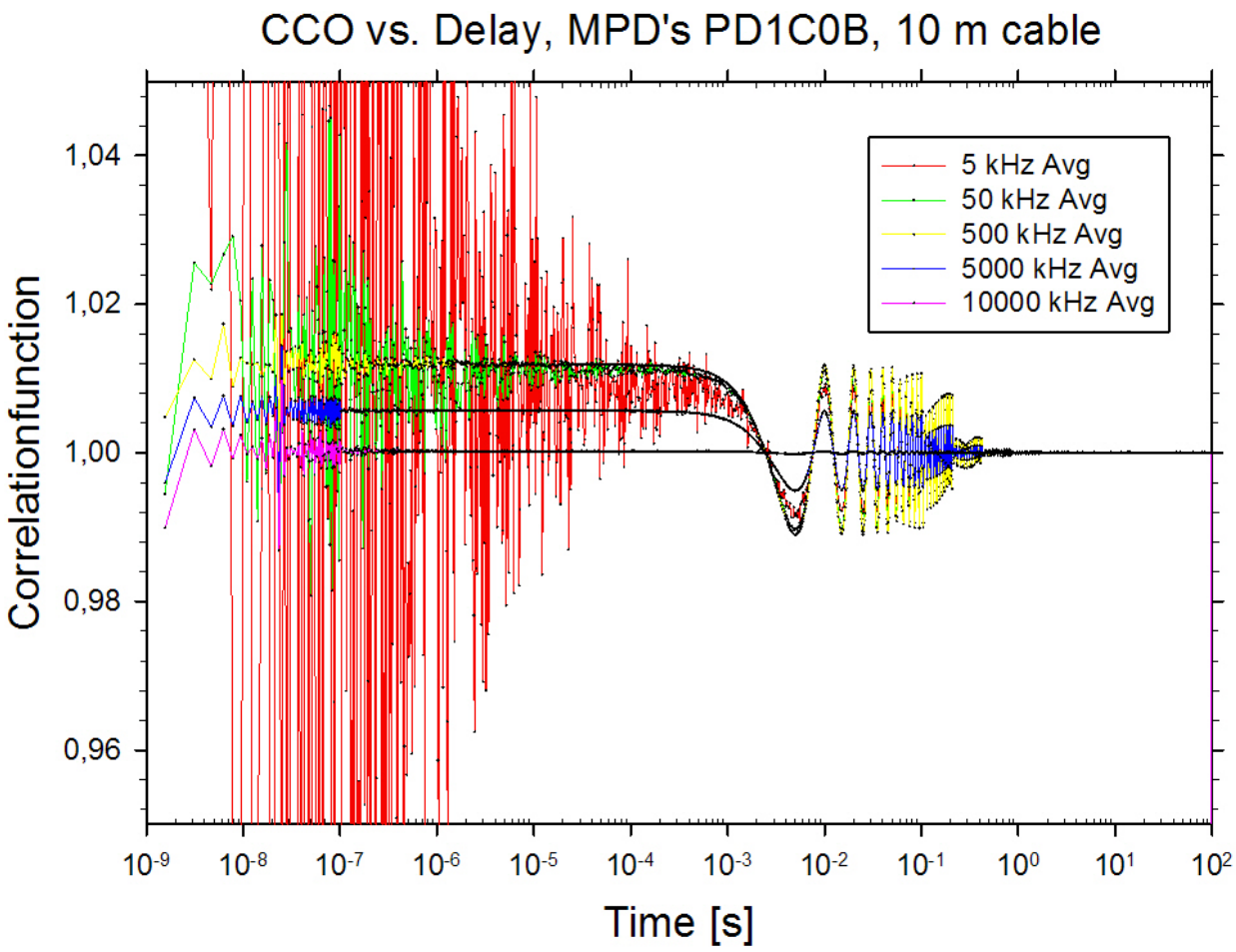

Figure A.30: Average normalized crosscorrelation function vs. time delay for **MPD's PDM series, PD1C0B** at various photon count rates using 10 m cable. Note that y-axis uses linear scaling and x-axis uses logarithmic scaling.

A.3 PerkinElmer's SPCM-100-PQ

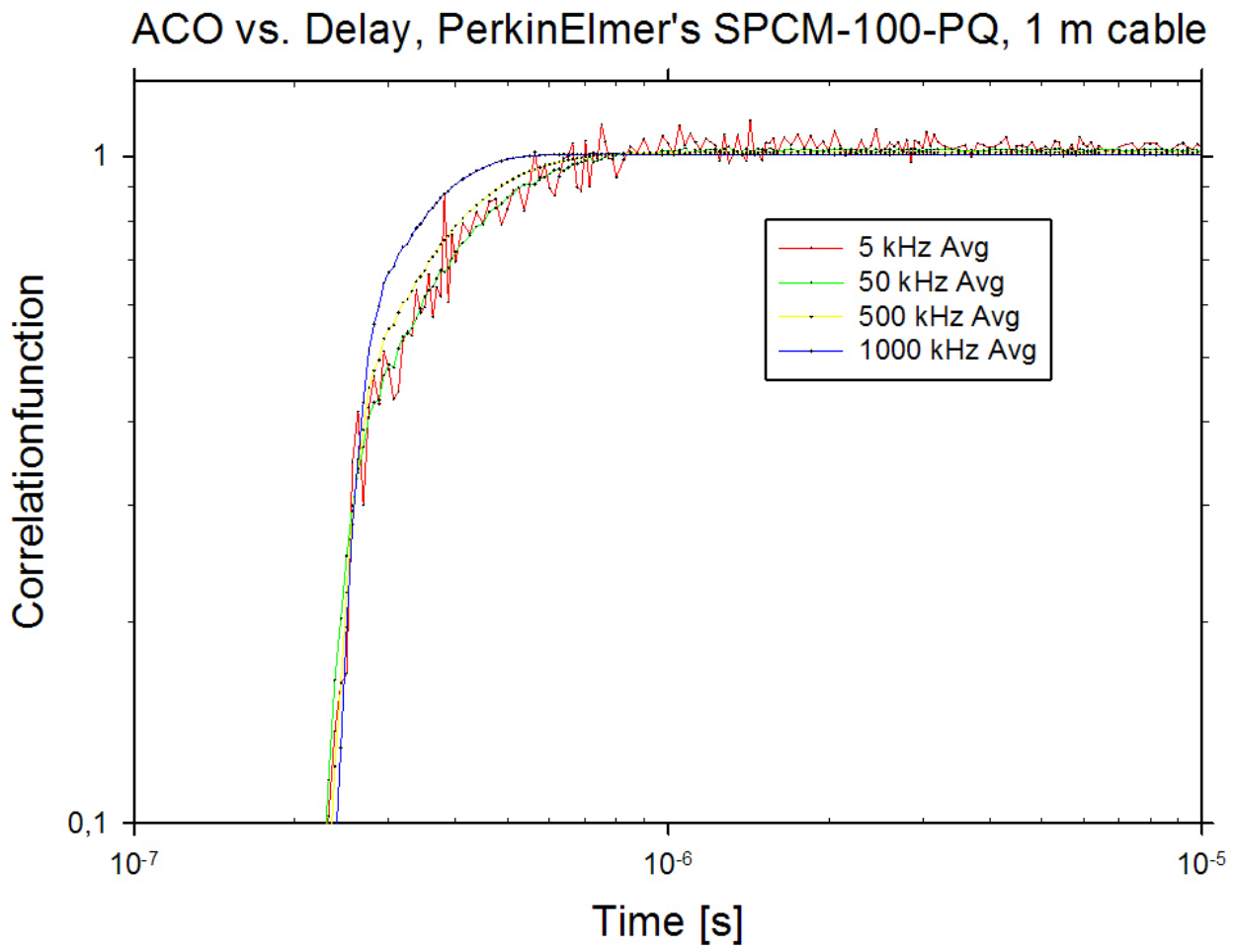

Figure A.31: Average normalized autocorrelation function vs. time delay for **PerkinElmer's SPCM-100-PQ** at various photon count rates using 1 m cable. Note that both axes use logarithmic scaling.

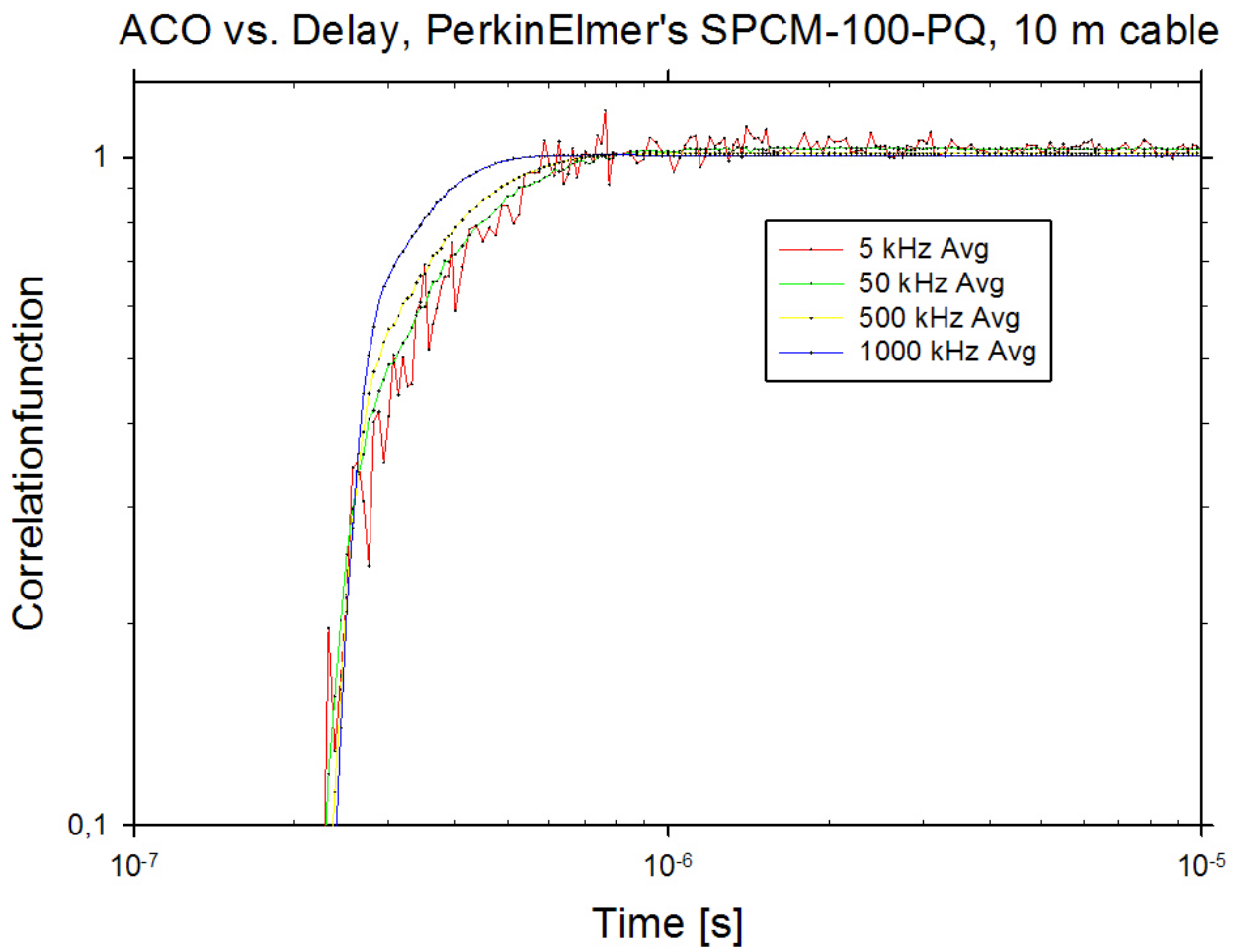

Figure A.32: Average normalized autocorrelation function vs. time delay for **PerkinElmer's SPCM-100-PQ** at various photon count rates using 10 m cable. Note that both axes use logarithmic scaling.

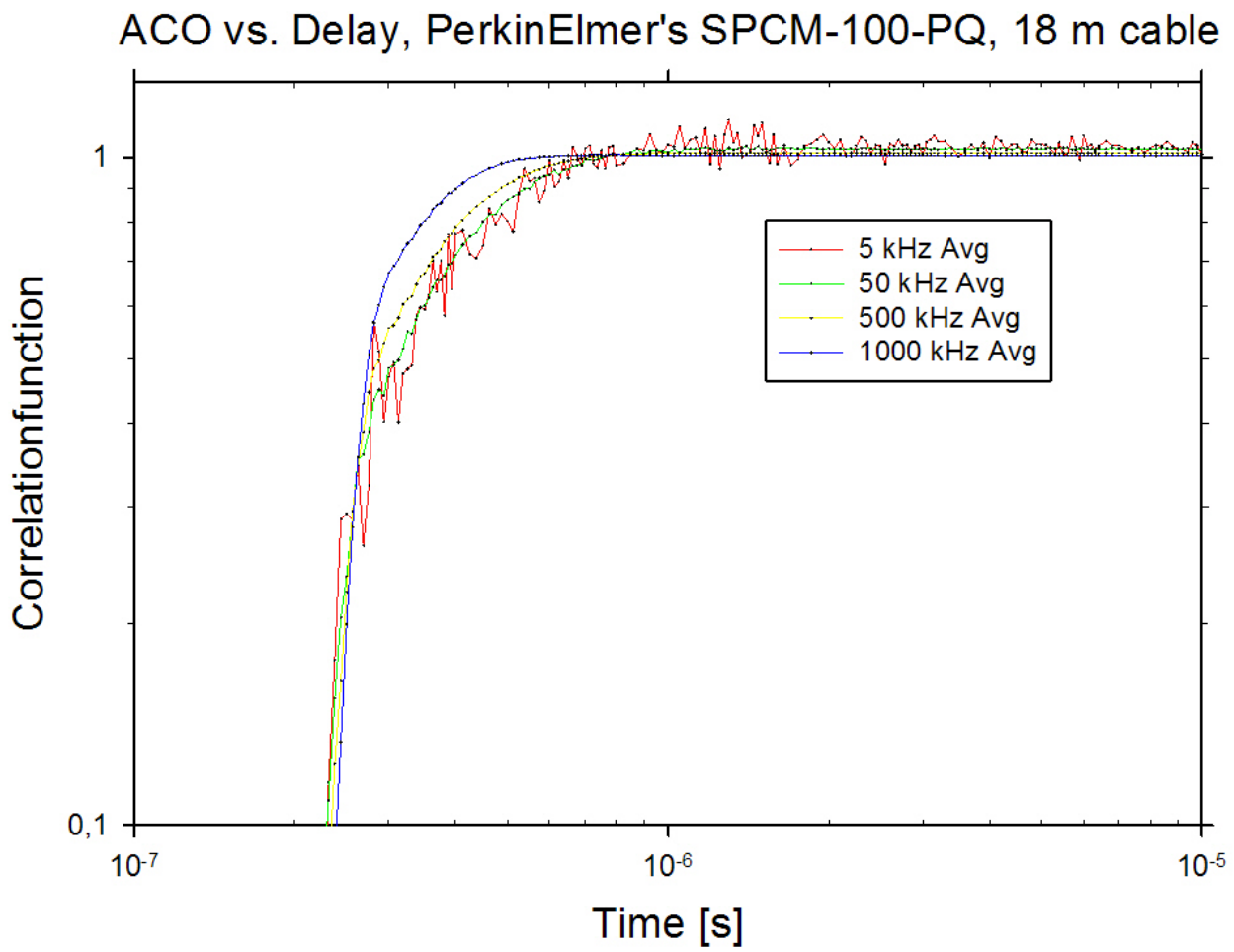

Figure A.33: Average normalized autocorrelation function vs. time delay for **PerkinElmer's SPCM-100-PQ** at various photon count rates using 18 m cable. Note that both axes use logarithmic scaling.

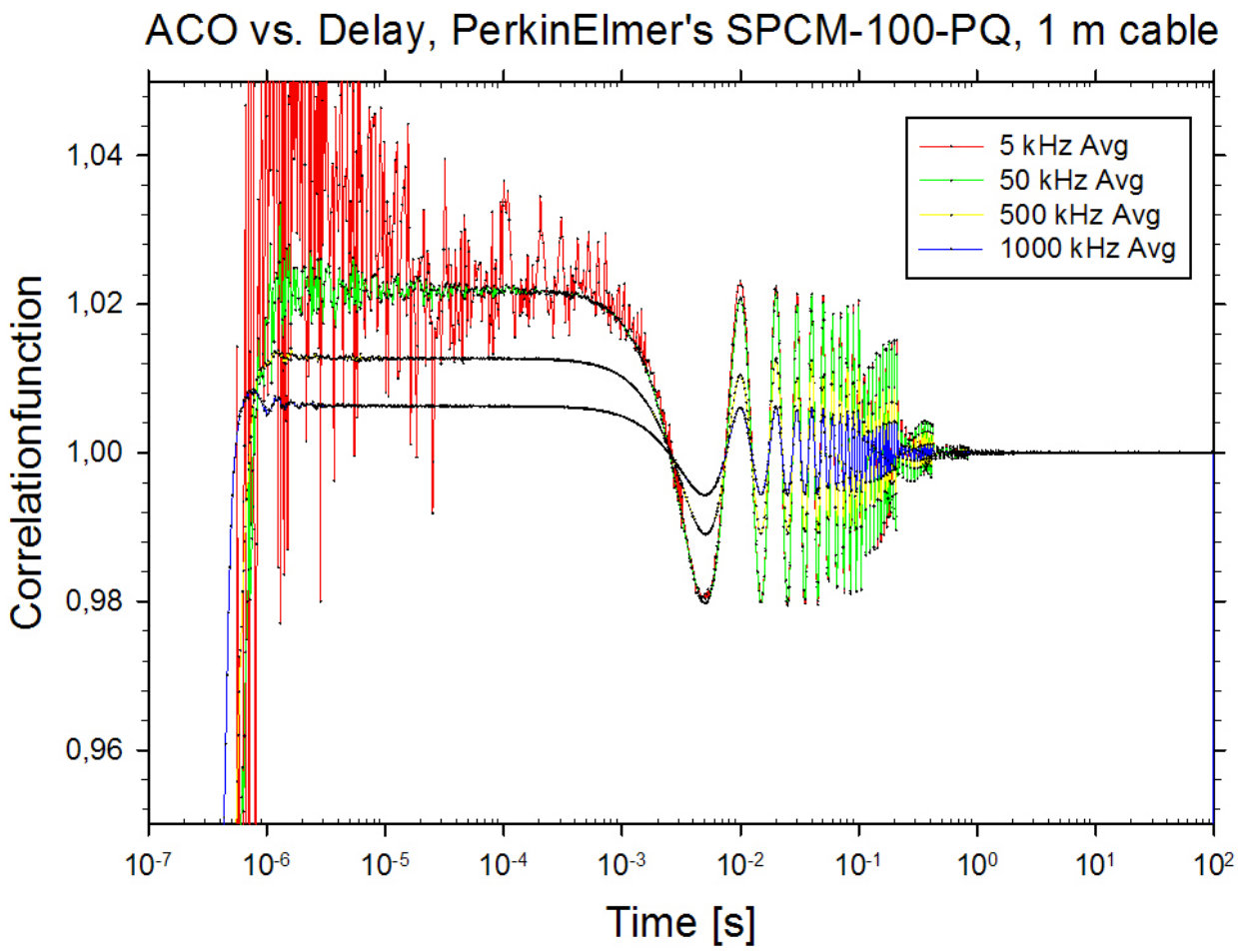

Figure A.34: Average normalized autocorrelation function vs. time delay for the **PerkinElmer's SPCM-100-PQ** at various photon count rates using 1 m cable. Note that y-axis uses linear scaling and x-axis uses logarithmic scaling.

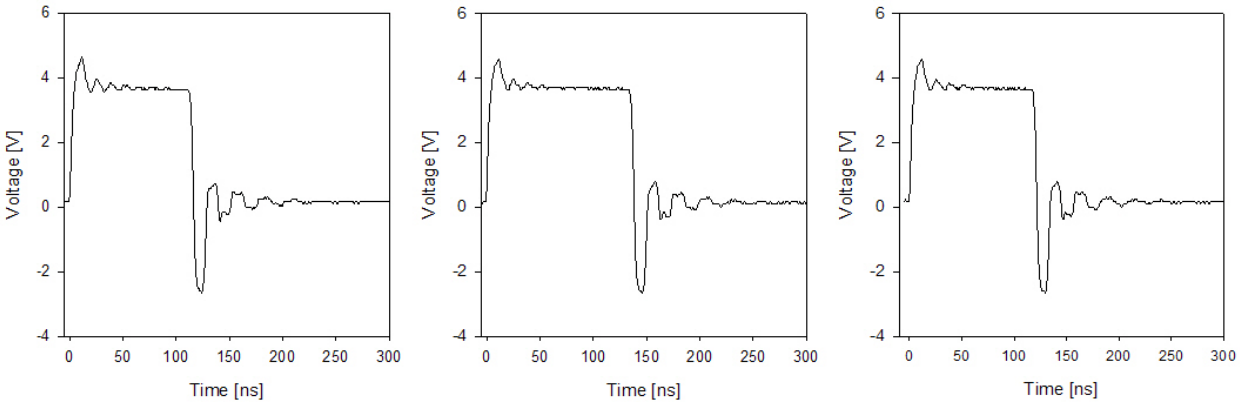

Figure A.35: Somewhat randomly picked waveforms (pulse shape) in the digital oscilloscope "Picoscope 5203" for some count rates, using the same setup as in the previous figure. From left to right: 5 kHz, 500 kHz, and 1000 kHz.

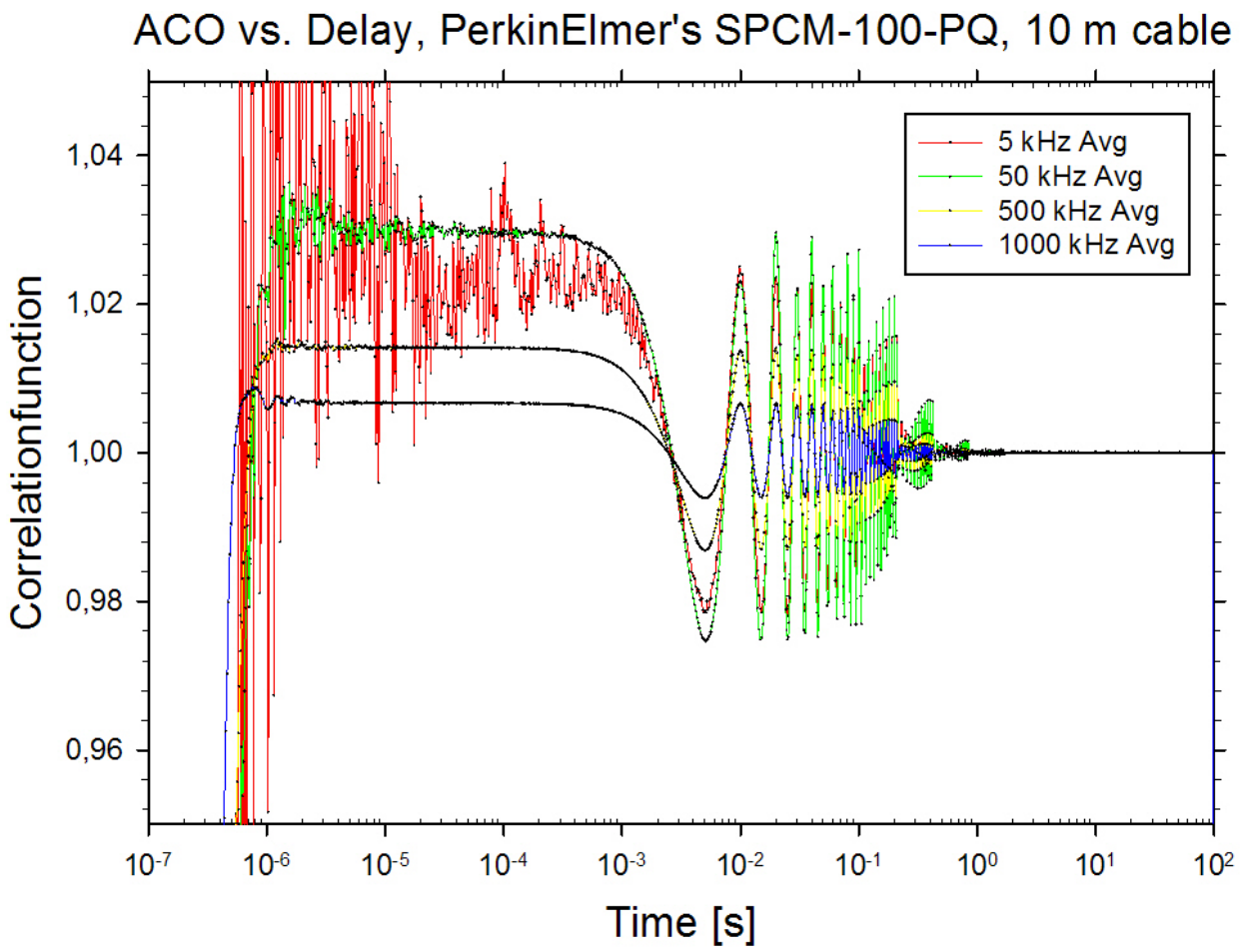

Figure A.36: Average normalized autocorrelation function vs. time delay for the **PerkinElmer's SPCM-100-PQ** at various photon count rates using 10 m cable. Note that y-axis uses linear scaling and x-axis uses logarithmic scaling.

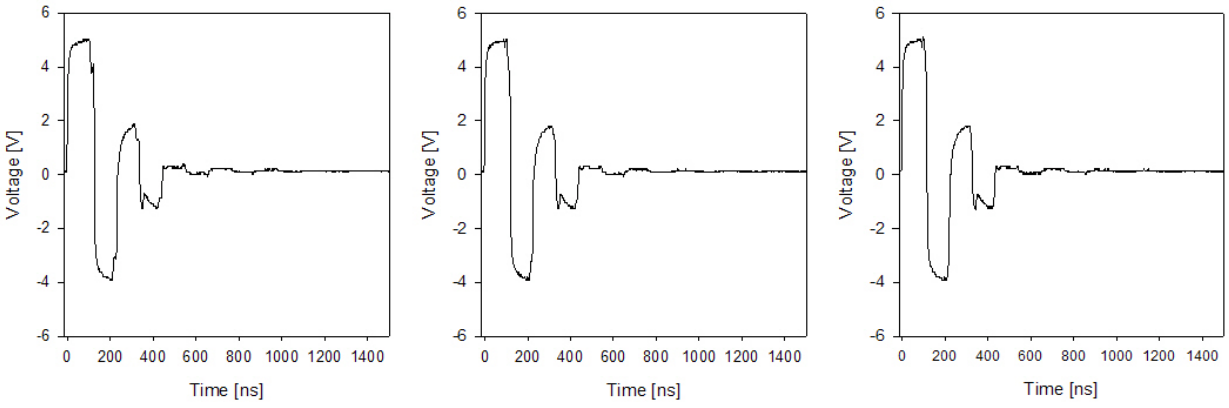

Figure A.37: Somewhat randomly picked waveforms (pulse shape) in the digital oscilloscope "Picoscope 5203" for some count rates, using the same setup as in the previous figure. From left to right: 5 kHz, 500 kHz, and 1000 kHz.

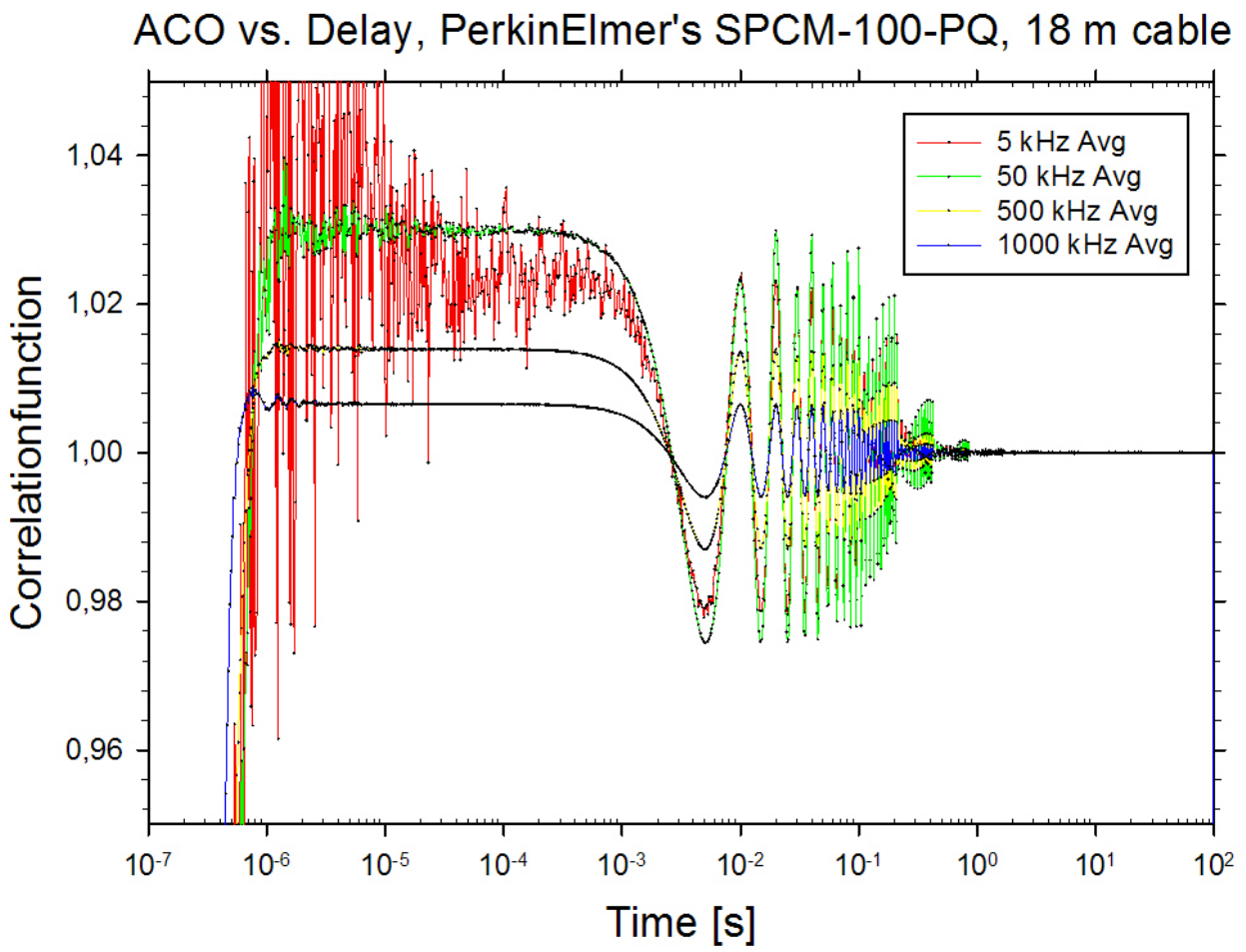

Figure A.38: Average normalized autocorrelation function vs. time delay for the **PerkinElmer's SPCM-100-PQ** at various photon count rates using 18 m cable. Note that y-axis uses linear scaling and x-axis uses logarithmic scaling.

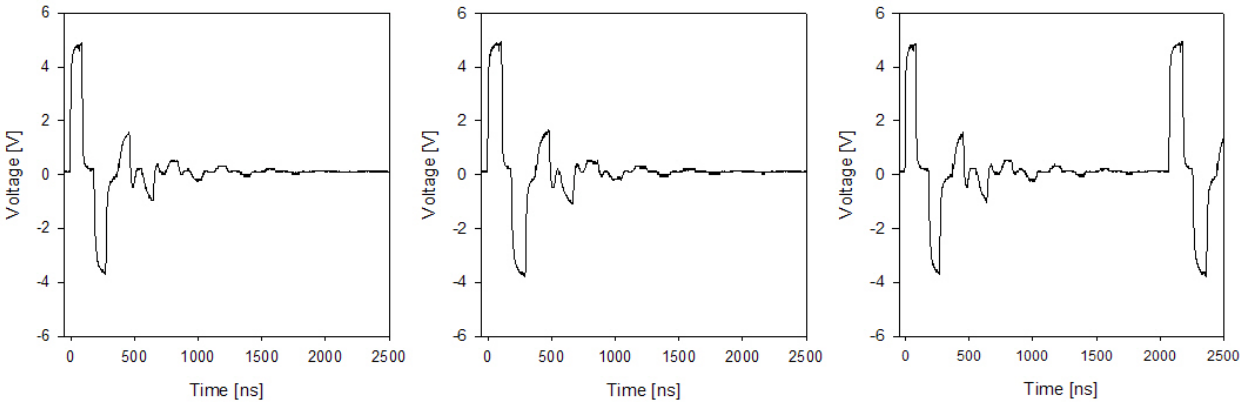

Figure A.39: Somewhat randomly picked waveforms (pulse shape) in the digital oscilloscope "Picoscope 5203" for some count rates, using the same setup as in the previous figure. From left to right: 5 kHz, 500 kHz, and 1000 kHz.

A.4 PerkinElmer's SPCM-AQR-14

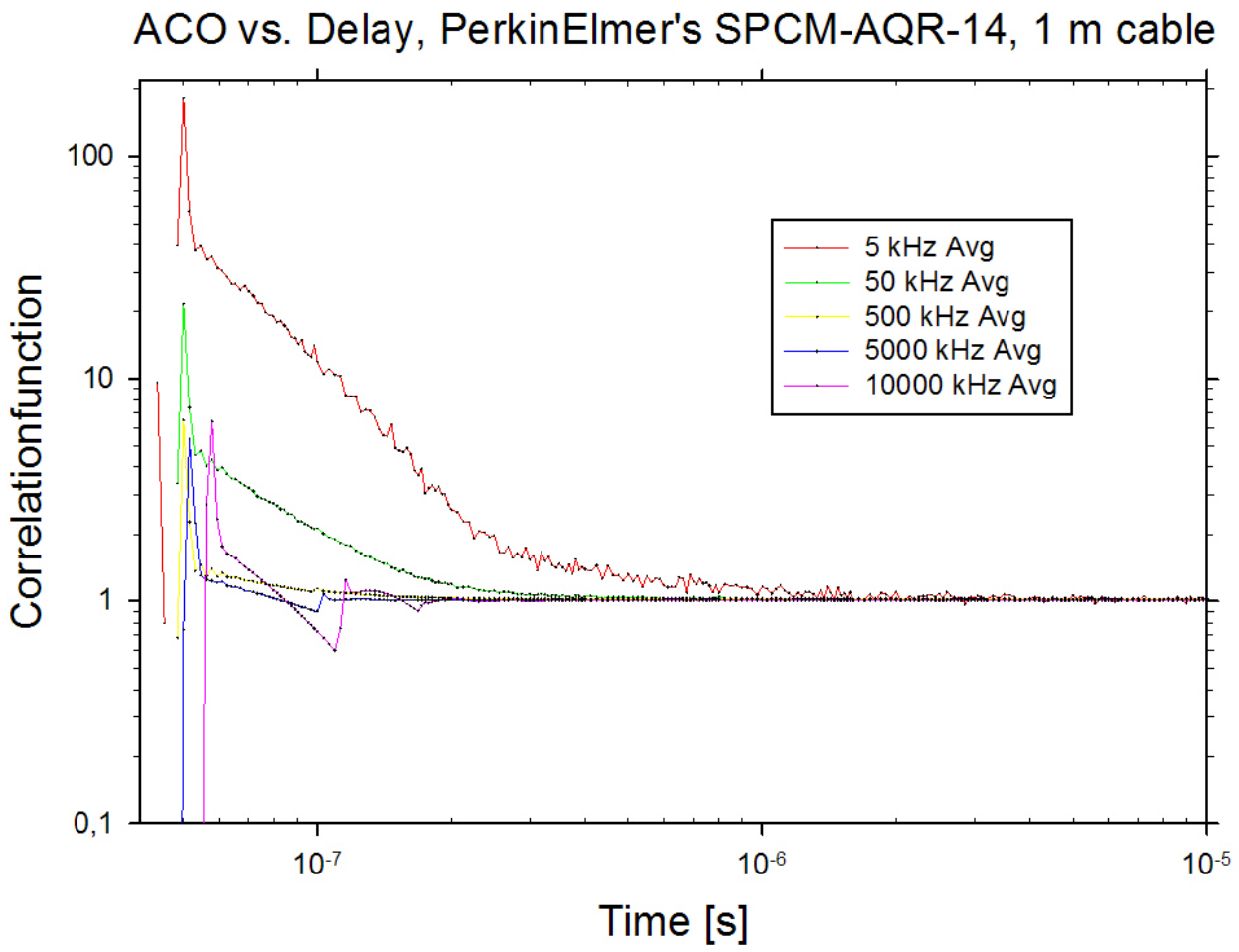

Figure A.40: Average normalized autocorrelation function vs. time delay for **PerkinElmer's SPCM-AQR-14** at various photon count rates using 1 m cable. Note that both axes use logarithmic scaling.

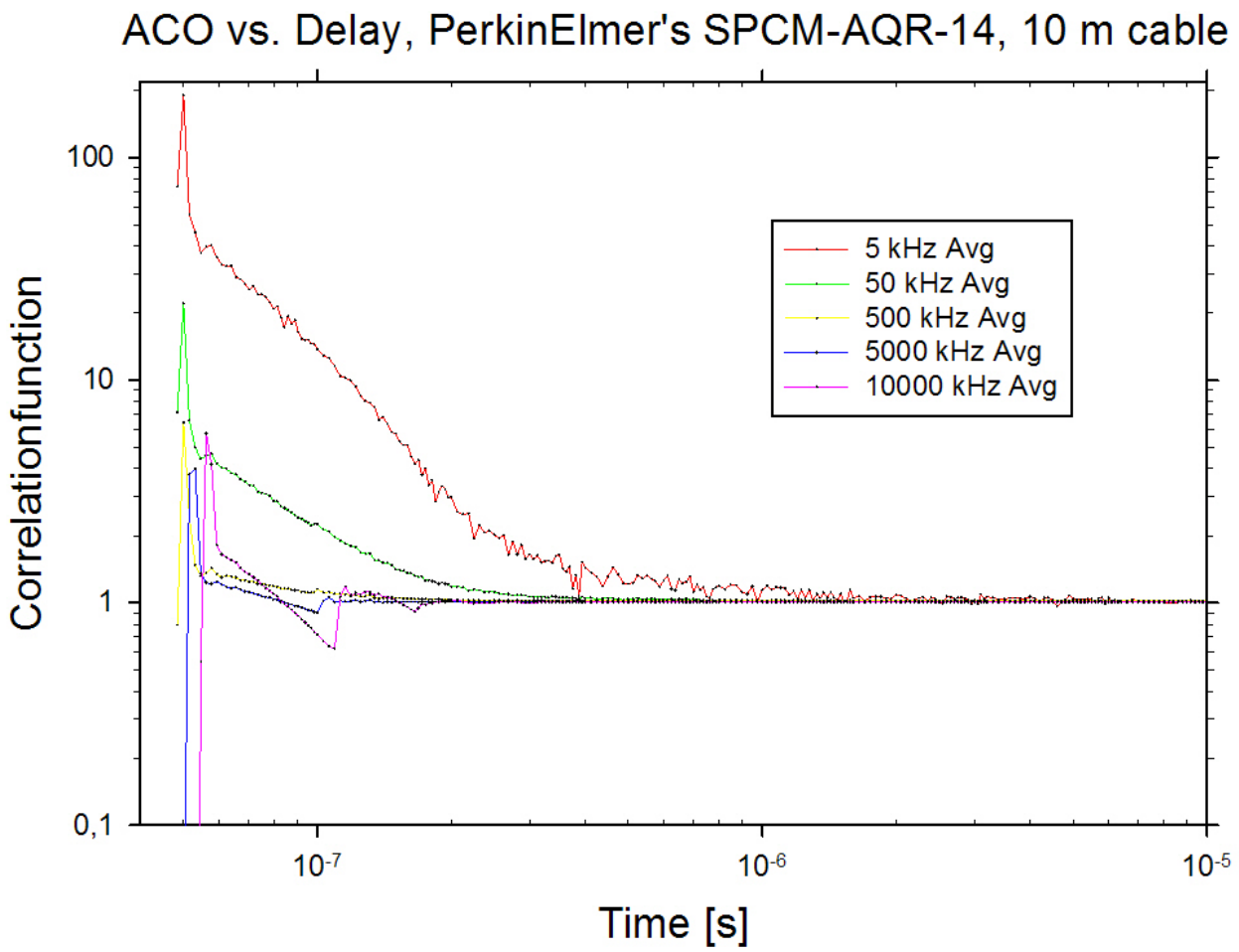

Figure A.41: Average normalized autocorrelation function vs. time delay for **PerkinElmer's SPCM-AQR-14** at various photon count rates using 10 m cable. Note that both axes use logarithmic scaling.

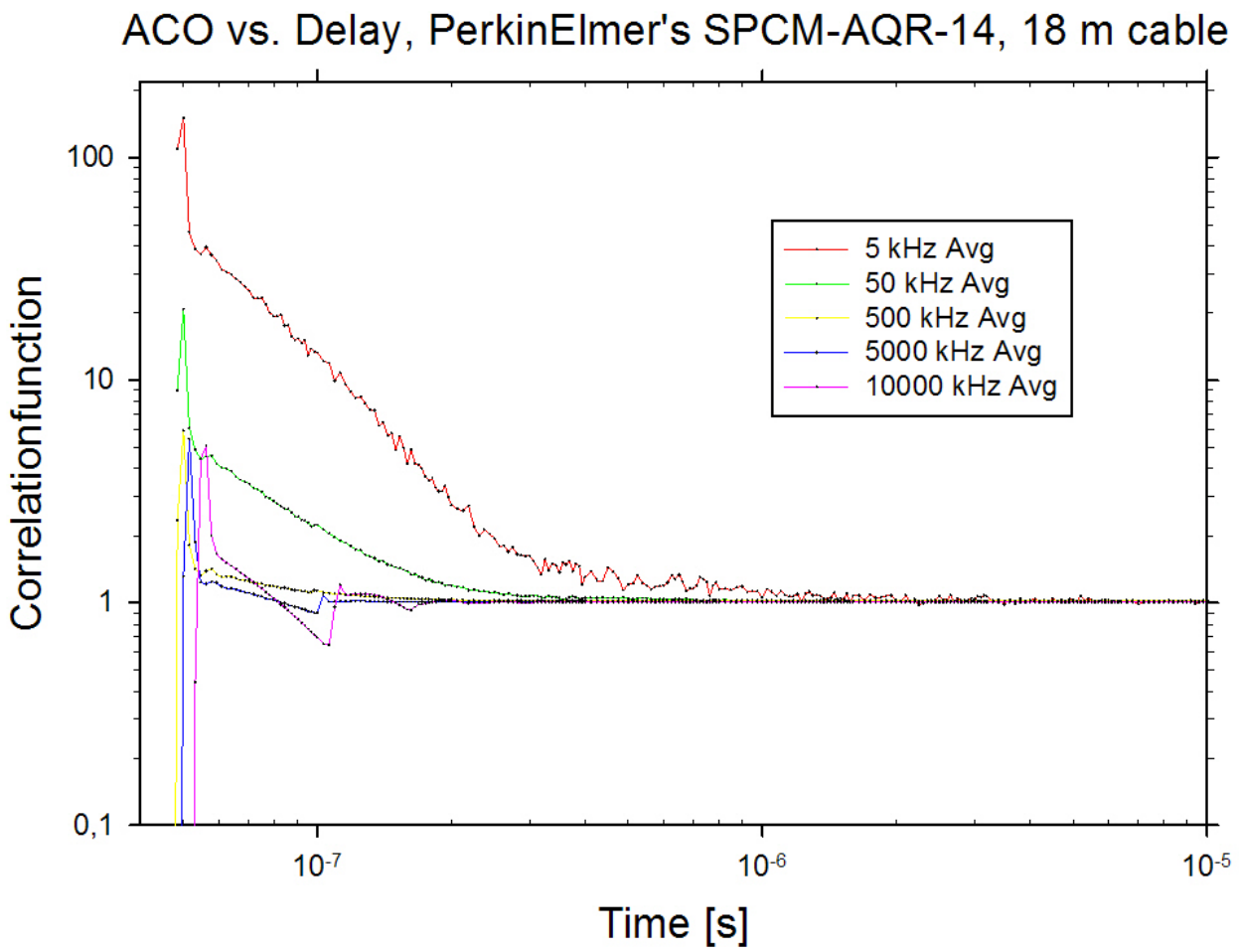

Figure A.42: Average normalized autocorrelation function vs. time delay for **PerkinElmer's SPCM-AQR-14** at various photon count rates using 18 m cable. Note that both axes use logarithmic scaling.

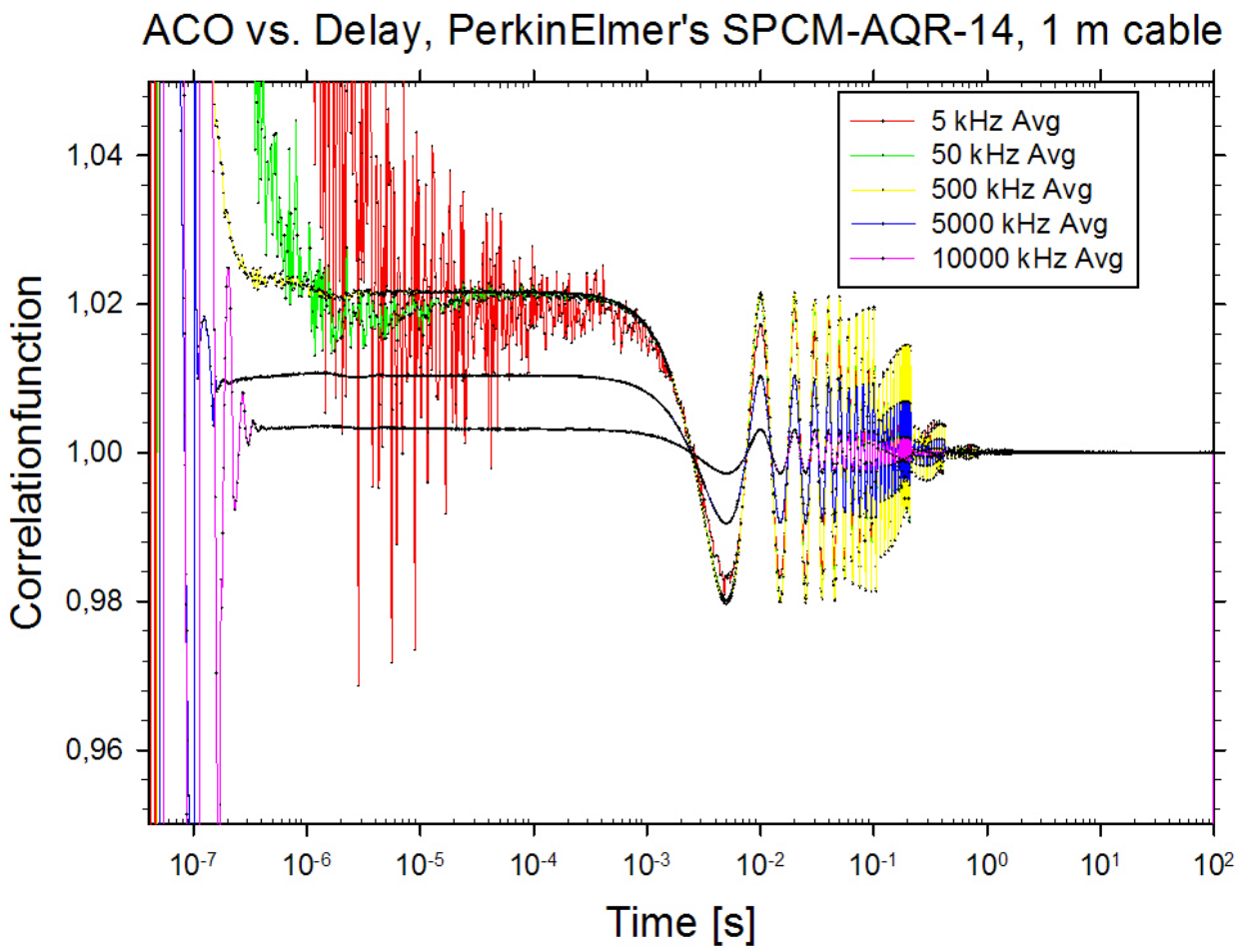

Figure A.43: Average normalized autocorrelation function vs. time delay for **PerkinElmer's SPCM-AQR-14** at various photon count rates using 1 m cable. Note that y-axis uses linear scaling and x-axis uses logarithmic scaling.

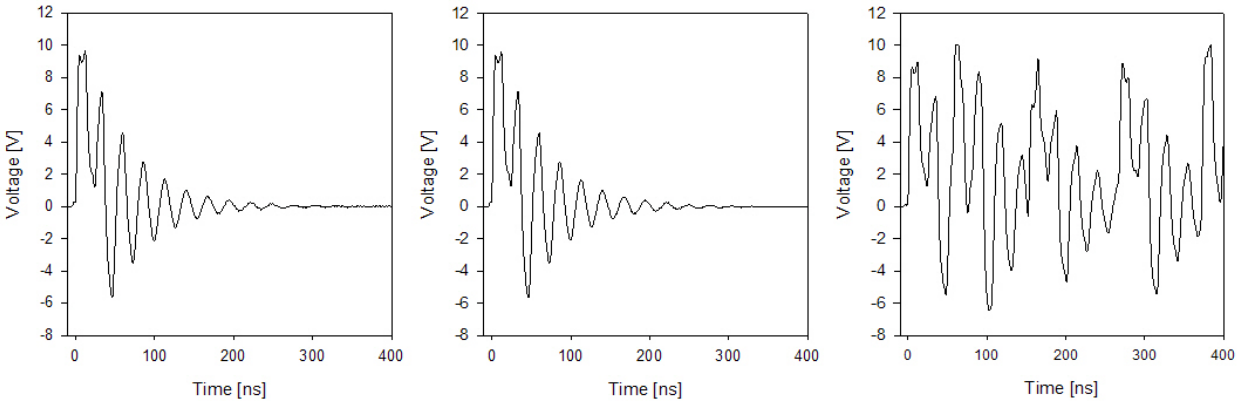

Figure A.44: Somewhat randomly picked waveforms (pulse shape) in the digital oscilloscope "Picoscope 5203" for some count rates, using the same setup as in the previous figure. From left to right: 5 kHz, 500 kHz, and 10000 kHz.

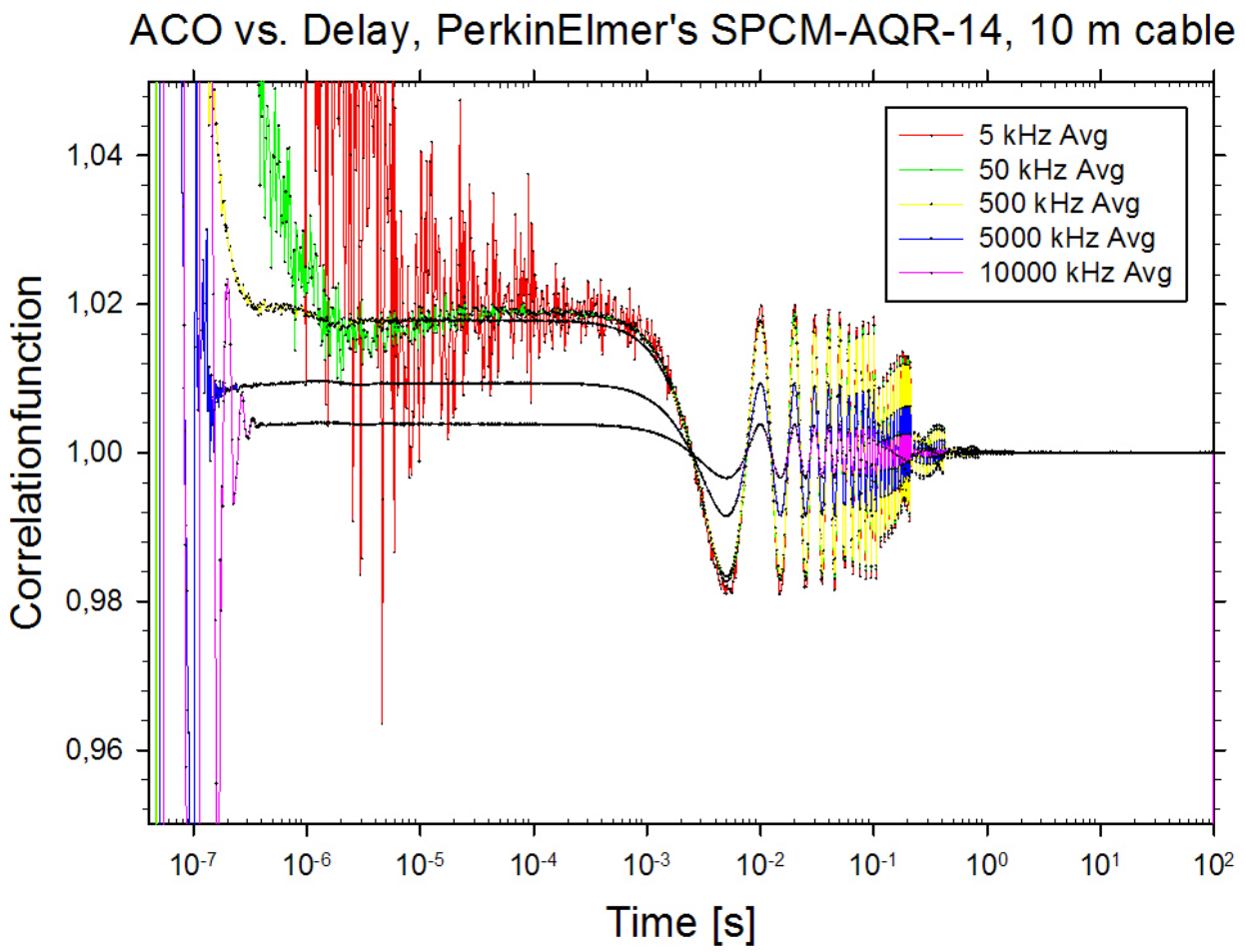

Figure A.45: Average normalized autocorrelation function vs. time delay for **PerkinElmer's SPCM-AQR-14** at various photon count rates using 10 m cable. Note that y-axis uses linear scaling and x-axis uses logarithmic scaling.

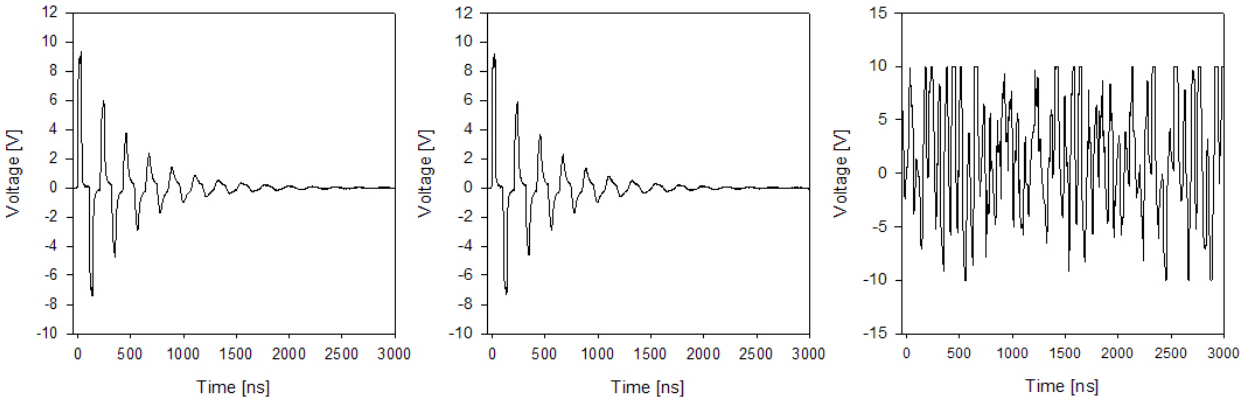

Figure A.46: Somewhat randomly picked waveforms (pulse shape) in the digital oscilloscope "Picoscope 5203" for some count rates, using the same setup as in the previous figure. From left to right: 5 kHz, 500 kHz, and 10000 kHz.

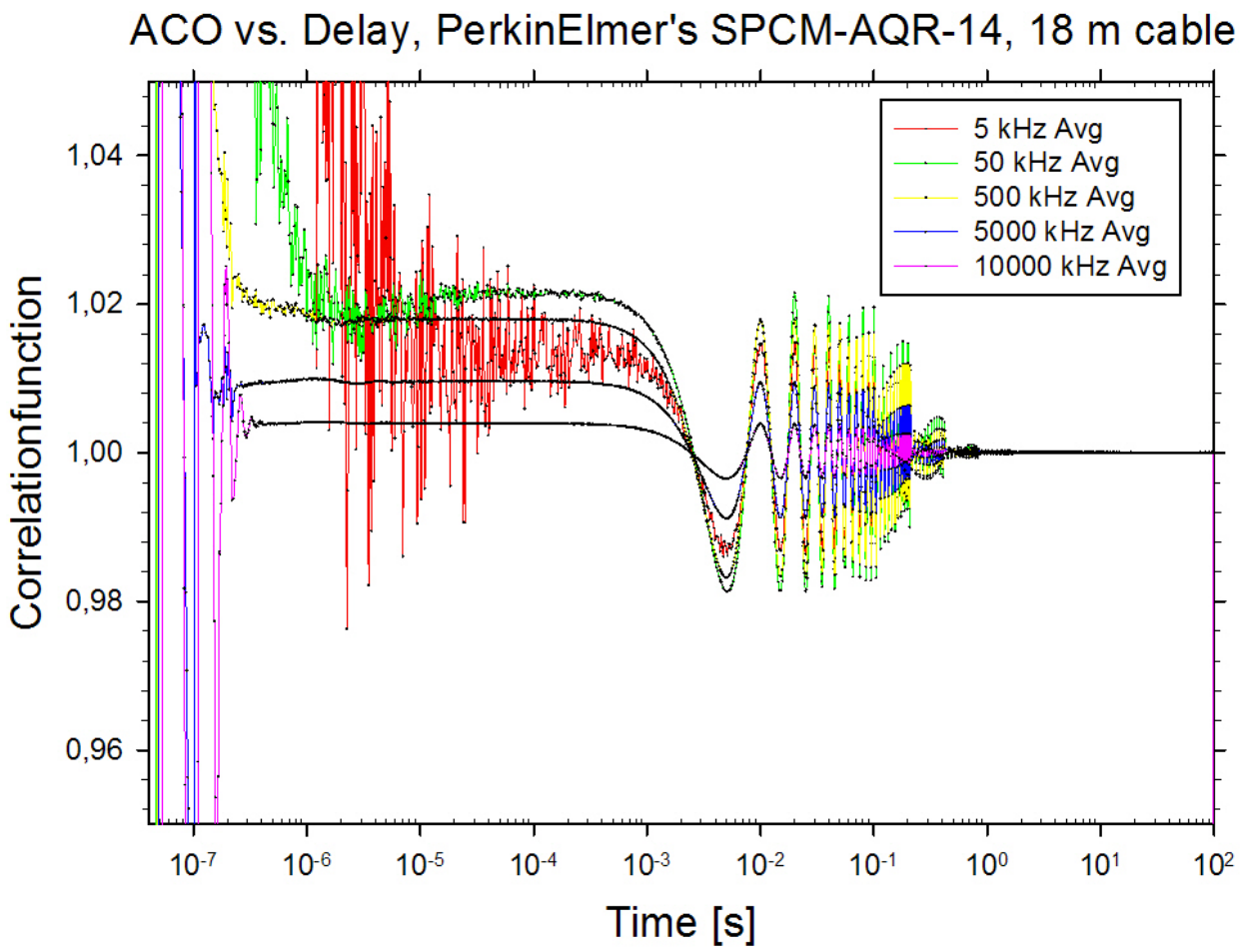

Figure A.47: Average normalized autocorrelation function vs. time delay for **PerkinElmer's SPCM-AQR-14** at various photon count rates using 18 m cable. Note that y-axis uses linear scaling and x-axis uses logarithmic scaling.

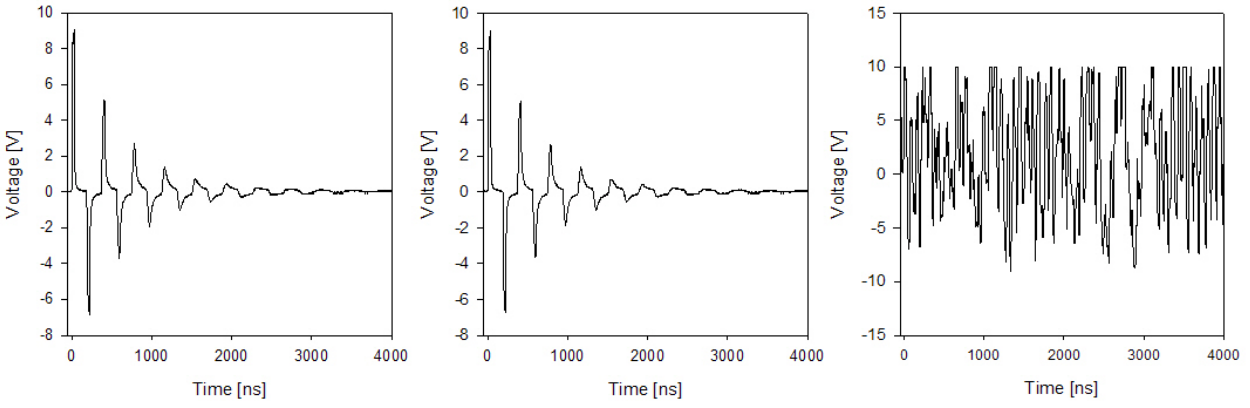

Figure A.48: Somewhat randomly picked waveforms (pulse shape) in the digital oscilloscope "Picoscope 5203" for some count rates, using the same setup as in the previous figure. From left to right: 5 kHz, 500 kHz, and 10000 kHz.

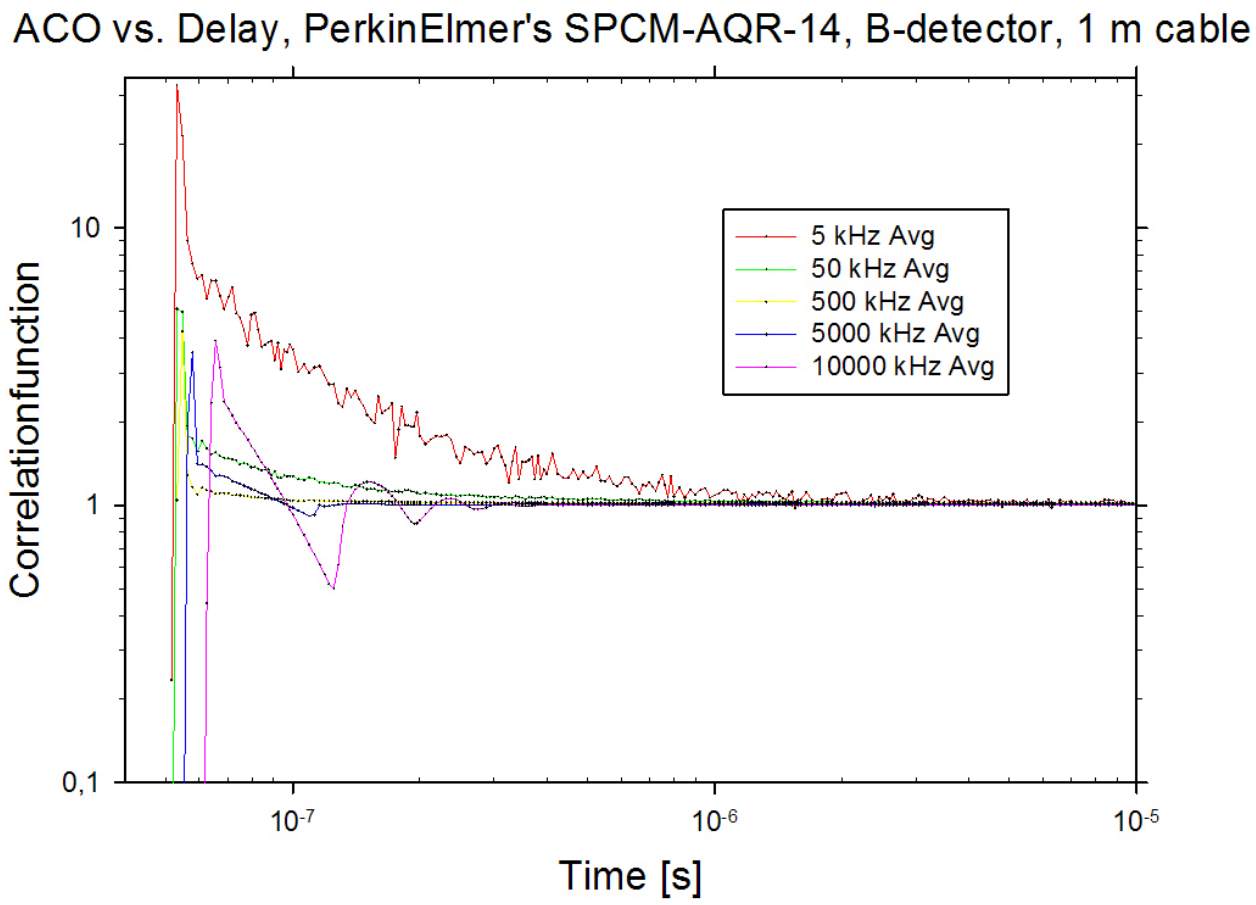

Figure A.49: Average normalized autocorrelation function vs. time delay for **PerkinElmer's SPCM-AQR-14**, using the 2nd detector (normally used for the B-channel in the hardware-correlator), at various photon count rates using 1 m cable. Note that y-axis uses linear scaling and x-axis uses logarithmic scaling.

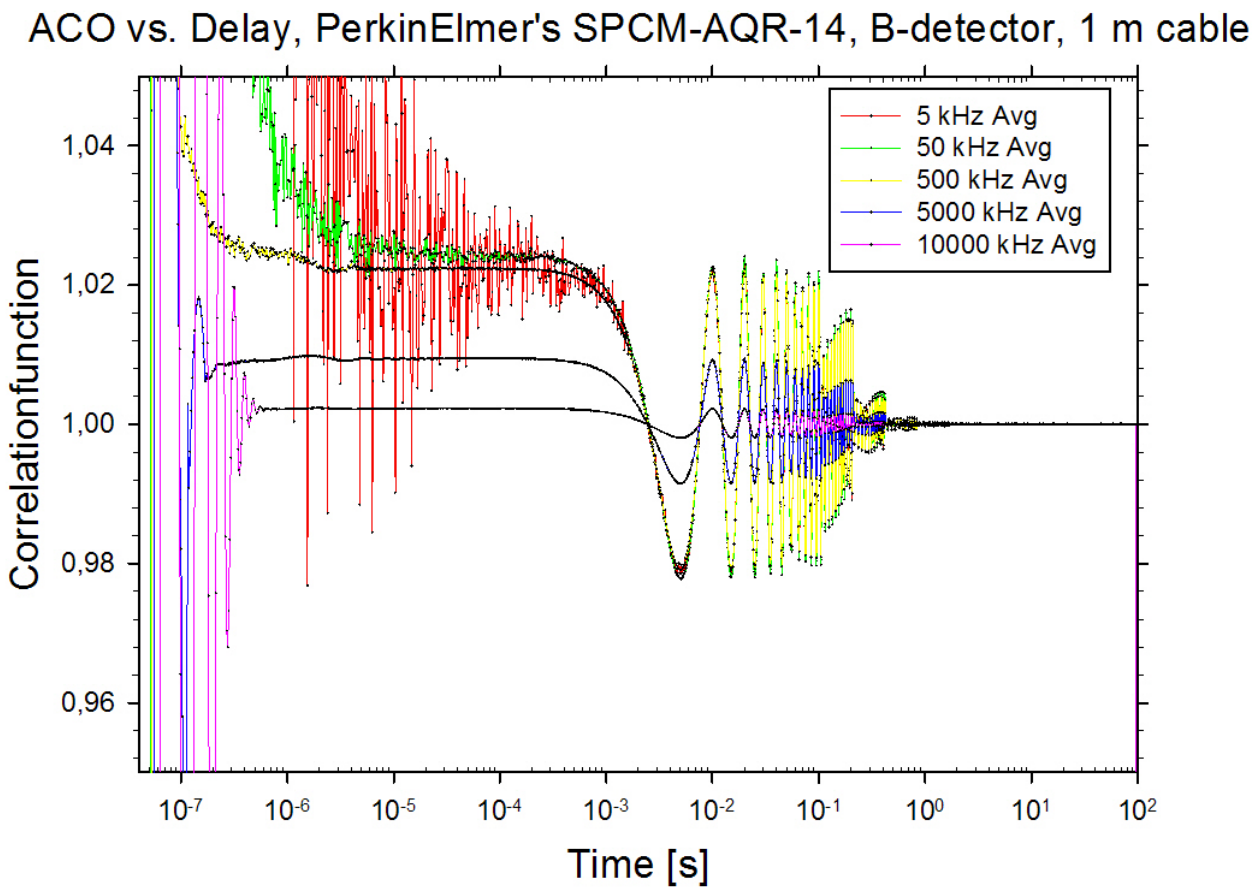

Figure A.50: Average normalized autocorrelation function vs. time delay for **PerkinElmer's SPCM-AQR-14**, using the 2nd detector (normally used for the B-channel in the hardware-correlator), at various photon count rates using 1 m cable. Note that y-axis uses linear scaling and x-axis uses logarithmic scaling.

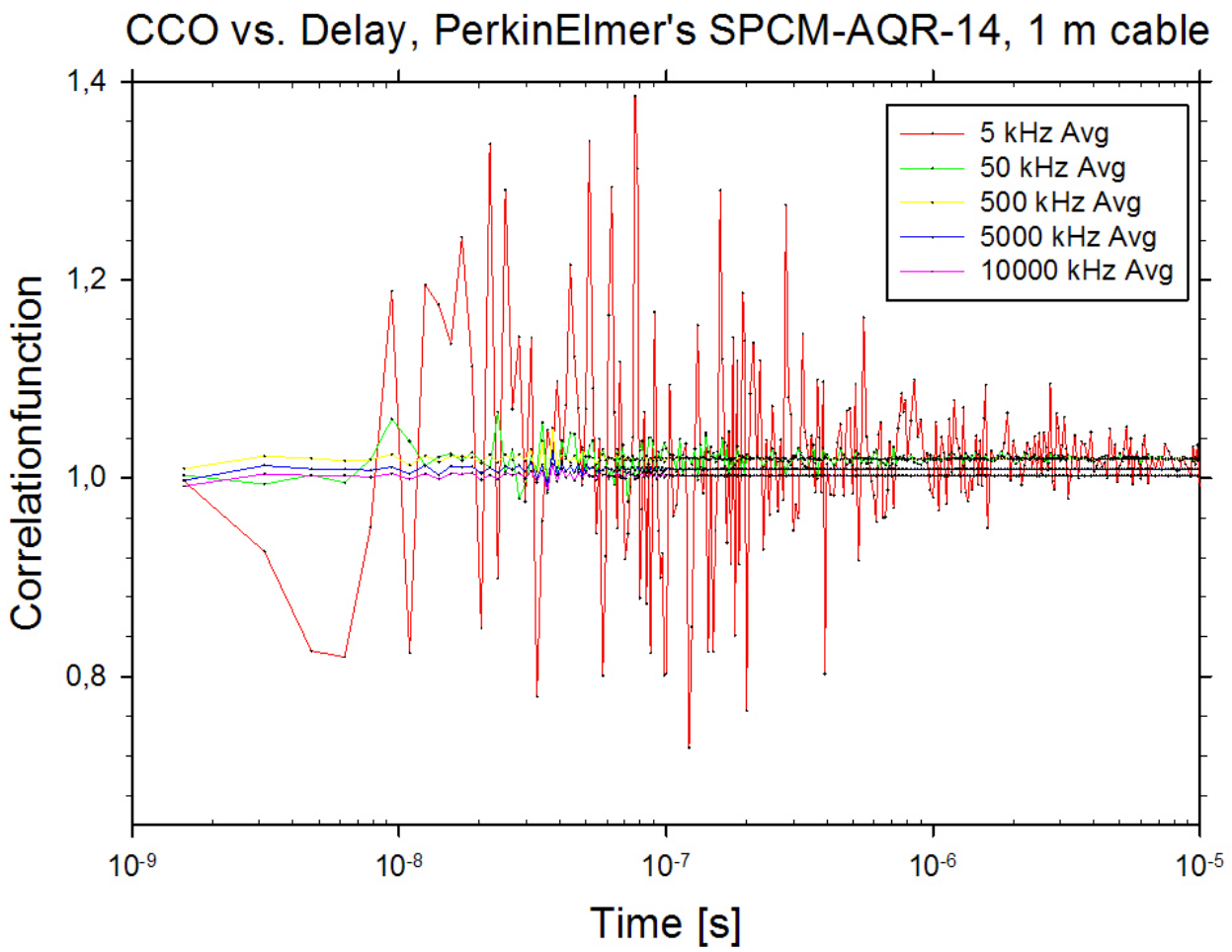

Figure A.51: Average normalized crosscorrelation function vs. time delay for **PerkinElmer's SPCM-AQR-14** at various photon count rates using 1 m cable. Note that y-axis uses linear scaling and x-axis uses logarithmic scaling.

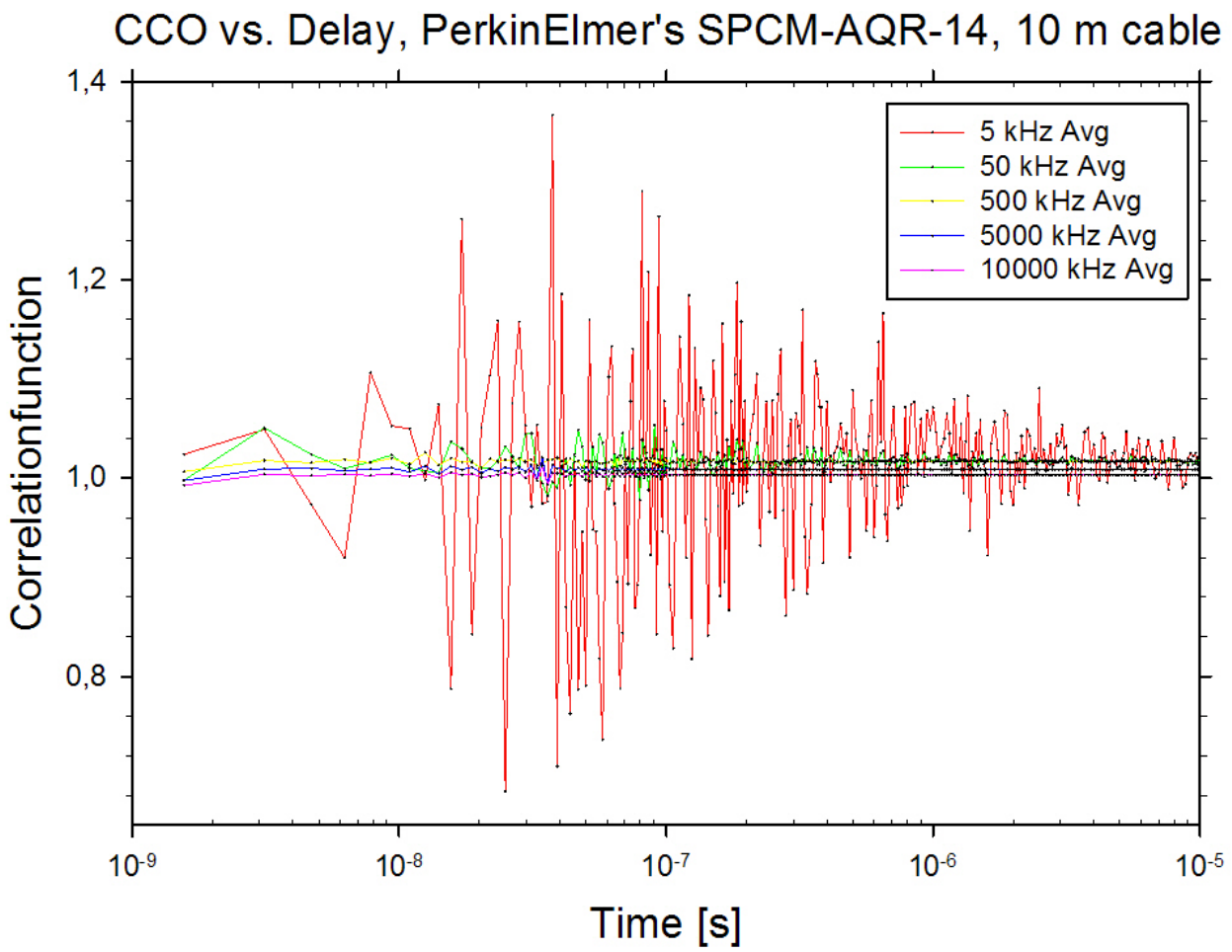

Figure A.52: Average normalized crosscorrelation function vs. time delay for **PerkinElmer's SPCM-AQR-14** at various photon count rates using 10 m cable. Note that y-axis uses linear scaling and x-axis uses logarithmic scaling.

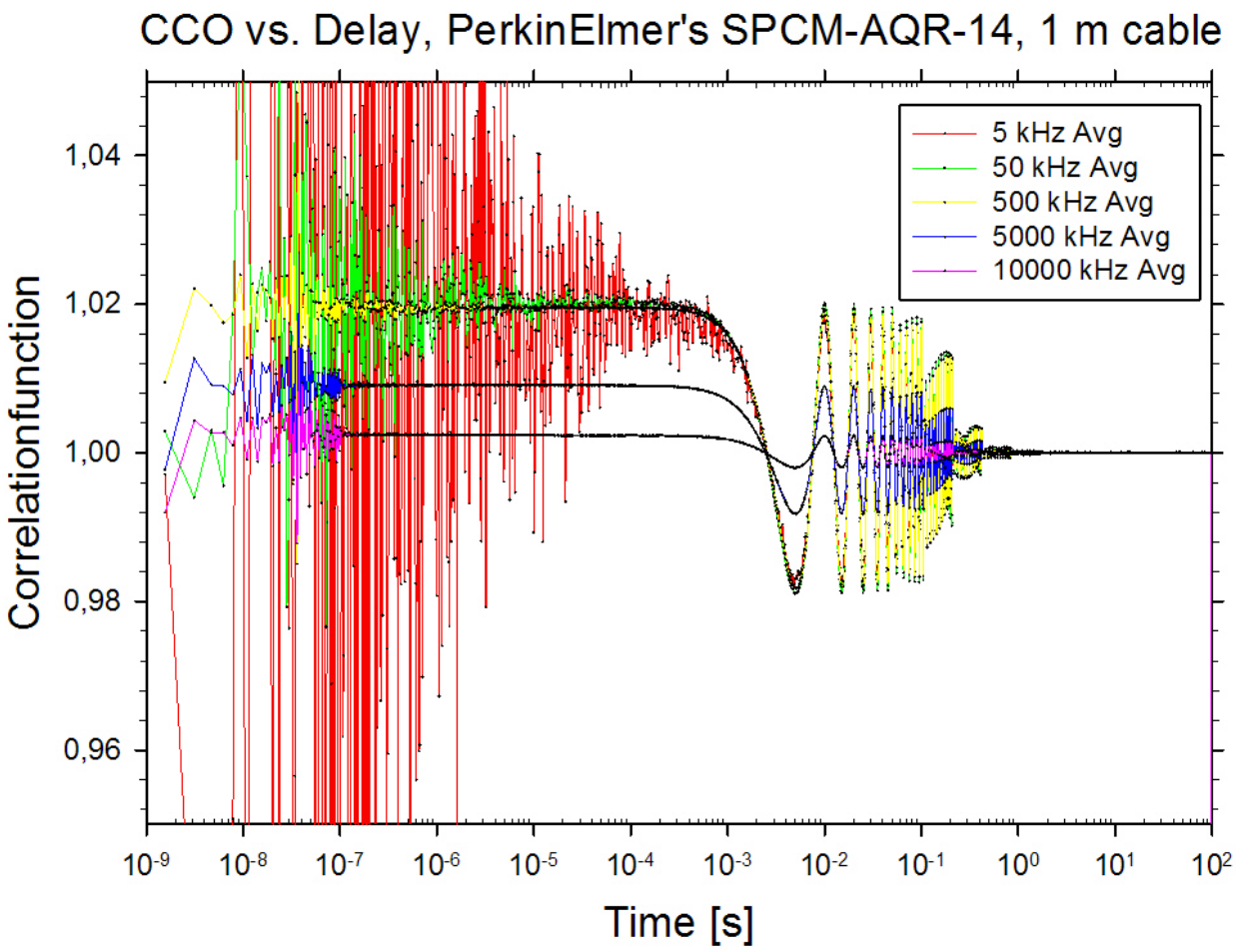

Figure A.53: Average normalized crosscorrelation function vs. time delay for **PerkinElmer's SPCM-AQR-14** at various photon count rates using 1 m cable. Note that y-axis uses linear scaling and x-axis uses logarithmic scaling.

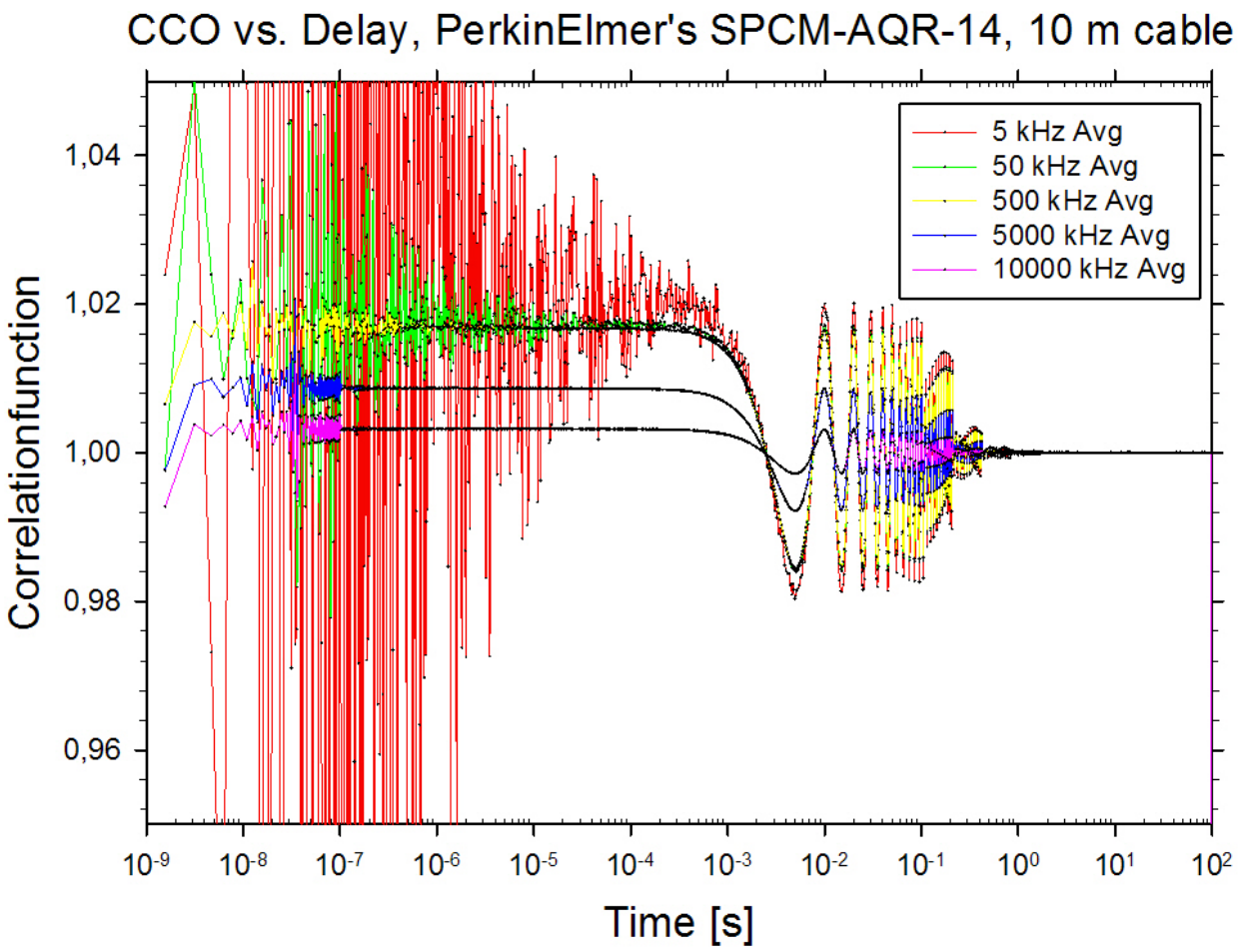

Figure A.54: Average normalized crosscorrelation function vs. time delay for **PerkinElmer's SPCM-AQR-14** at various photon count rates using 10 m cable. Note that y-axis uses linear scaling and x-axis uses logarithmic scaling.

A.5 SensL's PCDMini0100

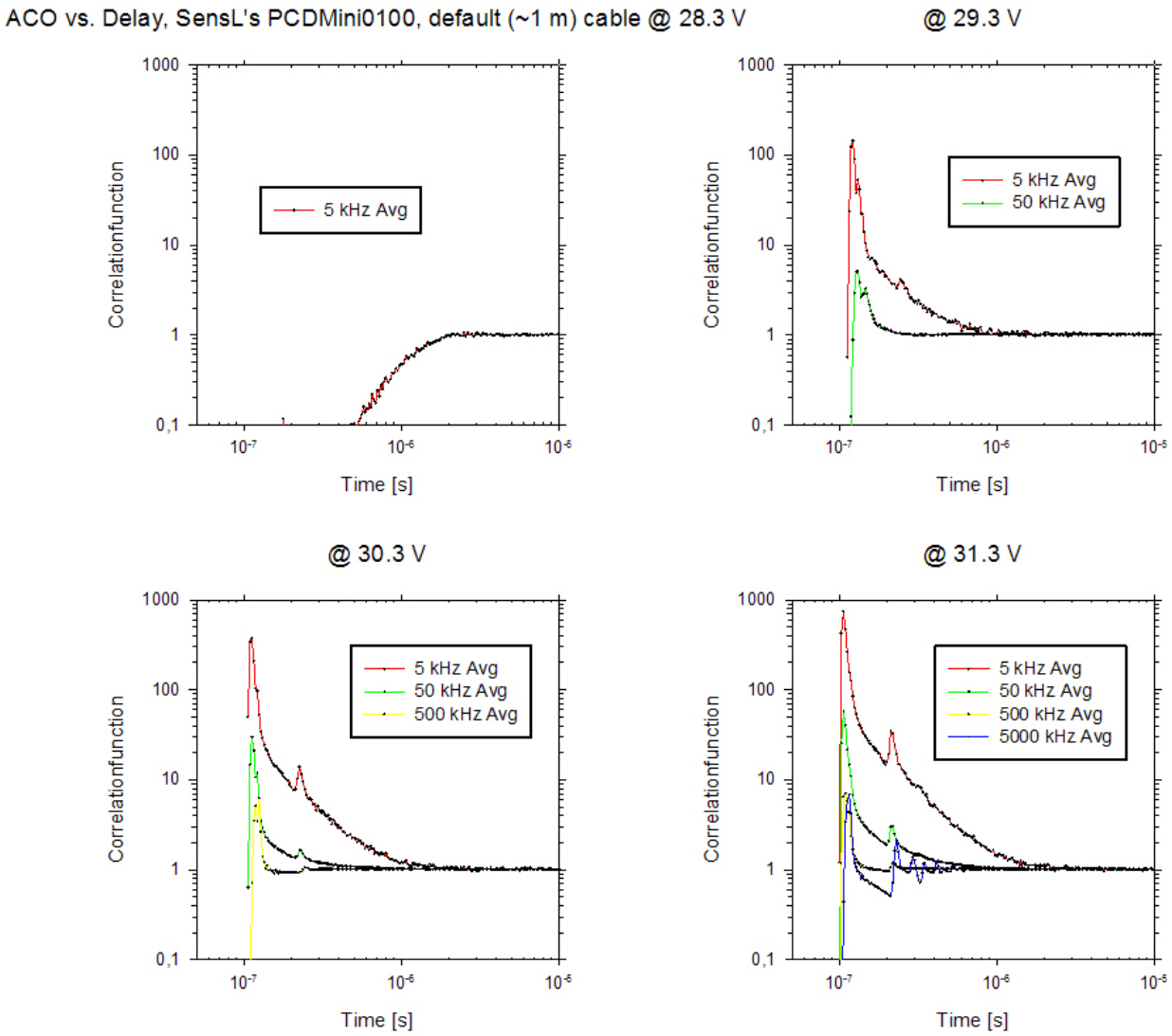

Figure A.55: Average normalized autocorrelation function vs. time delay for the **SensL's PCDMini0100** at various photon count rates and operating voltages using the default (1 m) cable. Note that both axes use logarithmic scaling.

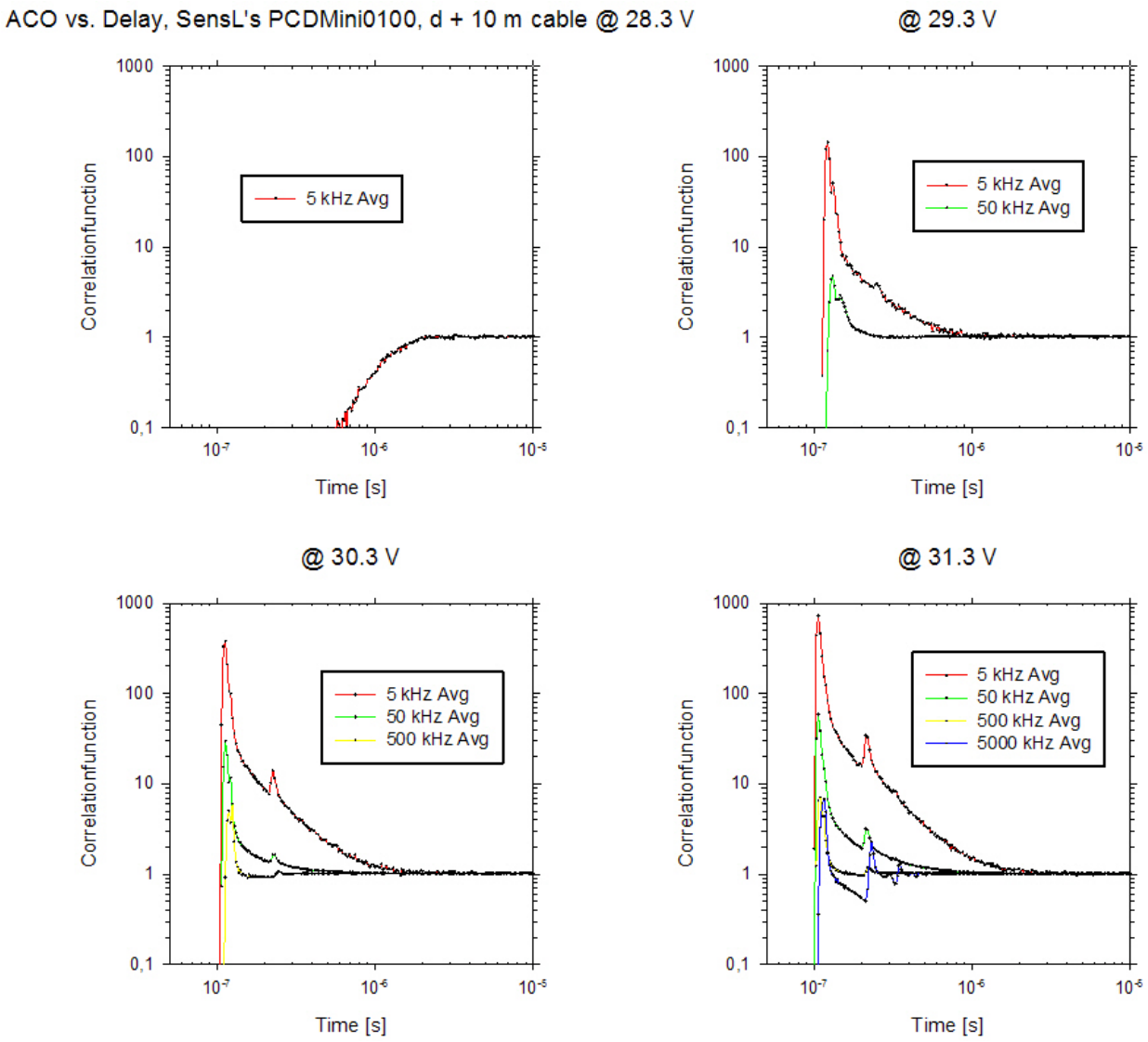

Figure A.56: Average normalized autocorrelation function vs. time delay for the **SensL's PCDMini0100** at various photon count rates and operating voltages using default (1 m) + 10 m cable. Note that both axes use logarithmic scaling.

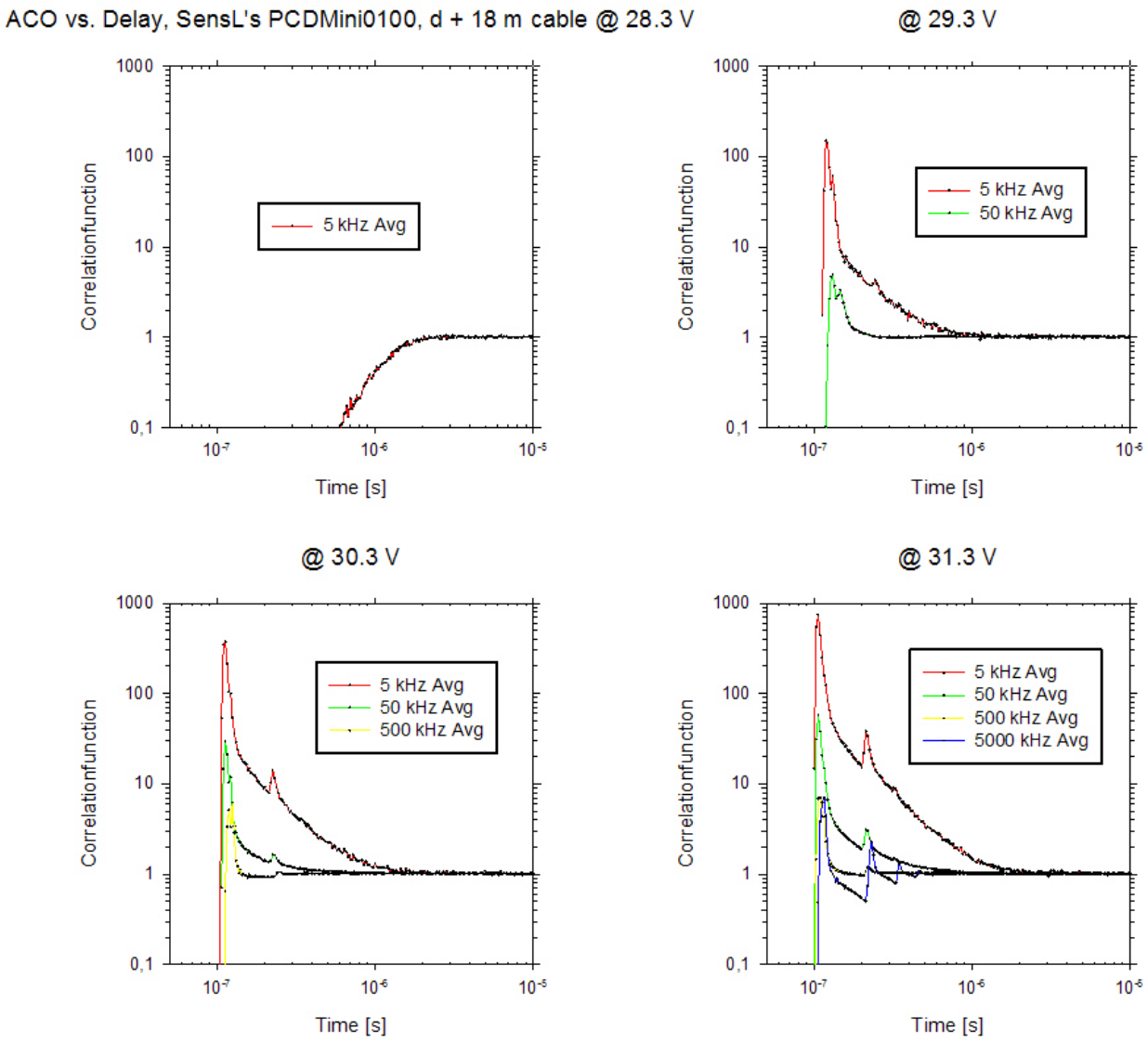

Figure A.57: Average normalized autocorrelation function vs. time delay for the **SensL's PCDMini0100** at various photon count rates and operating voltages using default (1 m) + 18 m cable. Note that both axes use logarithmic scaling.

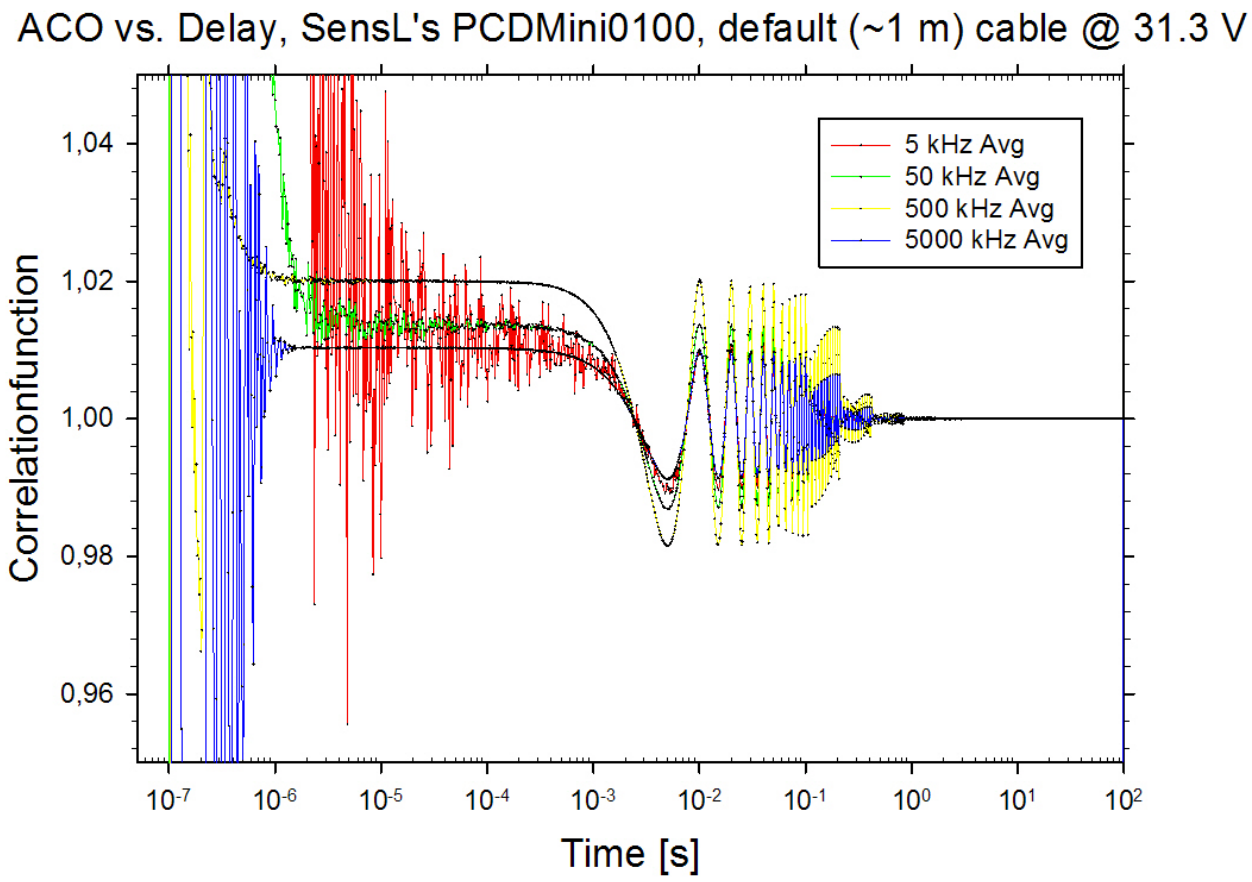

Figure A.58: Average normalized autocorrelation function vs. time delay for the **SensL's PCDMini0100** at various photon count rates and operating voltage 31.3 V using default (1 m) cable. Note that y-axis uses linear scaling and x-axis uses logarithmic scaling.

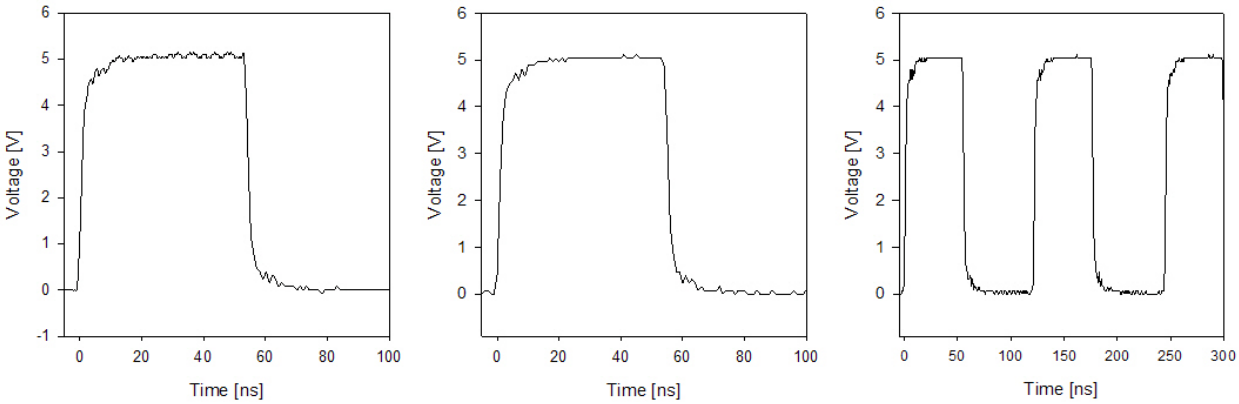

Figure A.59: Somewhat randomly picked waveforms (pulse shape) in the digital oscilloscope "Picoscope 5203" for some count rates, using the same setup as in the previous figure. From left to right: 5 kHz, 500 kHz, and 5000 kHz.

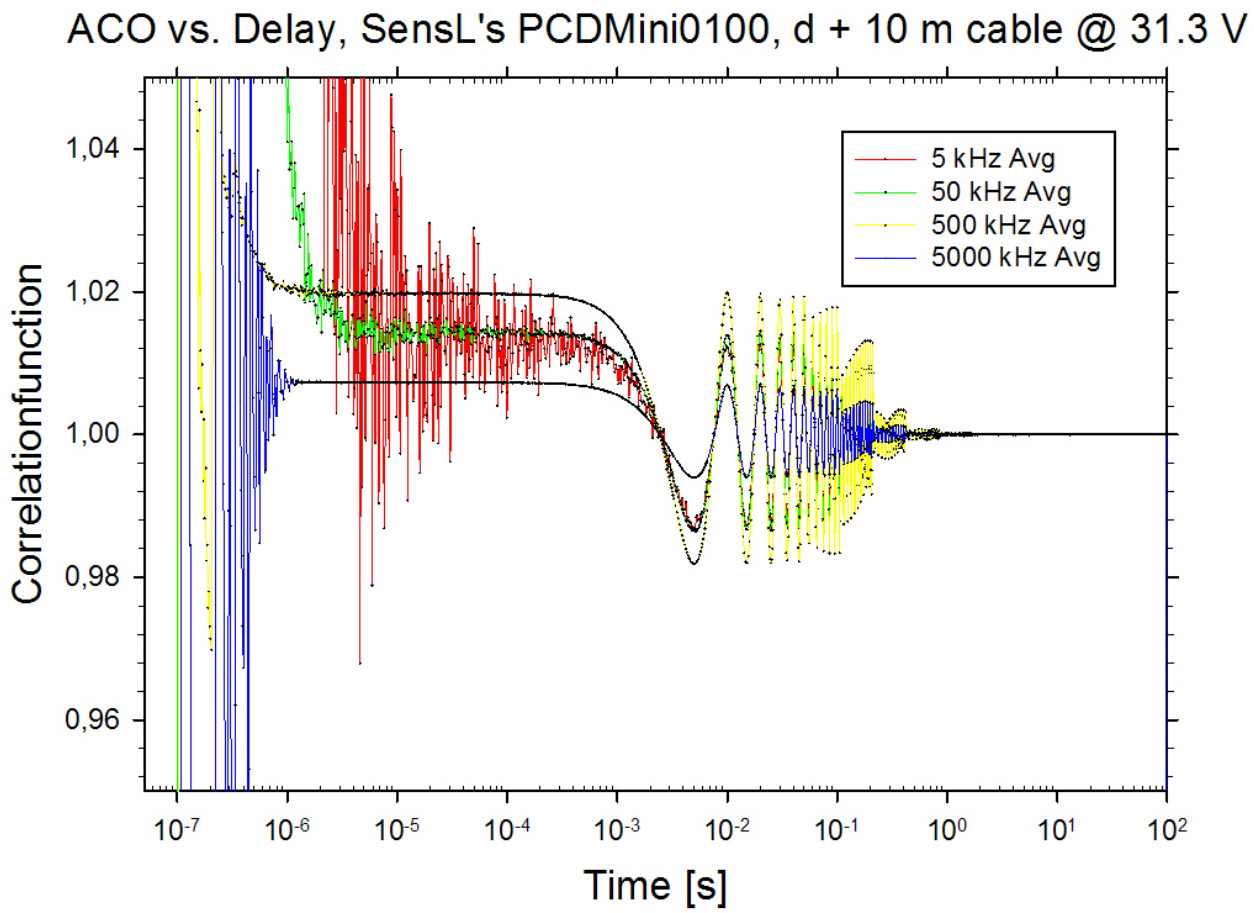

Figure A.60: Average normalized autocorrelation function vs. time delay for the **SensL's PCDMini0100** at various photon count rates and operating voltage 31.3 V using default (1 m) + 10 m cable. Note that y-axis uses linear scaling and x-axis uses logarithmic scaling.

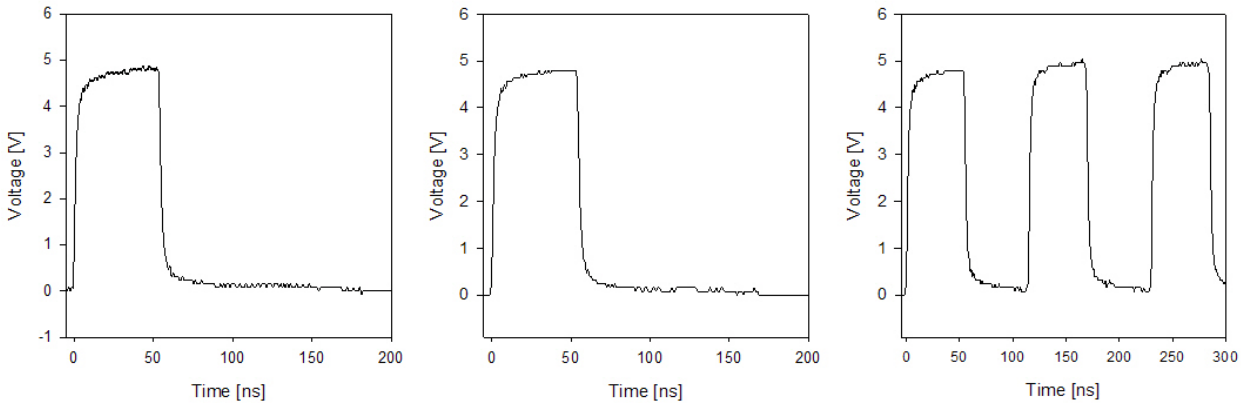

Figure A.61: Somewhat randomly picked waveforms (pulse shape) in the digital oscilloscope "Picoscope 5203" for some count rates, using the same setup as in the previous figure. From left to right: 5 kHz, 500 kHz, and 5000 kHz.

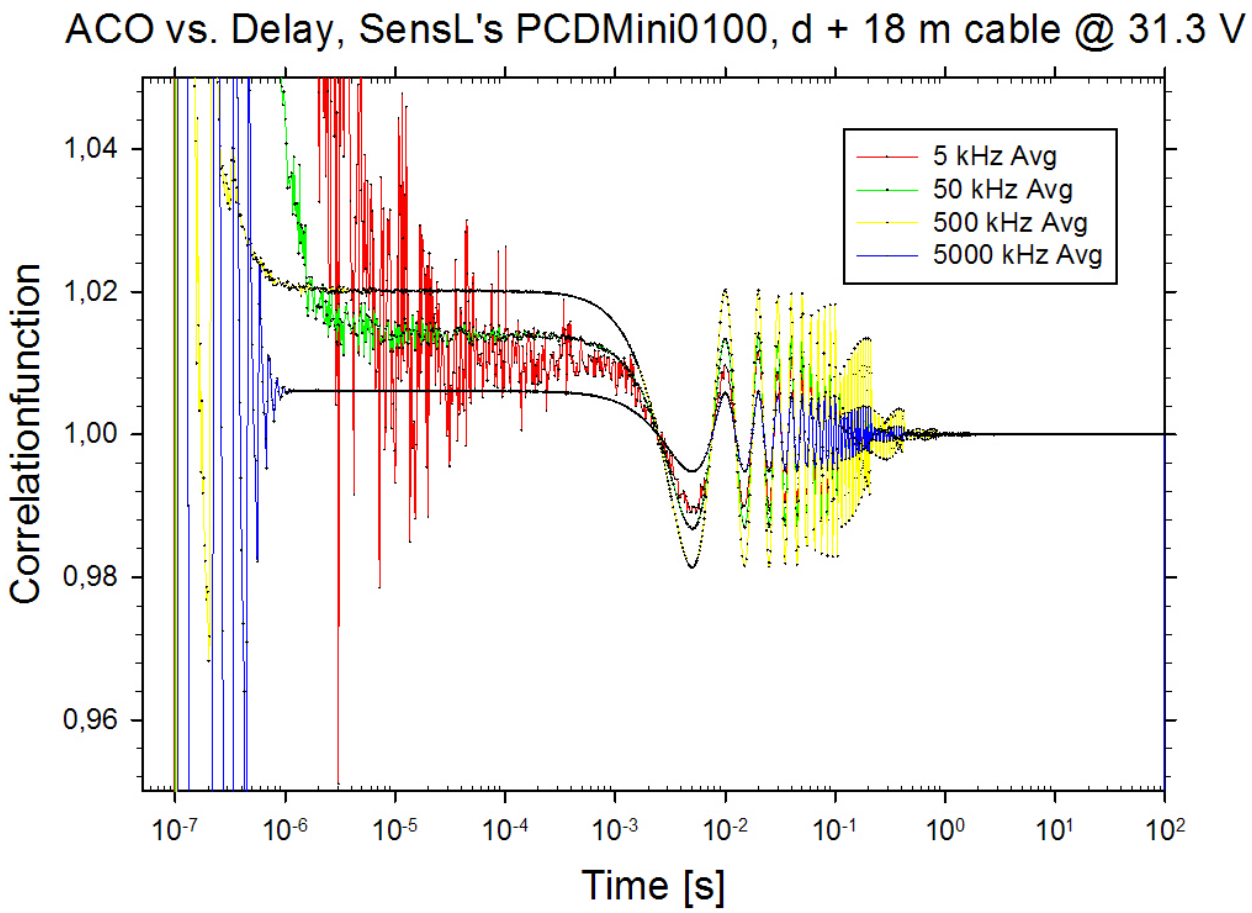

Figure A.62: Average normalized autocorrelation function vs. time delay for the **SensL's PCDMini0100** at various photon count rates and operating voltage 31.3 V using default (1 m) + 18 m cable. Note that y-axis uses linear scaling and x-axis uses logarithmic scaling.

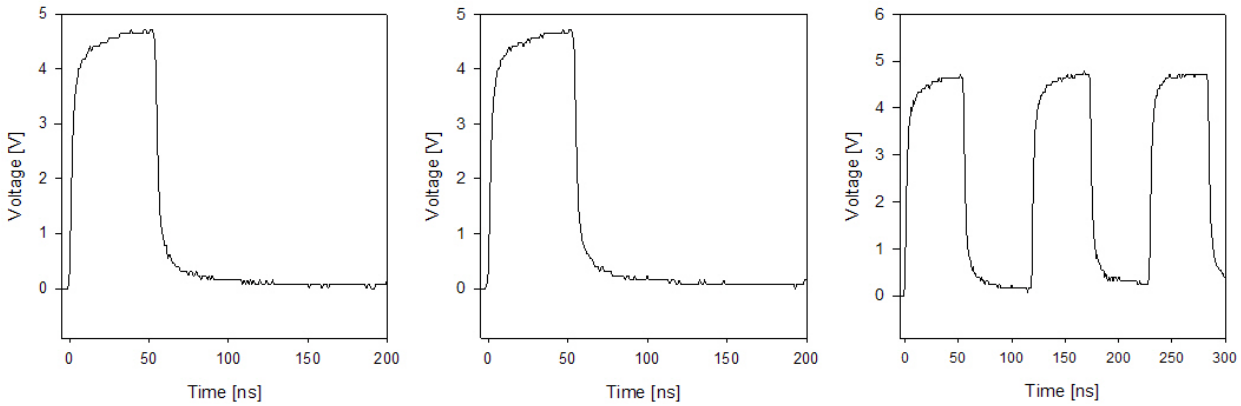

Figure A.63: Somewhat randomly picked waveforms (pulse shape) in the digital oscilloscope "Picoscope 5203" for some count rates, using the same setup as in the previous figure. From left to right: 5 kHz, 500 kHz, and 5000 kHz.

A.6 SensL's SPMPC

Note: Since the dark count rate is higher than 5 kHz, we could not measure at this level for these detectors.

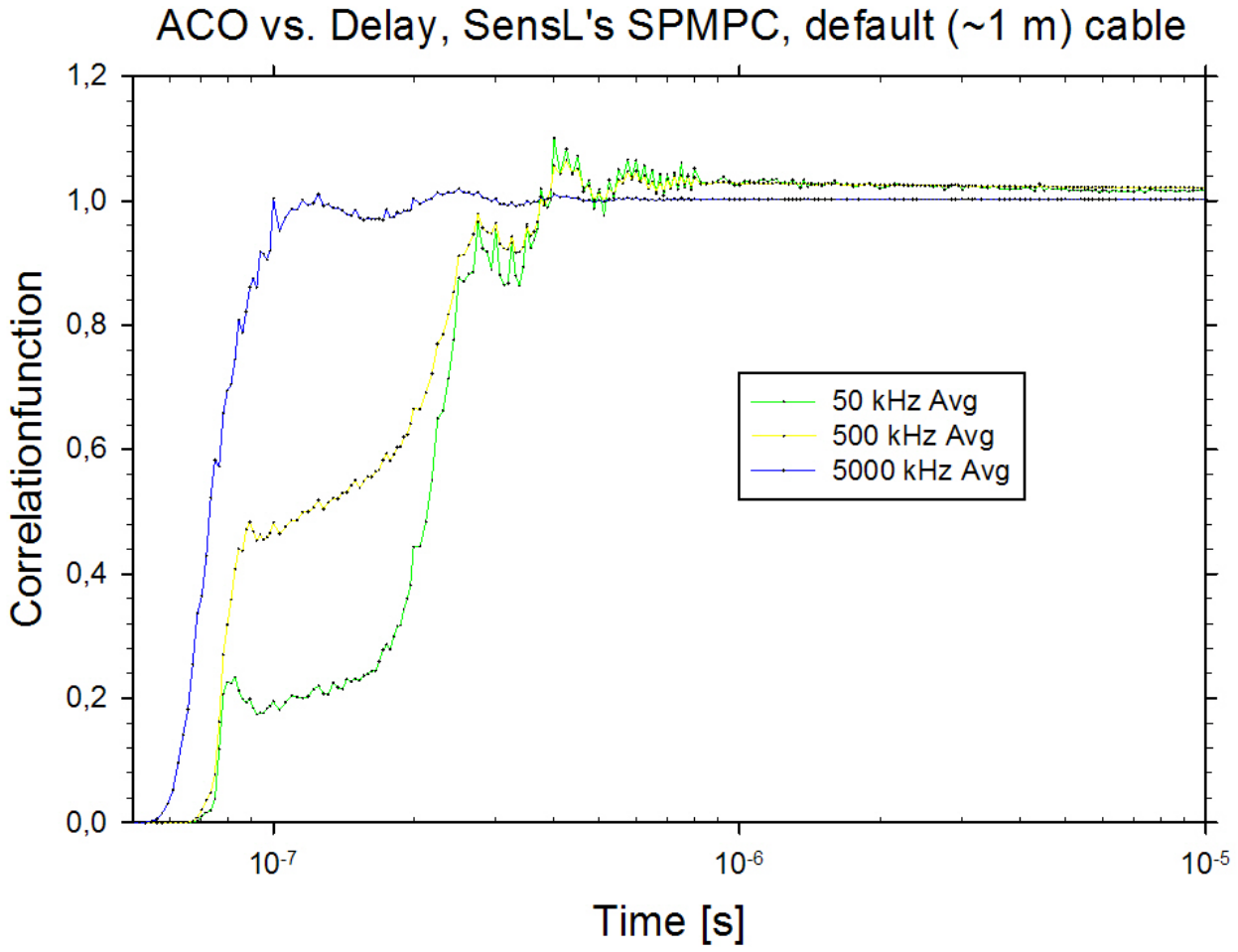

Figure A.64: Average normalized autocorrelation function vs. time delay for the **SensL's SPMPC** at various photon count rates using default (1 m) cable. Note that y-axis uses linear scaling and x-axis uses logarithmic scaling.

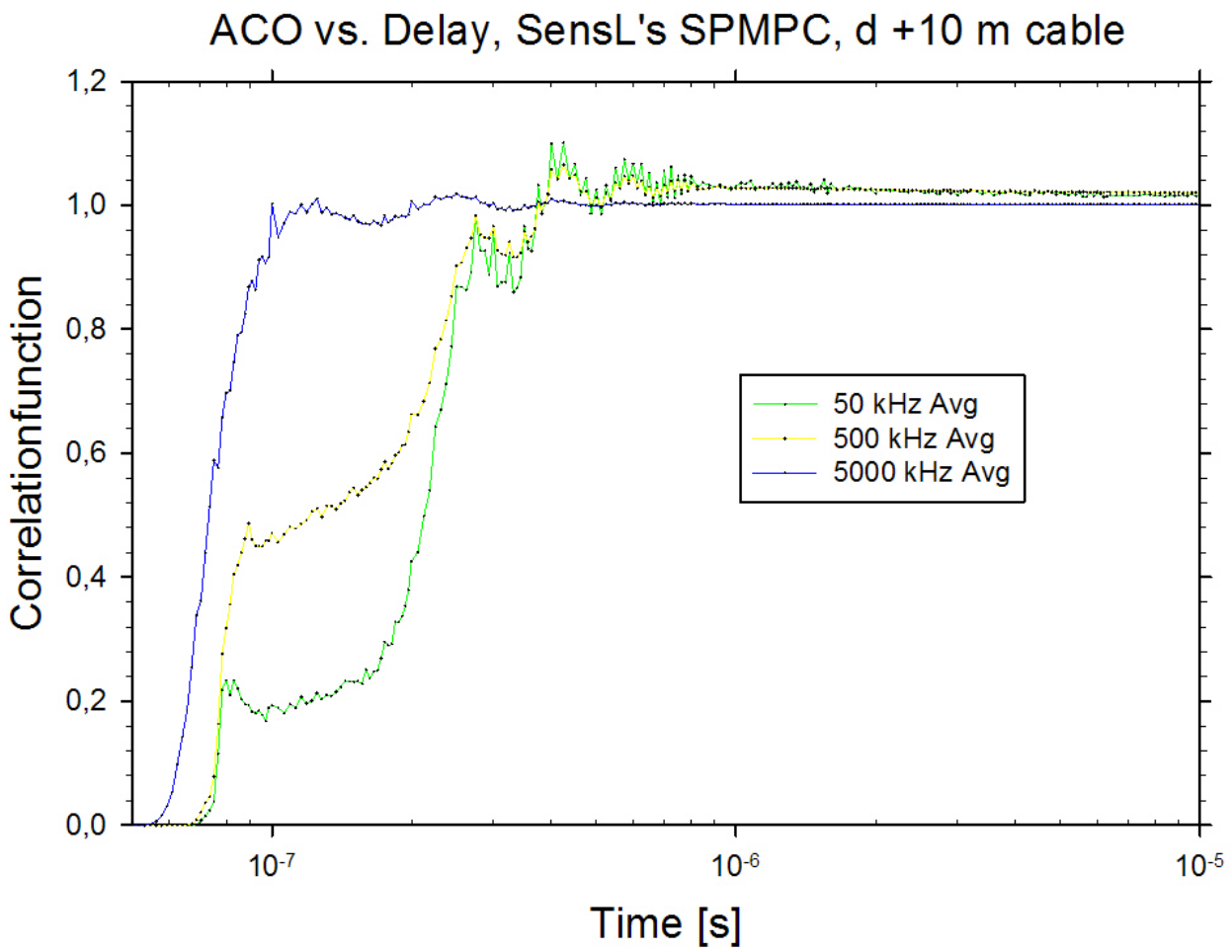

Figure A.65: Average normalized autocorrelation function vs. time delay for the **SensL's SPMPC** at various photon count rates using default (1 m) + 10 m cable. Note that y-axis uses linear scaling and x-axis uses logarithmic scaling.

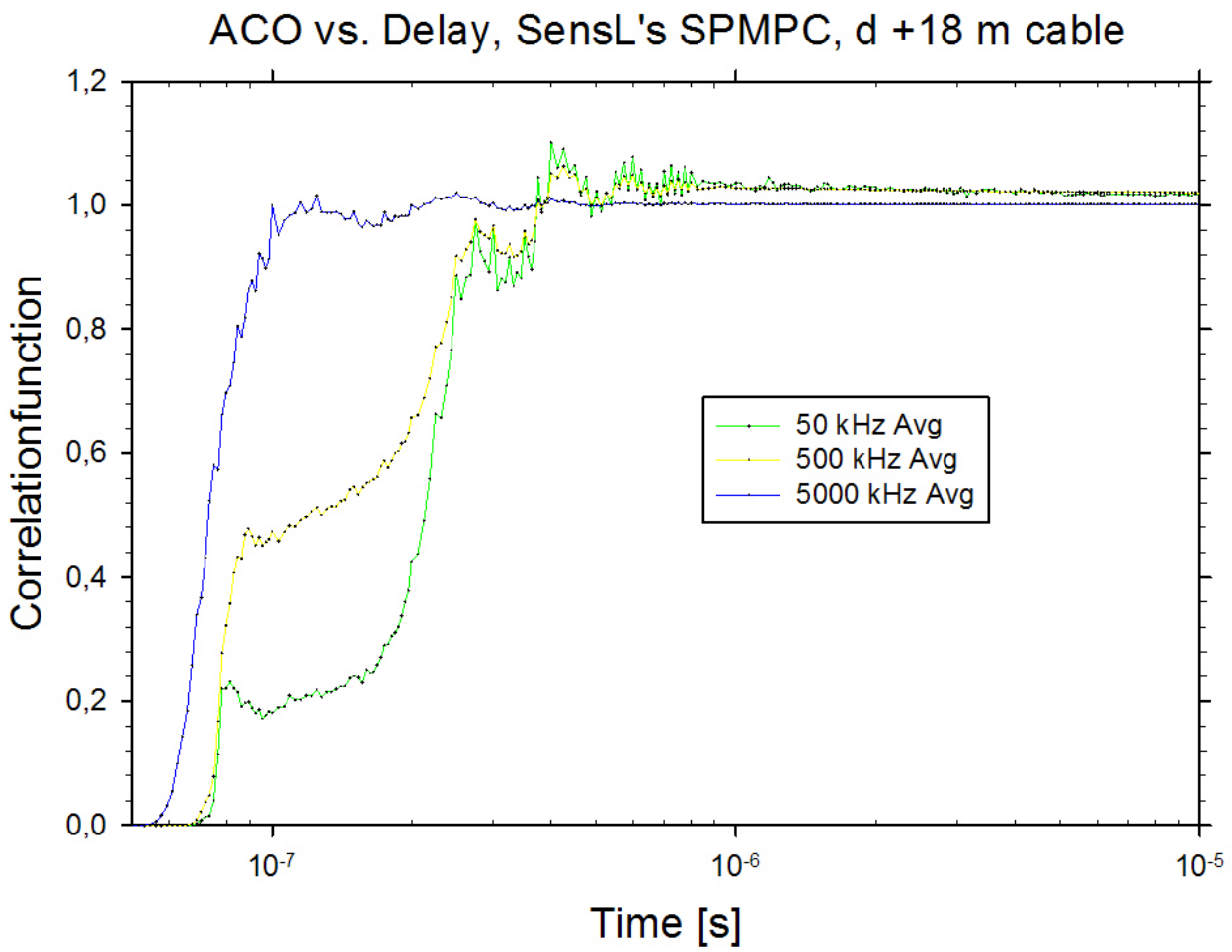

Figure A.66: Average normalized autocorrelation function vs. time delay for the **SensL's SPMPC** at various photon count rates using default (1 m) + 18 m cable. Note that y-axis uses linear scaling and x-axis uses logarithmic scaling.

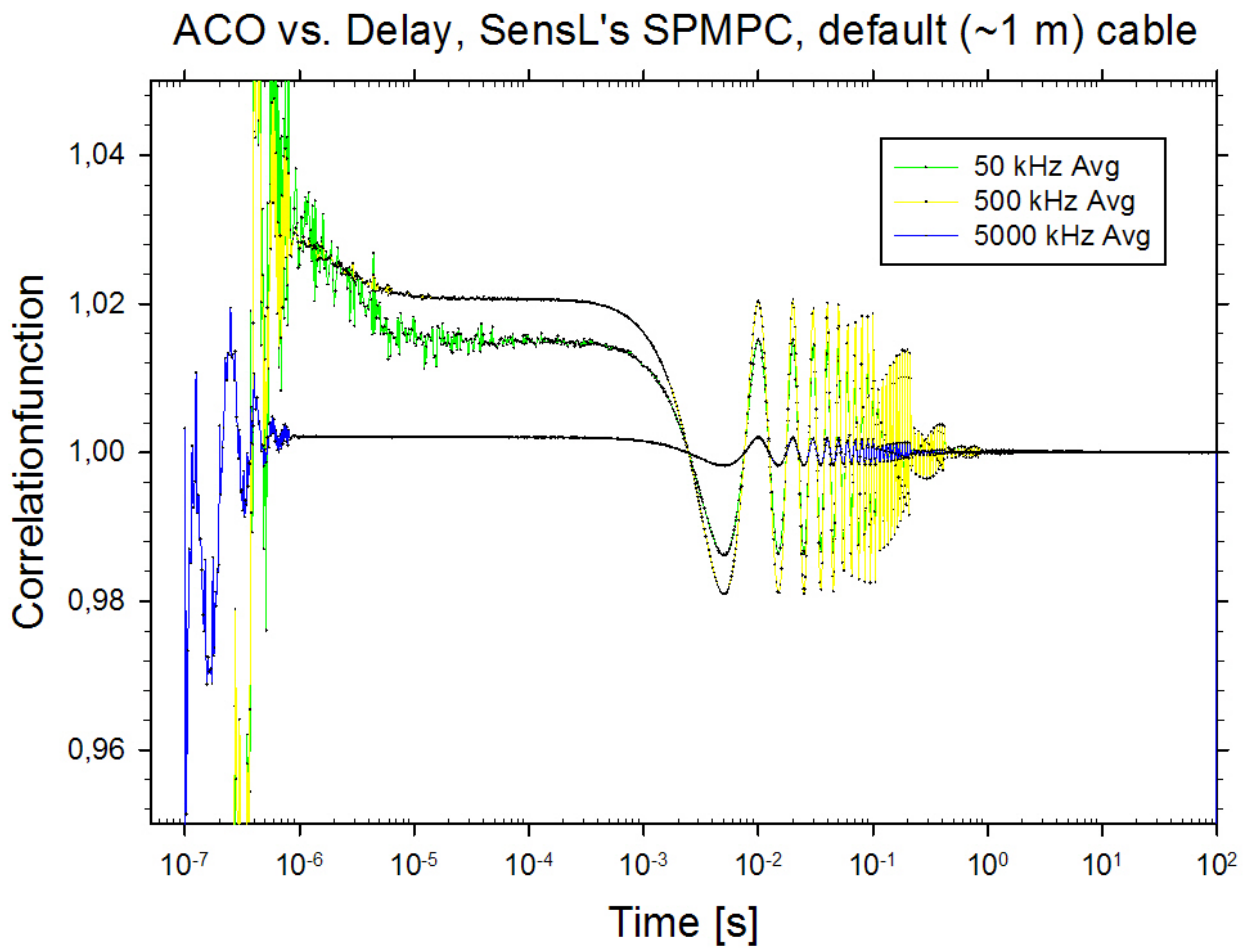

Figure A.67: Average normalized autocorrelation function vs. time delay for the **SensL's SPMPC** at various photon count rates using default (1 m) cable. Note that y-axis uses linear scaling and x-axis uses logarithmic scaling.

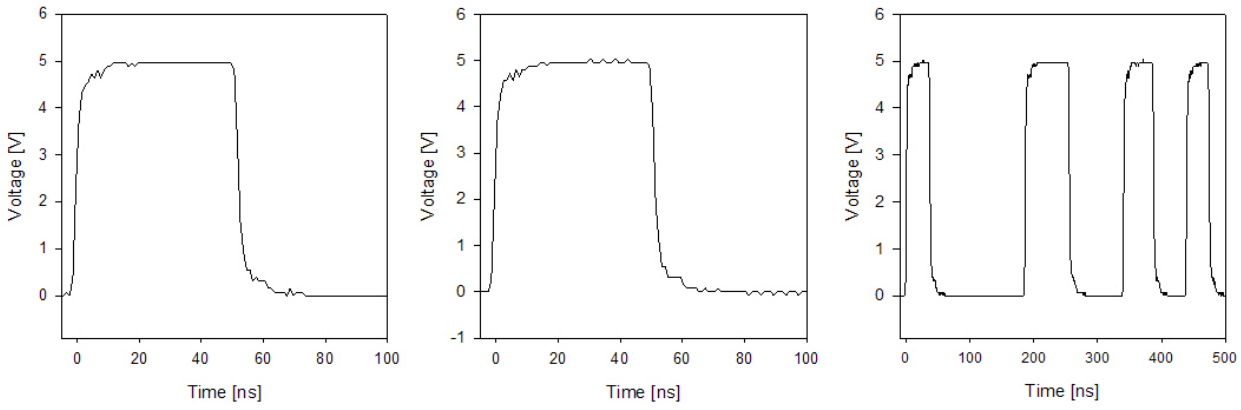

Figure A.68: Somewhat randomly picked waveforms (pulse shape) in the digital oscilloscope "Picoscope 5203" for some count rates, using the same setup as in the previous figure. From left to right: 50 kHz, 500 kHz, and 5000 kHz.

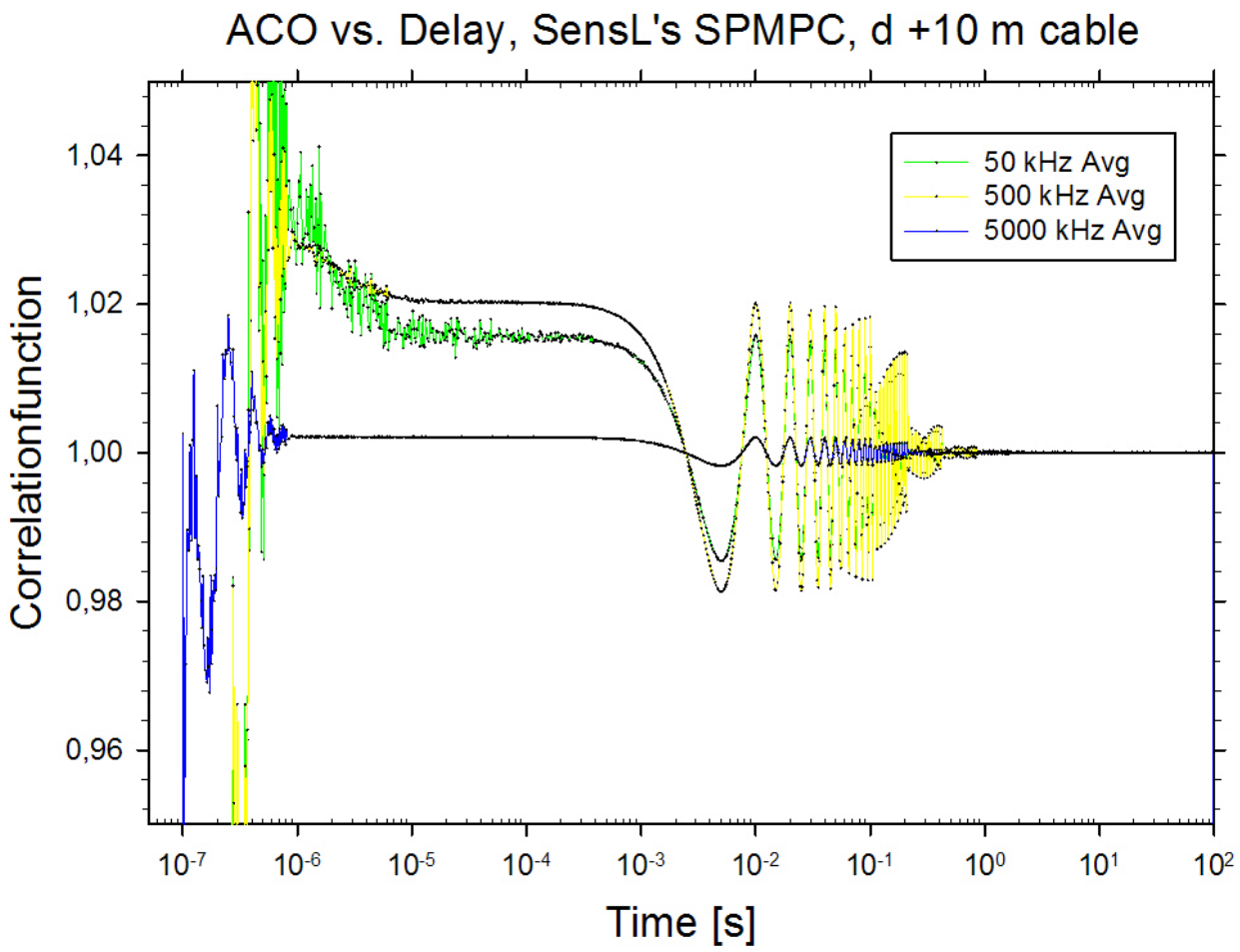

Figure A.69: Average normalized autocorrelation function vs. time delay for the **SensL's SPMPC** at various photon count rates using default (1 m) + 10 m cable. Note that y-axis uses linear scaling and x-axis uses logarithmic scaling.

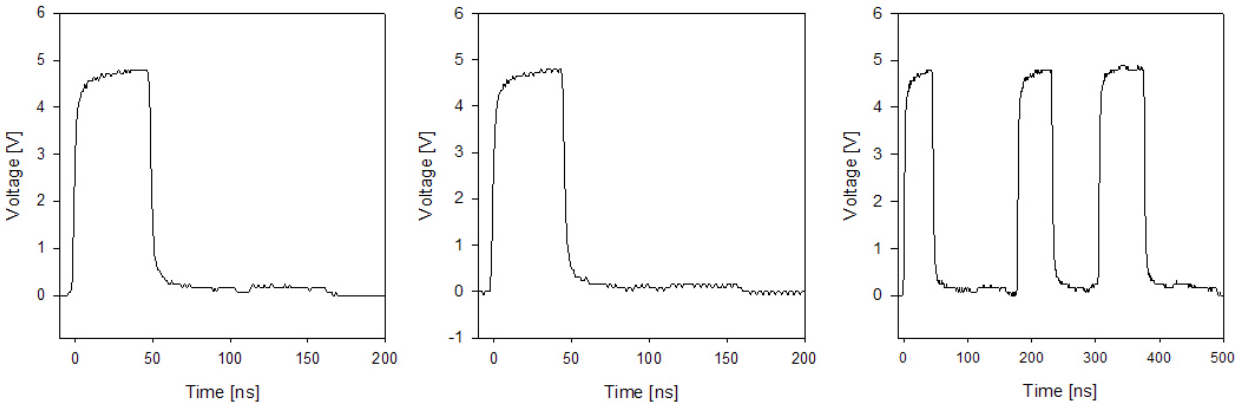

Figure A.70: Somewhat randomly picked waveforms (pulse shape) in the digital oscilloscope "Picoscope 5203" for some count rates, using the same setup as in the previous figure. From left to right: 50 kHz, 500 kHz, and 5000 kHz.

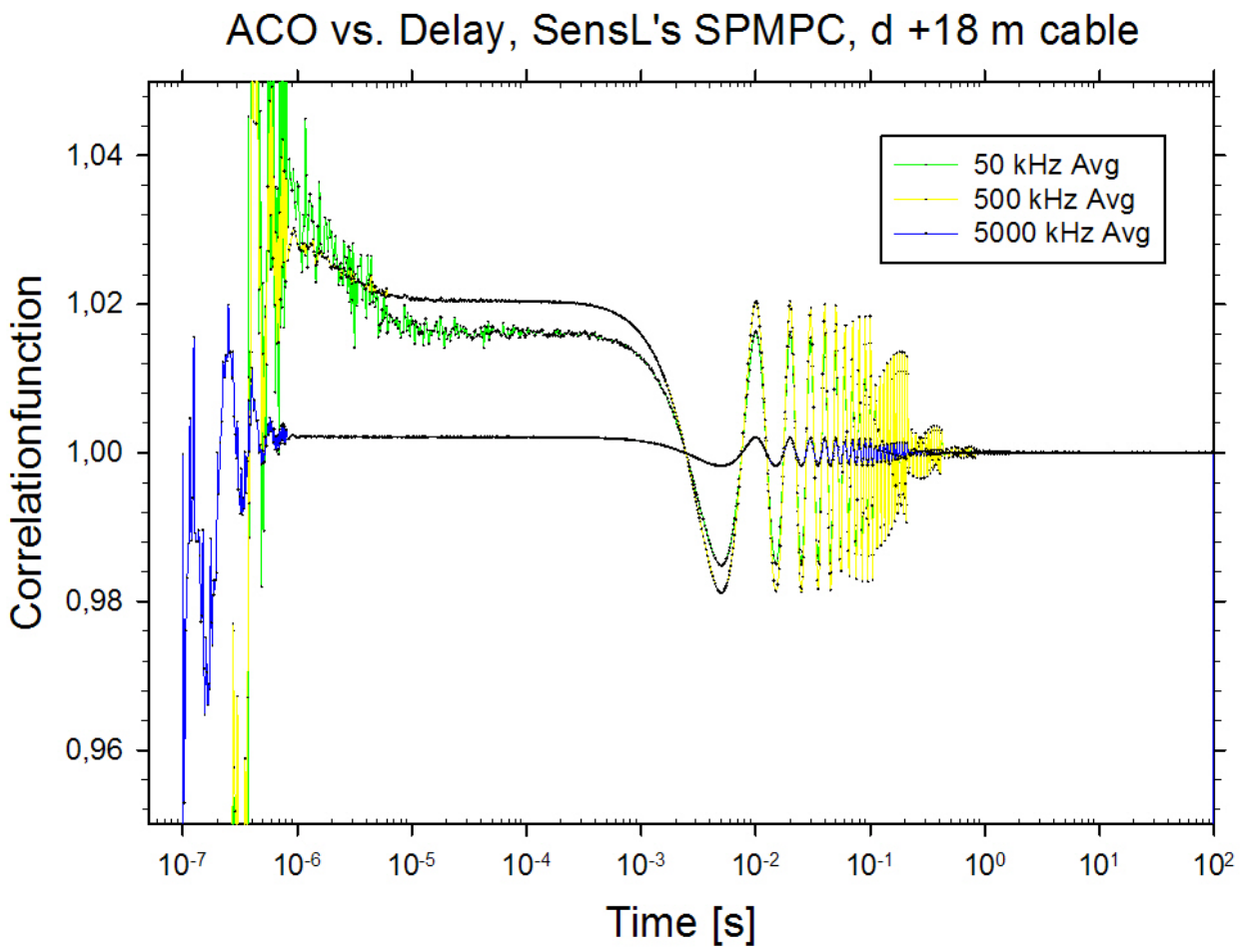

Figure A.71: Average normalized autocorrelation function vs. time delay for the **SensL's SPMPC** at various photon count rates using default (1 m) + 18 m cable. Note that y-axis uses linear scaling and x-axis uses logarithmic scaling.

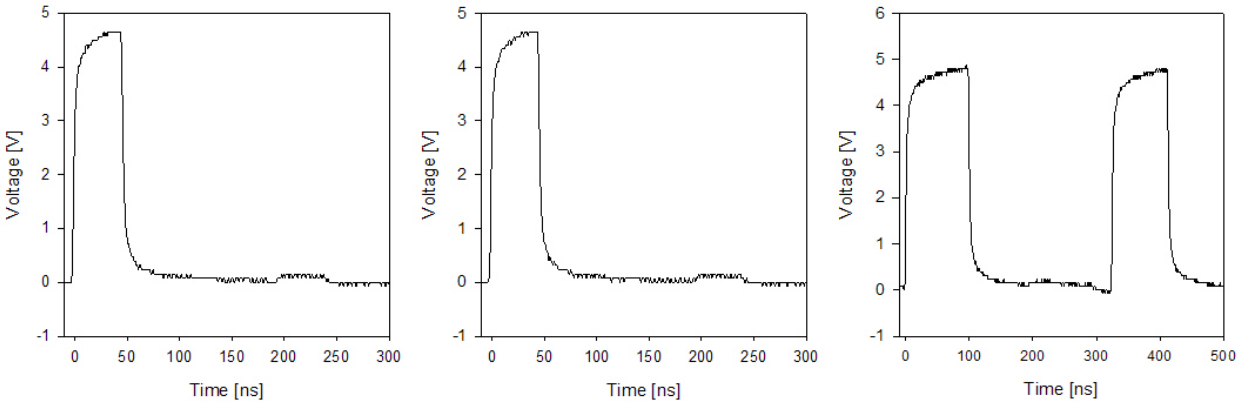

Figure A.72: Somewhat randomly picked waveforms (pulse shape) in the digital oscilloscope "Picoscope 5203" for some count rates, using the same setup as in the previous figure. From left to right: 50 kHz, 500 kHz, and 5000 kHz.

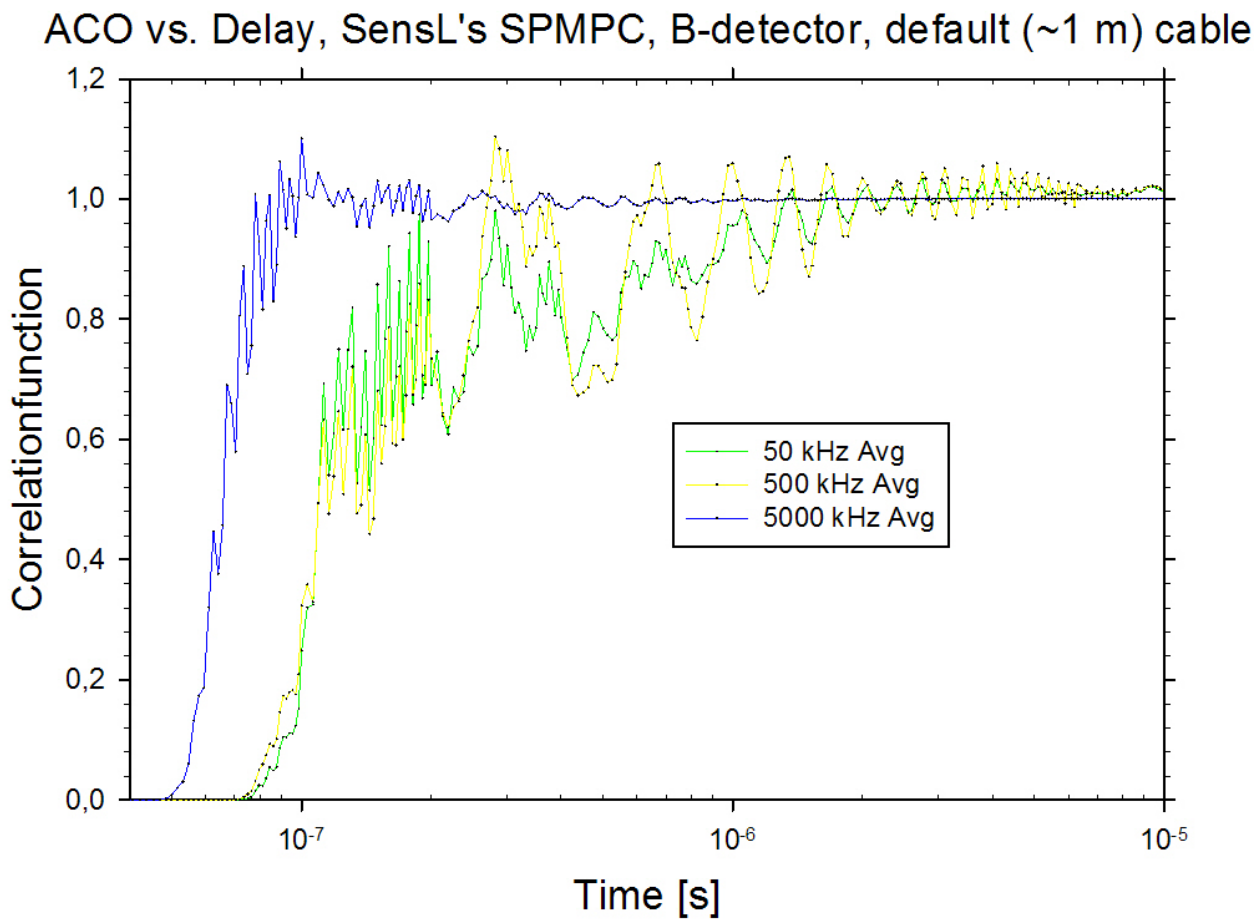

Figure A.73: Average normalized autocorrelation function vs. time delay for **SensL's SPMPC**, using the 2nd detector (normally used for the B-channel in the hardware-correlator), at various photon count rates using default (1 m) cable. Note that y-axis uses linear scaling and x-axis uses logarithmic scaling.

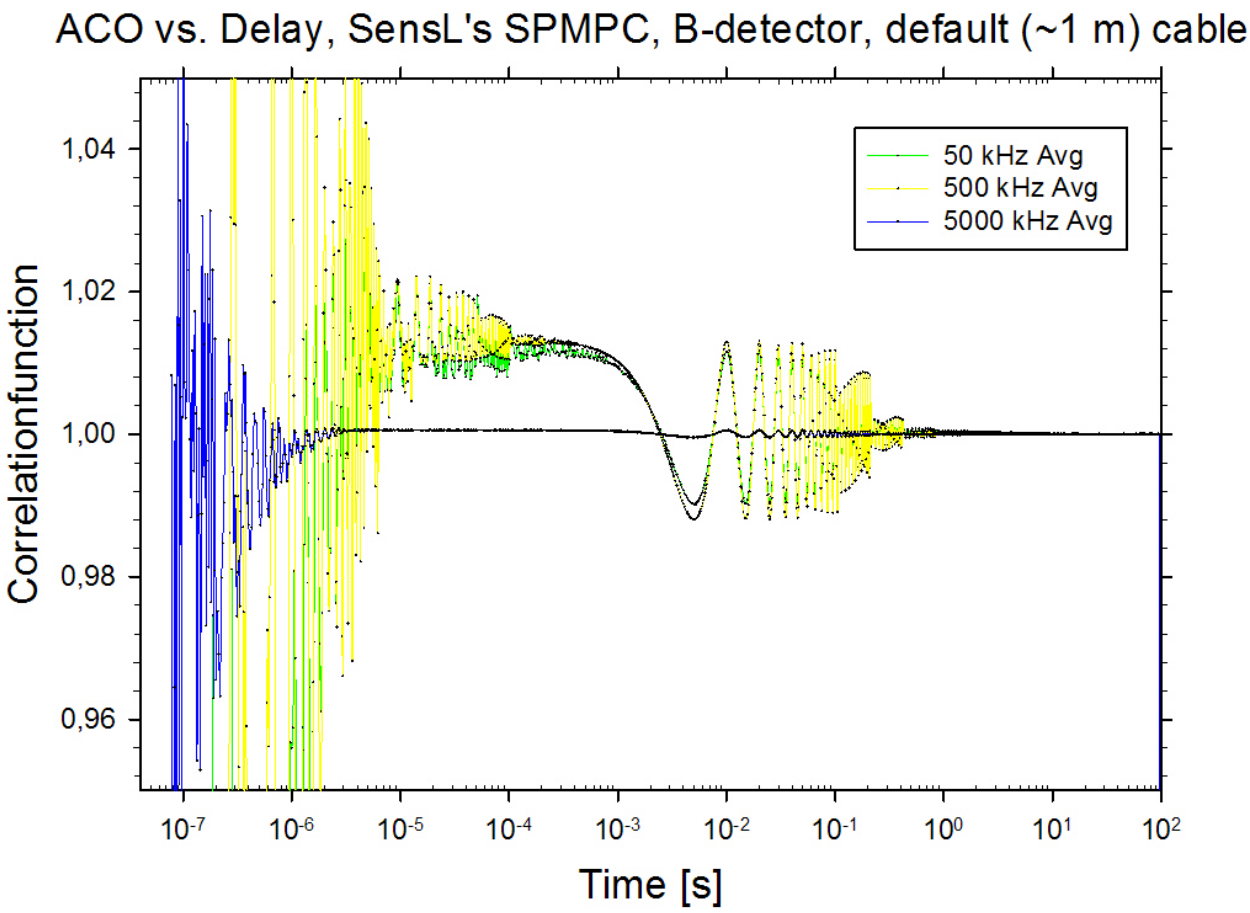

Figure A.74: Average normalized autocorrelation function vs. time delay for **SensL's SPMPC**, using the 2nd detector (normally used for the B-channel in the hardware-correlator), at various photon count rates using default (1 m) cable. Note that y-axis uses linear scaling and x-axis uses logarithmic scaling.

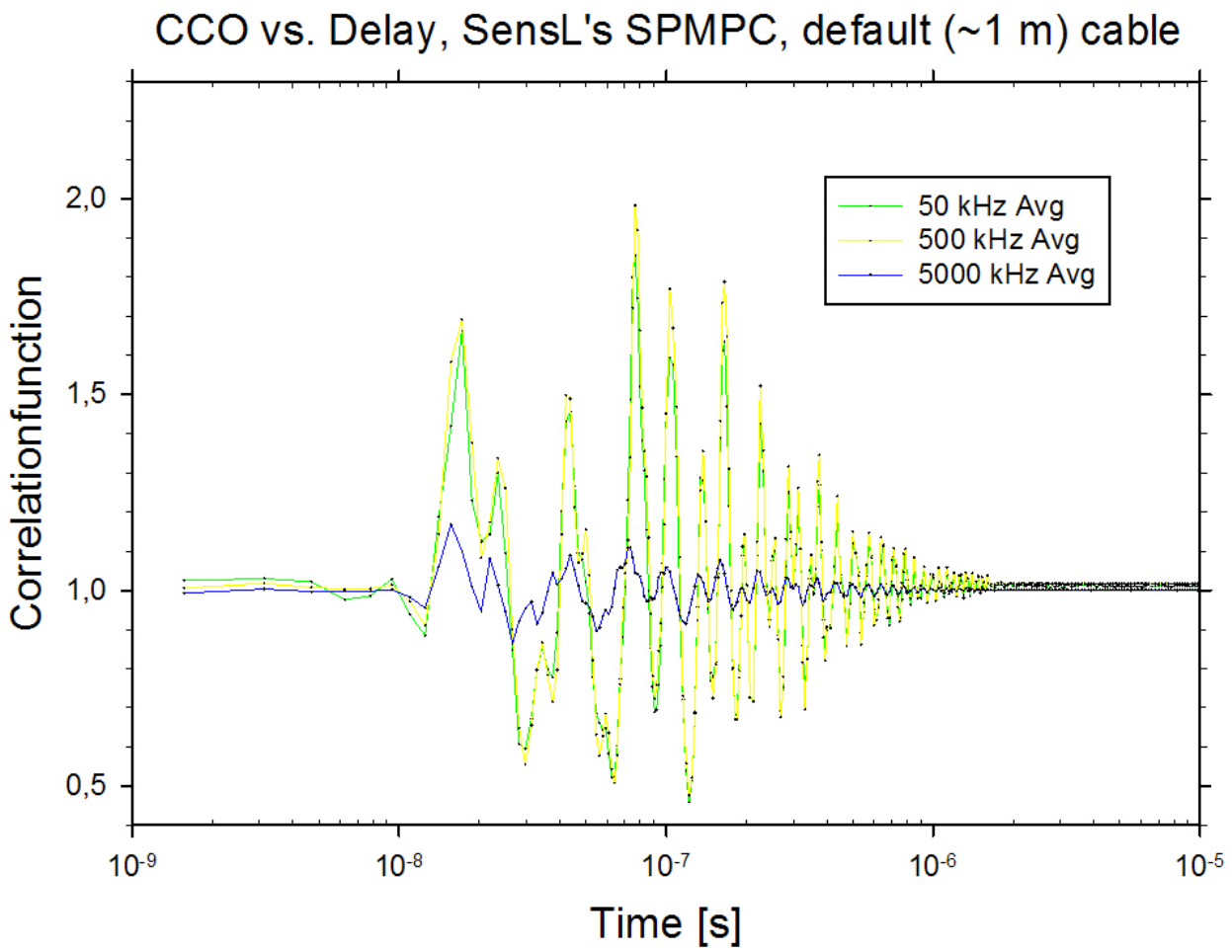

Figure A.75: Average normalized crosscorrelation function vs. time delay for the **SensL's SPMPC** at various photon count rates using default (1 m) cables. Note that y-axis uses linear scaling and x-axis uses logarithmic scaling.

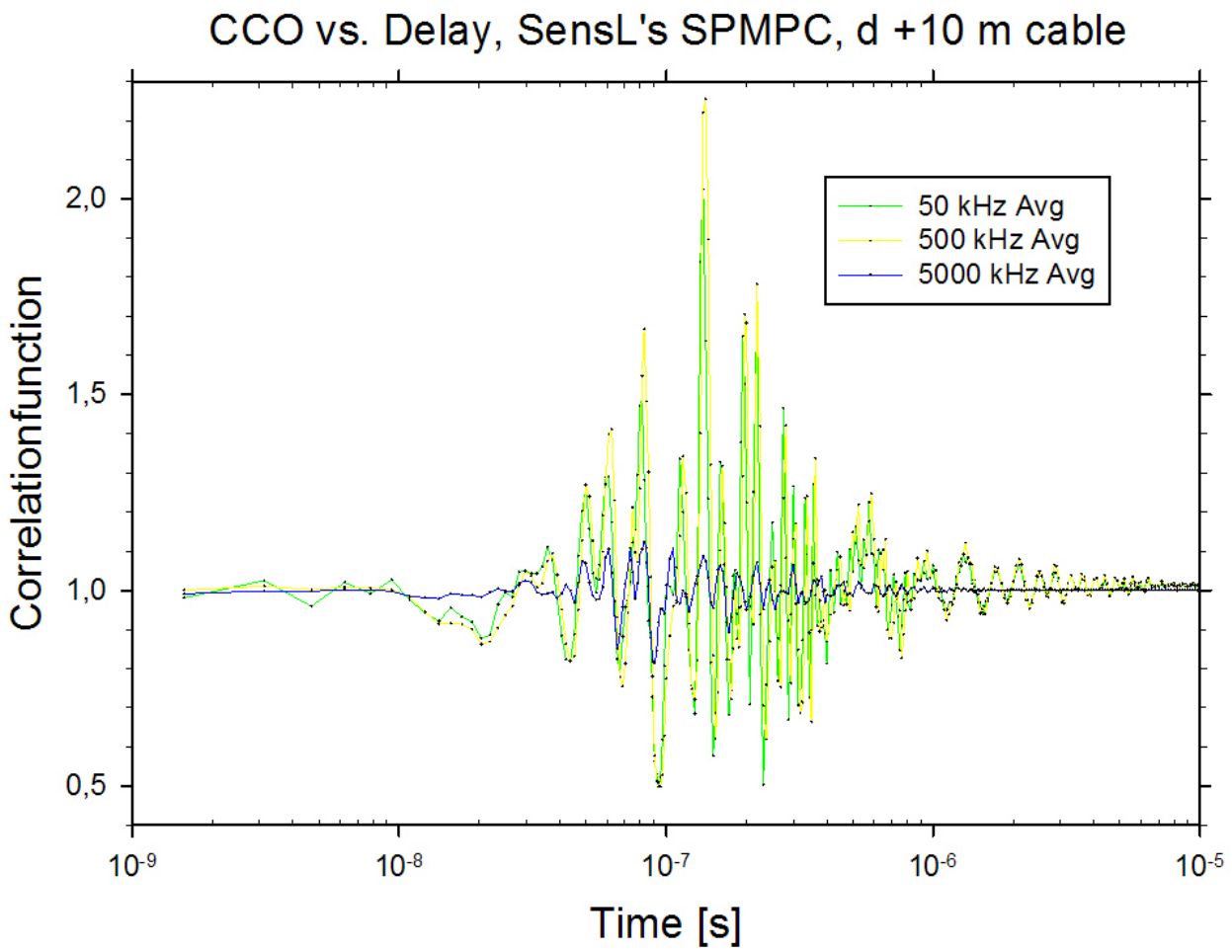

Figure A.76: Average normalized crosscorrelation function vs. time delay for the **SensL's SPMPC** at various photon count rates using default (1 m) + 10 m cables. Note that y-axis uses linear scaling and x-axis uses logarithmic scaling.

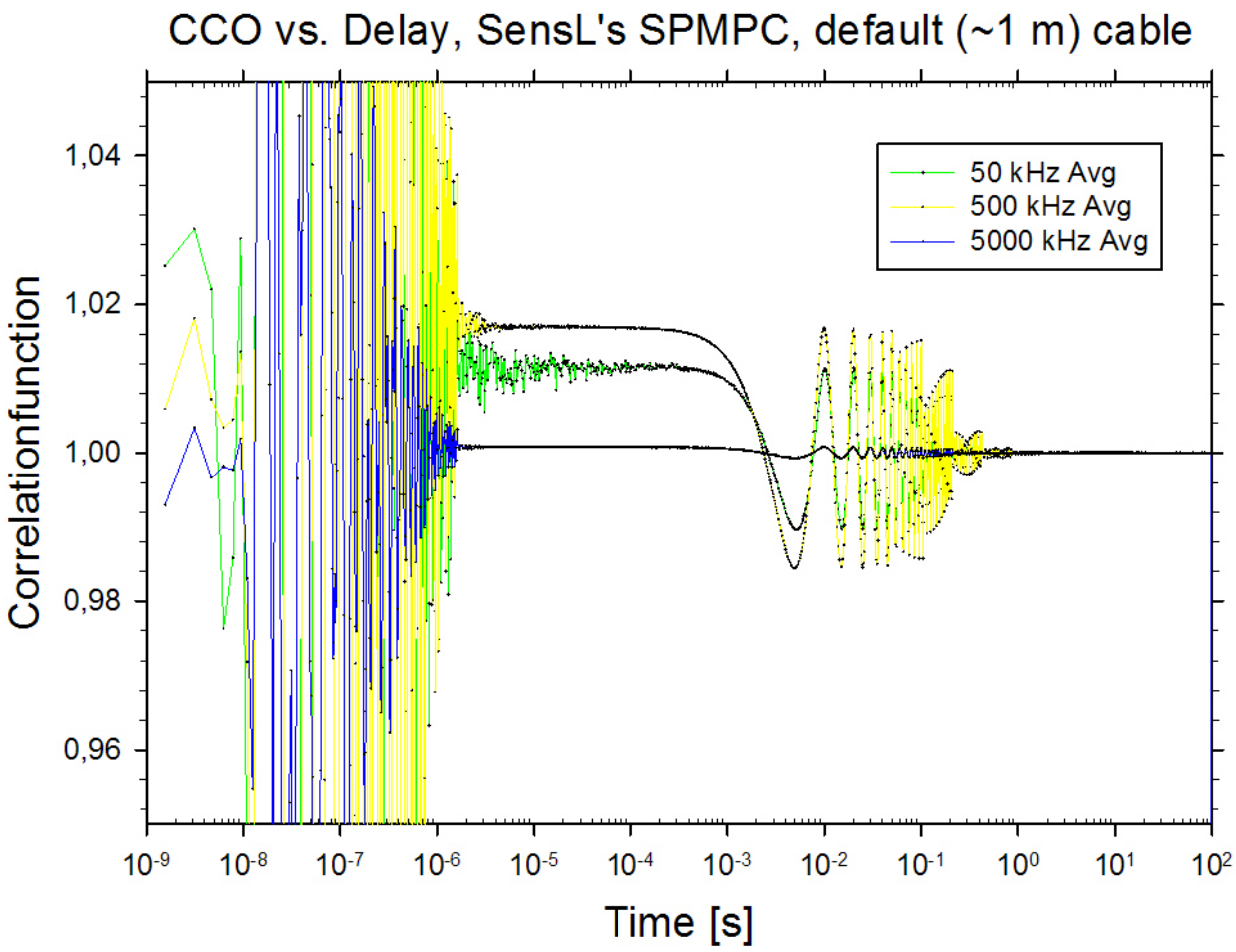

Figure A.77: Average normalized crosscorrelation function vs. time delay for the **SensL's SPMPC** at various photon count rates using default (1 m) cables. Note that y-axis uses linear scaling and x-axis uses logarithmic scaling.

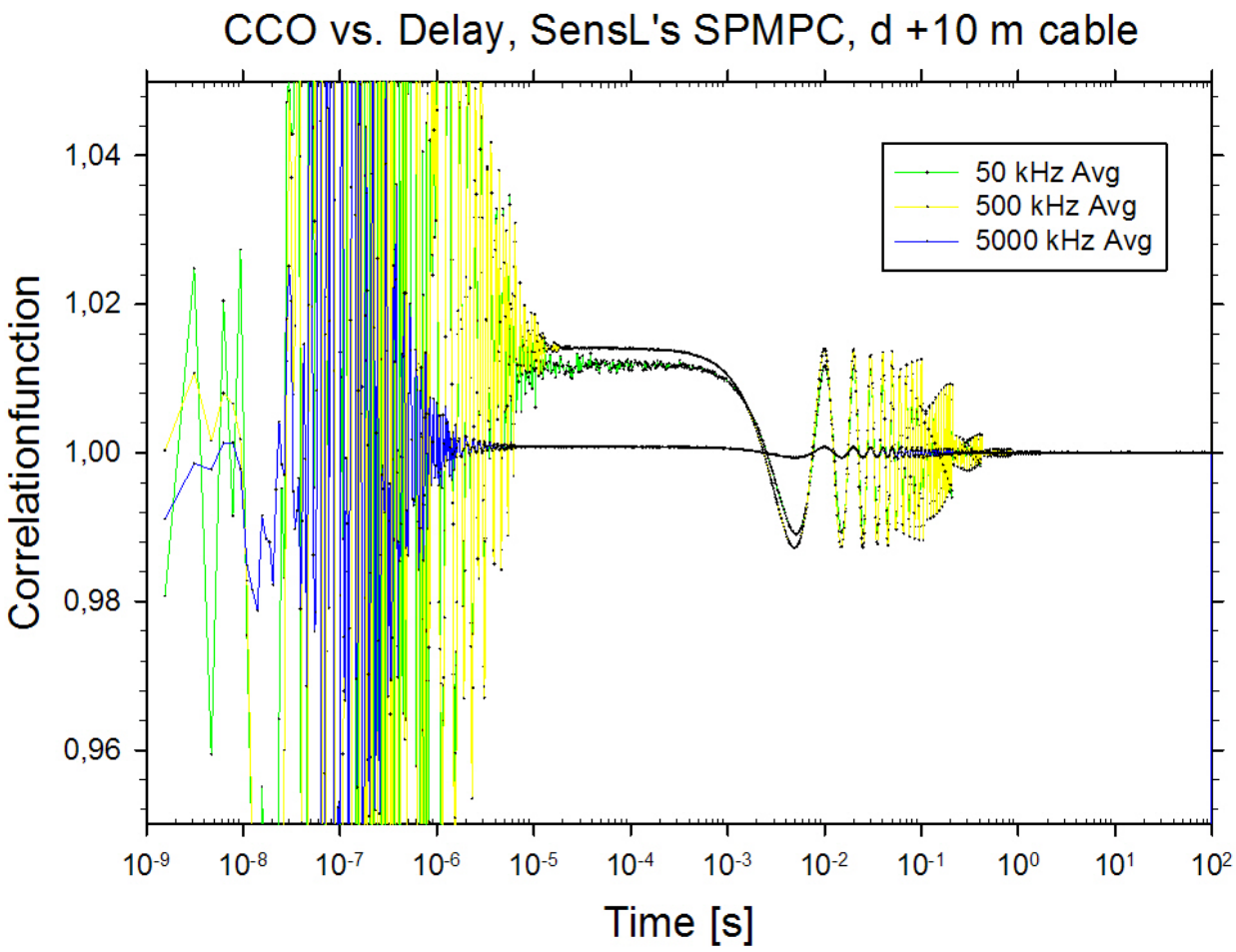

Figure A.78: Average normalized crosscorrelation function vs. time delay for the **SensL's SPMPC** at various photon count rates using default (1 m) + 10 m cables. Note that y-axis uses linear scaling and x-axis uses logarithmic scaling.